Technische Universität München
TUM School of Natural Sciences

Electromagnetic and power-suppressed effects in exclusive B decays

Jan-Niklas Toelstede

Vollständiger Abdruck der von der TUM School of Natural Sciences der Technischen Universität München zur Erlangung des akademischen Grades eines

Doktors der Naturwissenschaften (Dr. rer. nat.)

genehmigten Dissertation.

Vorsitz:
Prof. Dr. Bastian Märkisch

Prüfer*innen der Dissertation:
1. Prof. Dr. Martin Beneke
2. Prof. Dr. Lorenzo Tancredi

Die Dissertation wurde am 24.04.2023 bei der Technischen Universität München eingereicht und durch die TUM School of Natural Sciences am 08.06.2023 angenommen.

Electromagnetic and power-suppressed effects in exclusive B decays

Jan-Niklas Toelstede

Dissertation

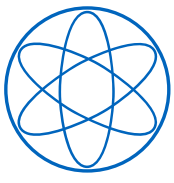

Physik-Department T31
Technische Universität
München

Abstract

In this thesis, we investigate corrections to the QCD factorization approach in exclusive, charmless B decays and study their relevance for future precision analyses. Using the framework of Heavy Quark Effective Theory and Soft-Collinear Effective Theory, we derive factorization formulas for two types of decays. For the radiative $\bar{B} \to \gamma\ell\nu$ decay, we extend the factorization analysis to the case of an off-shell hard-collinear photon and scalar interpolating currents with space-like separation. We estimate subleading power corrections in an operator product expansion that includes B-meson light-cone distribution amplitudes (LCDAs) of higher twist. Moreover, we employ sum rules using dispersion relations to obtain soft corrections induced by the leading power factorization and the $1/E_\gamma$- and, $1/m_b$-suppressed effects. The results provide constraints on exclusive matrix elements of the B meson from future lattice QCD calculations. For non-leptonic $\bar{B} \to M_1 M_2$ decays into light mesons, we show that the QCD factorization of the leading power amplitude can be generalized to include electromagnetic corrections. To this end, we consistently define the associated form factors and LCDAs in QCD$\times$QED. These objects are infrared divergent so that the non-radiative amplitude needs to be dressed with an ultrasoft function, accounting for the real emission of photons. For both radiative and non-leptonic decays, we use renormalization group techniques to resum large logarithms involving different scales. To complete our analysis, we provide numerical estimates for the subleading effects and QED corrections in the respective cases.

Zusammenfassung

In dieser Arbeit untersuchen wir Korrekturen zur QCD Faktorisierung in exklusiven, charmlosen B-Zerfällen und deren Relevanz für zukünftige Präzisionsanalysen. Mithilfe der effektiven Theorien schwerer Quarks und soft-kollinearer Moden leiten wir Faktorisierungsformeln für zwei Zerfallsarten her. Für den radiativen Zerfall $\bar{B} \to \gamma\ell\nu$ erweitern wir den Faktorisierungsansatz um den Fall von off-shell Photonen und skalaren interpolierenden Strömen mit raumartigem Abstand. Wir schätzen potenz-unterdrückte Korrekturen in einer Operatorproduktentwicklung ab, welche Lichtkegelverteilungsamplituden (LCDAs) des B Mesons zu höherer Twist-Ordnung beinhalten. Darüber hinaus nutzen wir Summenregeln aus Dispersionsrelationen, um weiche Korrekturen zu erhalten, die durch die Faktorisierung in führender Potenz und $1/E_\gamma$- und $1/m_b$-unterdrückte Terme induziert werden. Die Ergebnisse werden exklusive Matrixelemente des B Mesons durch zukünftige QCD Gitterrechnungen eingrenzen. Für nichtleptonische $\bar{B} \to M_1 M_2$ Zerfälle in leichte Endzustände zeigen wir, dass die QCD Faktorisierung der Amplitude um elektromagnetische Korrekturen erweitert werden kann. Hierfür definieren wir konsistent die assoziierten Formfaktoren und LCDAs in der vollen QCD×QED Theorie. Diese Objekte sind infrarot-divergent, sodass die nichtradiative Amplitude mit einer ultraweichen Funktion ausgestattet werden muss, welche die Emission reeller Photonen einschließt. Für sowohl den radiativen als auch den nicht-leptonischen Zerfall lösen wir die Renormierungsgruppengleichungen, um große Logarithmen verschiedener Skalen zu resummieren. Zuletzt liefern wir numerische Abschätzungen für die potenz-unterdrückten Terme und die QED Korrekturen in den entsprechenden Szenarien.

Contents

Chapter 1

Introduction

In 2012, the ATLAS [1] and CMS [2] experiments confirmed the existence of the Higgs boson, which was the last missing piece of the Standard Model (SM) of particle physics. These measurements completed the model built up by earlier works and discoveries, see [3–14] for some of the central publications and [15] for a review. Up to date, the SM is one of the most accurate theories that describes the fundamental interactions of matter, even though it is incomplete by several means. First of all, gravitation is not part of the SM and hence gravity-related phenomena like recently detected gravitational waves [16] or the nature of dark matter [17] are not explained. Moreover, the observation of neutrino oscillations [18, 19] which require neutrinos to be massive does not match the assumption of the model. In addition, the sources of CP-violation in the SM are not sufficient to create the observed matter-antimatter asymmetry in the universe. We could continue this list to include more unexplained phenomena, but apart from these rather obvious mismatches between the model and the real world, there are also more subtle tensions regarding measured quantities predicted by the SM. A paradigm in this context is the anomalous magnetic moment of the muon $(g-2)_\mu$ which describes the coupling to an external magnetic field and differs by 4.2σ to the SM prediction according to the findings in [20]. These kind of discrepancies may ultimately be related to effects of New Physics (NP).

The search for NP drives both theoretical and experimental physics towards increasing precision analyses in different branches of high energy physics. Generally, we expect to find NP effects in two ways: either directly or indirectly. A direct detection could be achieved by producing a new particle due to an increase of the center-of-mass energy in a (future) collider [21–23]. In contrast to the discovery of the Higgs boson, there is no further symmetry or guiding principle like the violation of perturbative unitarity (cured by the Higgs mechanism) which would indicate the existence of new phenomena between the electroweak and the Planck scale. Instead, the second promising strategy to find NP is to focus on methods allowing for a possible indirect detection based on a precise comparison between theoretical prediction and experimental measurement. The area of *Flavour Physics* represents an encouraging field where theory and experiment

have provided striking insights to the SM. Experiments at B factories like BaBar or Belle have shown that the decays of b-quark hadrons are especially suitable for precision studies [24]. From the theory side, this is supplemented by the fact that the B-meson mass is comparably large, so that perturbative calculations are possible and yield reliable results. Within the next decade, collider experiments like LHCb and Belle II increase their luminosity and detector efficiency and are thus expected to reach higher precision in various B-decay channels, see e.g. [25]. Therefore, it becomes even more desirable to study these decays and push theoretical calculations to the next frontier.

Charmless B decays in particular offer a broad variety of SM checks. In the past, there have been a couple of discrepancies and anomalies drawing attention due to their large tension compared to the SM theory prediction. One famous example in this regard is the discrepancy between the exclusive and inclusive determination of the CKM matrix element V_{ub} that deviates by 3.3σ [26].[1] Generally, we aim to resolve whether these tensions are real by sharpen theoretical calculations in specific decay channels. In this work, we focus on exclusive radiative $\bar{B} \to \gamma^{(*)}\ell\nu$ and non-leptonic $\bar{B} \to \pi\pi, \pi K$ decays. While the radiative decay can be used to measure V_{ub} and hadronic properties of the B meson, the non-leptonic decays are particularly sensitive to CP-violating strong and weak phases, required to constrain SM model parameters. We explain the aim of our analysis for both decay types in Sec. 1.1 and Sec. 1.2.

For precise theoretical calculations, it is necessary to disentangle all parameters and scales in the SM. Since we are interested in measurements much below the electroweak scale, fields with masses of $\mathcal{O}(m_W)$ or greater appear only virtually within Feynman diagrams. Their effects can be integrated out in an operator product expansion (OPE) and stored in Wilson coefficients, multiplying the operators of a low energy, non-renormalizable effective field theory (EFT) [29, 30]. The coefficient functions and coupling constants obey a renormalization group equation (RGE) that needs to be solved to resum large logarithms of the the b-quark and W-boson mass ratio $m_b/m_W \approx 5\%$. In practice, this improves the theoretical prediction since these logarithms could otherwise spoil the perturbative expansion when the strong coupling becomes large so that $\alpha_s \ln m_b^2/m_W^2 \sim \mathcal{O}(1)$. We refer to this as *renormalization group (RG) improved perturbation theory.*

At low energies, the nature of the strong interaction generally leads to the confinement of bound states like the B meson. This implies that hadronic matrix elements of EFT operators at the b-quark scale cannot be calculated perturbatively a priori. Instead, we parametrize the matrix elements by form factors that have to be determined experimentally or by lattice calculations in Quantum Chromodynamics (QCD). Due to scale evolution, the strong coupling α_s becomes smaller than unity and thus perturbative at scales above a few times Λ_{QCD}.[2] In the range up to m_b, we can use further EFT

[1] The anomalies in $B \to K^{(*)}\ell^+\ell^-$ decays, parametrized by the branching fractions $\mathcal{R}(K)$ and $\mathcal{R}(K^*)$, provide a counter example. They were intensively studied over the last decade and hinted towards a violation of lepton flavour universality. However, the tensions have been eliminated by the newest results from LHCb in December 2022 [27, 28].

[2] $\Lambda_{\text{QCD}} \approx 200 - 300$ MeV defines the scale at which α_s is formally infinite.

methods to compute the amplitudes of B-meson decays in a heavy-quark expansion. As a result, we obtain universal hadronic matrix elements that enter process-independently in different decay channels and are "multiplied" by process-dependent perturbative coefficients. Physically, these coefficients have to be understood as short-distance interactions of the partonic meson constituents that decouple in the heavy-quark limit from the non-perturtabive, long-distance fluctuations. We refer to this as the "factorization" of long- and short-distance physics.

In the following, we present the central ingredients and applications of the QCD factorization approach in the radiative $\bar{B} \to \gamma\ell\nu$ as well as non-leptonic $\bar{B} \to M_1 M_2$ decays. The aim of this thesis is to extend the leading power factorization formalism for both cases. For the first decay type, we consider more general correlation functions and estimate subleading power corrections in the heavy-quark expansion using an OPE and a dispersion relation. For the second type, we consider effects of Quantum Electrodynamics (QED) and develop a generalized QCD×QED factorization formula.

1.1 QCD factorization in $\bar{B} \to \gamma\ell\nu$

In experimental measurements, exclusive $\bar{B} \to \ell\nu$ and $\bar{B} \to \gamma\ell\nu$ decays have been analyzed to determine the CKM matrix element V_{ub}. When the photon in the final state becomes soft, the latter process cannot always be distinguished from a purely leptonic final state, so that it has to be viewed as a background process [31]. For an energetic photon with energy $E_\gamma \sim m_b \gg \Lambda_{\rm QCD}$, however, the $\bar{B} \to \gamma\ell\nu$ decay probes the intrinsic structure of the B meson. In this context, it is one of the simplest cases to analyze hadronic matrix elements and study QCD factorization as the process only involves one hadron.

The general idea of factorization is to decompose the amplitude (or cross section) of a process into more fundamental objects using a power expansion. In this way, one decouples long- from short-distance physics and achieves a separation of the scales by consequently applying EFT techniques. The natural scale of B decays is defined by the heavy b-quark mass $\Lambda_{\rm QCD} \ll m_b \ll m_W$ that determines the "hard" scale in the process. As we discussed in the introduction, fields with masses of order of the electroweak scale $\mathcal{O}(m_W)$ appear only virtually at the scale m_b. After integrating out these fields, we arrive at the electroweak Hamiltonian containing four-fermion interactions [32]. In the SM, the semi-leptonic $b \to u$ transition is mediated by the operator

$$\mathcal{H}_{\rm sl} = \frac{G_F V_{ub}}{\sqrt{2}} C_{\rm sl} Q_{\rm sl} \,, \qquad Q_{\rm sl} = [\bar{u}\gamma_\mu(1-\gamma_5)b][\bar{\ell}\gamma^\mu(1-\gamma_5)\nu_\ell] \,, \tag{1.1}$$

where G_F is the Fermi constant and $C_{\rm sl}$ the Wilson coefficient that contains the UV physics of the electroweak scale. In QCD-only, we have $C_{\rm sl} = 1$ to all orders in perturbation theory. The $\bar{B}_u$ meson decays weakly through the interaction in (1.1) and the amplitude for this decay is given by

$$\mathcal{A}(\bar{B}_u \to \gamma\ell^-\nu_\ell) = \frac{G_F V_{ub}}{\sqrt{2}} \big\langle \gamma\ell^-\nu_\ell \big| [\bar{\ell}\gamma^\mu(1-\gamma_5)\nu_\ell][\bar{u}\gamma_\mu(1-\gamma_5)b] \big| \bar{B}_u(p+q) \big\rangle \,, \tag{1.2}$$

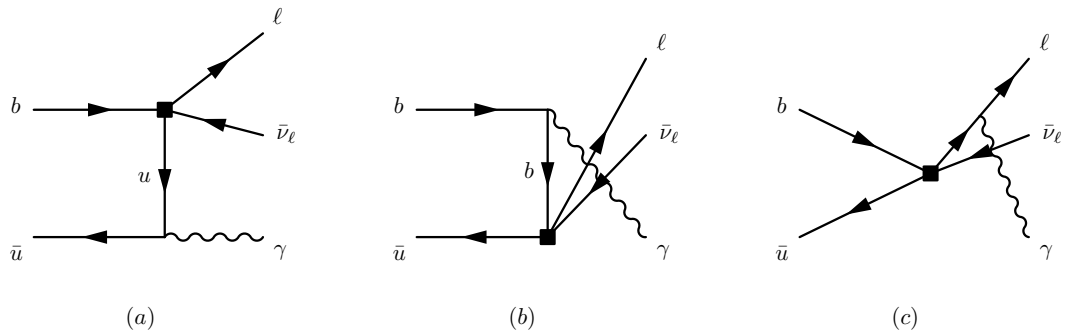

Figure 1.1: Tree level emission of the hard-collinear photon from (a) the light u-quark (b) the heavy b-quark and (c) the lepton. The box indicates the insertion of $Q_{\rm sl}$ in (1.1).

where a time-ordered product with an arbitrary number of QCD and QED current interactions is implicitly understood but no further insertions of weak operators are considered. Note that the B-meson momentum is displayed as the sum of the outgoing photon momentum p and the momentum q of the lepton pair $\ell\nu$. In the present context, we restrict ourselves to leading order (LO) in the electromagnetic coupling and focus on QCD-only effects. At LO, the photon can either be emitted from the final state lepton or the quarks of the B meson, see Fig. 1.1. We can decompose these three contributions according to [33]. The emission from the B-meson quarks are contained in the hadronic tensor

$$T_{\mu\nu}(p,q) = \int d^4x\, e^{ipx} \big\langle 0 \big| T\big\{ j_\mu^{\rm em}(x), j_\nu^{\rm weak}(0)\big\} \big| \bar{B}_u(p+q)\big\rangle \,. \tag{1.3}$$

The electromagnetic and the weak current are given by

$$j_\mu^{\rm em}(x) = \sum_{q\neq t} eQ_q \bar{q}\gamma_\mu q(x) \,, \qquad j_\nu^{\rm weak}(0) = \bar{u}\gamma_\nu(1-\gamma_5)b(0) \,, \tag{1.4}$$

where the electromagnetic coupling is $e^2 = 4\pi\alpha_{\rm em}$ and the electric charge of the up-type and down-type quarks $Q_u = 2/3$ and $Q_d = -1/3$ are factored out. Note that we focus on the hadronic part only since the sum over all spin and polarization states of the leptonic fields can be done trivially. The hadronic tensor in (1.3) can be further decomposed into the Lorentz structures

$$\begin{aligned} T_{\mu\nu}(p,q) = {} & \epsilon_{\mu\nu\lambda\rho} p^\lambda v^\rho F_V(E_\gamma) + [-i(vp)g_{\mu\nu} + iv_\mu p_\nu] F_A(E_\gamma) - i\frac{v_\mu v_\nu}{(vp)} f_B \\ & + \text{ terms with } p_\mu \,. \end{aligned} \tag{1.5}$$

The third term, proportional to $v_\mu v_\nu$, is fixed by the Ward identity of the amplitude and originates from the photon emission of the lepton. It involves the B-meson decay constant in QCD

$$\big\langle 0 \big| \bar{u}\gamma_\nu(1-\gamma_5)b(0) \big| \bar{B}_u(p+q)\big\rangle = if_B(p+q)_\nu \,, \tag{1.6}$$

which has to be determined non-perturbatively. In principle, also the form factors F_V and F_A defined by (1.5) have to be determined in this way. However, these objects can be decomposed (factorized) further into a product of perturbative coefficients and universal hadronic matrix elements (functions). Using the heavy-quark expansion, one finds [34, 35]

$$F_V(E_\gamma) = F_A(E_\gamma) = eQ_u f_B m_B \; C(E_\gamma;\mu) \int_0^\infty \frac{d\omega}{2E_\gamma\omega} J(2E_\gamma\omega;\mu)\phi_B(\omega;\mu) + \text{power corrections} \,. \tag{1.7}$$

Power corrections to this formula are of order $\Lambda_{\rm QCD}/E_\gamma \sim \Lambda_{\rm QCD}/m_b \ll 1$. The short-distance physics is contained within the hard and hard-collinear functions C and J. Their natural scales are $E_\gamma \sim m_b$ and $2E_\gamma\omega \sim \sqrt{\Lambda_{\rm QCD} m_b}$[3], at which the strong coupling is much smaller than unity and hence these objects can be calculated in perturbation theory. The remaining long-distance ("soft") physics of $\mathcal{O}(\Lambda_{\rm QCD})$ is parametrized by the non-perturbative matrix element

$$\big\langle 0\big|\bar{u}(x)[x,0]\not{x}\gamma_5 b(0)\big|\bar{B}(p+q)\big\rangle = itf_B m_B \int_0^\infty d\omega e^{-i\omega t}\phi_B(\omega;\mu) \,, \tag{1.8}$$

where $x^2 = 0$ is a light-like reference vector aligned with the direction of the photon. The meson velocity is defined by $p + q = m_B v$ and the implicit prescription on the Fourier transformation variable $t = vx - i0$ is induced by the analytic structure of the operator on the left-hand side in (1.8). $[x, 0]$ is a finite distance gauge-link that ensures gauge invariance of this operator. Its definition and origin will be explained in Chapter 2.

The function $\phi_B(\omega;\mu)$ is the leading-twist light-cone distribution amplitude (LCDA) of the B-meson defined in QCD. It is a process-independent matrix element that captures the two-particle contributions of the B-meson, approximately viewed as a b- and u-quark valence state, and was initially introduced in [36]. The first application of this function states back to the QCD factorization of the spectator scattering interactions in non-leptonic B decays, which is discussed in the next section 1.2. Although (1.8) reflects the light-like correlation between these valence states, the matrix element captures the entire soft fluctuations of the bound state. For this reason, it is traditionally defined in the framework Heavy Quark Effective Theory (HQET) rather than in QCD, which will be introduced in Chapter 2. The B LCDA enters in almost every exclusive decay involving the B meson and is convoluted with a hard-collinear function, which behaves like $1/\omega$ at tree-level. A central object that appearing on the amplitude level and eventually appearing in observable is therefore the first inverse moment [37]

$$\frac{1}{\lambda_B(\mu)} = \int_0^\infty \frac{d\omega}{\omega}\phi_B(\omega;\mu) \,. \tag{1.9}$$

[3]We count $\omega \sim \Lambda_{\rm QCD}$ even though we integrate ω in (1.7) to infinity. The variable ω can be associated with the typical momentum of the light u-quark that is of order $\mathcal{O}(\Lambda_{\rm QCD})$. We expect the B LCDA to favour this momentum configuration, so that $\phi_B(\omega) \sim \mathcal{O}(1)$ for $\omega \sim \Lambda_{\rm QCD}$ and is relatively suppressed otherwise.

Corrections at next-to-leading order (NLO) in the strong coupling introduce logarithmic modifications to this object that are discussed in later chapters. The value of inverse moment is typically given by $\lambda_B(1\text{ GeV}) = 460 \pm 160$ MeV [38, 39].

The inverse moment λ_B suffers from large uncertainties in experimental and lattice determinations and so far it has been a challenging task to obtain reliable constraints. Since lattice QCD simulations require space-like (Euclidean) separated correlation functions to implement sampling methods, the main difficulty is to find suitable objects that are eventually related to the time-like operator in (1.8). Recent works proposed several methods to match Euclidean correlators to the B-meson LCDA using EFTs and factorization [40, 41]. The current perspectives of lattice QCD in [42–44] motivate the application of corresponding techniques to correlation functions of the form (1.3). To this end, we consider the outgoing momentum in (1.3) to be off-shell with $p^2 < 0$, which provides a natural generalization to $\bar{B} \to \gamma^* \ell\nu$. A complete factorization of (1.3) in this case has already been derived for the four-lepton decay [45, 46]. In the context of lattice calculations, we view the resulting object as an arbitrary correlation function without an explicit embedding into a physical process. With this in mind and in addition to the electromagnetic vector and the weak axialvector current in (1.4), we analyze the correlation function (1.3) for (pseudo-)scalar currents. We further include power corrections to the leading power factorization result for both scalar and vector case based on the methods in [47]. This paves the way for precise future predictions of non-perturbative quantities in B decays such as ϕ_B and λ_B.

1.2 QED effects in non-leptonic $\bar{B} \to M_1 M_2$ decays

In the second part of this thesis, we consider the factorization of charmless, non-leptonic $\bar{B} \to M_1 M_2$ decays into two light final-state mesons. The QCD factorization formula for these decays has been etablished in [37, 48] and reads schematically

$$\langle M_1 M_2 | Q_i | \bar{B} \rangle = F^{BM_1} \times T_i^{\mathrm{I}} * f_{M_2}\phi_{M_2} + T_i^{\mathrm{II}} * f_{M_1}\phi_{M_1} * f_{M_2}\phi_{M_2} * f_B\phi_B \,. \tag{1.10}$$

The "$*$"-symbol denotes a convolution of the matching coefficients $T_i^{\mathrm{I/II}}$ with the meson LCDAs ϕ_{M_1} ϕ_{M_2} and ϕ_B. Usually, we refer to the first term in the formula (1.10) as the "form-factor term" and to the second one as the "hard spectator-scattering term." The formula holds in general for every operator Q_i of the electroweak Hamiltonian that mediates $b \to q$ transitions into light quarks $q = u, d, s$. On the left hand side of (1.10), the hard scattering kernels $T_i^{\mathrm{I/II}}$ can be calculated in perturbation theory since they contain physics at the scale m_b and $\sqrt{\Lambda_{\mathrm{QCD}} m_b}$. The kernel T_i^{II} can be further factorized into a hard and hard-collinear function, so that this term can be associated with a generalization of (1.7) in the case of two hadronic final states. Both short-distance kernels $T_i^{\mathrm{I,II}}$ are known up to $\mathcal{O}(\alpha_s^2)$ (NNLO) in QCD [49–56]. The form factor F^{BM_1} is "located" at zero momentum transfer towards the meson M_2 and contains information about the soft interactions between the B-meson and M_1, where the latter is defined to be the meson that picks up the light "spectator" quark of the B meson.

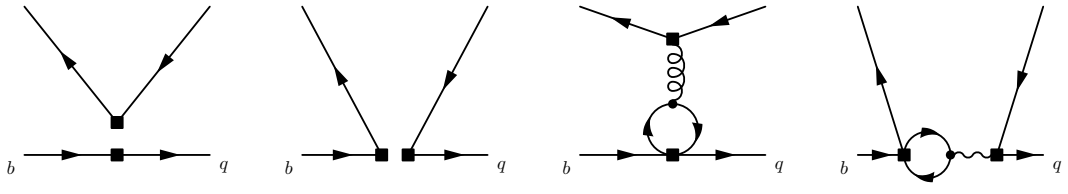

Figure 1.2: Different decay topologies for non-leptonic B decays with one weak effective $b \to q$ transition: We refer to the diagrams as (T) colour-allowed, (C) the colour-suppressed tree amplitudes, (P) colour-allowed QCD penguin and (EW) colour-suppressed electroweak penguin. The spectator quark line and annihilation topologies are not displayed.

Opposed to the radiative $\bar{B} \to \gamma \ell \nu$ decay, the decay of a B-meson into QCD final states is much more complex since we require non-perturbative information about three hadrons and their interactions. As such, we expect larger uncertainties for the prediction of these decays. Nevertheless, they are interesting to study since the theoretical structure involves many topologies, see Fig. 1.2, motivating different phenomenological analyses. For instance, one finds that the colour-suppressed electroweak penguin contribution dominantly affects the direct CP-asymmetries of different modes in $\bar{B} \to \pi K$ decays. The SM prediction turns out to be incompatible with the corresponding experimental data, leading to puzzling inconsistencies [57, 58]. In principle, NP models can be used to explain this tension to the SM. However, we observe that electroweak penguin amplitudes indirectly break the isospin symmetry, which holds between the u- and d-quark in QCD, and enter linearly in the asymmetries. QED can mimic these effects as it breaks isospin explicitly due to the different electric charges Q_u and Q_d. Hence one should properly include QED corrections in the SM predictions, before tailoring NP models to explain the tensions.

In general, the inclusion of QED effects may also become relevant beyond $\mathcal{O}(\alpha_s^2)$, which has been shown in numerous publications [59–65]. As an example, we observe in the analysis of $\bar{B}_s \to \mu^+ \mu^-$ that leading QED effects can be power-enhanced with respect to the QCD amplitude by a factor of m_B/Λ_{QCD}, where $m_B \gg \Lambda_{\text{QCD}}$ is the B-meson mass. Even though this is not the case for non-leptonic decays, it still displays the importance of these effects. Many of the recent works consider QED effects only as point-like up to the scale m_B, even though photons with energy above a few times Λ_{QCD} can resolve the inner partonic structure of the B-meson. In a proper framework, one has to deal with these structure-dependent terms by explicitly calculating them in a perturbative framework between the scale m_B and a few times Λ_{QCD}.

In this thesis, we show that the QCD factorization formula (1.10) can be extended to include QED effects using Soft-Collinear Effective Theory (SCET). The derivation follows our analysis in [66] and involves a two-step matching from the full weak effective theory onto SCET_I and SCET_II. We find that the QCD×QED factorization

formula takes the same form as in (1.10), even though it differs in complexity from its QCD analogue. The QED-generalized LCDA of the B-meson in particular acquires new phenomenological properties as it retains information about the charge and flight direction of the outgoing mesons through soft, light-like Wilson lines. The Wilson lines originate from the non-decoupling of soft photons when the external states are electrically charged. This is opposed to QCD-only, where soft gluons decouple since the external mesons are colour neutral. As a consequence, the hadronic matrix element of the B meson in QCD×QED contains soft rescattering phases, so that the function should rather be viewed as a "soft function" for the process. Therefore, we strictly omit the term "LCDA" in this context. Generally, matrix elements $\langle M_1 M_2|Q_i|\bar{B}\rangle$ become infrared (IR) divergent in the presence of virtual QED effects. A peculiar point lies in the inclusion of low-energetic ("ultrasoft") photons accounting for the IR behaviour of the hadronic matrix elements in the factorization formula. The IR-finite observable measured in the experiment is the branching fraction $\bar{B} \to M_1 M_2(\gamma)$, with an arbitrary number of ultrasoft photons in the final state. On a technical level, this requires that the non-radiative amplitude must be dressed with ultrasoft exponentiation factors, resumming logarithms below the scale of a few times $\Lambda_{\rm QCD}$ and above a threshold $\Delta E \ll \Lambda_{\rm QCD}$ for the photon energy, which is for theory and experiment convenient to be $\Delta E \approx 60$ MeV. In our computations, we calculate the first order QED corrections to the short-distance kernels for the current-current operators in the weak effective Hamiltonian and the scale evolution of the QED-generalized LCDAs. The latter analysis is based on the results of [67, 68]. In the numerical evaluation of QED effects, we restrict ourselves to the case of π and K mesons.

1.2.1 Comment on hadronic input

The decay constants, form factors and distribution amplitudes introduced in Sec. 1.1 and 1.2 can be determined from experimental measurements or lattice QCD calculations. For a review of lattice data, we refer to the most recent summary [69] and the references therein. Regarding the experimental side, the decay constants f_M of light and heavy pseudoscalar mesons $M = B, \pi, K$ are determined from their leptonic decays $M \to \ell\nu$ [15]. The $\bar{B} \to M_1$ form factors and the B-meson LCDA can be calculated by light-cone sum rules (LCSR), see [70–76] for a review of the method and their results. The determination of the light-meson LCDAs of pions and kaons uses similar methods [77–79]. We note that the information about the pion distribution function is much more precise due to the excellent data for the $\pi \to \gamma\gamma^*$ form factor from the BaBar and Belle experiment [80,81]. The distribution amplitudes are in general model-dependent. We discuss specific models for the case of light and heavy mesons in the main text alongside with numerical results.

1.3 Outline

The outline of this thesis is as follows. In Chapter 2, we review the formalism of the effective theories HQET and SCET to prove factorization in exclusive decays. We recapitulate that the effective theory approach traces back to a method of regions analysis in QCD. We use a scalar correlation function similar to $\bar{B} \to \gamma\ell\nu$ as a prime example for our computations. The basic results of this chapter build the bridge towards the calculation of subleading effects in Chapter 3. The $1/m_b$- and $1/E_\gamma$-suppressed terms can be calculated with a sum rule from a light-cone expansion of the hadronic correlation functions that is derived in 3.2. The results displayed in Sec. 3.3 are only valid in the tree-level approximation of the higher-twist LCDAs since we encounter endpoint-divergent integrals otherwise. In Chapter 4, we derive the QCD×QED factorization formula for $\bar{B} \to M_1 M_2$ decays. We consecutively match the full theory onto $\mathrm{SECT_I}$ in Sec. 4.2 and $\mathrm{SCET_{II}}$ in Sec. 4.3. The inclusion of ultrasoft effects is considered in Sec. 4.5. The resummation of logarithms due to QED effects is subject of Chapter 5. We analytically solve the renormalization group equations for the light-meson LCDAs and the soft functions to all orders in the strong and to first order in the electromagnetic coupling. The scale evolution for the light LCDAs, the soft and ultrasoft function are treated separately in Sec. 5.1–5.3. In the numerical analysis of Chapter 6, we compare the dispersive treatment of (pseudo-)scalar and (axial-)vector cases for the subleading corrections and discuss the model dependence of the results to some extent. We further provide numerical estimates of QED effects in $B \to \pi\pi$ and $B \to \pi K$ observables that enter through different terms in the factorization formula. We conclude in Chapter 7. The appendices A-F provide supplementary material for the renormalization and scale evolution of the collinear and soft functions.

Chapter 2

Basic concepts of QCD factorization

In this chapter, we review some of the basic methods to prove QCD factorization in hard-exclusive processes. To this end, we apply the framework to the specific case of the scalar correlation function

$$T(p,q) = \int d^4x e^{ipx} \langle 0 | T\{ j^{\text{em}}(x), j^{\text{weak}}(0)) \} | \bar{B}(p+q) \rangle = -vpF_S(vp, p^2) \,. \tag{2.1}$$

We define the scalar form factor F_S by this equation for later convenience. The outgoing momentum p is chosen to be off-shell with $p^2 < 0$ and the scalar currents are, similar to (1.4), given by

$$j^{\text{em}}(x) = \sum_{q \neq t} e_q \bar{q}(x) q(x) \,, \quad j^{\text{weak}}(0) = \bar{u}(0)(1-\gamma_5) b(0) \,. \tag{2.2}$$

The kinematics of this decay dictate that the correlation function can only depend on two kinematic invariants, that we choose to be the off-shellness p^2 and the "photon" energy $E_\gamma = vp$, which is of order of the hard scale m_b. Note that E_γ is related to the variable q^2 by momentum conservation $(p - m_B v)^2 = q^2$.

The example is chosen in strong analogy to the introductory $\bar{B} \to \gamma \ell \nu$ decay in Sec. 1.1 since there are several motivations to consider scalar currents. In general, the inclusion of scalar currents as well as tensor operators in the weak effective Hamiltonian is a typical way to account model-independently for NP effects at low energies, see e.g. [82] for an application in Λ_b decays. The main motivation to study the correlator in (2.1) was already mentioned in the introduction, namely that we can relate the Euclidean correlator to the light-like operator (1.8) using factorization. By applying the same methods to (2.1) and including power corrections, we can extract further information about hadronic matrix elements of the B meson. In the following, we stick to the analysis of scalar currents as it provides a simple playground for the application of basic QCD factorization techniques. A generalized factorization of the (axial-)vector case in (1.3) will be discussed in Chapter 3.

2.1 Heavy-quark expansion

The scalar form factor (2.1) can be factorized into more fundamental objects using the heavy quark expansion. The soft scale in this process is set by the scale $\Lambda_{\rm QCD}$. Since the momentum component $E_\gamma \sim m_b$ is large, there are two expansion parameters $\Lambda_{\rm QCD}/m_b \ll 1$ and $\Lambda_{\rm QCD}/E_\gamma \ll 1$. For the remainder of this section, we expand our results in the counting parameter $\lambda = \Lambda_{\rm QCD}/m_b$. Since the photon energy cannot be larger than m_b, the $1/E_\gamma$-corrections are strictly smaller than λ and thus we have $\Lambda_{\rm QCD}/E_\gamma < \lambda$ and treat the latter as an $\mathcal{O}(\lambda)$ correction for simplicity.

We highlight that the evaluation of the hadronic correlation function depends on the chosen reference frame in the intermediate steps of the calculation. The simplest and most convenient choice is to consider the B-meson rest frame, where the meson momentum is given by $p_B^\mu = m_B v^\mu$ with $v^\mu = (1,0,0,0)$. In good approximation, we can assume the b-quark to carry almost all of the momentum of the entire meson while the light quark momentum only fluctuates on scales of $\mathcal{O}(\Lambda_{\rm QCD})$. To define a suitable reference frame accounting for the large momentum transfer of the photon, we choose two light-like reference vectors

$$n_+^\mu = (1,0,0,1)\,, \qquad n_-^\mu = (1,0,0,-1)\,, \tag{2.3}$$

with $n_+ \cdot n_- = 2$. Any given momentum of the process can be decomposed in terms of these reference vectors

$$p^\mu = (n_- p)\frac{n_+^\mu}{2} + (n_+ p)\frac{n_-^\mu}{2} + p_\perp^\mu\,, \tag{2.4}$$

where the latter component is transverse with respect to the two vectors $n_\pm \cdot p_\perp = 0$. Note that we can rotate the frame such that the transverse component of the photon momentum $p_\perp = 0$ vanishes. The large momentum transfer is chosen to be in the n_--direction, so that $n_+ p \sim m_b$. We further assume the photon to be off-shell by order $p^2 \sim \lambda m_b^2$, which allows for a perturbative treatment in the following. This implies that the plus-component scales as $n_- p \sim \lambda m_b$.

To establish a factorization formula for (2.1), we apply the power counting of the momenta to the amplitude and expand to leading power (LP) in λ. The LP expression can be matched onto a simplified hadronic matrix element. Since perturbation theory is only valid above a few times $\Lambda_{\rm QCD}$ and the physics at this scale should be independent of the low-energetic, soft structure, we replace the hadronic state $\big|\bar{B}(p+q)\big\rangle$ with its leading partonic Fock state $\big|b(p_b)\bar{u}(l)\big\rangle$.[1] Throughout our calculations, we take the heavy quark momentum to be on-shell $p_b^\mu = m_b v^\mu$. The light quark momentum scales soft as $l^\mu \sim \lambda m_b$ and is taken to be off-shell in order to regulate IR divergences. Note that we cannot rotate the transverse component $l_\perp$ to zero since we already chose

[1] In general, we need to consider states involving more than two partons, e.g. $\big|b\bar{u}g\big\rangle$ or $\big|b\bar{u}q\bar{q}\big\rangle$, since the B meson is a bound state consisting of a sea of soft particles fluctuating at $\mathcal{O}(\Lambda_{\rm QCD})$. These contributions turn out to be power-suppressed due to additional internal propagators.

$p_\perp = 0$. At LO, the correlator in (2.1) is then given by

$$\begin{aligned} T^{(\mathrm{LO})} &= \bar{v}(l) e Q_u \frac{i(\not{p} - \not{l})}{(p-l)^2 + i0}(1-\gamma_5)u(p_b) + \bar{v}(l)(1-\gamma_5)\frac{i(\not{p}_b - \not{p} + m_b)}{(p_b-p)^2 - m_b^2 + i0} e Q_d u(p_b) \\ &= \frac{ieQ_u}{2(n_-p - n_-l + i0)}\bar{v}(l)\not{n}_-(1-\gamma_5)u(p_b)\Big(1 + \mathcal{O}(\lambda^{1/2})\Big) \\ &\equiv T^{(0)}\Big(1 + \mathcal{O}(\lambda^{1/2})\Big)\,, \end{aligned} \tag{2.5}$$

where, in the first line, the first term corresponds to the photon emission from the light quark and the second term to the emission from the heavy quark shown in Fig. 1.1a and b. Without knowing the λ-scaling of the spinors in (2.5), it is easy to see that the second term is relatively power-suppressed to the emission from the u-quark.

The central idea of factorization is now that the non-perturbative, soft physics can be stored in a universal, gauge invariant function. In Sec. 1.1 we already introduced the B-meson LCDA in (1.8) that fulfills this purpose. Note that we replace $z = tn_-$ in this section. The finite distance Wilson line is defined by

$$[tn_-, 0] \equiv \mathbf{P}\exp\left\{ig_s\int_0^t ds\; n_- G_s(sn_-)\right\} \tag{2.6}$$

and equals unity at tree-level. The operator $\mathbf{P}$ denotes the path-ordering of the exponential. To higher orders, its analytic structure enforces the position space LCDA Φ_B to have only poles in the upper half-plane of t. This implies that the momentum variable after Fourier transformation only has support for $\omega > 0$. More precisely, we have

$$\phi_B(\omega;\mu) = \int_{-\infty}^{\infty}\frac{dt}{2\pi}\, e^{i\omega t}\,\widetilde{\phi}_B(t - i0;\mu)\,, \tag{2.7}$$

$$\widetilde{\phi}_B(t;\mu) = \int_0^{\infty} d\omega\, e^{-i\omega t}\,\phi_B(\omega;\mu)\,. \tag{2.8}$$

We can calculate the LO contribution from the soft function by analyzing the tree-level matrix element with external partons. We find in the hadron and parton picture respectively

$$\int\frac{dt}{2\pi}e^{i\omega t}\big\langle 0\big|\bar{u}(tn_-)\not{n}_-\gamma_5 b(0)\big|\bar{B}(m_B v)\big\rangle = if_B m_B\phi_B(\omega;\mu)\,, \tag{2.9}$$

$$\int\frac{dt}{2\pi}e^{i\omega t}\big\langle 0\big|\bar{u}(tn_-)\not{n}_-\gamma_5 b(0)\big|b(p_b)\bar{u}(l)\big\rangle = \delta(\omega - n_-l)\bar{v}(l)\not{n}_-\gamma_5 u(p_b)\,. \tag{2.10}$$

The matrix element of $\big\langle 0\big|\bar{u}(tn_-)\not{n}_- b(0)\big|\bar{B}\big\rangle$ vanishes since the B-meson is a pseudoscalar state. Hence the operator has no overlap with the corresponding parity quantum number and partonic contributions of the form $\bar{v}(l)\not{n}_- u(p_b)$ can be neglected. By

comparing the two expressions in (2.9) and (2.10), we conclude that we need to replace

$$\bar{v}(l)\not{n}_-(1-\gamma_5)u(p_b) \to -if_B m_B \int_0^\infty d\omega\ \phi_B(\omega;\mu)\bigg|_{n_-l=\omega} \tag{2.11}$$

in the amplitude (2.5), where we set the spectator quark component $n_-l \to \omega$ before performing the ω integration. This is a greatly simplified version of the momentum space projector method [83] which generally involves a second function ϕ_- to parametrize the hadronic matrix element of (1.8) entirely.[2] We find for the LO amplitude

$$T^{(\mathrm{LO})} = eQ_u f_B m_B \int_0^\infty d\omega\ \frac{\phi_B(\omega;\mu)}{n_-p-\omega+i0}\bigg(1+\mathcal{O}(\lambda^{1/2})\bigg)\,. \tag{2.12}$$

For the form factor, we obtain

$$F_S^{(\mathrm{LO})}(E_\gamma,p^2) = eQ_u f_B m_B \int_0^\infty d\omega \frac{\phi_B(\omega;\mu)}{2E_\gamma\omega-p^2-i0}\,, \tag{2.13}$$

where the power corrections have been neglected. We emphasize that (2.13) respresents the LO factorization formula for the correlator defined in (2.1). We derived this result only by using power counting arguments for the momenta. The result can be extended to include radiative corrections, which is however more complicated due to the appearance of loop integrals. Generally, we expect at LP in the heavy quark expansion that the formula takes the form

$$F_S(E_\gamma,p^2) = eQ_u f_B m_B\ C_S(E_\gamma;\mu) \int_0^\infty d\omega\ \frac{\phi_B(\omega;\mu)}{2E_\gamma\omega-p^2-i0}\ J_S(2E_\gamma\omega,p^2;\mu) \tag{2.14}$$

to all orders in perturbation theory. We prove this result in Sec. 2.4 by matching QCD onto a combined HQET×SCET effective theory and determine the coefficient functions C_S and J_S at NLO.

2.2 Method of regions

Before introducing the HQET×SCET framework in the next section, we calculate the $\mathcal{O}(\alpha_s)$ corrections to the hadronic correlator (2.5) that can be used to determine the NLO coefficient functions. The corresponding one-loop diagrams are depicted in Fig. 2.1. We analyze the loop integrals using the method of regions [84, 85], which corresponds to an asymptotic expansion of the integrand based on a certain momentum scaling. In this approach, every loop momentum can be thought of as a sum of different modes induced by the power counting of the external momenta. We then compute the loop integrals for the distinct modes and add the results together, which is oftentimes simpler than calculating the entire integral at once. The method reveals the underlying

[2] The common definition follows from (3.9) in the limit $x^2 \to 0$.

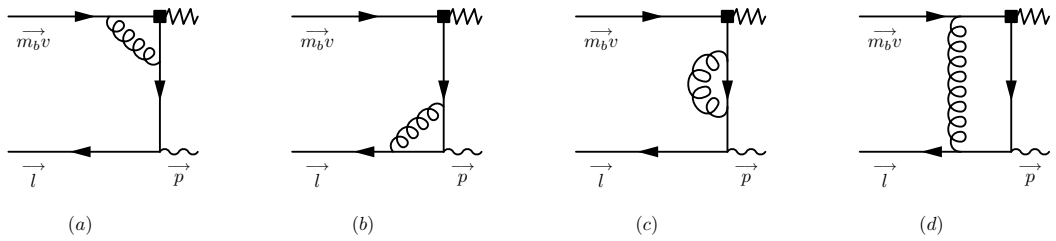

Figure 2.1: One-loop diagrams contributing to the correlator (2.1). The black box indicates the insertion of the weak $b \to u$ transition. We refer to (a) as the weak vertex correction, (b) the electromagnetic vertex correction, (c) the self-energy graph and (d) the box diagram.

structure of the factorization proof in terms of effective theories, which motivates a further discussion of the momentum modes and their field variables afterwards.

At LP in our scenario, there exist three relevant momentum regions which are classified by the λ-scaling of the loop momentum components $k \sim (k_+, k_-, k_\perp)$ according to the decomposition in (2.4). Note that we define $k_- \equiv n_+ k$ and $k_+ \equiv n_- k$. The regions are defined by the scalings

1. hard (h) $k \sim (1, 1, 1) m_b$,
2. hard-collinear (hc) $k \sim (\lambda, 1, \sqrt{\lambda}) m_b$,
3. soft (s) $k \sim (\lambda, \lambda, \lambda) m_b$.

In the following, we drop the factor of m_b in our notation, which can be always restored by dimensional analysis. Using these terms, we highlight that the b-quark momentum $m_b v$ scales hard, the photon momentum p hard-collinear and the spectator quark momentum l soft. In general, this list needs to be extended to other cases that can have different scalings, as we discuss in Sec. 2.3. We split up the correlation function in (2.1) as

$$T = T^{(\mathrm{LO})} + T^{(\mathrm{NLO})} + \ldots = T^{(0)} + \frac{\alpha_s C_F}{4\pi} T^{(1)} + \mathcal{O}(\alpha_s^2) \,, \tag{2.15}$$

where we drop the power corrections of $\mathcal{O}(\lambda)$ relative to the leading terms in $T^{(0)}$ and $T^{(1)}$. We emphasize that the full NLO result may contain IR divergences due to the non-perturbative nature of the matrix element at low-energies. The divergences appear in the soft region and are regulated by choosing the light quark momentum to be off-shell $l^2 \neq 0$. Throughout this thesis, we consider γ_5 in the naive dimensional regularization (NDR) scheme.

2.2.1 Hard region

In the hard region, the loop momentum scales as $k \sim (1,1,1)$. At LP, mainly the hard region of Fig. 2.1(a) contributes since other contributions from Fig. 2.1(b)-(d) are scaleless or even power-suppressed. The complete, non-expanded integral of diagram 2.1(a) reads

$$T^{(1a)} = 16\pi^2 e Q_u \tag{2.16}$$
$$\times\, \tilde{\mu}^{2\epsilon} \int \frac{d^dk}{(2\pi)^d} \frac{\bar{v}(l)(\not{p}-\not{l})\gamma_\mu(\not{p}+\not{k}-\not{l})(1-\gamma_5)(m_b\not{v}+\not{k}+m_b)\gamma^\mu u(p_b)}{[(p-l)^2+i0][(p+k-l)^2+i0][(m_bv+k)^2-m_b^2+i0][k^2+i0]} \,.$$

We expand every term in the integrand to LP in λ. For the hard-collinear u-quark propagator, this implies

$$\frac{\not{p}+\not{k}-\not{l}}{(p+k-l)^2+i0} = \frac{(n_+p)\frac{\not{n}_-}{2}+\not{k}}{k^2+(n_+p)(n_-k)+i0} + \mathcal{O}(\lambda^{1/2}) \,, \tag{2.17}$$

when the loop momentum k counts hard. In total, the hard region at LP is given by

$$T_{\rm h}^{(1a)} = \frac{8\pi^2 e Q_u}{[n_-p - n_-l + i0]}$$
$$\times\, \tilde{\mu}^{2\epsilon} \int \frac{d^dk}{(2\pi)^d} \frac{\bar{v}(l)\not{n}_-\gamma_\mu(\not{p}+\not{k})(1-\gamma_5)(m_b\not{v}+m_b+\not{k})\gamma^\mu u(p_b)}{[k^2+i0][k^2+2m_bv\cdot k+i0][k^2+(n_+p)(n_-k)+i0]} \,. \tag{2.18}$$

This integral can be calculated with conventional methods by introducing Feynman parameters. We obtain the leading power result

$$T_{\rm h}^{(1a)} = T^{(0)}\bigg(\frac{4}{\epsilon_{\rm UV}} - \frac{1}{\epsilon^2} - \frac{2}{\epsilon}\bigg[1+\ln\frac{\mu}{n_+p}\bigg] + 2 - \frac{\pi^2}{12} + 8\ln\frac{\nu}{m_b} - 4\ln\frac{\mu}{m_b}$$
$$+ \frac{2}{1-r}\ln r + \ln^2 r - 2\ln^2\frac{\mu}{n_+p} + 2{\rm Li}_2\bigg(1-\frac{1}{r}\bigg)\bigg) + \mathcal{O}(\lambda) \,, \tag{2.19}$$

where we defined the ratio $r = n_+p/m_b$. In the hard region, we distinguish between the scale ν that originates from the UV divergence and the IR scale μ. Both types can easily be separated within the calculation. The IR divergences will be cancelled by the corresponding UV divergences in the hard-collinear and soft region while the UV divergence has to be renormalized in the full theory. An important observation for this mechanism to work is that the Dirac structure in the numerator can be reduced to the LO object $T^{(0)}$ in (2.5), which we have shown to be equivalent to the soft matrix element (2.11) at tree-level.

For completeness, we remark that the hard region of the box diagram is power suppressed while the hard region of the electromagnetic vertex and the self-energy graph are scaleless. More precisely, we have

$$T_{\rm h}^{(1b)} = T^{(0)}\bigg(\frac{4}{\epsilon_{\rm UV}} - \frac{4}{\epsilon} + 4\ln\frac{\nu^2}{\mu^2}\bigg) \,, \tag{2.20}$$

$$T_{\rm h}^{(1c)} = T^{(0)}\bigg(-\frac{1}{\epsilon_{\rm UV}} + \frac{1}{\epsilon} - \ln\frac{\nu^2}{\mu^2}\bigg)\,, \tag{2.21}$$

which is required for later purposes. Note that for axial-vector currents in (1.3), these contributions cancel exactly since the poles of both hard regions agree up to a relative sign.

2.2.2 Hard-collinear region

The hard-collinear region with $k \sim (\lambda, 1, \sqrt{\lambda})$ contributes in all cases except the box diagram from Fig. 2.1(d), which is again power-suppressed. For the weak vertex correction, the hard-collinear region is given by

$$\begin{aligned} T_{\rm hc}^{(1a)} &= 32\pi^2(-i)\,T^{(0)} \\ &\quad\times\tilde{\mu}^{2\epsilon}\int\frac{d^dk}{(2\pi)^d}\frac{(n_+p+n_+k)}{[k^2+i0][(n_-p+n_-k-n_-l)(n_+p+n_+k)-k_\perp^2+i0][n_+k+i0]} \\ &= T^{(0)}\bigg(\frac{2}{\epsilon^2}+\frac{2}{\epsilon}\bigg[1+\ln\frac{\mu^2}{(n_+p)(n_-l-n_-p)}\bigg]+4-\frac{\pi^2}{6} \\ &\quad+2\ln\frac{\mu^2}{(n_+p)(n_-l-n_-p)}+\ln^2\frac{\mu^2}{(n_+p)(n_-l-n_-p)}\bigg)\,. \end{aligned} \tag{2.22}$$

For the electromagnetic vertex correction, we obtain

$$\begin{aligned} T_{\rm hc}^{(1b)} &= 16\pi^2\,T^{(0)} \\ &\quad\times\tilde{\mu}^{2\epsilon}\int\frac{d^dk}{(2\pi)^d}\frac{d(k-l)^2+2(n_+p)(n_-l-n_-k)+(d-2)(n_-p)(n_+l-n_+k)}{[k^2+i0][(k-l)^2+i0)][(n_+p+n_+k)(n_-p+n_-k-n_-l)+i0]} \\ &= T^{(0)}\bigg(\frac{2}{\epsilon}-\frac{2}{\epsilon}\frac{n_-p}{n_-l}\ln\frac{n_-p-n_-l}{n_-p}+2+4\ln\frac{\mu^2}{(n_+p)(n_-l-n_-p)} \\ &\quad-2\ln\frac{\mu^2}{(n_+p)(n_-l-n_-p)}+\frac{n_-p}{n_-l}\ln\frac{n_-p-n_-l}{n_-p}\bigg[-2\ln\frac{\mu^2}{-p^2}+\ln\frac{n_-p-n_-l}{n_-p}\bigg]\bigg)\,. \end{aligned} \tag{2.23}$$

For the self-energy graph of the hard-collinear propagator, we have

$$\begin{aligned} T_{\rm hc}^{(1c)} &= 32\pi^2(-i)\,T^{(0)} \\ &\quad\times\tilde{\mu}^{2\epsilon}\int\frac{d^dk}{(2\pi)^d}\frac{(2-d)((1-\frac{n_+k}{n_+p})(p-l)^2+(n_+k)(n_-p-n_-l)+(n_-k)(n_+p))}{[(p-l)^2+i0][k^2+i0][(p+k-l)^2+i0]} \\ &= T^{(0)}\bigg(-\frac{1}{\epsilon}-\ln\frac{\mu^2}{(n_+p)(n_-l-n_-p)}-1\bigg)\,. \end{aligned} \tag{2.24}$$

2.2.3 Soft region

For soft momentum $k \sim (\lambda, \lambda, \lambda)$, the self-energy graph in Fig. 2.1(c) is scaleless since the u-quark line is hard-collinear. In all other cases, the soft region leads at least to finite results of the integration. For the weak vertex, we have

$$\begin{aligned} T_{\rm s}^{(1a)} &= 32\pi^2(-i)T^{(0)}\,\tilde{\mu}^{2\epsilon}\int\frac{d^dk}{(2\pi)^d}\frac{1}{[k^2+i0][2v\cdot k+i0][n_-p+n_-k-n_-l+i0]} \\ &= T^{(0)}\bigg(-\frac{1}{\epsilon^2}-\frac{2}{\epsilon}\ln\frac{\mu}{n_-p-n_-l}-\frac{3}{4}\pi^2-\frac{1}{2}\ln^2\frac{\mu^2}{(n_-p-n_-l)^2}\bigg)\,. \end{aligned} \tag{2.25}$$

For the electromagnetic vertex we find

$$\begin{aligned} T_{\rm s}^{(1b)} &= 32\pi^2(-i)T^{(0)}\,\tilde{\mu}^{2\epsilon}\int\frac{d^dk}{(2\pi)^d}\frac{(n_-k-n_-l)}{[k^2+i0][(k-l)^2+i0][n_-p+n_-k-n_-l+i0]} \\ &= T^{(0)}\bigg(\frac{2}{\epsilon}+\frac{2}{\epsilon}\frac{n_-p}{n_-l}\ln\frac{n_-p-n_-l}{n_-p}+2\ln\frac{\mu^2}{-l^2}+2\frac{n_-p}{n_-l}\ln\frac{\mu^2}{-l^2}\ln\frac{n_-p-n_-l}{n_-p} \\ &\quad +4+\frac{n_-p}{n_-l}\ln^2\frac{n_-p-n_-l}{n_-p}+4\frac{n_-p}{n_-l}\mathrm{Li}_2\bigg(1-\frac{n_-p}{n_-p-n_-l}\bigg)\bigg)\,. \end{aligned} \tag{2.26}$$

The box graph contributes with the finite integral

$$\begin{aligned} T_{\rm s}^{(1d)} &= 16\pi^2 eQ_u \\ &\quad\times\int\frac{d^4k}{(2\pi)^4}\frac{(n_+p)\,\bar{v}(l)\not{v}(\not{k}-\not{l})\not{n}_-(1-\gamma_5)u(p_b)}{[k^2+i0][2v\cdot k+i0][(k-l)^2+i0][(n_+p)(n_-k-n_-l)+p^2+i0]}\,. \end{aligned} \tag{2.27}$$

The explicit result of this integration involves generically complicated hypergeometric functions [86,87]. For this reason, we refrain from a detailed analysis and point towards (A.12) and (A.15), where we show that this integral cancels exactly after matching onto the effective theory.

We note that the IR divergences in the soft region are entirely regulated by the off-shell spectator momentum $l^2 \neq 0$, so that the results (2.25)-(2.27) are IR-finite. All divergences therefore arise from the UV region of the integration. For instance, the UV double pole in (2.25) is a combination of the limits $n_+k, k_\perp \to \infty$ in the integration. The single pole in (2.26) originates from $n_+k \to \infty$. In the hard-collinear region, divergences can arise from both the UV and the IR. The results in particular contain divergencs from $n_+k, k_\perp \to 0$ that cancel the UV divergences of the soft region. The sum of divergences in the soft and hard-collinear region together exactly correspond to the IR divergences of the hard region. In this way, we reproduce the full theory result from the sum of all regions

$$T^{(1)} = T_{\rm h}^{(1)} + T_{\rm hc}^{(1)} + T_{\rm s}^{(1)}\,. \tag{2.28}$$

This decomposition is exact to all orders in λ. In (2.28), we refer to the leading power integrals given by (2.18)-(2.27). A more detailed, pictorial analysis of the divergent structure and interplay between different regions can be found in Fig. 2 of [88] for the case of heavy-to-light form factors. The pole cancellation between the different regions allows for a systematic renormalization of each sector, which is properly done in the framework of effective theories.

2.3 Heavy Quark and Soft-Collinear Effective Theory

The loop momentum virtuality $k^2 \sim \lambda^2 \ll \lambda \ll 1$ introduces a hierarchy of scales, which corresponds to $\Lambda_{\rm QCD} \ll \sqrt{\Lambda_{\rm QCD} m_b} \ll m_b$. At the scales m_b and $\sqrt{\Lambda_{\rm QCD} m_b}$, the strong interaction still lies in the perturbative regime, so that the hard and hard-collinear contributions in (2.18)-(2.24) yield an accurate result for the correlator in this region. Together with the explicit results from the last section, this motivates to integrate out the high-oscillating modes of the quark and gluon fields so that only the soft region is reproduced by an effective theory. The perturbative results then enter with the corresponding matching coefficients. Technically, this is done by splitting the fields into different variables that contain the hard(-collinear) and soft modes in an EFT framework. In the following, we distinguish between two effective theories. While Heavy Quark Effective Theory (HQET) deals with the modes of the massive, heavy b-quark, Soft-Collinear Effective Theory (SCET) focuses on soft and energetic light degrees of freedom that are assumed to be massless. The large scale in SCET refers to the momentum transfer in a distinct direction which is typically $\mathcal{O}(m_b)$. We integrate out the hard modes for both light and heavy quark fields at the scale m_b and the hard-collinear modes at the scale $\sqrt{\Lambda_{\rm QCD} m_b}$. Even though these EFTs have different characteristics, we treat them on equal ground in the matching calculation, so that we generally need to consider interactions between the light and heavy quark fields via hard(-collinear) and soft gluons.

To review the fundamental properties of HQET and SCET, we consider the QCD Lagrangian containing the heavy quark field Q and a light quark field q

$$\mathcal{L}_{\rm QCD} = \bar{Q}(i\not{D} - m_Q)Q + \bar{q} i\not{D} q \,, \tag{2.29}$$

where the Yang-Mills Lagrangian accompanied with gauge-fixing and ghost terms is implicitly understood. The heavy quark inside a meson carries almost all of the momentum and can therefore be parametrized by $p_Q = m_Q v + k_{\rm res}$, where the residual momentum is $\mathcal{O}(\Lambda_{\rm QCD})$. We define two components of the heavy quark field

$$h_v(x) = e^{i m_Q v\cdot x}\left(\frac{1+\not{v}}{2}\right)Q(x) \,, \qquad H_v(x) = e^{i m_Q v\cdot x}\left(\frac{1-\not{v}}{2}\right)Q(x) \,, \tag{2.30}$$

which in sum yield $Q(x) = \exp(-i m_Q v\cdot x)(h_v + H_v)(x)$. The scaling of the two fields in (2.30) can be inferred from the analysis of the propagators

$$\big\langle 0\big|T\big\{h_v(x), \bar{h}_v(0)\big\}\big|0\big\rangle = \left(\frac{1+\not{v}}{2}\right)\int \frac{d^4p}{(2\pi)^4}\frac{i(\not{p}+m_Q)}{p^2-m_Q^2+i0}e^{-i(p-m_Q v)x}\left(\frac{1+\not{v}}{2}\right)$$

$$= \left(\frac{1+\not{v}}{2}\right) \int \frac{d^4k}{(2\pi)^4} \frac{i(\not{k} + m_Q \not{v} + m_Q)}{k^2 + 2m_Q v\cdot k + i0} e^{-ikx} \left(\frac{1+\not{v}}{2}\right)$$

$$= \int \frac{d^4k}{(2\pi)^4} \frac{i(1+\not{v})}{2v\cdot k + i0} e^{-ikx} + \mathcal{O}(\lambda^{7/2}) \,, \tag{2.31}$$

$$\big\langle 0\big|T\big\{H_v(x), \bar{H}_v(0)\big\}\big|0\big\rangle = -i\delta^{(4)}(x)\left(\frac{1-\not{v}}{4}\right) + \mathcal{O}(\lambda^{9/2}) \,. \tag{2.32}$$

In the second line, we substituted the momentum $p \to m_Q v + k$, where the remaining loop momentum $k^\mu \sim \lambda$ scales soft. From the second to third line, we expanded in the expression to leading power in λ, so that we find

$$\big\langle 0\big|T\big\{h_v(x), \bar{h}_v(0)\big\}\big|0\big\rangle \sim \lambda^3 \,. \tag{2.33}$$

We conclude that the small field component scales as $h_v \sim \lambda^{3/2}$. Equivalently, we find $H_v \sim \lambda^2$ from (2.32) since $\delta^{(4)}(x) \sim \lambda^4$ for soft fluctuations, which implies that the field variable H_v is power-suppressed. This fact can also be observed on the level of the Lagrangian: Plugging in (2.30) into the Lagrangian (2.29), we find that the field h_v propagates as a massless degree of freedom while H_v propagates with a mass of $2m_Q$. We can integrate out the heavy mode at tree level by deriving the formal solution to the equation of motion

$$H_v(x) = \frac{1}{2m_Q + iv\cdot D} i\vec{\not{D}}_\perp h_v(x) \,, \tag{2.34}$$

where $\vec{\not{D}}_\perp = \not{D} - \not{v} v\cdot D$. After replacing (2.34) in the Lagrangian, we obtain

$$\mathcal{L}_{\rm HQET} = \bar{h}_v iv\cdot D h_v + \bar{h}_v i\vec{\not{D}}_\perp \frac{1}{2m_Q + iv\cdot D} i\vec{\not{D}}_\perp h_v = \mathcal{L}^{(0)}_{\rm HQET} + \mathcal{O}\left(\frac{1}{m_Q}\right) . \tag{2.35}$$

The replacement in (2.34) strictly corresponds to field redefinition that leads to the appearance of a Jacobian in the path integral. However, it can be shown by gauge invariance that the Jacobian is just an irrelevant constant. The HQET Lagrangian $\mathcal{L}^{(0)}_{\rm HQET} = \bar{h}_v iv\cdot D h_v$ contains the leading interactions between the heavy quark and hard-collinear and soft gluon fields. Note that the covariant derivative $iv\cdot D$ only contains the soft gluon field since the hard-collinear part vanishes due to momentum conservation. Furthermore, we assume a mass term $\delta m \bar{h}_v h_v$ to be absent.[3]. In perturbative calculations, the Feynman rules of HQET are given by

$$\frac{i(1+\not{v})}{2v\cdot k + i0} \,, \qquad ig_s v^\mu T^a \,, \tag{2.36}$$

for the heavy quark propagator in (2.31) and the quark-gluon interaction, respectively. For a complete review of the EFT formalism, we refer to original publications and lectures of HQET [90–93].

[3]In a proper framework, the residual mass term $\delta m \sim \Lambda_{\rm QCD}$ must be included in order to cancel UV renormalons from HQET operator matrix elements, see [89] for a detailed discussion.

Momentum modes and scaling			
hard (h)	$p \sim (1,1,1)$		
hard-collinear (hc)	$p \sim (\lambda,1,\sqrt{\lambda})$	hard-anti-collinear (h$\bar{\text{c}}$)	$p \sim (1,\lambda,\sqrt{\lambda})$
collinear (c)	$p \sim (\lambda^2,1,\lambda)$	anti-collinear ($\bar{\text{c}}$)	$p \sim (1,\lambda^2,\lambda)$
soft (s)	$p \sim (\lambda,\lambda,\lambda)$		

Table 2.1: Momentum scaling $p \sim (p_+, p_-, p_\perp)$ according to the light-cone decomposition in (2.4). We define $\lambda = \Lambda_{\rm QCD}/m_b$ and neglect an overall factor of m_b in our notation. The anti-collinear modes are not relevant to the present context of this Chapter, but will appear in $\bar{B} \to M_1 M_2$ decays involving an additional direction of large momentum transfer. We use the label $\text{C} = \text{hc}, \text{c}$ as a generalized index that contains both (hard-)collinear modes.

SCET was developed by a series of publications addressing heavy quark decays into light, energetic particles [88, 94–99]. It is deeply connected to the method of regions approach presented in the last section. The treatment of the light quark fields in SCET is more subtle compared to heavy quark fields in HQET as we deal with additional modes. In general, the light quark field can be decomposed into different components

$$q(x) = \xi_{\rm C}(x) + \eta_{\rm C}(x) + q_{\rm s}(x) \,, \tag{2.37}$$

such that the collinear fields have collinear momentum scaling and the soft field soft scaling. Note that the label $\text{C} = (\text{hc}, \text{c})$ may include an additional collinear mode scaling as $p \sim (\lambda^2, 1, \lambda)$, which is relevant in the context of Chapter 4. A complete list of the momentum labels and their light-cone components can be found in Table 2.1. For the remainder of this section, we assume C to have hard-collinear scaling, i.e. $p \sim (\lambda, 1, \sqrt{\lambda})$. Similar to the heavy quark case, the two components ξ_C and η_C are defined by projections on the light-cone

$$\xi_{\rm C}(x) = P_+ q(x) \equiv \frac{\not{n}_- \not{n}_+}{4} q(x) \,, \qquad \eta_{\rm C}(x) = P_- q(x) \equiv \frac{\not{n}_+ \not{n}_-}{4} q(x) \,. \tag{2.38}$$

The projectors fulfill standard relations $P_\pm^2 = P_\pm$, $P_\pm P_\mp = 0$ and $P_+ + P_- = 1$. Following the same analysis as in (2.31), we find that the propagators of these fields scale as

$$\big\langle 0 \big| T\big\{\xi_{\rm C}(x), \bar{\xi}_{\rm C}(0)\big\} \big| 0 \big\rangle = \int \frac{d^4k}{(2\pi)^4} \frac{i(n_+k)\frac{\not{n}_-}{2}}{k^2 + i0} e^{-ikx} \sim \mathcal{O}(\lambda) \,, \tag{2.39}$$

$$\big\langle 0 \big| T\big\{\eta_{\rm C}(x), \bar{\eta}_{\rm C}(0)\big\} \big| 0 \big\rangle = \int \frac{d^4k}{(2\pi)^4} \frac{i(n_-k)\frac{\not{n}_+}{2}}{k^2 + i0} e^{-ikx} \sim \mathcal{O}(\lambda^2) \,, \tag{2.40}$$

$$\langle 0|T\{q_s(x),\bar{q}_s(0)\}|0\rangle = \int \frac{d^4k}{(2\pi)^4}\frac{i\not{k}}{k^2+i0}e^{-ikx} \sim \mathcal{O}(\lambda^3)\ . \tag{2.41}$$

Note that we assume the loop momentum to have hard-collinear and soft scaling, respectively. We conclude that $\xi_C \sim \lambda^{1/2}$, $\eta_C \sim \lambda$ and $q_s \sim \lambda^{3/2}$. This analysis can be extended to the gauge sector, yielding a power counting for the collinear and soft gluon fields, shown in Table 2.2. Analogously to HQET, we proceed by deriving the equations of motion at tree level to eliminate the power-suppressed collinear field

$$\eta_C(x) = \frac{1}{in_+D}i\not{D}_\perp\frac{\not{n}_+}{2}\xi_C(x) + \frac{1}{in_+D}\not{\mathcal{C}}_C\frac{\not{n}_+}{2}q_s(x)\ . \tag{2.42}$$

The leading term in this expression is proportional to ξ_C since q_s is power-suppressed. After integrating out the field operator η_C in (2.29), we obtain the leading power SCET Lagrangian

$$\mathcal{L}^{(0)}_{\text{SCET}} = \bar{\xi}_C\left(in_-D + i\not{D}_{C\perp}\frac{1}{in_+D_C}i\not{D}_{C\perp}\right)\frac{\not{n}_+}{2}\xi_C + \bar{q}_s i\not{D}q_s\ . \tag{2.43}$$

The subleading terms to this Lagrangian have been derived in [99, 100]. It can be shown that the tree-level SCET Lagrangian is exact and requires no renormalization, see e.g. [97]. The renormalization is therefore fully contained in the operator matching. Furthermore, we emphasize that the derivative in_-D in (2.43) still contains soft gauge fields, so that collinear fields interact with soft gluons at LP. This interaction can be removed by a decoupling transformation discussed in Sec. 2.4.1. When both collinear modes in C are present, we usually refer to (2.43) as the SCET_I Lagrangian. After integrating out the hard-collinear mode, we refer to the theory as SCET_II which only involves the remaining collinear and soft fields (c,s). Finally, we note that one can trivially extend the Lagrangian to include several collinear directions $n_{\pm i}$ with $n_{+i}\cdot n_{-j} = 2\delta_{ij}$ by adding copies of the Lagrangian (2.43) to the effective theory.

2.3.1 Gauge invariance

The leading power HQET×SCET Lagrangian given by (2.35) and (2.43) admits a set of fundamental symmetries. First and foremost, the effective theory respects gauge invariance inherited from QCD. In the effective theory, each field transforms separately under the gauge group, which can be viewed as a direct sum of collinear and soft gauge transformations

$$V_C(x) = e^{i\alpha^a_C(x)T^a}\ , \qquad V_s(x) = e^{i\alpha^a_s(x)T^a}\ . \tag{2.44}$$

The transformations act on fields as

$$\xi_C \to V_C\xi_C\ ,\quad q_s \to q_s\ ,\qquad G^\mu_C \to V_C G^\mu_C V_C^\dagger + \frac{i}{g_s}V_C\left[D^\mu_s, V_C^\dagger\right]\ ,\quad G^\mu_s \to G^\mu_s\ , \tag{2.45}$$

Scaling of field components		
Heavy quark	soft	$h_v \sim \lambda^{3/2}\,, \quad H_v \sim \lambda^2$
Light quark	hard-collinar	$\xi_{\rm hc} \sim \lambda^{1/2}\,, \quad \eta_{\rm hc} \sim \lambda$
	collinear	$\xi_{\rm c} \sim \lambda\,, \quad \eta_{\rm c} \sim \lambda^2$
	soft	$q_{\rm s} \sim \lambda^{3/2}$
Gauge field	hard-collinear	$n_-G_{\rm hc} \sim \lambda\,, \quad n_+G_{\rm hc} \sim 1\,, \quad G_{\rm hc\perp} \sim \lambda^{1/2}$
	collinear	$n_-G_{\rm c} \sim \lambda^2\,, \quad n_+G_{\rm c} \sim 1\,, \quad G_{\rm c\perp} \sim \lambda$
	soft	$G^\mu_{\rm s} \sim \lambda$

Table 2.2: Scaling of field variables for different momentum modes, which follows from the analysis of the respective propagators. For the quark fields, we explicitly derived the counting in (2.31),(2.32) and (2.40)–(2.41). The scaling of the gauge field components can be inferred by the same arguments [101].

$$\xi_{\rm C} \to V_{\rm s}\xi_{\rm C}\,, \quad q_{\rm s} \to V_{\rm s}q_{\rm s}\,, \quad G^\mu_{\rm C} \to V_{\rm s}G^\mu_{\rm C}V_{\rm s}^\dagger\,, \quad G^\mu_{\rm s} \to V_{\rm s}G^\mu_{\rm s}V_{\rm s}^\dagger + \frac{i}{g_s}V_{\rm s}\big[\partial^\mu, V_{\rm s}^\dagger\big]\,, \tag{2.46}$$

where $D^\mu_{\rm s} = \partial^\mu - ig_sG^\mu_{\rm s}$ only contains the soft gauge field. The collinear fields transform under both collinear and soft gauge transformations since they interact with the soft modes via the leading power Lagrangian. The soft fields on the other hand do not transform under the collinear gauge transformation. For this reason, the field decomposition and redefinition in (2.37) and (2.42) is only valid at tree-level as it does not respect gauge symmetry at NLO. To maintain gauge invariance, we have to account for a consistent transformation by replacing the soft field according to

$$q_{\rm s}(x) \to W(x)q_{\rm s}(x)\,, \tag{2.47}$$

where we construct the object W such that the full theory field q transforms homogeneously under the entire gauge group. For details of the precise construction based on the properties of Wilson lines, we refer to [102].[4] For our purposes, it is sufficient to introduce the semi-infinite collinear and soft Wilson lines

$$W_{\rm C}(x) = \mathbf{P}\exp\left\{ig_s\int_{-\infty}^0 ds\, n_+G_{\rm C}(x+sn_+)\right\}\,, \tag{2.48}$$

$$S_{n_-}(x) = \mathbf{P}\exp\left\{ig_s\int_{-\infty}^0 ds\, n_-G_{\rm s}(x+sn_-)\right\}. \tag{2.49}$$

At LP, the Wilson line in (2.47) is given by $W = W_C$. The soft Wilson line carries the label of the collinear direction. The label distinguishes the soft Wilson line originating

[4] In [102] the Wilson line W is written as a product $WZ^\dagger$ involving the full gauge field and its soft part, which ensures the correct transformation properties.

from collinear lines to the ones associated to the anti-collinear direction n_+ that will appear in Chapter 4. Note that we can construct finite distance Wilson lines from a product of two semi-infinite lines

$$[x,y] = S_{n_-}(x) S_{n_-}^\dagger(y) \,, \tag{2.50}$$

which appeared in the definition of the B-meson LCDA in (1.8) and (2.6). The advantage of using (2.48) and (2.49) is their simple transformation under the collinear and soft gauge group

$$W_{\rm C} \to V_{\rm C} W_{\rm C} \,, \quad S_{n_-} \to S_{n_-} \qquad \text{and} \qquad W_{\rm C} \to V_{\rm s} W_{\rm C} V_{\rm s}^\dagger \,, \quad S_{n_-} \to V_{\rm s} S_{n_-} \,. \tag{2.51}$$

This implies for the finite distance Wilson line to transform as $[x,y] \to V_{\rm s}(x)[x,y]V_{\rm s}^\dagger(y)$. We emphasize that the transformations for the collinear Wilson line only hold at LP and are more complicated otherwise.

We can use the collinear Wilson lines to define gauge-invariant building blocks in the effective theory and construct operators that respect gauge symmetry ad hoc. We define

$$\chi_{\rm C} = W_{\rm C}^\dagger(x)\xi_{\rm C}(x) \,, \qquad \mathcal{G}_{\rm C}^\mu(x) = W_C^\dagger(x)[iD_{\rm C}^\mu W_{\rm C}](x) \,, \tag{2.52}$$

which are clearly invariant under the collinear gauge transformations but still transform under the soft gauge group. This allows for a simple construction of invariant operators, for instance

$$J^{(\rm B1)}(s_1,s_2;0) \sim \bar\chi_{\rm C}(s_1 n_+) \not{\mathcal{G}}_{\rm C\perp}(s_2 n_+) \Gamma h_v(0) \,, \tag{2.53}$$

that reflects three-particle interactions between a heavy quark, a collinear quark and a gluon field with an arbitrary Dirac structure Γ. We shifted the position space variable of the heavy quark field to zero, which can always be done after multipole expanding the field operator and using translational invariance, so that the operator counts homogeneously of order $\mathcal{O}(\lambda^{3/2})$. The precise origin and definition of A- and B-type operators will be clarified in the next section.

2.3.2 Reparametrization invariance

The definition of HQET×SCET strictly depends on the choice of the reference vectors v^μ and $n_\pm^\mu$. We can reparametrize these vectors by explicit transformations that leave the scaling of momenta and fields invariant [103–105]. More precisely, the effective theory stays separately invariant under the transformations

$$v^\mu \to v^\mu + \delta v^\mu \,, \qquad n_\pm^\mu \to (1\pm\alpha) n_\pm^\mu \,, \qquad n_\pm^\mu \to n_\pm^\mu \pm \epsilon_\perp^\mu \,, \tag{2.54}$$

when $\alpha \sim \mathcal{O}(1)$, $\epsilon_\perp^\mu \sim \mathcal{O}(\lambda^{1/2})$ and the normalization $(v+\delta v)^2 = 1$ is maintained. This reparametrization invariance imposes contraints on subleading operators. As a consequence, we can use the invariance to construct a suitable basis of HQET×SCET

operators that are fixed up to next-to-leading power (NLP) and simplify matching calculations in QCD.

A concrete example where this symmetry applies is the matching of the QCD heavy-to-light current onto HQET×SCET, which is frequently used to parametrize matrix elements in decays of heavy mesons into light particles. The matching equation reads[5]

$$\bar{q}\Gamma_X b(0) = \int d\hat{s}\, \hat{C}_X^{(\mathrm{A0})i}(\hat{s};\mu)\, J_X^{(\mathrm{A0})i}(s;0) + \int d\hat{s}_1 d\hat{s}_2\, \hat{C}_X^{(\mathrm{B1})i}(\hat{s}_1,\hat{s}_2;\mu) J_X^{(\mathrm{B1})i}(s_1,s_2;0) + \dots \,, \tag{2.55}$$

where $\hat{s} = (n_+p)s$ is the large component of the energetic light quark or gluon and $\Gamma_X = \{1, \gamma_5, \gamma^\mu, \gamma^\mu\gamma_5, \sigma^{\mu\nu}\}$ an arbitrary Dirac matrix. The A-type and B-type operators label whether the operator contains two-particle or three-particle contributions. A complete matching of the heavy-to-light current for all possible Dirac matrices up to NNLO can be found in [49, 105–107]. Since we restrict ourselves to scalar operators, we consider the two currents

$$J_S^{(\mathrm{A0})}(s,0) = \bar{\chi}_{\mathrm{C}}(sn_+)(1-\gamma_5)\left(1 - \frac{1}{in_+\overleftarrow{\partial}} i\overleftarrow{\partial}_\perp\right) h_v(0) \,, \tag{2.56}$$

$$J_S^{(\mathrm{B1})}(s_1,s_2,0) = \frac{1}{m_b}\bar{\chi}_{\mathrm{C}}(s_1n_+)\not{\mathcal{G}}_{C,\perp}(s_2n_+)(1+\gamma_5)h_v(0) \,, \tag{2.57}$$

which are of $\mathcal{O}(\lambda^2)$ and $\mathcal{O}(\lambda^{5/2})$ respectively. Note that the term proportional to $\overleftarrow{\partial}$ in (2.56) is fixed by reparametrization invariance, but power-suppressed as it counts as $\mathcal{O}(\lambda^{5/2})$. This is an explicit example how the form of the operators on the right hand side of (2.55) is dictated by symmetry arguments. The Wilson coefficient $C_S^{(\mathrm{A0})}$ in momentum space depends on the large component n_+p and is obtained by Fourier transformation

$$C_S^{(\mathrm{A0})}(n_+p;\mu) = \int d\hat{s} e^{isn_+p} \hat{C}_S^{(\mathrm{A0})}(\hat{s};\mu) \,. \tag{2.58}$$

We refrain from giving more details about the (B1) operator as it will drop out by power counting arguments in the following.

Contrary to the heavy-to-light case, the matching of the electromagnetic current in (2.2) onto SCET differs slightly in its computation. We replace $u \to \xi_{\mathrm{C}} + \eta_{\mathrm{C}} + W_C q_s$ together with (2.42) at LP, which is correct up to $\mathcal{O}(\lambda^{3/2})$. For the scalar current, we find that two terms in the expansion are relevant:

$$\bar{q}q(x) = j_{\xi\xi}^{(3/2)}(x) + j_{\xi q}^{(2)}(x) + \mathcal{O}(\lambda^{5/2}) \,. \tag{2.59}$$

[5] Here, we do not distinguish between the UV and IR scale dependence, which is however explicitly done in Sec. 2.4.2.

The effective currents are given by

$$j^{(3/2)}_{\xi\xi} = \bar{\xi}_{\rm C}\frac{1}{in_+D}i\not{D}_\perp\frac{\not{n}_+}{2}\xi_{\rm C} + \text{h.c.}\,, \tag{2.60}$$

$$j^{(2)}_{\xi q} = \bar{q}_s\chi_C + \text{h.c.} \tag{2.61}$$

We do not express the current $j^{(3/2)}_{\xi\xi}$ in terms of the gauge invariant building blocks (2.52) for later convenience.

Lastly, we note that HQET admits the heavy-quark spin-symmetry at LP in $1/m_Q$. However, this symmetry has no direct application in our context.

2.4 Factorization

The effective theory description from Sec. 2.3 allows us to systematically derive and prove factorization for the scalar correlator (2.1). In the following, we use (2.55) and (2.59) to match the currents from QCD to SCET and express the correlator in terms of SCET fields. We further replace the QCD B-meson state by its HQET equivalent $\big|\bar{B}(p+q)\big\rangle \to \sqrt{m_B}\big|\bar{B}(v)\big\rangle$.[6] At LP, we find

$$T(p,v) = eQ_u\sqrt{m_B}C_S(E_\gamma;\mu)\int d^4x e^{ipx}\big\langle 0\big|T\left\{\left(j^{(3/2)}_{\xi\xi} + j^{(2)}_{\xi q}\right)(x), J_S^{(\rm A0)}(0;0)\right\}\big|\bar{B}(v)\big\rangle + \mathcal{O}(\lambda)\,, \tag{2.62}$$

where we redefined the matching coefficient $C_S^{(\rm A0)} \to C_S$ to account for the renormalization of the scalar electromagnetic current in QCD. In (2.1), the collinear and soft fields in the currents (2.60) and (2.61) carry an implicit u-quark flavour label since the contribution from the heavy-quark current is power-suppressed. Note that we used the translation invariance $\phi(x) = e^{ix\mathcal{P}}\phi(0)e^{-ix\mathcal{P}}$ for the collinear field of $J_S^{(\rm A0)}$ to perform the $\hat{s}$-integral from (2.58).

In order to explain the structure of (2.62), several comments must be made. The first observation is that the LP correlator counts as $T \sim \lambda^{1/2}$ and hence power-corrections are $\mathcal{O}(\lambda)$ as indicated. The counting can be inferred from the tree-level expression, where the two light u-quark fields are contracted to a hard-collinear propagator

$$\begin{aligned} T(p,v) &\propto \int d^4x e^{ipx}\big\langle 0\big|\bar{u}(x)\; u_{\rm hc}(x)\bar{u}_{\rm hc}(0)\; b(0)\big|\bar{B}(v)\big\rangle \\ &\sim \frac{1}{\lambda^2}\cdot\lambda^{3/2}\cdot\lambda^{1/2}\cdot\lambda^{1/2}\cdot\lambda^{3/2}\cdot\frac{1}{\lambda^{3/2}} \sim \lambda^{1/2}\,. \end{aligned} \tag{2.63}$$

[6] The additional factor of $\sqrt{m_B}$ accounts for a mass-independent normalization of the B-meson state in HQET, $\langle\bar{B}(v')|\bar{B}(v)\rangle = (2\pi)^3 2v^0\delta^{(3)}(\vec{v}-\vec{v}')$. We conclude that $|\bar{B}\rangle \sim \lambda^{-3/2}$ since the delta-distribution counts as $1/\Lambda^3_{\rm QCD}$ with the spatial momentum only fluctuating at $\mathcal{O}(\Lambda_{\rm QCD})$.

The external u-quark and b-quark fields overlap with the B-meson state and therefore have the soft scaling of $\lambda^{3/2}$. We anticipate that the exponential $e^{ipx} \sim \mathcal{O}(1)$, so that the position variable scales as $x^\mu \sim (1, 1/\lambda, 1/\sqrt{\lambda})$ since p is hard-collinear. Hence, the integral measure counts as $d^4x \sim \lambda^{-2}$. On the EFT side, we consequently need to collect all effective operators such that the entire object contributes at $\mathcal{O}(\lambda^{1/2})$ or, equivalently, the product of operators within the time-ordered product scales as $T\{\ldots\} \sim \lambda^4$. Simultaneously, we have to match the quantum numbers of the external state. From these requirements, we immediately conclude that contributions with the B-type current $J_S^{(\mathrm{B1})} \sim \lambda^{5/2}$ in (2.57) are absent, since the product $j_{\xi\xi}^{(3/2)} J_S^{(\mathrm{B1})} \sim \lambda^4$ but has no light quark field q_s to overlap with the B-meson. To add further soft fields in an expression containing only collinear fields, we require an insertion of the subleading Lagrangian

$$\mathcal{L}_{\xi q}^{(1/2)} = \bar{q}_\mathrm{s} W_\mathrm{C}^\dagger i \not{D}_\perp \xi_\mathrm{C} + \text{ h.c.} \tag{2.64}$$

that adds another power of $\lambda^{1/2}$. For the B-type currents, this implies that their contribution can be at least of $\mathcal{O}(\lambda)$ so that they are subleading. The situation for the A-type current is different as the product $j_{\xi\xi}^{(3/2)} J_S^{(\mathrm{A0})} \sim \lambda^{7/2}$ allows for an insertion of (2.64). Hence, this term contributes at leading power, in addition to the tree-level term $j_{\xi q}^{(2)} J_S^{(\mathrm{A0})} \sim \lambda^4$. Note that the term $\not{\partial}_\perp$ in the A-type current (2.56) does not contribute due to its additional power suppression. In the following, we define the two contributions arising from this analysis separately

$$\hat{T}^1 = \int d^4x e^{ipx} \big\langle 0 \big| T\big\{ j_{\xi q}^{(2)}(x), \bar{\chi}_\mathrm{C}^{(u)}(1-\gamma_5) h_v(0) \big\} \big| \bar{B}(v) \big\rangle \,, \tag{2.65}$$

$$\hat{T}^2 = i \int d^4y \int d^4x e^{ipx} \big\langle 0 \big| T\big\{ \mathcal{L}_{\xi q}^{(1/2)}(y), j_{\xi\xi}^{(3/2)}(x), \bar{\chi}_\mathrm{C}^{(u)}(1-\gamma_5) h_v(0) \big\} \big| \bar{B}(v) \big\rangle \,, \tag{2.66}$$

where we factored out the coefficient $T = eQ_u \sqrt{m_B} C_S \hat{T}$ in front.

2.4.1 Decoupling transformation

We emphasize that the collinear fields in the correlator (2.62) as well as in the reduced objects (2.65) and (2.66) still interact with soft gluons via the leading power SCET Lagrangian (2.43). The soft-collinear interaction appears in the derivative term $in_- D$ and can be removed by the decoupling transformation

$$\xi_\mathrm{C}(x) = S_{n_-}(x_-) \xi_\mathrm{C}^{(0)}(x) \,, \qquad G_\mathrm{C}^\mu(x) = S_{n_-}(x_-) G_\mathrm{C}^{(0)\mu}(x) S_{n_-}^\dagger(x_-) \,. \tag{2.67}$$

This transformation decouples the soft from the collinear modes, so that $in_- D_\mathrm{C}$ only contains the collinear gauge field at LP, see [101] for details. In the remainder of this section, we assume that this decoupling has been done and we drop the index (0) for the collinear fields. The reduced correlator (2.65) takes the form

$$\hat{T}^1(p,v) = \int d^4x e^{ipx} \big\langle 0 \big| T\big\{ \bar{q}_\mathrm{s}^{(u)} S_{n_-}(x_-) \chi_\mathrm{C}^{(u)}(x), \bar{\chi}_\mathrm{C}^{(u)}(1-\gamma_5) S_{n_-}^\dagger h_v(0) \big\} \big| \bar{B}(v) \big\rangle$$

$$= \int d^4x e^{ipx} \langle 0 | T\{\chi_{\mathrm{C}\alpha}^{(u)}(x), \bar{\chi}_{\mathrm{C}\beta}^{(u)}\} | 0 \rangle \times [1-\gamma_5]_{\beta\gamma}$$

$$\times \left\langle 0 \middle| T\{\bar{q}_{\mathrm{s}\alpha}^{(u)} S_{n_-}(x_-) S_{n_-}^\dagger h_{v\gamma}(0)\} \middle| \bar{B}(v) \right\rangle , \tag{2.68}$$

where we can now factorize the collinear and soft matrix elements at LP due to the absence of soft-collinear interactions. The indices α, β, γ refer to the Dirac algebra while the colour structure is implicitly understood. We multipole expanded the position space argument of the soft function since factors of $x_-\partial \sim \lambda$ and $x_\perp \partial \sim \lambda^{1/2}$ yield an additional power-suppression when acting on soft fields. Therefore, the soft function depends only on one variable $x_- = tn_-$, where $t = vx$.

In (1.8) we defined the B-LCDA (soft function) in QCD. In the framework of HQET, the leading-twist LCDA is defined by

$$\left\langle 0 \middle| \bar{q}_{\mathrm{s}\alpha}(tn_-)[tn_-, 0] h_{v\gamma}(0) \middle| \bar{B}(v) \right\rangle = -\frac{iF_B(\mu)}{2} \left[\left(\frac{1+\not{v}}{2} \right) \gamma_5 \right]_{\gamma\alpha} \Phi_+(t - i0; \mu)$$

$$+ \dots \tag{2.69}$$

The omitted terms are proportional to $\not{n}_-$ and annihilated by the properties of the collinear function $\langle 0 | T\{\chi_{\mathrm{C}}, \bar{\chi}_{\mathrm{C}}\} | 0 \rangle$. Therefore, they are not relevant in the present context. However, these terms need to be included for NLP computations in Chapter 3, more precisely in (3.9). Note that we combined the two semi-infinite Wilson lines into $[tn_-, 0] = S_{n_-}(tn_-) S_{n_-}^\dagger(0)$ introduced in (2.6). The difference to the QCD definition lies in the presence of the heavy quark field h_v and the mass-independent state $\left| \bar{B}(v) \right\rangle$, changing the scale dependence of the function ϕ_+ compared to ϕ_B. This further implies that the static decay constant $F_B(\mu)$ in HQET defined by the local matrix element

$$\left\langle 0 \middle| \bar{q}_{\mathrm{s}}(0) \not{n}_- \gamma_5 h_v(0) \middle| \bar{B}(v) \right\rangle = iF_B(\mu) \tag{2.70}$$

is scale dependent. It can be related to the QCD decay constant via [91]

$$F_B(\mu) = f_B \sqrt{m_B} K^{-1}(\mu) = f_B \sqrt{m_B} \left[1 + \frac{\alpha_s C_F}{4\pi} \left(3 \ln \frac{\mu}{m_b} + 2 \right) + \mathcal{O}(\alpha_s^2) \right] . \tag{2.71}$$

The HQET operator on the right hand side of (2.69) retains the analytical structure compared to QCD, so that the Fourier transformation is, analogously to (2.7) and (2.8), given by

$$\phi_+(\omega; \mu) = \int \frac{dt}{2\pi} e^{i\omega t} \Phi_+(t - i0; \mu) , \qquad \Phi_+(t; \mu) = \int_0^\infty d\omega e^{-i\omega t} \phi_+(\omega; \mu) \tag{2.72}$$

and the function in momentum space is supported for $\omega > 0$. We emphasize that the local limit $t \to 0$ in (2.69) does not commute in general with the inclusion of radiative corrections [38]. The normalization $\Phi_+(0; \mu) = 1$ induced by (2.69) and (2.71) therefore only holds at tree level.

Employing (2.69) and (2.72), the first contribution to the correlator in (2.65) takes the form

$$\hat{T}^1(p,q) = -\frac{iF_B(\mu)}{2}\int_0^\infty d\omega\ \phi_+(\omega;\mu)\left[(1-\gamma_5)\left(\frac{1+\not{v}}{2}\right)\gamma_5\right]_{\beta\alpha} \times \int d^4x e^{i(p-\omega v_+)x}\big\langle 0\big|T\big\{\chi_{\mathrm{C}\alpha}^{(u)}(x),\bar{\chi}_{\mathrm{C}\beta}^{(u)}\big\}\big|0\big\rangle\ . \tag{2.73}$$

The matrix element in the second line involves only fermion fields living at the hard-collinear scale. Therefore, this object can be identified with a hard-collinear (jet) function. We define

$$\int d^4x e^{i(p-\omega v_+)x}\big\langle 0\big|T\big\{\chi_{\mathrm{C}\alpha}^{(u)}(x),\bar{\chi}_{\mathrm{C}\beta}^{(u)}(0)\big\}\big|0\big\rangle = \frac{-i}{\omega - n_-p - i0}\left[\frac{\not{n}_-}{2}\right]_{\alpha\beta} J_1(\omega,p;\mu)\ , \tag{2.74}$$

where $v_+^\mu = {n_+}^\mu/2$ is inherited from the Fourier transform of the LCDA. Note that the matrix element has to be proportional to $[\not{n}_-/2]_{\alpha\beta}$ due to the intrinsic structure of the hard-collinear propagator (2.39) in SCET. The prefactor $-i/(\omega - n_-p - i0)$ is chosen for convenience. In total, the first contribution can be written as

$$\hat{T}^1(p,q) = -\frac{F_B(\mu)}{2}\int_0^\infty \frac{d\omega}{\omega - n_-p - i0} J_1(\omega,p;\mu)\phi_+(\omega;\mu)\ , \tag{2.75}$$

which admits the structure of the factorization formula in (1.7). We can derive an equivalent form for the second term (2.66)

$$\hat{T}^2(p,q) = -\frac{F_B(\mu)}{2}\int_0^\infty \frac{d\omega}{\omega - n_-p - i0} J_2(\omega,p;\mu)\phi_+(\omega;\mu)\ . \tag{2.76}$$

In this case, the jet function is defined by

$$i\int d^4y e^{-i\omega v_+ y}\int d^4x e^{ipx}\big\langle 0\big|\big\{[W_{\mathrm{C}}^\dagger i\not{D}_\perp \xi_{\mathrm{C}}^{(u)}]_\alpha(y), j_{\xi\xi}^{(3/2)}(x),\chi_{\mathrm{C}\beta}^{(u)}(0)\big\}\big|0\big\rangle = \frac{-i}{\omega - n_-p - i0}\left[\frac{\not{n}_-}{2}\right]_{\alpha\beta} J_2(\omega,p;\mu)\ . \tag{2.77}$$

Again, the intrinsic structure of the fields including their projectors lead to the fact that the matrix element on the right hand side of (2.77) is proportional to $\not{n}_-/2$. Finally, we combine (2.74) (2.77) together with the definition $T = -vpF_S$ to obtain the complete factorization formula

$$F_S(E_\gamma,p^2) = eQ_u f_B m_B K^{-1}(\mu) C_S(E_\gamma;\mu)\int_0^\infty \frac{d\omega}{2E_\gamma\omega - p^2} J(2E_\gamma\omega,p^2;\mu)\phi_+(\omega;\mu)\ , \tag{2.78}$$

where $J = J_1 + J_2$. Note that the hard-collinear function only depends on the hard-collinear scales $2E_\gamma\omega$ and p^2, where ϕ_+ is assumed to be dominated by the support from $\omega \sim \Lambda_{\mathrm{QCD}}$. This completes the formal derivation of the QCD factorization for (2.1) at LP.

2.4.2 Renormalization

In order to derive the NLO expressions for the hard and hard-collinear matching coefficients C and J in (2.78), we properly match the full onto the effective theory. This matching is deeply connected to the method of regions computation in QCD from Sec. 2.2, but requires renormalization on both the QCD and the HQET×SCET side. We renormalize the UV divergences on the QCD side by first multiplying the correlator with the external on-shell quark field renormalization factors for the b- and the u-quark at one-loop

$$Z_b^{(1)} = -\frac{1}{2}\left(\frac{1}{\epsilon_{\rm UV}} + \frac{2}{\epsilon} + \ln\frac{\nu^2}{m_b^2} + 2\ln\frac{\mu^2}{m_b^2} + 4\right), \tag{2.79}$$

$$Z_u^{(1)} = -\frac{1}{2}\left(\frac{1}{\epsilon_{\rm UV}} - \frac{1}{\epsilon} + \ln\frac{\nu^2}{\mu^2}\right), \tag{2.80}$$

where $Z_i = 1 + Z_i^{(1)}\alpha_s C_F/4\pi$. Even though the on-shell renormalization factor of the light quark field vanishes, we separate UV and IR scales to track the origin of the divergences. In fact, the on-shell factors correspond to the hard region of the external field renormalization. After adding these factors, the full theory result still contains a UV divergence that needs to be subtracted by an additional renormalization factor, corresponding to the $\overline{\rm MS}$ renormalization of the scalar heavy-to-light currents in QCD

$$Z_{\rm QCD}^{(1)} = \frac{6}{\epsilon_{\rm UV}}\,. \tag{2.81}$$

In this way, the product $Z_{\rm QCD}^{-1} Z_b Z_u T$ ultimately becomes UV finite. We emphasize that the UV divergences from the hard region in (2.19)–(2.21) match the ones from the complete QCD result, which are removed by the renormalization. Hence, the remaining divergences in the combination $T_{\rm h} + Z_b^{(1)} + Z_u^{(1)} - Z_{\rm QCD}^{(1)}$ are of infrared nature. They are cancelled by the sum of all hard-collinear and soft contributions. On the HQET×SCET side, we therefore introduce the counter term in the $\overline{\rm MS}$ scheme

$$Z_C^{(1)} = -\frac{1}{\epsilon^2} - \frac{5}{2\epsilon} - \frac{2}{\epsilon}\ln\frac{\mu}{n_+p}\,, \tag{2.82}$$

which renders the hard region finite. Hence, we find that the hard matching coefficient equals the renormalized hard region and obtain

$$\begin{aligned} C_S(E_\gamma;\mu,\nu) = 1 + \frac{\alpha_s C_F}{4\pi}\Bigg(&12\ln\frac{\nu}{m_b} - 11\ln\frac{\mu}{m_b} - \frac{\pi^2}{12} \\ &- 2\ln^2\frac{\mu}{2E_\gamma} + 2{\rm Li}_2\left(1-\frac{1}{r}\right) + \ln^2 r + \frac{2}{1-r}\ln r\Bigg)\,. \end{aligned} \tag{2.83}$$

The scale ν corresponds to the UV renormalization scale in QCD while the scale μ is associated with the factorization scale appearing in the hard-collinear and soft region. The result agrees with [106, 108].

Using the same arguments, we renormalize the sum of all hard-collinear contributions (2.22), (2.23) and (2.24) in the $\overline{\text{MS}}$ scheme and remove the UV and IR divergences that cancel with the hard and soft region respectively. We obtain the hard-collinear matching coefficient

$$J_S(2E_\gamma\omega, p^2;\mu) = 1 + \frac{\alpha_s C_F}{4\pi}\bigg(\ln^2\frac{\mu^2}{2E_\gamma\omega - p^2} + 3\ln\frac{\mu^2}{2E_\gamma\omega - p^2} - \frac{\pi^2}{6} + 5 \\ - \frac{p^2}{2E_\gamma\omega}\ln\frac{p^2 - 2E_\gamma\omega}{p^2}\bigg(\ln\frac{\mu^2}{-p^2} + \ln\frac{\mu^2}{2E_\gamma\omega - p^2}\bigg)\bigg) . \tag{2.84}$$

As a crosscheck, this result can also be obtained by calculating the object directly from the SCET definitions in (2.74) and (2.77). The derivation together with the corresponding SCET Feynman rules can be found in Appendix A. In this context, we also discuss the cancellation of the soft region on both sides of the matching equation.

2.5 Resummation

The hard matching coefficient (2.83) contains logarithms involving the scale ratios μ/m_b and μ/n_+p, that become large when μ is chosen to be of order of the hard-collinear or soft scale. The same is true for logarithms of the jet function, evaluated at the hard or soft scale and vice versa. These logarithms spoil the convergence of the fixed-order perturbative expansion when $\alpha_s \ln\mu/m_b \sim \alpha_s \ln\mu/n_+p \sim \mathcal{O}(1)$.

We can resum large logarithms by solving the renormalization group (RG) of the hard, jet and the soft function, to which we refer as RG improved perturbation theory. In this way, the coefficients in (2.78) are evaluated at their natural hard(-collinear) or soft scale and then evolved to a common reference scale. In the following, we restrict ourselves to the renormalization of the hard and soft function and choose μ to be of order of the hard-collinear scale. This approach simplifies the treatment of the jet function as it does not contain large logarithms at the hard-collinear scale and hence resummation is not required. A proper treatment, including the resummation of hard-collinear logarithms, can be found for instance in [109] for the case of deep-inelastic scattering.

The RGE for the hard coefficient C_S can be derived from the counter term (2.82) using the running of the strong coupling in QCD, given by $d\alpha_s/d\ln\mu = -2\epsilon\alpha_s$. We find at one-loop

$$\frac{d}{d\ln\mu}C_S(E_\gamma;\mu,\nu) = -\frac{\alpha_s C_F}{\pi}\bigg[\ln\frac{\mu}{2E_\gamma} + \frac{11}{4}\bigg]C_S(E_\gamma;\mu,\nu) , \\ \frac{d}{d\ln\nu}C_S(E_\gamma;\mu,\nu) = \frac{3\alpha_s C_F}{\pi}C_S(E_\gamma;\mu,\nu) . \tag{2.85}$$

The distinction between the scales μ and ν is used to separate effects from the QCD and SCET renormalization. Since the result should be overall independent with respect to the chosen reference scales, we often use one common scale in practice. For $\mu = \nu$, the RGE can be expressed more generally to any loop-order as

$$\frac{d}{d\ln\mu} C_S(E_\gamma;\mu) = \left[-\Gamma_{\text{cusp}}(\alpha_s) \ln\frac{\mu}{2E_\gamma} + \gamma(\alpha_s) \right] C_S(E_\gamma;\mu) \,. \tag{2.86}$$

The scale evolution is determined by the functions

$$\Gamma_{\text{cusp}}(\alpha_s) = \sum_{n=0} \Gamma_n \left(\frac{\alpha_s}{4\pi}\right)^{n+1} , \qquad \gamma(\alpha_s) = \sum_{n=0} \gamma_n \left(\frac{\alpha_s}{4\pi}\right)^{n+1} . \tag{2.87}$$

The former term is called the cusp anomalous dimension and appears as a universal feature of heavy-to-light currents in HQET, related to the finite distance Wilson line $[tn_-, 0]$ in (2.69) [110, 111]. The latter anomalous dimension γ in (2.87) involves two contributions from the running coupling at five and four flavours respectively. The NNLO results for Γ_{cusp} and γ are given in [107]. The evolution of the strong coupling α_s is determined by the beta function

$$\beta^{\text{QCD}}(\alpha_s) = \frac{d\alpha_s}{d\ln\mu} = -2\alpha_s \sum_{n=0} \beta_n^{\text{QCD}} \left(\frac{\alpha_s}{4\pi}\right)^{n+1} . \tag{2.88}$$

The coefficients β_n^{QCD} are known up to the five-loop order [112]. As discussed in the introduction, we have $\beta^{\text{QCD}}(\alpha_s) < 0$ for the flavour content of the SM such that the strong coupling becomes large at lower energies and formally infinite at the scale $\Lambda_{\text{QCD}} \approx 200 - 300$ MeV depending on the number of active flavours. Technically, the effective theory contains four active flavours so that $\alpha_s(n_f = 5)$ needs to be matched to $\alpha_s(n_f = 4)$ at the scale m_b. Starting at two-loop, this matching is discontinuous. The matching relations can be found in [113, 114].

The RGE (2.86) can be solved by the simple ansatz

$$\begin{aligned} C_S(E_\gamma;\mu) &= U_1(E_\gamma;\mu,\mu_{\text{h}})\; C_S(E_\gamma;\mu_{\text{h}}) \,, \\ U_1(E_\gamma;\mu,\mu_{\text{h}}) &= \exp\left(\int_{\mu_{\text{h}}}^{\mu} \frac{d\mu'}{\mu'} \big[-\Gamma_{\text{cusp}}(\alpha_s(\mu')) \ln\frac{\mu'}{\mu_{\text{h}}} + \gamma(\alpha_s(\mu')) \big] \right) . \end{aligned} \tag{2.89}$$

The evolution function $U_1(E_\gamma;\mu,\mu_{\text{h}})$ evolves the coefficient from an arbitrary hard scale $\mu_h \sim \mathcal{O}(m_b)$ to another reference scale μ. Note that we assume that the decoupling of the b-quark flavour in γ has been done. The derivation for the anomalous dimension of the B-meson decay constant in HQET and the LCDA follows an equivalent derivation. We obtain the resummed expressions

$$F_B(\mu) = U_2(\mu,\mu_{\text{h}}) F_B(\mu_{\text{h}}) \,, \tag{2.90}$$

$$\phi_+(\omega;\mu) = \int_0^\infty d\omega'\, U_{\rm s}(\omega,\omega';\mu,\mu_{\rm s})\ \phi_+(\omega';\mu_{\rm s})\ , \tag{2.91}$$

where the evolution function U_2 is obtained from the factor U_1 by sending $\Gamma_{\rm cusp} \to 0$ and replacing γ according to Appendix A of [33]. In general, the hard reference scale of the decay constant and the matching coefficient can be different. However, we choose them to be equal for convenience. At one-loop, the evolution factor of the B-meson LCDA from a soft scale $\mu_{\rm s} \sim \mathcal{O}(\Lambda_{\rm QCD})$ is given in (5.92). We present more details about the derivation and properties of the soft function evolution in Chapter 5. We emphasize that the μ-dependence between the evolution functions cancels in the form factor (2.78), so that

$$\frac{d}{d\ln\mu} F_S(E_\gamma, p^2) = 0\ . \tag{2.92}$$

Hence, the complete result does not depend on the factorization scale μ. We refrain from verifying (2.92) explicitly and instead refer to [115] where this has been done for the case of the (axial-)vector form factors. Nevertheless, this observation justifies to choose the factorization scale μ arbitrarily.

In RG-improved perturbation theory, we distinguish between different approximations depending on their accuracy. The leading-logarithmic (LL) resummation corresponds to the solution of (2.86) with the one-loop expressions for $\Gamma_{\rm cusp}$ and the tree-level for γ. The next-to-leading logarithmic (NLL) resummation uses two-loop $\Gamma_{\rm cusp}$ and one-loop γ etc., see Table 1 in [101].

Chapter 3

Subleading effects in B-meson correlators

In the last chapter we derived the QCD factorization for the scalar form factor (2.78) at LP in the heavy-quark expansion. We expect the power corrections to the factorization formula to be of order $\mathcal{O}(5-10\%)$. In general, it turns out to be conceptually difficult to access these corrections in the traditional SCET framework due to the appearance of *endpoint divergences*. Based on the discussion for the scalar form factor in Chapter 2, the central problem can be paraphrased as follows: In a naive attempt, one would calculate NLP corrections by expanding the tree-level expression (2.5) and the integrands in the method of regions computation from Sec. 2.2 up to the next order in λ. However, this approach fails since convolution integrals at NLP in SCET generally become divergent at the boundary of the integration range. A simple example in this context is the evaluation of the heavy-quark emission in Fig. 1.1b. Using the momentum space projector method, we find that this contribution can be matched to

$$\xi_S^{(b)} = \frac{eQ_d f_B m_B}{2E_\gamma m_b}\left(1-\frac{2m_b}{E_\gamma}\right)\int_0^\infty d\omega\ \phi_+(\omega;\mu)\ . \tag{3.1}$$

Even though ϕ_+ vanishes linearly for $\omega\to 0$, the behaviour for $\omega\to\infty$ dictated by the RGE leads to $\phi_+(\omega)\propto\omega^{-1-a}$ with $-1<a<0$ and hence (3.1) diverges beyond tree-level. Physically, the divergence originates from an overlap with a region of different virtuality. Up to date, there exists no formal EFT framework to consistently handle endpoint divergences. Instead, the general strategy is to reshuffle the divergences from the different regions by introducing refactorization conditions, so that each region again only contains its natural scale. This analysis requires a careful case-by-case study and is not pursued in this work. For an overview of the recent research activity see e.g. [116–122].

Our aim is to estimate power corrections by a complementary approach. More precisely, we want to compute corrections to the scalar form factor $F_S(E_\gamma,p^2)$ in (2.1) as well as for the vector form factors $F_V(E_\gamma,p^2)$ and $F_A(E_\gamma,p^2)$ in (1.5) with a small off-shellness $p^2\approx-\Lambda_{\rm QCD}^2$ where $p^2<0$. These can be used for a comparison with future lattice QCD calculations which serves as our motivation. The main results for

the (axial)-vector form factors appearing in this chapter already exist in the literature. They can be inferred from [46, 47] and are not discussed in detail.

To access the $1/E_\gamma$ and $1/m_b$ power corrections, we use a dispersion relation for the correlation functions in (2.1) and (1.3). The correlators are dominated by hard-collinear $x^2 \sim 1/\sqrt{m_b \Lambda_{\rm QCD}}$ and soft $x^2 \sim 1/\Lambda_{\rm QCD}^2$ region. The former can be accessed by an OPE and involves higher-twist functions of the B-meson LCDA. The latter contains long-distance physics and cannot be calculated in perturbation theory, but the dispersion relation allows us to estimate the soft correction to the form factors by a sum rule. We can show that both contributions describe the subleading effects to a sufficient accuracy. In what follows, we parametrize the NLP corrections to the form factors by

$$F_S(E_\gamma, p^2) = \frac{eQ_u f_B m_B R_S(E_\gamma, p^2; \mu)}{2E_\gamma \lambda_B(E_\gamma, p^2; \mu)} + \xi_S(E_\gamma, p^2) \,, \tag{3.2}$$

$$F_V(E_\gamma, p^2) = \frac{eQ_u f_B m_B R(E_\gamma, p^2; \mu)}{2E_\gamma \lambda_B(E_\gamma, p^2; \mu)} + \xi(E_\gamma, p^2) + \Delta\xi(E_\gamma, p^2) \,, \tag{3.3}$$

$$F_A(E_\gamma, p^2) = \frac{eQ_u f_B m_B R(E_\gamma, p^2; \mu)}{2E_\gamma \lambda_B(E_\gamma, p^2; \mu)} + \xi(E_\gamma, p^2) - \Delta\xi(E_\gamma, p^2) \,. \tag{3.4}$$

The factor $R_{\{S\}}$ contains the radiative corrections at LP. For the scalar case, the factor is determined at NLO through the expressions in (2.83) and (2.84). We define the generalized inverse moment as

$$\frac{1}{\lambda_B(E_\gamma, p^2; \mu)} = 2E_\gamma \int_0^\infty \frac{d\omega}{2E_\gamma \omega - p^2} \, \phi_+(\omega; \mu) \,. \tag{3.5}$$

All NLP effects such as (3.1) are absorbed into ξ_S, ξ and $\Delta\xi$. Based on the above discussion about endpoint divergences, we emphasize that we do not consider radiative corrections to the subleading terms. For the vectorial form factors, the decomposition into symmetry-preserving and symmetry-breaking parts ξ and $\Delta\xi$ has originally been introduced in [33]. In the following, we develop the fundamental ideas to calculate ξ_S, ξ and $\Delta\xi$ with the scalar case at hand.

3.1 Higher-twist corrections

For $x^2 \sim 1/\sqrt{m_b \Lambda_{\rm QCD}}$, the hard-collinear propagator can be expanded in an OPE according to the heavy quark limit $x^2 \to 0$. The NLP terms in this expansion yield the hard-collinear corrections to the form factors. For the scalar correlator, the $1/E_\gamma$- and $1/m_b$-corrections to (2.1) at tree-level can be obtained from the identity $b = h_v + H_v$ and the equation of motion for the heavy mode H_v in (2.34) in HQET. We obtain two separate terms

$$T^{1/E_\gamma} = \sqrt{m_B} \int d^4x e^{ipx} \big\langle 0 \big| T\big\{ j^{\rm em}(x), \bar{u}(1-\gamma_5) h_v(0) \big\} \big| \bar{B}(v) \big\rangle \,, \tag{3.6}$$

$$T^{1/m_b} = \frac{\sqrt{m_B}}{2m_b}\int d^4x e^{ipx}\langle 0|T\{j^{\rm em}(x),\bar u(1-\gamma_5)i\not{D}h_v(0)\}|\bar B(v)\rangle\,. \tag{3.7}$$

In the first expression, the corrections are associated with the $1/E_\gamma$ terms originating from an expansion of the hard-collinear propagator up to NLP. The second term is already $1/m_b$-suppressed so that the hard-collinear propagator only enters at tree level. In both cases, we consider the expansion in a soft gluon background since the inclusion of hard-collinear gluons would correspond to loop corrections beyond our accuracy, and actually lead to divergent integrals. The propagator of the hard-collinear quark fields can be expanded as [123]

$$\begin{aligned}\langle 0|T\{q_{\rm hc}(x)\bar q_{\rm hc}(0)\}|0\rangle = \frac{i\not{x}}{2\pi x^4} - \frac{1}{8\pi^2x^2}\int_0^1 du\big\{ig_s\widetilde G_{\lambda\rho}(ux)x^\lambda\gamma^\rho\gamma_5\\ + (2u-1)g_sG_{\lambda\rho}(ux)x^\lambda\gamma^\rho\big\} + \dots\,,\end{aligned} \tag{3.8}$$

where the dual field strength tensor is defined by $\widetilde G_{\lambda\rho} = \epsilon_{\lambda\rho\alpha\beta}G^{\alpha\beta}/2$. We emphasize once more that the gluon fields in (3.8) only contain soft modes. In addition to the expansion of the hard-collinear propagator, we need to include the next-to-leading terms in the two-particle LCDA

$$\begin{aligned}\langle 0|\bar q_{\rm s}(x)[x,0]\Gamma h_v(0)|\bar B(v)\rangle = -\frac{iF_B(\mu)}{2}{\rm tr}\bigg[\gamma_5\Gamma\bigg(\frac{1+\not{v}}{2}\bigg)\bigg\{\Phi_+(t;\mu) + x^2G_+(t;\mu)\\ - \frac{\not{x}}{2vx}\big[(\Phi_+-\Phi_-)(t;\mu) + x^2(G_+-G_-)(t;\mu)\big]\bigg\}\bigg]\,,\end{aligned} \tag{3.9}$$

for the leading term in (3.8). For the remaining chapter, we omit the soft index $q_{\rm s}$ for the light quark field. Due to the analytic structure of the operator on the left-hand side of (3.9), the functions Φ_- and $G_\pm$ inherit the same $i0$-prescription as the function ϕ_+. The Fourier transformed functions ϕ_- and $g_\pm$ are equivalently obtained by (2.72). At tree-level, the limits $x\to 0$ and $vx\to 0$ imply the normalization

$$\int_0^\infty d\omega\;\phi_\pm(\omega;\mu) = 1\,,\qquad \int_0^\infty d\omega\;[\phi_+-\phi_-](\omega;\mu) = 0\,, \tag{3.10}$$

where the latter also holds true for the distribution functions $G_\pm$. For the subleading terms in (3.8), the appearance of soft gluon tensors requires the introduction of three-particle LCDAs which are defined by [124]

$$\begin{aligned}\langle 0|\bar q(x)g_sG_{\lambda\rho}(ux)x^\rho\Gamma h_v(0)|\bar B(v)\rangle = \frac{F_B(\mu)}{2}{\rm tr}\bigg[\gamma_5\Gamma\bigg(\frac{1+\not{v}}{2}\bigg)\\ \times\bigg\{(\not{v}v_\lambda-\gamma_\lambda vx)(\Psi_A-\Psi_V) - i\sigma_{\lambda\rho}x^\rho\Psi_V - x_\lambda X_A + x_\lambda\frac{\not{x}}{vx}Y_A\bigg\}(vx,uvx;\mu)\bigg]\,,\end{aligned} \tag{3.11}$$

$$\langle 0|\bar{q}(x)ig_s\widetilde{G}_{\lambda\rho}(ux)x^\rho\gamma_5\Gamma h_v(0)|\bar{B}(v)\rangle = \frac{F_B(\mu)}{2}\mathrm{tr}\left[\gamma_5\Gamma\left(\frac{1+\not{v}}{2}\right)\right. \tag{3.12}$$
$$\left.\times\left\{(\not{x}v_\lambda-\gamma_\lambda vx)(\widetilde{\Psi}_A-\widetilde{\Psi}_V)-i\sigma_{\lambda\rho}x^\rho\widetilde{\Psi}_V-x_\lambda\widetilde{X}_A+x_\lambda\frac{\not{x}}{vx}\widetilde{Y}_A\right\}(vx,uvx;\mu)\right].$$

The Fourier transformation to momentum space is generically given by

$$\psi(\omega_1,\omega_2;\mu)=\int\frac{dx_1}{2\pi}\int\frac{dx_2}{2\pi}e^{-i\omega_1x_1-i\omega_2x_2}\Psi(x_1,x_2;\mu)\,. \tag{3.13}$$

We emphasize that the functions defined by (3.9), (3.11) and (3.12) differ in their power counting which is usually referred to as twist in this context. We present further details on the twist expansion in Appendix B, including the analysis of the small ω-behaviour for the LCDAs. In our case, four combinations of the three-particle LCDAs are relevant

$$\begin{aligned}&\Phi_3=\Psi_V-\Psi_A\,,\\ &\Phi_4=\Psi_V+\Psi_A\,,\qquad \Psi_4=\Psi_V-X_A\,,\qquad \widetilde{\Psi}_4=-\Psi_A+\widetilde{X}_A\,,\end{aligned} \tag{3.14}$$

which are of twist-3 and twist-4, respectively. After using (3.8) and applying the higher-twist definitions (3.9)–(3.12), the $1/E_\gamma$ term (3.6) in position space becomes

$$\begin{aligned}T^{1/E_\gamma}=&\frac{eQ_uf_Bm_B}{2\pi^2}\int d^4x\,\frac{e^{ipx}}{x^4}\,(vx)\\ &\times\left\{\Phi_+(vx)+x^2G_+(vx)-\frac{x^2}{2(vx)^2}\big\{\Phi_+(vx)-\Phi_-(vx)\big\}\right.\\ &\left.+\frac{x^2}{4}\int_0^1du\left[2u\Phi_3+(2u-2)\Phi_4+(2u-1)\Psi_4-\widetilde{\Psi}_4\right](vx,uvx)\right\}.\end{aligned} \tag{3.15}$$

We perform the Fourier transformation using the integrals in Appendix B.1. For the $1/E_\gamma$ contribution to ξ_S, we find

$$\begin{aligned}\xi_S^{1/E_\gamma}(E_\gamma,p^2)=&\frac{eQ_uf_Bm_B}{4E_\gamma^2}\left\{\int_0^\infty\frac{4E_\gamma^2d\omega}{(2E_\gamma\omega-p^2)^2}[\omega^2\phi_+(\omega)-4g_+(\omega)]\right.\\ &+2\int_0^\infty\frac{2E_\gamma d\omega}{2E_\gamma\omega-p^2}\left(-\omega\phi_+(\omega)+\int_0^\omega d\omega'[\phi_+-\phi_-](\omega')\right)\\ &+\int_0^\infty d\omega_1\int_0^\infty d\omega_2\left(\frac{4E_\gamma^2[\psi_4+\widetilde{\psi}_4+2\phi_4](\omega_1,\omega_2)}{(2E_\gamma\omega_1-p^2)(2E_\gamma(\omega_1+\omega_2)-p^2)}\right.\\ &\left.\left.+\frac{2}{\omega_2}[\phi_3+\phi_4+\psi_4](\omega_1,\omega_2)\left[\frac{2E_\gamma}{2E_\gamma(\omega_1+\omega_2)-p^2}-\frac{1}{\omega_2}\ln\frac{2E_\gamma(\omega_1+\omega_2)-p^2}{2E_\gamma\omega_1-p^2}\right]\right)\right\}.\end{aligned} \tag{3.16}$$

Opposed to the real photon limit $p^2 \to 0$, the denominator is regularized by the off-shellness $p^2 < 0$, so that all integrals are endpoint finite. To our accuracy, we assume the tree-level normalization in (3.10) and neglect four-particle contributions like $qGGh_v$ or $qqqh_v$. The latter implies that we can further simplify the above expressions using the equation of motion for the light fields, commonly referred to as Wandzura-Wilczek (WW) relations, see [124]. Imposing the relations from Appendix B.2, the result in (3.17) drastically simplifies to

$$\begin{aligned}\xi_S^{1/E_\gamma}(E_\gamma, p^2) = \frac{eQ_u f_B m_B}{4E_\gamma^2}\Bigg\{ &\frac{\bar\Lambda}{\lambda_B(E_\gamma,p^2)} + \int_0^\infty \frac{2E_\gamma d\omega}{2E_\gamma\omega - p^2}\int_0^\omega d\omega'[\phi_+ - \phi_-](\omega') \\ &+ \int_0^\infty \frac{2E_\gamma d\omega}{2E_\gamma\omega - p^2}\left[\omega^2\frac{d}{d\omega}\phi_+(\omega) - 8\frac{d}{d\omega}g_+(\omega) - \omega[\phi_+ + \phi_-](\omega)\right] \\ &+ \int_0^\infty \frac{2E_\gamma d\omega_1}{2E_\gamma\omega_1 - p^2}\int_0^\infty \frac{2E_\gamma d\omega_2}{2E_\gamma(\omega_1+\omega_2) - p^2}[\psi + \widetilde{\psi}_4 + 2\phi_4](\omega_1,\omega_2)\Bigg\}\,. \end{aligned} \tag{3.17}$$

To calculate the $1/m_b$-corrections, we only require the leading term of the propagator in (3.8) since the corresponding term already enters with a factor $1/m_b$ from the equation of motion of the heavy quark field h_v. We eliminate the derivative acting on h_v in (3.7) by using the HQET operator identity [125]

$$\begin{aligned}\bar q(x)\Gamma\vec D_\lambda h_v(0) = \partial_\lambda[\bar q(x)\Gamma h_v(0)] - \left(\frac{\partial}{\partial x^\lambda}\bar q(x)\right)\Gamma h_v(0) \\ - i\int_0^1 du\bar u\bar q(x) g_s G_{\lambda\rho}(ux)x^\rho\Gamma h_v(0)\,, \end{aligned} \tag{3.18}$$

where $\bar u = 1-u$. Note that the derivative in the first term on the right-hand side acts on the entire operator $[\bar q(x)\Gamma h_v(0)]$. Taking the B to vacuum matrix, this contribution equals

$$\begin{aligned}\big\langle 0\big|\partial_\lambda[\bar q(x)\Gamma h_v(0)]\big|\bar B(v)\big\rangle &= \lim_{y\to 0}\frac{\partial}{\partial y^\lambda}\big\langle 0\big|\bar q(x+y)\Gamma h_v(y)\big|\bar B\big\rangle \\ &= \lim_{y\to 0}\frac{\partial}{\partial y^\lambda}e^{-i\bar\Lambda vy}\big\langle 0\big|\bar q(x)\Gamma h_v(0)\big|\bar B\big\rangle \\ &= -i\bar\Lambda v_\lambda\big\langle 0\big|\bar q(x)\Gamma h_v(0)\big|\bar B(v)\big\rangle\,. \end{aligned} \tag{3.19}$$

Similar to the $1/E_\gamma$ case, we evaluate the matrix element together with the latter two terms of (3.18) by applying the LCDA definitions above. In total, we obtain

$$\begin{aligned}T^{1/m_b} = &\frac{eQ_u f_B m_B}{4\pi^2 m_b}\int d^4x\frac{e^{ipx}}{x^4}vx\Bigg\{\bar\Lambda\Phi_+(vx) - i\Phi_+'(vx) \\ &- \frac{i}{vx}(\Phi_+ - \Phi_-)(vx) + 2ivx\int_0^1 du\bar u\Phi_3(vx,uvx)\Bigg\}\,, \end{aligned} \tag{3.20}$$

where the prime in the first line denotes the derivative with respect to the position space variable vx. After performing Fourier transformation and applying the WW relations, the contribution to the scalar form factor reads

$$\xi_S^{1/m_b}(E_\gamma,p^2)=\frac{eQ_uf_Bm_B}{4m_bE_\gamma}\bigg\{\frac{\bar\Lambda}{\lambda_B(E_\gamma,p^2)}-\int_0^\infty d\omega\frac{2E_\gamma\omega[\phi_++\phi_-](\omega)}{2E_\gamma\omega-p^2}$$
$$+2\int_0^\infty\frac{2E_\gamma d\omega_1}{2E_\gamma\omega_1-p^2}\int_0^\infty\frac{2E_\gamma d\omega_1}{2E_\gamma(\omega_1+\omega_2)-p^2}\phi_3(\omega_1,\omega_2)\,. \tag{3.21}$$

Note that we neglected the photon emission from the b-quark in (3.20) and (3.21), which we compute separately. In this case, the correlation function can be matched to

$$T^{(b)}=-\frac{eQ_df_Bm_B}{2E_\gamma m_b}(vp)\bigg(1-\frac{2m_b}{E_\gamma}\bigg)\,, \tag{3.22}$$

$$\xi_S^{(b)}(E_\gamma,p^2)=\frac{eQ_df_Bm_B}{2E_\gamma m_b}\bigg(1-\frac{2m_b}{E_\gamma}\bigg)\,. \tag{3.23}$$

Without the tree-level approximation, this result was already stated in (3.1).

3.1.1 Results for the (axial-)vector case

The derivation for the NLP contributions for the vector form factors in (3.3) and (3.4) follows the same arguments as for the scalar case. Rather than giving a precise derivation, we summarize the results which in part have been presented in [47]. In position space, we obtain

$$T_{\mu\nu}^{1/E_\gamma}=\frac{eQ_uf_Bm_B}{2\pi^2}\int d^4x\,\frac{e^{ipx}}{x^4}\left[-\epsilon_{\mu\nu\rho\sigma}x^\rho v^\sigma+i(vx)g_{\mu\nu}\right]$$
$$\times\bigg\{\Phi_+(vx)+x^2G_+(vx)-\frac{x^2}{4}\int_0^1du\left[(2u-1)\Psi_4-\widetilde\Psi_4\right](vx,uvx)\bigg\}\,, \tag{3.24}$$

$$T_{\mu\nu}^{1/m_b}=\frac{eQ_uf_Bm_B}{4\pi^2m_b}\int d^4x\,\frac{e^{ipx}}{x^4}\left[\epsilon_{\mu\nu\lambda\rho}x^\lambda v^\rho-i(vx)g_{\mu\nu}\right]\bigg\{-\bar\Lambda\Phi_+(vx)+i\Phi_+'(vx)$$
$$+\frac{i}{vx}(\Phi_+-\Phi_-)(vx)-2i(vx)\int_0^1du\bar u\Phi_3(vx,uvx)\bigg\}\,, \tag{3.25}$$

$$T_{\mu\nu}^{(b)}=\frac{eQ_df_Bm_B}{2E_\gamma m_b}[\epsilon_{\mu\nu\lambda\rho}p^\lambda v^\rho+i(vp)g_{\mu\nu}]\Phi_+(0;\mu)\,, \tag{3.26}$$

where we neglected terms proportional to p_μ since they do not contribute to the form factors F_V and F_A. We find the symmetry-preserving contribution ξ and symmetry-breaking part $\Delta\xi$ defined in (3.3) and (3.4) by performing the Fourier transformation

and compare the result with the definition in (1.3). For the tree-level and WW approximation, we find

$$\xi^{1/E_\gamma} = \frac{eQ_u f_B m_B}{4E_\gamma^2}\bigg\{ -2 + \int_0^\infty \frac{2E_\gamma d\omega}{2E_\gamma\omega - p^2}\,\omega\phi_+(\omega) + 2\int_0^\infty d\omega \ln\left(\omega - \frac{p^2}{2E_\gamma}\right)\phi_-^{\mathrm{t3}}(\omega) \\ - \int_0^\infty \frac{2E_\gamma d\omega_1}{2E_\gamma\omega_1 - p^2}\int_0^\infty \frac{2E_\gamma d\omega_2}{2E_\gamma\omega_2 - p^2}[\psi_4 + \widetilde{\psi}_4](\omega_1,\omega_2)\left[1 - \frac{p^2}{2E_\gamma(\omega_1+\omega_2) - p^2}\right]\bigg\}\,, \tag{3.27}$$

$$\Delta\xi^{1/E_\gamma} = \frac{eQ_u f_B m_B}{4E_\gamma^2}\int_0^\infty d\omega \frac{2E_\gamma d\omega}{2E_\gamma\omega - p^2}\,\omega\phi_+(\omega)\,, \tag{3.28}$$

and

$$\xi^{1/m_b} = \xi_S^{1/m_b}\,, \qquad \Delta\xi^{1/m_b} = 0\,, \qquad \xi^{(b)} = 0\,, \qquad \Delta\xi^{(b)} = \frac{eQ_d f_B m_B}{2E_\gamma m_b}\,. \tag{3.29}$$

We emphasize that the $1/m_b$ corrections in (3.29) agree to the previous scalar result (3.21). Within our approximation, we observe that no endpoint-divergent convolutions appear in the results for the scalar and vector form factors.

3.1.2 Twist-5 and twist-6 contributions

In addition to the twist-3 and twist-4 contributions, there are some terms of twist-5 and twist-6 that give rise to $1/E_\gamma^2$ corrections entering ξ_S, ξ and $\Delta\xi$. The corresponding tree-level diagrams are depicted in Fig. 3.1 and involve the insertion of the $\langle\bar{u}u\rangle$ vacuum condensate. In diagrams (a)–(d), the exchanged gluon has hard-collinear virtuality. Hence, we can calculate these contributions using standard methods, such as the projector method discussed in Appendix C.2. Out of the four diagrams, we find that only diagram (a) contributes at $\mathcal{O}(1/E_\gamma^2)$ with

$$\xi_{S,\mathrm{tw56}}^{(a)} = -\xi_{\mathrm{tw56}}^{(a)} = -\frac{eQ_u f_B m_B g_s^2 C_F\langle\bar{u}u\rangle}{12p^2E_\gamma}\int_0^\infty \frac{d\omega}{2E_\gamma\omega - p^2}\,\phi_-^{\mathrm{WW}}(\omega)\,. \tag{3.30}$$

At this accuracy, we neglect the twist-3 contribution of ϕ_-, so that only the WW part appears in the above results. The gluon exchanged in diagrams (e) and (f) is soft and thus, we can not extract the condensate term perturbatively. Instead, we again use the expansion of the hard-collinear propagator in a soft background. For diagram (e), there are two relevant terms in this expansion. In d space-time dimensions, they read

$$\langle 0|T\{q_{\mathrm{hc}}(x),\bar{q}_{\mathrm{hc}}(x)\}|0\rangle \supset \frac{\Gamma\left(\frac{d}{2}-1\right)}{8\pi^2(-x^2)^{\frac{d}{2}-1}}\int_0^1 du u\bar{u}\not{x} g_s(D_\lambda G^{\lambda\rho})(ux)x_\rho \\ + \frac{\Gamma\left(\frac{d}{2}-2\right)}{16\pi^2(-x^2)^{\frac{d}{2}-2}}\int_0^1 du\left(u\bar{u} - \frac{1}{2}\right) g_s(D_\lambda G^{\lambda\rho})(ux)\gamma_\rho\,. \tag{3.31}$$

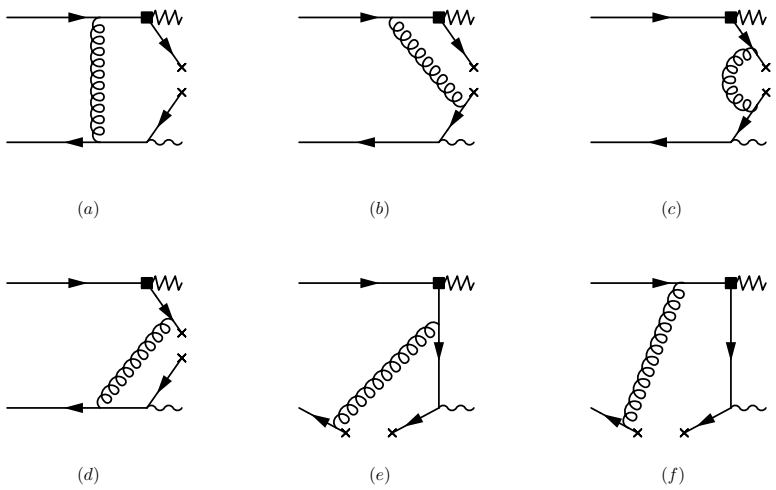

Figure 3.1: $\mathcal{O}(\alpha_s)$ corrections with one insertion of the vacuum condensate $\langle\bar{u}u\rangle$.

After using the equation of motion $(D_\lambda G^{\lambda\rho})^a = -g_s\bar{q}\gamma^\rho T^a q$, we obtain four-quark operators of the form $[\bar{u}u][\bar{u}b]$, in which we replace $u_\alpha\bar{u}_\beta \to -\delta_{\alpha\beta}\langle\bar{u}u\rangle/12$. Performing the Fourier transformation with the help of Appendix B.1, we find

$$\xi^{(e)}_{S,\text{tw56}} = -\frac{eQ_u f_B m_B g_s^2 C_F\langle\bar{u}u\rangle}{12p^2E_\gamma}\int_0^\infty \frac{d\omega}{2E_\gamma\omega - p^2}\,[\phi_+ + \phi_-^{\text{WW}}](\omega)\,, \tag{3.32}$$

$$\xi^{(e)}_{\text{tw56}} = -\frac{eQ_u f_B m_B g_s^2 C_F\langle\bar{u}u\rangle}{24p^2E_\gamma}\int_0^\infty \frac{d\omega}{2E_\gamma\omega - p^2}\,\phi_-^{\text{WW}}(\omega)\,, \tag{3.33}$$

$$\Delta\xi^{(e)}_{\text{tw56}} = \frac{eQ_u f_B m_B g_s^2 C_F\langle\bar{u}u\rangle}{24p^2E_\gamma}\int_0^\infty \frac{d\omega}{2E_\gamma\omega - p^2}\,\phi_+(\omega)\,. \tag{3.34}$$

Diagram (f) can be obtained in a hybrid approach using the $\mathcal{O}(1/x^2)$ terms in (3.8) and inserting one QCD interaction vertex for the b-quark, which produces a hard-collinear heavy-quark propagator. This procedure ensures that the exchanged gluon is soft, but does not provide an explicit condensate contribution. In fact, the corresponding term is part of the twist-5 amplitude g_- and hence at least $\mathcal{O}(1/E_\gamma^3)$.

3.2 Dispersion relation

For soft contributions from $x^2 \sim 1/\Lambda^2_{\text{QCD}}$, the hadronic matrix elements cannot be evaluated by an OPE in the heavy quark limit. However, we can relate the form factors at negative $p^2 < 0$ to the physical spectrum using a dispersion relation. This approach has been introduced for the $\gamma\gamma^* \to \pi$ form factor in [126] and applied to the $\bar{B} \to \gamma\ell\nu$ decay in [47, 127]. Again, we only consider the analysis of the scalar form factor to keep the discussion simple as the results for the vector case follow by simple replacements.

The physical spectrum contains cuts and poles along the positive real p^2 axis corresponding to single particle and bound states. To factor out these contributions, we insert a complete set of states between the currents in (2.1) so that

$$\begin{aligned} T(p,q) &= \int d^4x e^{ipx} \sum\!\!\!\!\!\!\int_X \Big\{ \theta(x^0) \big\langle 0 \big| j^{\text{em}}(x) \big| X \big\rangle \big\langle X \big| j^{\text{weak}}(0) \big| \bar{B}(p+q) \big\rangle \\ &\quad + \theta(-x^0) \big\langle 0 \big| j^{\text{weak}}(0) \big| X \big\rangle \big\langle X \big| j^{\text{em}}(x) \big| \bar{B}(p+q) \big\rangle \Big\} \\ &= \sum\!\!\!\!\!\!\int_X \frac{i(2\pi)^3 \delta^{(3)}(\vec{p} - \vec{p}_X)}{p^0 - p_X^0 + i0} \big\langle 0 \big| j^{\text{em}}(0) \big| X \big\rangle \big\langle X \big| j^{\text{weak}}(0) \big| \bar{B}(p+q) \big\rangle + \dots \,, \end{aligned} \tag{3.35}$$

where the Heaviside functions $\theta(\pm x^0)$ originates from the time-ordered product [128]. In the second line, we performed the position space integral after using translational invariance. The omitted term corresponds to the second integration for $x^0 < 0$ and contains a factor of $p^0 + p_X^0 - i0$ in the denominator. Since $p^0, p_X^0 > 0$, this term will not contribute to the dispersion relation. We take the imaginary part of (3.35) to obtain the spectral representation

$$\begin{aligned} \text{Im} F_S^{\text{had}}(E_\gamma, p^2) &= \frac{i}{2E_\gamma} \sum\!\!\!\!\!\!\int_X (2\pi)^4 \delta^{(4)}(p - p_X) \big\langle 0 \big| j^{\text{em}}(0) \big| X \big\rangle \big\langle X \big| j^{\text{weak}}(0) \big| \bar{B}(p+q) \big\rangle \\ &= \pi f_\sigma F_{B\to\sigma}(E_\gamma, p^2)\ \delta(p^2 - m_\sigma^2) + \theta(p^2 - s_0) \text{Im} F_S^{\text{had}}(E_\gamma, p^2) \,. \end{aligned} \tag{3.36}$$

We singled out the lowest-lying scalar resonance σ, sometimes referred to as $f_0(500)$, with mass m_σ in the narrow-width approximation [15]. The parameter s_0 defines an effective continuum threshold. To find the last line, we further defined the scalar meson decay constant and the $B \to \sigma$ form factor by

$$\big\langle 0 \big| j^{\text{em}}(0) \big| \sigma(p) \big\rangle = -i f_\sigma m_\sigma \,, \tag{3.37}$$

$$\big\langle \sigma(p) \big| j^{\text{weak}}(0) \big| \bar{B}(p+q) \big\rangle = \frac{vp}{m_\sigma} F_{B\to\sigma}(E_\gamma, p^2) \,. \tag{3.38}$$

Note that the additional factor of i ensures that the matrix element $i\langle 0|j^{\text{em}}|\sigma\rangle$ is real. The spectral representation (3.36) shows that there are no hadronic contributions for $p^2 < 0$. We can therefore relate the form factor for negative p^2 to the physical spectrum using Cauchy's integral theorem and deforming the contour to enclose the discontinuities on the positive real p^2-axis. We find

$$F_S^{\text{had}}(E_\gamma, p^2) = \frac{f_S F_{B\to\sigma}(E_\gamma, p^2 = m_\sigma^2)}{m_\sigma^2 - p^2} + \frac{1}{\pi} \int_{s_0}^\infty ds\, \frac{\text{Im} F_S^{\text{had}}(E_\gamma, s)}{s - p^2} \,. \tag{3.39}$$

We neglect the m_σ^2 dependence in the factor $F_{B\to\sigma}(E_\gamma, p^2 = m_\sigma^2) = F_{B\to\sigma}(E_\gamma)$ in the following. In Chapter 2, we calculated the scalar form factor for hard-collinear photon

momentum using QCD factorization. Above the threshold s_0, we assume that the continuum can be approximated by the partonic model $\mathrm{Im}F_S^{\mathrm{had}} = \mathrm{Im}F_S^{\mathrm{QCDF}}$, to which we refer as quark-hadron duality. For $p^2 < 0$, we observe that the jet function (2.84) does not contain imaginary parts from the hard-collinear logarithms. Therefore, we obtain a similar dispersion relation to (3.39)

$$F_S^{\mathrm{QCDF}}(E_\gamma, p^2) = \frac{1}{\pi}\int_0^\infty ds\, \frac{\mathrm{Im}\, F_S^{\mathrm{QCDF}}(E_\gamma, s)}{s - p^2}\,, \tag{3.40}$$

where $\mathrm{Im}F(s) = (F(s + i0) - F(s - i0)/(2i)$. We emphasize that no subtraction term in the dispersion relation appears due to the asymptotic behaviour of the QCD factorization result for $p^2 \to \infty$. Both the hadronic and the perturbative form factor can be related by a Borel transformation in the variable p^2. This transformation acts on an arbitrary function $F(p^2)$ as [129]

$$\mathcal{B}_{M^2} F(p^2) = \lim_{\substack{-p^2, n\to\infty \\ -p^2/n = M^2}} \frac{(-p^2)^{n+1}}{n!}\left(\frac{d}{dp^2}\right)^n F(p^2)\,. \tag{3.41}$$

For $p^2 \to \infty$, we assume that the hadronic correlator coincides with the QCD factorization due to the absence of particle poles and continuum cuts. Hence, we equate the Borel transformed expressions for (3.39) and (3.40)

$$\mathcal{B}_{M^2} F_S^{\mathrm{had}}(E_\gamma, p^2) = \mathcal{B}_{M^2} F_S^{\mathrm{QCDF}}(E_\gamma, p^2)\,. \tag{3.42}$$

The transformation (3.41) acts on the form factor denominators as

$$\mathcal{B}_{M^2}\left(\frac{1}{(s-p^2)^n}\right) = \frac{1}{(n-1)!}\frac{\exp\left(-\frac{s}{M^2}\right)}{M^{2(n-1)}} \tag{3.43}$$

for $n > 1$ and thus trades the variable p^2 for the Borel parameter M. Physically, the Borel parameter exponentially suppresses contributions from higher states in the continuum. It therefore improves the theoretical prediction as it reduces the error of the quark-hadron duality assumption. In practice, the parameter is chosen to be of the order of the hard-collinear scale and varied in a small numerical window to ensure the independence of the result on M. We discuss the choice of the Borel parameter in Chapter 6. After subtracting the continuum contribution from the left-hand side of (3.42), we find

$$f_\sigma F_{B\to\sigma}(E_\gamma) = \frac{1}{\pi}\int_0^{s_0} ds\, e^{-(s-m_\sigma^2)/M^2}\, \mathrm{Im}\, F_S^{\mathrm{QCDF}}(E_\gamma, s)\,. \tag{3.44}$$

We insert (3.44) into (3.39) and obtain

$$F_S(E_\gamma, p^2) = \frac{1}{\pi}\int_{s_0}^\infty \frac{ds}{s-p^2}\, \mathrm{Im}\, F_S^{\mathrm{QCDF}}(E_\gamma, s)$$

$$+\frac{1}{\pi}\int_0^{s_0}\frac{ds}{m_\sigma^2-p^2}\,\mathrm{Im}\,F_S^{\mathrm{QCDF}}(E_\gamma,s)\,e^{-(s-m_\sigma^2)/M^2}$$

$$=F_S^{\mathrm{QCDF}}(E_\gamma,p^2)+\xi_S^{\mathrm{soft}}(E_\gamma,p^2)\,. \tag{3.45}$$

In the last line, we added and subtracted the integral $\int_0^{s_0}$ to recover the QCD factorization result in (3.40). We conclude that the remaining term ξ_S^{soft} entirely originates from soft interactions. The definition

$$\xi_S^{\mathrm{soft}}(E_\gamma,p^2)=\frac{1}{\pi}\int_0^{s_0}\frac{ds}{s-p^2}\left[\frac{s-p^2}{m_\sigma^2-p^2}e^{-(s-m_\sigma^2)/M^2}-1\right]\mathrm{Im}\,F_S^{\mathrm{QCDF}}(E_\gamma,s) \tag{3.46}$$

$$=\int_0^{\frac{s_0}{2E_\gamma}}\frac{d\omega'}{2E_\gamma\omega'-p^2}\left[\frac{2E_\gamma\omega'-p^2}{m_\sigma^2-p^2}e^{-(2E_\gamma\omega'-m_\sigma^2)/M^2}-1\right]\Phi_S^{\mathrm{eff}}(\omega';\mu)$$

holds for arbitrary $p^2<0$, while the imaginary part of the QCD factorization form factor $F_S^{\mathrm{QCDF}}(E_\gamma,s)$ is calculated for hard-collinear $s>0$. For later purposes, we parametrized the integral in the second line in terms of the variable $\omega'=s/2E_\gamma$. We defined the effective function

$$\Phi_S^{\mathrm{eff}}(\omega';\mu)=\frac{2E_\gamma}{\pi}\,\mathrm{Im}\,F_S^{\mathrm{QCDF}}(E_\gamma,2E_\gamma\omega')\,, \tag{3.47}$$

which turns out to be equivalent to the B-meson LCDA at LO in the factorization approach. At NLO, the LCDA gets modified due to hard-collinear corrections from the jet function.

We remark that (3.46) represents the soft correction to the scalar form factor F_S. For the (axial-)vector case, the derivation follows almost the exact same steps. The main difference is the appearance of vector currents in (3.35), so that the vector meson resonances ρ and ω instead of σ contribute as the lowest-lying resonance. We combine both contributions into one generalized form factor with equal mass $m_\rho\approx m_\omega$. The corresponding formula reads

$$\xi_{\{V,A\}}^{\mathrm{soft}}(E_\gamma,p^2)=\int_0^{\frac{r_0}{2E_\gamma}}\frac{d\omega'}{2E_\gamma\omega'-p^2}\left[\frac{2E_\gamma\omega'-p^2}{m_\rho^2-p^2}e^{-(2E_\gamma\omega'-m_\rho^2)/M^2}-1\right]\Phi_{\{V,A\}}^{\mathrm{eff}}(\omega';\mu)\,,$$

$$\Phi_{\{V,A\}}^{\mathrm{eff}}(\omega';\mu)=\frac{2E_\gamma}{\pi}\,\mathrm{Im}\,F_{\{V,A\}}^{\mathrm{QCDF}}(E_\gamma,2E_\gamma\omega')\,, \tag{3.48}$$

where the indices refer to the contributions from V and A that have to be matched onto the ξ and $\Delta\xi$ parametrization in (3.3) and (3.4). Note that (3.48) can be obtained from (3.46) upon replacing $m_\sigma\to m_\rho$ and $s_0\to r_0$. The latter accounts for a different continuum threshold in the physical spectrum of scalar and vector mesons.

3.3 Soft corrections

In this section, we present the result for the soft corrections induced by the LP factorization formula and the higher-twist results in Sec. 3.1 for both scalar and (axial-)vector

case. For the latter, we require the generalization to (1.7) for an off-shell photon with $p^2 < 0$. We restrict ourselves to the transverse part of the correlation function $T^{\perp}_{\mu\nu}$, in which the currents are given by $\gamma^{\perp}_{\mu} \otimes \gamma^{\perp}_{\nu}(1-\gamma_5)$. The corresponding factorization theorem acquires a similar form to (2.78):

$$F_{\{V,A\}}(E_\gamma, p^2) = eQ_u f_B m_B K^{-1}(\mu) C_V^{(\mathrm{A0})}(E_\gamma;\mu) \int_0^\infty \frac{d\omega}{2E_\gamma\omega - p^2} J(2E_\gamma\omega, p^2;\mu)\phi_+(\omega;\mu)\,. \tag{3.49}$$

We remark that the coefficient $C_V^{(\mathrm{A0})}$ in this formula in fact refers to the matching coefficient of the heavy-to-light current from QCD to SCET since the electromagnetic and weak vector currents do not require UV renormalization in QCD. Both matching coefficients can be found in the literature [108, 115] and are given by

$$\begin{aligned} C_V^{(\mathrm{A0})}(E_\gamma;\mu) &= 1 + \frac{\alpha_s C_F}{4\pi}\bigg(-5\log\frac{\mu}{m_b} - 2\log^2\frac{\mu}{2E_\gamma} + 2\mathrm{Li}_2\left(1-\frac{1}{r}\right) - 6 - \frac{\pi^2}{12} \\ &\quad + \log^2 r + \frac{2-3r}{1-r}\log r\bigg)\,, \end{aligned} \tag{3.50}$$

$$\begin{aligned} J(2E_\gamma\omega, p^2;\mu) &= 1 + \frac{\alpha_s C_F}{4\pi}\bigg(\ln^2\frac{\mu^2}{2E_\gamma\omega - p^2} - \frac{\pi^2}{6} - 1 \\ &\quad - \frac{p^2}{2E_\gamma\omega}\ln\frac{p^2 - 2E_\gamma\omega}{p^2}\left(\ln\frac{\mu^2}{-p^2} + \ln\frac{\mu^2}{2E_\gamma\omega - p^2} + 3\right)\bigg)\,. \end{aligned} \tag{3.51}$$

For the longitudinal components, the formula (1.7) admits a more complicated structure which we do not consider, see [46].

3.3.1 LP contributions

To calculate the soft corrections from the LP factorization up to NLO in (2.78) and (3.49), we use the identities from Appendix D.1. In both cases, the soft form factor takes the form

$$\begin{aligned} \xi^{\mathrm{soft}}_{S,\mathrm{NLO}}(E_\gamma, p^2) &= eQ_u f_B m_B K^{-1}(\mu)\, C_S(E_\gamma;\mu) \\ &\quad \times \int_0^{\frac{s_0}{2E_\gamma}} \frac{d\omega'}{2E_\gamma\omega' - p^2}\left[\frac{2E_\gamma\omega' - p^2}{m_\sigma^2 - p^2}\, e^{-(2E_\gamma\omega' - m_\sigma^2)/M^2} - 1\right] \phi_S^{\mathrm{eff}}(\omega';\mu)\,, \end{aligned} \tag{3.52}$$

$$\begin{aligned} \xi^{\mathrm{soft}}_{\mathrm{NLO}}(E_\gamma, p^2) &= eQ_u f_B m_B K^{-1}(\mu)\, C_V^{(\mathrm{A0})}(E_\gamma;\mu) \\ &\quad \times \int_0^{\frac{r_0}{2E_\gamma}} \frac{d\omega'}{2E_\gamma\omega' - p^2}\left[\frac{2E_\gamma\omega' - p^2}{m_\rho^2 - p^2}\, e^{-(2E_\gamma\omega' - m_\rho^2)/M^2} - 1\right] \phi^{\mathrm{eff}}(\omega';\mu)\,, \end{aligned} \tag{3.53}$$

$$\Delta\xi^{\mathrm{soft}}_{\mathrm{NLO}}(E_\gamma, p^2) = 0\,. \tag{3.54}$$

For convenience, we redefined (3.47) to $\Phi_S^{\text{eff}} = eQ_u f_B m_B K^{-1} C\, \phi_S^{\text{eff}}$. For the scalar case, the effective function is given by

$$\begin{aligned}\phi_S^{\text{eff}}(\omega';\mu) = \phi_+(\omega';\mu) + \frac{\alpha_s(\mu)C_F}{4\pi}\Bigg\{ &\left(\ln^2\frac{\mu^2}{2E_\gamma\omega'} + 3\ln\frac{\mu^2}{2E_\gamma\omega'} + \frac{\pi^2}{6} + 5\right)\phi_+(\omega';\mu) \\ &+ 2\ln\frac{\mu^2}{2E_\gamma\omega'}\int_{\omega'}^{\infty} d\omega\,\omega' \ln\frac{\omega-\omega'}{\omega'}\frac{d}{d\omega}\frac{\phi_+(\omega;\mu)}{\omega} \\ &- \left(2\ln\frac{\mu^2}{2E_\gamma\omega'} + 3\right)\int_0^{\omega'} d\omega \ln\frac{\omega'-\omega}{\omega'}\frac{d}{d\omega}\phi_+(\omega;\mu) \\ &+ \int_0^{\omega'} d\omega \ln^2\frac{\omega'-\omega}{\omega'}\frac{d}{d\omega}\left[\frac{\omega'}{\omega}\phi_+(\omega;\mu) + \phi_+(\omega;\mu)\right]\Bigg\}\,. \end{aligned} \tag{3.55}$$

For the vector case, we have

$$\begin{aligned}\phi^{\text{eff}}(\omega';\mu) = \phi_+(\omega';\mu) + \frac{\alpha_s(\mu)C_F}{4\pi}\Bigg\{ &\left(\ln^2\frac{\mu^2}{2E_\gamma\omega'} + \frac{\pi^2}{6} - 1\right)\phi_+(\omega';\mu) \\ &+ \left(2\ln\frac{\mu^2}{2E_\gamma\omega'} + 3\right)\int_{\omega'}^{\infty} d\omega\,\omega' \ln\frac{\omega-\omega'}{\omega'}\frac{d}{d\omega}\frac{\phi_+(\omega;\mu)}{\omega} \\ &- 2\ln\frac{\mu^2}{2E_\gamma\omega'}\int_0^{\omega'} d\omega \ln\frac{\omega'-\omega}{\omega'}\frac{d}{d\omega}\phi_+(\omega;\mu) \\ &+ \int_0^{\omega'} d\omega \ln^2\frac{\omega'-\omega}{\omega'}\frac{d}{d\omega}\left[\frac{\omega'}{\omega}\phi_+(\omega;\mu) + \phi_+(\omega;\mu)\right]\Bigg\}. \end{aligned} \tag{3.56}$$

Generally, we consider the hard matching coefficients C_S, C_V and K as well as the B-meson LCDA in (3.52) and (3.53) to include the resummed evolution factors up to NLL accuracy based on the discussion in Sec. 2.5. To this end, we recall that the RGE for the scalar coefficient slightly differs from [107] due to the additional UV renormalization of the scalar electromagnetic current in QCD in the correlation function (2.1). The corresponding μ-dependence is compensated by the single-logarithmic term in the scalar jet function (2.84).

3.3.2 NLP contributions

The higher-twist contributions correct the QCD factorization result at NLP and therefore enter the soft form factor through the dispersion relation. Up to twist-4, we define

$$\begin{aligned}\xi^{\text{soft}}_{S,\text{tw34}}(E_\gamma,p^2) = \frac{eQ_u f_B m_B}{2E_\gamma}\int_0^{\frac{s_0}{2E_\gamma}}\frac{d\omega'}{2E_\gamma\omega'-p^2}\left[\frac{2E_\gamma\omega'-p^2}{m_\sigma^2-p^2}e^{-(2E_\gamma\omega'-m_\sigma^2)/M^2}-1\right]\Xi_{S,1}(\omega') \\ + \frac{eQ_u f_B m_B}{2m_b}\int_0^{\frac{s_0}{2E_\gamma}}\frac{d\omega'}{2E_\gamma\omega'-p^2}\left[\frac{2E_\gamma\omega'-p^2}{m_\sigma^2-p^2}e^{-(2E_\gamma\omega'-m_\sigma^2)/M^2}-1\right]\Xi_{S,2}(\omega')\,. \end{aligned} \tag{3.57}$$

An analogous definition holds for the vector case upon replacing $s_0 \to r_0$, $m_\sigma \to m_\rho$

$$\xi^{\text{soft}}_{\text{tw34}}(E_\gamma, p^2) = \frac{eQ_u f_B m_B}{2E_\gamma} \int_0^{\frac{r_0}{2E_\gamma}} \frac{d\omega'}{2E_\gamma\omega' - p^2} \left[\frac{2E_\gamma\omega' - p^2}{m_\rho^2 - p^2} e^{-(2E_\gamma\omega' - m_\rho^2)/M^2} - 1 \right] \Xi_1(\omega')$$

$$+ \frac{eQ_u f_B m_B}{2m_b} \int_0^{\frac{r_0}{2E_\gamma}} \frac{d\omega'}{2E_\gamma\omega' - p^2} \left[\frac{2E_\gamma\omega' - p^2}{m_\rho^2 - p^2} e^{-(2E_\gamma\omega' - m_\rho^2)/M^2} - 1 \right] \Xi_2(\omega') \,. \tag{3.58}$$

The coefficient functions are calculated from the results in Sec. 3.1, where we again use the relations from the Appendices B.2 and D.1. From (3.17), (3.21), (3.27) and (3.29), we obtain

$$\Xi_{S,1}(\omega) = (\bar\Lambda - \omega)\phi_+(\omega) - 2\omega\phi_-^{\text{WW}}(\omega) + \omega\phi_-^{\text{t3}}(\omega) - \int_0^\omega d\omega' \phi_-^{\text{t3}}(\omega') \tag{3.59}$$

$$+ \int_0^\infty \frac{d\omega_2}{\omega_2} [\psi_4 + \widetilde{\psi}_4 + 2\phi_4](\omega, \omega_2) - \int_0^\omega \frac{d\omega_2}{\omega_2} [\psi_4 + \widetilde{\psi}_4 + 2\phi_4](\omega - \omega_2, \omega_2) \,,$$

$$\Xi_{S,2}(\omega) = (\bar\Lambda - \omega)\phi_+(\omega) - \omega\phi_-(\omega) + 2\int_0^\infty \frac{d\omega_2}{\omega_2} \phi_3(\omega, \omega_2) - 2\int_0^\omega \frac{d\omega_2}{\omega_2} \phi_3(\omega - \omega_2, \omega_2) \,,$$

$$\Xi_1(\omega) = -2\int_0^\omega d\omega' \phi_-^{\text{t3}}(\omega') - 2\omega\phi_-^{\text{WW}}(\omega) + \frac{d}{d\omega}(\omega^2\phi_+(\omega)) \tag{3.60}$$

$$- \left(\int_0^\omega d\omega_1 \int_{\omega-\omega_1}^\infty \frac{d\omega_2}{\omega_2} \frac{\partial}{\partial\omega_1} + \int_0^\omega d\omega_2 \int_{\omega-\omega_2}^\infty \frac{d\omega_1}{\omega_1} \frac{\partial}{\partial\omega_2} \right) [\psi_4 + \widetilde{\psi}_4](\omega_1, \omega_2) \,,$$

$$\Xi_2(\omega) = \Xi_{S,2}(\omega) \,. \tag{3.61}$$

For the symmetry-breaking term (3.28), we find

$$\Delta\xi^{\text{soft}}_{\text{tw34}} = \frac{eQ_u f_B m_B}{2E_\gamma} \int_0^{\frac{r_0}{2E_\gamma}} \frac{d\omega'}{2E_\gamma\omega' - p^2} \left[\frac{2E_\gamma\omega' - p^2}{m_\rho^2 - p^2} e^{-(2E_\gamma\omega' - m_\rho^2)/M^2} - 1 \right] \omega'\phi_+(\omega') \,. \tag{3.62}$$

The twist-5 and twist-6 terms in (3.30) and (3.32)–(3.34) sum up to

$$\xi^{\text{soft}}_{S,\text{tw56}} = \frac{-\mathcal{N}_u}{12p^2E_\gamma} \int_0^{\frac{s_0}{2E_\gamma}} \frac{d\omega'}{2E_\gamma\omega' - p^2} \left[\frac{2E_\gamma\omega' - p^2}{m_\sigma^2 - p^2} e^{-(2E_\gamma\omega' - m_\sigma^2)/M^2} - 1 \right]$$

$$\times [\phi_+ + 2\phi_-^{\text{WW}}](\omega') \,, \tag{3.63}$$

$$\xi^{\text{soft}}_{\text{tw56}} = \frac{\mathcal{N}_u}{24p^2E_\gamma} \int_0^{\frac{r_0}{2E_\gamma}} \frac{d\omega'}{2E_\gamma\omega' - p^2} \left[\frac{2E_\gamma\omega' - p^2}{m_\rho^2 - p^2} e^{-(2E_\gamma\omega' - m_\rho^2)/M^2} - 1 \right] \phi_-^{\text{WW}}(\omega') \,, \tag{3.64}$$

$$\Delta\xi^{\text{soft}}_{\text{tw56}} = \frac{\mathcal{N}_u}{24p^2E_\gamma} \int_0^{\frac{r_0}{2E_\gamma}} \frac{d\omega'}{2E_\gamma\omega' - p^2} \left[\frac{2E_\gamma\omega' - p^2}{m_\rho^2 - p^2} e^{-(2E_\gamma\omega' - m_\rho^2)/M^2} - 1 \right] \phi_+(\omega') \,, \tag{3.65}$$

where we introduced the normalization constant $\mathcal{N}_u \equiv eQ_u f_B m_B g_s^2 C_F \langle\bar u u\rangle$ for convenience. This completes our calculation of the NLP corrections at $\mathcal{O}(1/E_\gamma^2)$. We present first qualitative numerical estimates in Chapter 6.

Chapter 4

QCD×QED Factorization

The QCD factorization framework as it was presented in Chapter 2 is the state-of-the-art tool to parametrize and calculate precision observables of non-leptonic decays. Although its technical difficulties at NLP, the results compete up to now with the experimental precision from LHCb and Belle II. However, to obtain profound predictions in the future, it is necessary to improve the theoretical calculations beyond the LP accuracy in QCD-only. As discussed at the beginning of Chapter 3, there are ongoing efforts to derive a consistent framework for QCD factorization at NLP in the heavy-quark expansion which is accompanied by higher-order perturbative calculations for the matching coefficient functions at LP.

So far, QED corrections in B decays have barely been investigated even though they could be of similar size as NLP and $\mathcal{O}(\alpha_s^2)$ corrections. In non-leptonic B decays, QED effects are usually taken into account by dressing the QCD-only amplitude with Bloch-Nordsieck factors below the scale Λ_{QCD} that resum collinear and soft logarithms up to the B-meson mass scale m_B. This approach assumes the B meson to be point-like up to distances of order $1/m_B$, which is conceptually wrong above the scale Λ_{QCD}. In this regime, photons can resolve the partonic substructure of hadrons that are typically confined to a size of order $1/\Lambda_{\text{QCD}}$. Beyond the scale m_B, one furthermore needs to include QED effects as well as their running in the Wilson coefficients of the weak effective operators.

In this chapter, we address the incomplete treatment of QED effects in charmless, non-leptonic $\bar{B} \to M_1 M_2$ decays into light final-state mesons $M_i = \pi, K$. Note that the meson M_1 is specifically defined to pick up the spectator quark. Our analysis is based on [66] and the follow-up publications [68, 130] that consider the renormalization of LCDAs for light and heavy mesons. For decays into heavy (charmed) mesons, we refer to [67]. We consider the following three separate aspects depending on their energy range:

i) Above the scale m_B, QED effects can be added to the Wilson coefficients of the weak effective operators in a standard manner by using the results of [131].

ii) Between the scale m_B and $\Lambda_{\rm QCD}$, we can extend the QCD factorization approach, schematically given in (1.10), to a combined QCD×QED factorization formula that takes a similar form as in QCD-only

$$\begin{aligned}\big\langle M_1M_2\big|Q_i\big|\bar B\big\rangle = im_B^2\bigg\{&\mathcal{F}_{Q_2}^{BM_1}(0)\int_0^1 du\,T_{i,Q_2}^{\rm I}f_{M_2}\Phi_{M_2}(u)\\&+\int_0^1 du\,dv\int_{-\infty}^{\infty}d\omega\,T_{i,Q_2}^{\rm II}(u,v,\omega)f_{M_1}\Phi_{M_1}(v)f_{M_2}\Phi_{M_2}(u)f_B\Phi_{B,\otimes}(\omega)\bigg\}\,.\end{aligned}\tag{4.1}$$

Q_i denotes an operator of the weak effective Hamiltonian, mediating a $b\to q$ transition. Here, the mesons M_1 and M_2 are strictly assumed to be massless and hence carry the energy of $m_B/2$ each while flying in back-to-back directions.

iii) Below the scale $\Lambda_{\rm QCD}$, the meson masses cannot be neglected. We further include an arbitrary number of ultrasoft photons in the final state of $\bar B\to M_1M_2(\gamma)$ with total energy $\Delta E\ll\Lambda_{\rm QCD}$. This is necessary to render the entire process IR finite in QED since the non-radiative amplitude $\big\langle M_1M_2\big|Q_i\big|B\big\rangle$ becomes IR divergent once virtual QED corrections are considered. The energy difference allows for perturbative calculations in a theory of point-like mesons [62].

We emphasize that the above statements are valid at the corresponding scales up to a small window below and above a few times $\Lambda_{\rm QCD}$. In this energy range, QED interacts with a strongly coupled system that requires a non-perturbative matching to the effective theory environment.

The second point ii), accounting for the structure-dependent contributions, turns out to be the most difficult and novel part which will be the main focus of this chapter. The formula (4.1) describes factorization for the four possible final-state charge combinations $\otimes=(Q_1,Q_2)=(0,0),(-,0),(0,-),(+,-)$. The flipped combinations can be obtained by CP invariance of the full QCD×QED theory. Compared to QCD-only, the essential difference is that the form factor $\mathcal{F}^{BM_1}$ and the hard scattering kernels $T^{\rm I/II}$ depend on the electric charge Q_2 and implicitly on the direction of flight of the second meson M_2 that is produced by the weak interaction. The QED-generalized definitions of the light and heavy meson LCDAs Φ_M and $\Phi_{B,\otimes}$ inherit the same attributes but require an additional modification depending on the charge combination of the external states. While for light mesons these generalizations are quite natural, the B-meson LCDA becomes a rather complicated object that contains soft physics at the scale $\Lambda_{\rm QCD}$. Almost every modification in this context is related to the non-decoupling of soft photons from electrically charged mesons. For the heavy meson LCDA, this leads to the appearance of soft rescattering phases and it therefore should rather be viewed as a soft function to the process so that we omit the term "LCDA" in the following. To this end, we conclude that the non-perturbative objects become process-dependent.

To prove the factorization formula (4.1), we derive the hard scattering kernels at $\mathcal{O}(\alpha_s^0\alpha_{\rm em})$ by consecutively matching the full QCD×QED theory onto HQET×SCET$_{\rm I}$ and HQET×SCET$_{\rm II}$. Opposed to the radiative $\bar B\to\gamma\ell\nu$ decay discussed in Chapter 2,

the external states are collinear objects, such that we need to distinguish between hard-collinear and collinear modes in the process. SCET_I therefore refers to a theory of light fields including soft, collinear and hard-collinear scaling while SCET_II only contains the soft and collinear modes. We introduce the operator basis for both EFTs in Sec. 4.1 and discuss the SCET_I matching in Sec. 4.2 alongside with the renormalization of QED-generalized heavy-to-light currents and light-meson LCDAs. The matching onto SCET_II in Sec. 4.3 integrates out the hard-collinear modes and factorizes the spectator scattering term in (4.1). We introduce soft rearrangement factors to consistently separate soft and collinear scales. The case of $Q_2 \neq 0$ is particularly interesting since soft photons do not decouple from the $B \to M_1$ transition, which contains soft spectator scattering contributions. In this case, the QED-generalized form factor $\mathcal{F}^{BM_1}$ in SCET can be replaced by a QCD×QED form factor of the semi-leptonic $\bar{B} \to M_1 \ell^- \bar{\nu}_\ell$ decay. We present the precise formalism for this replacement in Sec.4.2.4.

To address point iii), we introduce the ultrasoft function below Λ_QCD in Sec. 4.5 that accounts for the real emission of an arbitrary number of ultrasoft photons with total energy $\Delta E \ll \Lambda_\text{QCD}$. For photons at this scale, perturbative calculations can be done in an effective theory where mesons have point-like QED coupling. In a standard framework, the IR singularities of virtual QED effects cancel with the corresponding divergences from the phase space integration after calculating the decay width. This is qualitatively different in QED where the non-perturbative objects entering (4.1) retain the IR divergences of the non-radiative amplitude. In practice, we therefore consider the form factors and LCDAs as well as the ultrasoft function as separately IR/UV regularized objects. The resummation of the collinear and soft logarithms $m_{M_i}/\Lambda_\text{QCD}$ and $\Delta E/\Lambda_\text{QCD}$ is subject of Chapter 5.

4.1 Matching equation

The B meson decays weakly into light final states through $b \to u$ transitions in the effective Hamiltonian. Generally, there are many operators and topologies that contribute to the decay into (non-leptonic) pseudoscalars, some of which we presented in Fig. 1.2. We restrict ourselves to the case of current-current operators $Q_{1,2}$ in the Hamiltonian

$$\mathcal{H}_\text{eff} = \frac{G_F}{\sqrt{2}} V_{uD}^* V_{ub} \left(C_1(\nu) Q_1 + C_2(\nu) Q_2\right) + \text{h.c.} \tag{4.2}$$

The generalization to other operators may follow in future works. We choose to work within the CMM operator basis [132] where

$$\begin{aligned} Q_1 &= [\bar{u}\gamma^\mu T^a (1-\gamma_5) b][\bar{D}\gamma_\mu T^a (1-\gamma_5) u] \,, \\ Q_2 &= [\bar{u}\gamma^\mu (1-\gamma_5) b][\bar{D}\gamma_\mu (1-\gamma_5) u] \,. \end{aligned} \tag{4.3}$$

T^a denotes the SU(3) colour generator in the fundamental representation and $D = d, s$ the down-type quark flavour. At tree level, the operator Q_2 is generated after integrating out the W boson and the operator Q_1 is induced by renormalization. The

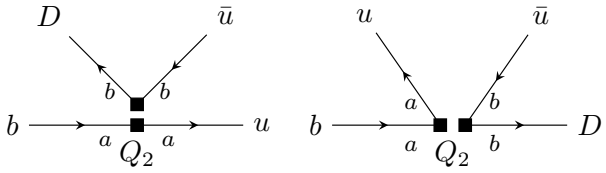

Figure 4.1: "Right" and "wrong" insertions of the operator Q_2, respectively. The indices a and b denote the colour flow.

Wilson coefficients $C_{1,2}(\nu)$ include the QED corrections from the electroweak field content. Depending on the flavour structure, the insertion of an operator Q_i is referred to as "right" or "wrong" insertion corresponding to colour-allowed and colour-suppressed amplitudes respectively, see Fig. 4.1. For neutral $Q_{M_2} = 0$, only the wrong insertion contributes to the decay while for charged M_2 the right insertion enters. At tree level, the Dirac structure for the wrong insertion can be rearranged using (colour) Fierz transformations, see equation (24) of [133].

4.1.1 SCET$_\mathrm{I}$ operator basis

Both right and wrong insertions of Q_i can be matched onto operators in the effective theory. In Chapter 2, we presented the fundamental steps of this procedure in the simple framework of scalar currents. For the case at hand, the operators in HQET×SCET$_\mathrm{I}$ side are given by a combination of A0- and B1-type heavy-to-light currents and an anti-collinear operator[1]

$$\mathcal{O}^{\mathrm{I}}(t) = [\bar{\chi}^{(q_1)}_{\bar{\mathrm{C}}}(tn_-)\frac{\not{n}_-}{2}(1-\gamma_5)\chi^{(u)}_{\bar{\mathrm{C}}}(0)][\bar{\chi}^{(q_2)}_{\mathrm{C}}(0)\not{n}_+(1-\gamma_5)h_v(0)]\,, \tag{4.4}$$

$$\mathcal{O}^{\mathrm{II}\gamma}(t,s) = \frac{1}{m_b}[\bar{\chi}^{(q_1)}_{\bar{\mathrm{C}}}](tn_-)\frac{\not{n}_-}{2}(1-\gamma_5)\chi^{(u)}_{\bar{\mathrm{C}}}(0)][\bar{\chi}^{(q_2)}_{\mathrm{C}}(0)\frac{\not{n}_+}{2}\not{\mathcal{A}}_{\perp\mathrm{C}}(sn_+)(1+\gamma_5)h_v(0)]\,. \tag{4.5}$$

The gluon operator $\mathcal{O}^{\mathrm{IIg}}$ is obtained upon replacing $\not{\mathcal{A}}_{\perp\mathrm{C}} \to \not{\mathcal{G}}_{\perp\mathrm{C}}$, where the latter was defined in (2.52). In the anti-collinear fermion fields, the u-quark flavour of the outgoing anti-quark is fixed while $q_{1,2} = u, d, s$ are not restricted. The collinear Wilson line W_C in QCD-only from (2.48) gets multiplied by the corresponding QED exponential

$$W^{(q)}_{\mathrm{C}}(x) = \exp\left\{iQ_q e\int_{-\infty}^{0} ds\, n_+A_{\mathrm{C}}(x+sn_+)\right\} W_{\mathrm{C}}(x)\,, \tag{4.6}$$

[1] In [66] we distinguished between two operator types, depending on the total electric charge of the meson M_2. Here, we use a compact notation and only separate the results for the hard-scattering kernels.

where $Q_q = 2/3, -1/3$ labels the up- and down-type electric quark charge. The fields $\chi_{\bar{\mathrm{C}}}$ and $\mathcal{A}_{\perp\mathrm{C}}$ are the gauge-invariant building blocks defined in (2.52) with QED

$$\chi_{\mathrm{C}}^{(q)} = [W_{\mathrm{C}}^{(q)}]^\dagger \xi_{\mathrm{C}}^{(q)} , \qquad \mathcal{A}_{\mathrm{C}\perp}^{\mu} = e\left[A_{\mathrm{C}\perp}^{\mu} - \frac{i\partial_\perp^\mu n_+ A_{\mathrm{C}}}{in_+\partial}\right] . \tag{4.7}$$

Note that the photon field is just the abelian version of the gluon field. For the anti-collinear fields, analogous definitions and conventions with the replacements $C \to \bar{C}$ and $n_+ \to n_-$ apply. We recall that the labels C and $\bar{\mathrm{C}}$ refer to both collinear and hard-collinear scalings given in Table 2.1. The labels c and $\bar{\mathrm{c}}$ solely correspond to the (anti-)collinear λ-scaling.

The matching equation for each operator Q_i is given by

$$Q_i(0) = \int d\hat{t}\, \widetilde{H}_{i,Q_2}^{\mathrm{I}}(\hat{t})\, \mathcal{O}^{\mathrm{I}}(t) + \int d\hat{t} d\hat{s}\, \widetilde{H}_{i,Q_2}^{\mathrm{II}}(\hat{t},\hat{s})\, \mathcal{O}^{\mathrm{II}}(t,s) . \tag{4.8}$$

We emphasize that the right and wrong insertions of both operators Q_i of the full theory can be matched onto the same $\mathcal{O}^{\mathrm{I/II}}$ operators. The wrong insertion applies for the case of $Q_2 = 0$ and the right insertion for $Q_2 = -1$. The difference is encoded in the hard matching coefficients $H^{\mathrm{I/II}}$ obtained from a partonic calculation. Their Fourier transformation is given by

$$H_i^{\mathrm{I}}(u) = \int d\hat{t} \widetilde{H}_i^{\mathrm{I}}(\hat{t}) e^{iu\hat{t}} , \qquad H_i^{\mathrm{II}}(u,v) = \int d\hat{t} d\hat{s} \widetilde{H}_i^{\mathrm{II}}(\hat{t},\hat{s}) e^{iu\hat{t}+iv\hat{s}} , \tag{4.9}$$

where $0 < u, v < 1$ and $\hat{t} = m_B t$ and $\hat{s} = m_B s$ are the rescaled variables that involve the hard scale associated to the large energy transfer. We omit the charge label Q_2 in the following until we present the final results.

A standard power counting analysis shows that the operators scale as $\mathcal{O}^{\mathrm{I}} \sim \lambda^3$ and $\mathcal{O}^{\mathrm{II}} \sim \lambda^{7/2}$ when pure hard-collinear scaling for the fields is assumed. Hence, we would naively expect the second operator to be power-suppressed. However, we require an additional insertion of subleading $\mathcal{L}_{\xi q}$ Lagrangians with different powers to match the quantum numbers of the external states

$$i\int d^4x T\{\mathcal{O}^{\mathrm{I}}(t), \mathcal{L}_{\xi q}^{(1)}(x)\} \sim i\int d^4x T\{\mathcal{O}^{\mathrm{II}}(t,s), \mathcal{L}_{\xi q}^{(1/2)}(x)\} \sim \lambda^4 . \tag{4.10}$$

This is related to the fact that the operator $\mathcal{O}^{\mathrm{II}}$ can be associated with the transverse photon polarizations only as discussed in Appendix C.2. We conclude that both operators contribute at the same power. Note that after matching onto $\mathrm{SCET_{II}}$, the four external light quarks of the outgoing mesons have collinear scalings $\xi_{c,\bar{c}} \sim \lambda$ so that the power is reduced by another factor of λ^2 in total and the operators count as $\mathcal{O}(\lambda^6)$ effectively. Furthermore, the external states scaling as $\lambda^{-3/2}$ for the B meson and λ^{-2} for the light mesons contribute to the power counting.[2] Altogether, the LP amplitude therefore is of order $\mathcal{O}(\lambda^{5/2})$, consistent with QCD-only.

[2]This property follows from the normalization of light meson states. The light-meson mass introduces an additional factor of λ compared to the heavy meson, see (2.62).

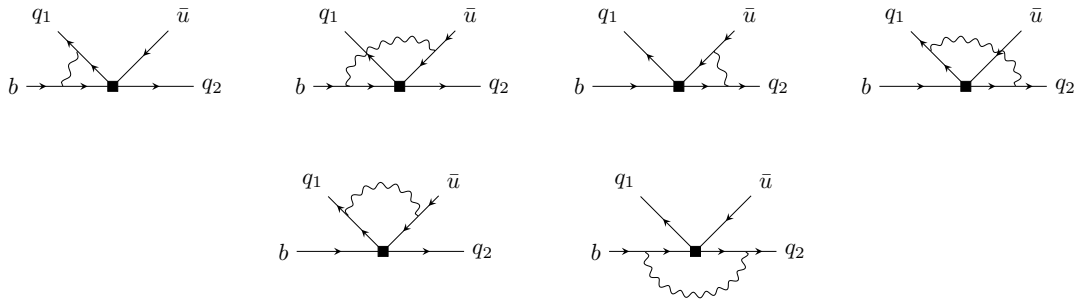

Figure 4.2: One-loop corrections to the four-point transition amplitude $b \to q_1 \bar{u} q_2$. The box denotes a right or wrong insertion of the operators Q_1 and Q_2 in (4.3).

4.1.2 Hard region computation

The factorization in SCET_I is based on integrating out the hard region in a method of regions approach we discussed in Sec. 2.2. To calculate the hard region, we proceed in complete analogy to the derivation in Chapter 2 and replace the external states in the non-radiative matrix element in the partonic picture

$$\big\langle M_1(p) M_2(q) \big| Q_i \big| \bar{B}(p+q) \big\rangle \to \big\langle \bar{q}(p_q) q_2(p_{q_2}) q_1(q_{q_1}) \bar{u}(q_u) \big| Q_i \big| b(m_b v) \bar{q}_\text{s}(l) \big\rangle \,. \tag{4.11}$$

We work in the B-meson rest frame where $p_B = m_B v$, such that the momenta of the two outgoing mesons are parametrized by $p^\mu = E_{M_1} n_-^\mu$ and $q^\mu = E_{M_2} n_+^\mu$, where $E_{M_1} = E_{M_2} = m_B/2$ and $n_\pm^\mu$ defined in (2.3). Most generally, the momenta of the leading valence quark states can be parametrized by

$$\begin{aligned}
p_b^\mu &= m_b v^\mu + k_\text{res}^\mu \,, & l^\mu &= \omega \frac{n_+^\mu}{2} + l_\perp^\mu + l_- \frac{n_-^\mu}{2} \,, \\
k_{q_1}^\mu &= u E_{M_2} n_+^\mu + k_{q_1\perp}^\mu + \frac{k_{q_1}^2}{2 u E_{M_2}} \frac{n_-^\mu}{2} \,, & k_{\bar{u}}^\mu &= \bar{u} E_{M_2} n_+^\mu + k_{\bar{u}\perp}^\mu + \frac{k_{\bar{u}}^2}{2 \bar{u} E_{M_2}} \frac{n_-^\mu}{2} \,, \\
k_{q_2}^\mu &= v E_{M_1} n_+^\mu + k_{q_2\perp}^\mu + \frac{k_{q_2}^2}{2 v E_{M_1}} \frac{n_+^\mu}{2} \,, & k_{\bar{q}}^\mu &= \bar{v} E_{M_1} n_+^\mu + k_{\bar{q}\perp}^\mu + \frac{k_{\bar{q}}^2}{2 \bar{v} E_{M_1}} \frac{n_+^\mu}{2} \,.
\end{aligned} \tag{4.12}$$

In what follows, we can typically neglect the residual momentum k_res^μ of the b-quark as well as the transverse component of the (anti-)collinear quarks that are all of $\mathcal{O}(\Lambda_\text{QCD})$. The off-shellness k_q^2 for the light quarks has to be kept to regulate the soft and collinear IR divergences in the soft and collinear matrix elements, even though they are of subleading order $\mathcal{O}(\Lambda_\text{QCD}^2)$.

The $\mathcal{O}(\alpha_\text{em})$ corrections to (4.11) can arise from i) one-loop (form factor) and ii) tree-level (spectator scattering) interactions, which have hard and hard-collinear virtualities respectively. The spectator quark momentum $l \sim (\lambda, \lambda, \lambda)$ scales soft and appears only in the spectator scattering term since it requires a hard-collinear interaction to

turn collinear in the M_1 final state. In this section, we focus on the hard one-loop effects of the form factor terms i) and calculate the one-loop corrections to the four-point amplitude $b \to q_1 \bar{u} q_2$. The corresponding Feynman diagrams are depicted in Fig. 4.2. The hard-collinear spectator-scattering is computed in Sec. 4.4. To explain the fundamental steps of the calculation, we restrict ourselves to the computation of the hard region of the first diagram in Fig. 4.2 for the right insertion of the operator Q_2. For this particular case, the partonic calculation yields

$$R_{\rm h}^{(1a)} = -ie^2 Q_d Q_{q_1} \tilde{\mu}^{2\epsilon} \int \frac{d^dk}{(2\pi)^d} \frac{1}{[(k+k_{q_1})^2+i0][k^2+2m_b vk+i0][k^2+i0]} \tag{4.13}$$

$$\times [\bar{u}(k_{q_2})\gamma^\mu(1-\gamma_5)(m_b \not{v} + m_b + \not{k}_{q_1})\gamma^\nu u(p_b)][\bar{u}(k_{q_1})\gamma_\nu(\not{k}+\not{k}_{q_1})\gamma_\mu(1-\gamma_5)v(k_{\bar{u}})] \,,$$

$$= \frac{\alpha_{\rm em} Q_d Q_{q_1}}{4\pi}\left[\left(\frac{1}{\epsilon_{\rm UV}} - \frac{1}{\epsilon^2} - \frac{1}{\epsilon}\left(2 + \ln\frac{\mu^2}{m_B^2} - 2\ln u\right) - 2 - \frac{\pi^2}{12} + \frac{2-3u}{\bar{u}}\ln u - \ln^2 u\right.\right.$$

$$\left.\left. + \ln\frac{\nu^2}{m_B^2} - 2\ln\frac{\mu^2}{m_B^2} + 2\ln u \ln\frac{\mu^2}{m_B^2} - \frac{1}{2}\ln^2\frac{\mu^2}{m_B^2} + 2{\rm Li}_2\left(-\frac{\bar{u}}{u}\right)\right)\langle \mathcal{O}^{\rm I}\rangle + \frac{3}{4\epsilon_{\rm UV}}\langle \mathcal{E}^{\rm I}\rangle\right] .$$

The results for the wrong insertion including the remaining diagrams can be found in Appendix C.1. At LP, we do not distinguish between the b-quark pole mass m_b and the B-meson mass m_B since the difference is $\mathcal{O}(\lambda^{1/2})$. We treat γ_5 in the NDR scheme and define the tree-level matrix elements in (4.13)

$$\langle \mathcal{O}^{\rm I}\rangle = [\bar{u}(k_{q_1})\frac{\not{n}_-}{2}(1-\gamma_5)v(k_{\bar{u}})][\bar{u}(k_{q_2})n_+(1-\gamma_5)u(p_b)] \,, \tag{4.14}$$

$$\langle \mathcal{E}^{\rm I}\rangle = [\bar{u}(k_{q_1})\frac{\not{n}_-}{2}(1-\gamma_5)\gamma_\perp^\mu\gamma_\perp^\nu v(k_{\bar{u}})][\bar{u}(k_{q_2})n_+(1-\gamma_5)\gamma_{\perp\nu}\gamma_{\perp\mu}u(p_b)] \,. \tag{4.15}$$

Note that the external spinors refer to the LP momentum components in (4.12) and therefore coincide in QCD×QED and HQET×SCET$_{\rm I}$. Hence, we conclude that the hard region can be reduced to two operator structures. The first term corresponds to the operator $\mathcal{O}^{\rm I}$ defined in (4.4), while the second operator originates from an evanescent contribution that was not present at tree level. At the one-loop order in $d \neq 4$, it cannot be removed by a Fierz transformation. Instead, we extend the operator basis to include evanescent operators that account for "Fierz related" expressions. These operators enter with a UV pole that requires renormalization and generally can enter matrix elements $\langle Q_i\rangle$ with finite terms of the form $\mathcal{O}(\epsilon)/\epsilon_{\rm UV}$. On the QCD×QED-side, we therefore define the evanescent operators

$$E_1^{(1)} = \bar{u}\gamma^\mu\gamma^\nu\gamma^\rho T^a(1-\gamma_5)b \;\; \bar{D}\gamma_\mu\gamma_\nu\gamma_\rho T^a(1-\gamma_5)u - 16Q_1 \,,$$

$$E_2^{(1)} = \bar{u}\gamma^\mu\gamma^\nu\gamma^\rho(1-\gamma_5)b \;\; \bar{D}\gamma_\mu\gamma_\nu\gamma_\rho(1-\gamma_5)u - 16Q_2 \,, \tag{4.16}$$

which vanish in $d = 4$ space-time dimensions. In the following, we show that the renormalization of these operators removes the UV pole proportional to $\langle \mathcal{E}^{\rm I}\rangle$ appearing in the last line of (4.13).

4.1.3 Renormalization of the hard region

In Chapter 2, we observed that the hard matching coefficient corresponds to the renormalized hard region, which included the external field and current renormalization. In the present context, we additionally encounter UV divergent as well as finite terms from the evanescent operators. To consistently renormalize the hard region, we follow the procedure in [53]. The matrix element of an operator Q_i takes the general form

$$\langle Q_i \rangle = \left\{ A_i^{(0)} + \frac{\alpha_{\rm em}}{4\pi} \left[A_i^{(1)} + Z_{\rm ext}^{(1)} A_i^{(0)} + Z_{ij}^{(1)} A_j^{(0)} \right] + \mathcal{O}(\alpha_{\rm em}^2) \right\} \left\langle \mathcal{O}^{\rm I/II} \right\rangle^{(0)} \ , \tag{4.17}$$

where $\langle \mathcal{O} \rangle^{(0)}$ denotes HQET×SCET$_{\rm I}$ operator at tree-level. At the one-loop order, the tree-level factor $A_i^{(0)}$ is multiplied with the on-shell $\overline{\rm MS}$ factors

$$Z_b^{(1)} = -\frac{Q_d^2}{2} \left(\frac{1}{\epsilon_{\rm UV}} + \frac{2}{\epsilon} + 4 + \ln \frac{\nu^2}{m_b^2} + 2 \ln \frac{\mu^2}{m_b^2} \right) , \tag{4.18}$$

$$Z_q^{(1)} = -\frac{Q_q^2}{2} \left(\frac{1}{\epsilon_{\rm UV}} - \frac{1}{\epsilon} + \ln \frac{\nu^2}{\mu^2} \right) . \tag{4.19}$$

The light quark factor is strictly included for every $q = q_1, \bar{u}, q_2$, so that the external factor $Z_{\rm ext}^{(1)} = Z_b^{(1)} + \sum_q Z_q^{(1)}$ consists of four contributions in total. The remaining UV divergences are absorbed into the current renormalization

$$Z_{ij}^{(1)} = \frac{1}{\epsilon_{\rm UV}} \begin{pmatrix} 6Q_uQ_d & 0 & \frac{1}{4}(Q_u^2 + Q_d^2 + 2Q_uQ_d) & 0 \\ 0 & 6Q_uQ_d & 0 & \frac{1}{4}(Q_u^2 + Q_d^2 + 2Q_uQ_d) \end{pmatrix} , \tag{4.20}$$

where the coloumn index j refers to the extended operator basis $(Q_1, Q_2, E_1^{(1)}, E_2^{(1)})$. We emphasize that $Z_{ij}^{(1)}$ includes the renormalization for the evanescent operators defined in (4.16). From (4.17), we can read off the hard matching coefficients

$$H_i^{\rm I/II(0)} = A_i^{(0)} \ , \tag{4.21}$$

$$H_i^{\rm I(1)} = A_i^{(1)} + \left(Z_{\rm ext}^{(1)} - Y^{(1)} \right) A_i^{(0)} + Z_{ij}^{(1)} A_j^{(0)} \ . \tag{4.22}$$

In the second line, we subtracted the factor $Y^{(1)}$ that removes the IR divergences in hard region corresponding to the UV renormalization for the operator $\mathcal{O}^{\rm I}$ in HQET×SCET$_{\rm I}$. We remark that (4.17) and (4.22) hold for both right and wrong insertion of the operators Q_i and in particular for $\mathcal{O}^{\rm I}$ and $\mathcal{O}^{\rm II}$ simultaneously. Since the latter operator is a tree-level contribution, we omitted the corresponding index in (4.22). In principle, the evanescent contributions also need to be included for the wrong insertion on the EFT side. However, the difference $Y^{(1)} - \widetilde{Y}^{(1)}$ turns out to be $\mathcal{O}(\epsilon)$ and can thus be neglected since we renormalize the difference $\mathcal{O}^{\rm I} - \widetilde{\mathcal{O}}^{\rm I}$ to zero.

4.2 SCET$_\mathrm{I}$ factorization

To renormalize the hard region consistently, we need to determine the UV renormalization in SCET$_\mathrm{I}$ and therefore derive the operator renormalization $Y^{(1)}$ of $\mathcal{O}^{\mathrm{I/II}}$. We recall that at LP soft and (anti)-collinear modes interact separately through the leading SCET Lagrangian (2.43). On the EFT side, both operators involve the anti-collinear building block $\bar{\chi}^{(q_1)}(tn_-)\not{n}_-(1-\gamma_5)\chi^{(u)}/2$ that is multiplied to the A0- and B1-type currents. We factorize both structures in (4.4) and (4.5) by applying the decoupling transformation (2.67) to the anti-collinear fields

$$\xi^{(q)}_{\bar{\mathrm{C}}}(x) \to S^{(q)}_{n_+}(x)\xi^{(q)}_{\bar{\mathrm{C}}}(x)\,, \qquad\qquad G^{\mu}_{\bar{\mathrm{C}}}(x) \to S_{n_+}(x)G^{(0)}_{\bar{\mathrm{C}}}(x)S^{\dagger}_{n_+}(x)\,. \tag{4.23}$$

The QED-generalized soft Wilson line is defined by

$$S^{(q)}_{n_\pm}(x) = \exp\left\{-iQ_q e\int_0^\infty ds\, n_\pm A_s(x+sn_\pm)\right\} S_{n_\pm}(x), \tag{4.24}$$

where $S_{n_\pm}$ refers to the QCD definition in (2.49) with one exception: The decoupling corresponds to outgoing (anti-)particles such that the $i0$-prescription must be adjusted. Hence, we use

$$S_{n_\pm}(x) \to \mathbf{P}\exp\left\{-ig_s\int_0^\infty ds\, n_\pm G_\mathrm{s}(x+sn_\pm)\right\}. \tag{4.25}$$

Note that the QCD part of the Wilson line (4.24) for the decoupling of $A^{\mu}_{\bar{\mathrm{C}}}$ combines to unity. Since $U(1)$ is abelian, the anti-collinear photon field requires no decoupling transformation. As a consequence, the anti-collinear building block factorizes from the heavy-to-light currents. After decoupling, the SCET$_\mathrm{I}$ operators read

$$\mathcal{O}^{\mathrm{I}}(t) = [\bar{\chi}^{(q_1)}_{\bar{\mathrm{C}}}(tn_-)\frac{\not{n}_-}{2}(1-\gamma_5)\chi^{(u)}_{\bar{\mathrm{C}}}(0)][\bar{\chi}^{(q_2)}_{\mathrm{C}}(0)\not{n}_+(1-\gamma_5)S^{\dagger(Q_{M_2})}_{n_+}h_v(0)]\,, \tag{4.26}$$

$$\begin{aligned}\mathcal{O}^{\mathrm{II}\gamma}(t,s) = {}& \frac{1}{m_b}[\bar{\chi}^{(q_1)}_{\bar{\mathrm{C}}}](tn_-)\frac{\not{n}_-}{2}(1-\gamma_5)\chi^{(u)}_{\bar{\mathrm{C}}}(0)] \\ & \times [\bar{\chi}^{(q_2)}_{\mathrm{C}}(0)\frac{\not{n}_+}{2}\not{\mathcal{A}}_{\perp\mathrm{C}}(sn_+)(1+\gamma_5)S^{\dagger(Q_{M_2})}_{n_+}h_v(0)]\,.\end{aligned} \tag{4.27}$$

The soft Wilson line $S^{\dagger(Q_{M_2})}_{n_+} = S^{\dagger(q_1)}_{n_+}S^{(u)}_{n_+}$ is the combination from the decoupling of the anti-collinear fields and is located at the origin. The QCD part of this Wilson line cancels and the position space argument tn_- in the first field has been multipole expanded. Due to the factorization of the anti-collinear sector, we can split the renormalization factor into two contributions

$$Y^{(1)}(u,v) = Z^{(1)}_J\delta(u-v) + Z^{(1)}_{\bar{\mathrm{C}}}(u,v)\,. \tag{4.28}$$

In QCD-only, the renormalization kernel (4.28) corresponds to the serparate divergent parts of the soft-collinear and anti-collinear building blocks. As we see in the following,

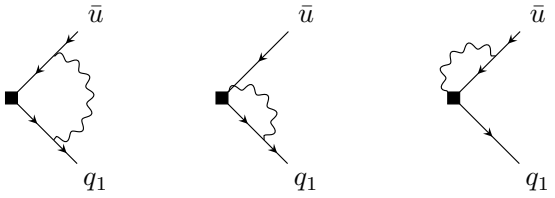

Figure 4.3: One-loop diagrams at $\mathcal{O}(\alpha_{\rm em})$ that contribute to the anomalous dimensions of the operator (4.29).

this will not be the case for QED a priori since soft photons between the meson M_2 and the $B \to M_1$ transition do not decouple when M_2 is electrically charged. Nevertheless, the meson M_2 can be already factorized at the scale m_b due to the soft rearrangement presented in 4.2.3.

4.2.1 Anti-collinear kernel

We first address the calculation of $Z_{\bar{\rm C}}^{(1)}$, that is the renormalization of the anti-collinear operator

$$\mathcal{O}_{\bar{\rm C}}(u) = \int \frac{d\hat{t}}{2\pi} e^{-i\hat{t}u} [\bar{\chi}_{\bar{\rm C}}^{(q_1)}(tn_-) \frac{\not{n}_-}{2}(1-\gamma_5)\chi_{\bar{\rm C}}^{(u)}(0)] \,, \tag{4.29}$$

where $\hat{t} = 2E_{M_1}t$. The QED corrections involve three diagrams, depicted in Fig. 4.3. We calculate the matrix elements with the external quark momenta in (4.12) and neglect the transverse component. The off-shellness serves as a regulator for soft and collinear IR divergences and has to be kept. Hence all poles are of UV nature. The renormalization factor including the external $\overline{\rm MS}$ field renormalization is defined by

$$\mathcal{O}_{\bar{\rm C}}^{\rm ren}(u) = \int_0^1 dv \; Z_{\bar{\rm C}}(u,v;\mu) \; \mathcal{O}_{\bar{\rm C}}^{\rm bare}(v) \,. \tag{4.30}$$

The bare diagrams are given by

$$\begin{aligned}
\langle \mathcal{O}_{\bar{\rm C}} \rangle^{(1a)} &= 2ie^2 Q_{q_1} Q_u \langle \mathcal{O}_{\bar{\rm C}} \rangle^{(0)} \tilde{\mu}^{2\epsilon} \int \frac{d^dk}{(2\pi)^d} \frac{(1-\epsilon)\; \vec{k}_\perp^{\,2} \; \delta(u-v-n_-k/2E_{M_1})}{[k^2+i0][(k-k_{q_1})^2+i0][(k+k_u)^2+i0]} \\
&= \frac{\alpha_{\rm em} Q_{q_1} Q_u}{4\pi} \frac{2}{\epsilon} \left\{ \theta(v-u)\theta(u) \frac{u}{v} + \theta(u-v) \frac{\bar{u}}{\bar{v}} \right\} \langle \mathcal{O}_{\bar{\rm C}} \rangle^{(0)} + \mathcal{O}(\epsilon^0) \,, \qquad (4.31) \\
\langle \mathcal{O}_{\bar{\rm C}} \rangle^{(1b)} &= 2ie^2 Q_{q_1} \langle \mathcal{O}_{\bar{\rm C}} \rangle^{(0)} \\
&\quad \times \tilde{\mu}^{2\epsilon} \int \frac{d^dk}{(2\pi)^d} \frac{n_-(k+k_{q_1}) \left(Q_u \delta(u-v-n_-k/2E_{M_1}) - Q_{q_1} \delta(u-v) \right)}{[k^2+i0][n_-k+i0][(k+k_{q_1})^2+i0]}
\end{aligned}$$

$$= \left\{ \frac{\alpha_\mathrm{em} Q_{q_1} Q_u}{4\pi} 2\Gamma(\epsilon) \left(\frac{4\pi\tilde{\mu}^2}{-k_{q_1}^2}\right)^\epsilon \frac{\theta(v-u)\theta(u)}{v} \left(1-\frac{u}{v}\right)^{-1-\epsilon} \left(\frac{u}{v}\right)^{1-\epsilon} \right.$$

$$\left. - \frac{\alpha_\mathrm{em} Q_{q_1}^2}{4\pi} \frac{2\Gamma(\epsilon)\Gamma(-\epsilon)\Gamma(2-\epsilon)}{\Gamma(2-2\epsilon)} \left(\frac{4\pi\tilde{\mu}^2}{-k_{q_1}^2}\right)^\epsilon \delta(u-v) \right\} \langle \mathcal{O}_{\bar{\mathrm{C}}} \rangle^{(0)} + \mathcal{O}(\epsilon^0) \,, \quad (4.32)$$

$$\langle \mathcal{O}_{\bar{\mathrm{C}}} \rangle^{(1c)} = 2ie^2 Q_u \langle \mathcal{O}_{\bar{\mathrm{C}}} \rangle^{(0)}$$

$$\times \tilde{\mu}^{2\epsilon} \int \frac{d^dk}{(2\pi)^d} \frac{n_-(k+k_u)\left(Q_{q_1}\delta(u-v+n_-k/2E_{M_1}) - Q_u\delta(u-v)\right)}{[k^2+i0][n_-k+i0][(k+k_u)^2+i0]}$$

$$= \left\{ \frac{\alpha_\mathrm{em} Q_{q_1} Q_u}{4\pi} 2\Gamma(\epsilon) \left(\frac{4\pi\tilde{\mu}^2}{-k_u^2}\right)^\epsilon \frac{\theta(u-v)}{\bar{v}} \left(\frac{u-v}{\bar{v}}\right)^{-1-\epsilon} \left(\frac{\bar{u}}{\bar{v}}\right)^{1-\epsilon} \right.$$

$$\left. - \frac{\alpha_\mathrm{em} Q_u^2}{4\pi} \frac{2\Gamma(\epsilon)\Gamma(-\epsilon)\Gamma(2-\epsilon)}{\Gamma(2-2\epsilon)} \left(\frac{4\pi\tilde{\mu}^2}{-k_u^2}\right)^\epsilon \delta(u-v) \right\} \langle \mathcal{O}_{\bar{\mathrm{C}}} \rangle^{(0)} + \mathcal{O}(\epsilon^0) \,. \quad (4.33)$$

In the results above, the variable u refers to the Fourier-conjugate variable t of the anti-collinear operator while v is the variable of the external momenta. To avoid confusion, we note that we used u for the anti-collinear momenta before in the parametrization (4.12).

The non-local terms proportional to $\theta(u-v)$ in (4.32) and (4.33) may contain additional divergences, which can arise in the limit $u \to v$ from the convolution with the operator $\mathcal{O}_{\bar{\mathrm{C}}}(u)$. We extract the true UV behaviour by introducing the plus-distribution (in the variable u)

$$\int_0^1 du \left[\dots\right]_+^{(u)} f(u) \equiv \int_0^1 du \left[\dots\right] (f(u) - f(v)) \,, \quad (4.34)$$

which regulates divergences from the limit $u \to v$. Then, the total result from (4.31)–(4.33) including the light quark renormalization takes the form

$$V(u,v) = Q_{q_1} Q_u \left[\left(1 + \frac{1}{v-u}\right) \frac{u}{v} \theta(v-u) + \left(1 + \frac{1}{u-v}\right) \frac{1-u}{1-v} \theta(u-v) \right]_+^{(u)} \quad (4.35)$$

$$+ \delta(u-v) \left((Q_{q_1} - Q_u)^2 \left(\frac{1}{\epsilon} + \frac{3}{4}\right) + (Q_{q_1} - Q_u) \left(Q_{q_1} \ln \frac{\mu^2}{-k_{q_1}^2} - Q_u \ln \frac{\mu^2}{-k_{\bar{u}}^2} \right) \right) .$$

For convenience, we defined

$$Z_{\bar{\mathrm{C}}}^{(1)}(u,v) = -\frac{2}{\epsilon} V(u,v) \,. \quad (4.36)$$

For $q_1 = u$, the meson is electrically neutral and the first line of (4.35) vanishes. In this case, we obtain the ERBL evolution kernel [134–136] that describes the scale evolution of light-meson LCDAs. From the neutral case, the QCD limit can be obtained by sending $\alpha_\mathrm{em} Q_u^2 \to \alpha_s C_F$. For $q_1 = d, s$ when the meson is electrically charged, the

renormalization factor contains a $1/\epsilon^2$ pole and depends on the off-shellness $k_{q_1}^2$ and k_u^2. The former implies that the LCDA kernel has a cusp logarithm. From the latter follows that the anomalous dimension a priori is ill-defined since it depends on the IR regulators. The corresponding logarithmic terms in (4.32) and (4.33) originate from the limit where the photon momentum becomes soft. Hence, it can be interpreted as a soft overlap with the remaining heavy-to-light operator. We discuss the cancellation of the soft overlap contribution between the (anti-)collinear operators in Sec. 4.2.3.

4.2.2 Generalized heavy-to-light current

After the decoupling of the anti-collinear sector, the operator $\mathcal{O}^{\mathrm{I}}$ contains the QED-generalized heavy-to-light current that we define as

$$\mathcal{J}^{(\mathrm{A0})}(0,0) = \bar{\chi}_C^{(q_2)}(0)\not{n}_+(1-\gamma_5)S_{n_+}^{\dagger(Q_{M_2})}h_v(0)\ . \tag{4.37}$$

The operator renormalizes locally with $\mathcal{J}^{\mathrm{ren}} = Z_J^{(1)}\mathcal{J}^{\mathrm{bare}}$. As discussed below (4.27), the soft Wilson line with charge Q_{M_2} originates from the anti-collinear q_1- and u-quark fields. It inherits the off-shellness of the external quark momenta, which can be seen from a simple analysis of an outgoing anti-collinear propagator with incoming soft momentum k

$$\frac{\not{k}_{q_1}-\not{k}}{(k_{q_1}-k)^2+i0} \approx \frac{n_-k_{q_1}\frac{\not{n}_+}{2}}{n_-k_{q_1}(n_+k-\delta_{\bar{\mathrm{c}}})}\ . \tag{4.38}$$

Consequently, we need to replace $n_+k - i0 \to n_+k - \delta_{\bar{\mathrm{c}}}$ for the Feynman rule in the soft Wilson line

$$\frac{-eQ_{M_2}n_+^\mu}{n_+k-\delta_{\bar{\mathrm{c}}}}\ , \qquad \delta_{\bar{\mathrm{c}}} \equiv \frac{k_{q_1}^2}{(n_-k_{q_1})} + i0 = \frac{k_{\bar{u}}^2}{(n_-k_{\bar{u}})} + i0\,, \tag{4.39}$$

which arises from the first-order expansion $S_{n_+}^{\dagger(Q_{M_2})}(0) \approx 1 - \frac{eQ_{M_2}}{in_+\partial - i0}n_+A_{\mathrm{s}}(0) + \mathcal{O}(e^2)$. This was already discussed in Appendix A of [60]. The definition of $\delta_{\bar{\mathrm{c}}}$ in (4.39) imposes a relation between the off-shellness of the q_1- and the $\bar{u}$-quark of the meson M_2. At first sight, those should be independent, however, we require equality in (4.39) so that the identity $S^{\dagger Q_{M_2}} = S^{\dagger(q_1)}S^{(u)}$ is maintained. In addition, we introduce an off-shellness for the light quark q_2 according to (4.12). Including the $\overline{\mathrm{MS}}$ renormalization factors for h_v and ξ_c, we obtain

$$\begin{aligned} Z_J^{(1)} = &-Q_d^2\left\{\frac{1}{\epsilon^2}+\frac{1}{\epsilon}\left[L+\frac{5}{2}\right]\right\} + 2Q_{M_2}Q_d\left\{\frac{1}{\epsilon^2}+\frac{1}{\epsilon}\left[L+\frac{3}{2}+i\pi\right]\right\} \\ &- Q_{M_2}^2\frac{1}{\epsilon}\left[L+\frac{3}{2}+2\ln\left(\frac{-\delta_{\bar{\mathrm{c}}}}{\mu}\right)+i\pi\right], \end{aligned} \tag{4.40}$$

where we defined

$$L \equiv \ln\left(\frac{\mu^2}{m_B^2}\right)\ . \tag{4.41}$$

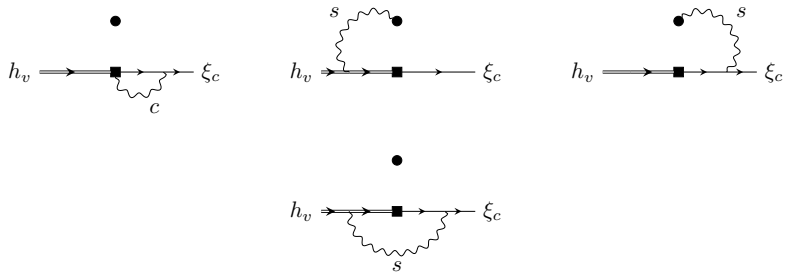

Figure 4.4: $\mathcal{O}(\alpha_\mathrm{em})$ corrections to the generalized heavy-to-light current (4.37) in SCET$_\mathrm{I}$. The black dot represents the soft Wilson line $S_{n_+}^{\dagger(Q_{M_2})}$. Diagrams for the external field renormalization are not shown.

We recover the QCD result [53] for the renormalization of the heavy-to-light current from the neutral case $Q_{M_2} = 0$ together with the replacement $Q_d^2 \to C_F$. At one-loop in QED-only, the renormalization of the second heavy-to-light current

$$\mathcal{J}^{(\mathrm{B1})}(0,s,0) = \frac{1}{m_b}[\bar{\chi}_\mathrm{C}^{(q_2)}(0)\frac{\not{n}_+}{2}\mathcal{A}_{\perp\mathrm{C}}(sn_+)(1+\gamma_5)S_{n_+}^{\dagger(Q_{M_2})}h_v(0)] \tag{4.42}$$

agrees with Z_J in (4.40) due to the absence of photon self-interactions.[3] Both (A0)- and (B1)-type currents are multiplied with the same anti-collinear operator $\mathcal{O}_{\bar{\mathrm{C}}}$. Hence the operator $\mathcal{O}^\mathrm{II}$ renormalizes in the same way as $\mathcal{O}^\mathrm{I}$ at this order.

4.2.3 Soft rearrangement

From the one-loop counter terms (2.82) with (4.35) and (4.40), we obtain the operator renormalization for the SCET$_\mathrm{I}$ operator

$$\begin{aligned} Y^{(1)}(u,v) = \delta(u-v)\Bigg(&- Q_d^2\left\{\frac{1}{\epsilon^2}+\frac{1}{\epsilon}\left[L+\frac{5}{2}\right]\right\} + 2Q_{M_2}Q_u\left\{\frac{1}{\epsilon^2}+\frac{1}{\epsilon}\left[L+\frac{3}{2}+i\pi\right]\right\} \\ &+ \frac{2}{\epsilon}Q_{M_2}\Big[Q_d\ln u - Q_u\ln(1-u)\Big]\Bigg) \\ &- \frac{2}{\epsilon}Q_u\left(Q_u+Q_{M_2}\right)\left[\left(1+\frac{1}{v-u}\right)\frac{u}{v}\theta(v-u)+\left(1+\frac{1}{u-v}\right)\frac{\bar{u}}{\bar{u}}\theta(u-v)\right]_+ . \end{aligned} \tag{4.43}$$

An important observation is that the result does not depend on the off-shellness of the external quarks, more precisely the IR regularization. For an electrically charged meson with $Q_{M_2} \neq 0$, the IR regulators appear in each of the separate sectors and prevent a consistent factorization. We can restore factorization of the anti-collinear

[3] Furthermore, the renormalization of the current operator does not depend on the Dirac structure between the soft and collinear fields.

sector and the $\bar{B} \to M_1$ transition by introducing a soft rearrangement that removes the overlap between those two. To this end, we consider similar to [60] the vacuum matrix element[4]

$$\left|\langle 0|\left[S_{n_-}^{(Q_{M_2})} S_{n_+}^{\dagger(Q_{M_2})}\right](0)\,|0\rangle\right| \equiv R_c^{(Q_{M_2})} R_{\bar{c}}^{(Q_{M_2})} \tag{4.44}$$

that defines the two rearrangement factors R_c and $R_{\bar{c}}$. In dimensional regularization, the on-shell vacuum matrix element (4.44) vanishes to all orders in the electromagnetic coupling as soft Wilson lines only produce scaleless integrals. However, we recall that the soft Wilson lines still inherit the off-shellness from the (anti-)collinear momenta after the soft decoupling. For the collinear direction n_-, we this implies a similar replacement to (4.38) and (4.39) for the Feynman rule with incoming momentum k, that is

$$\frac{1}{n_- k - i0} \to \frac{1}{n_- k - \delta_{\rm c}}\,, \qquad \delta_{\rm c} \equiv \frac{k_{\bar{u}}^2}{n_+ k_{\bar{u}}} + i0 = \frac{k_q^2}{n_+ k_q} + i0\,. \tag{4.45}$$

We expand the Wilson lines up to one-loop order and find

$$\begin{aligned}\langle 0|(S_{n_-}^{(Q_{M_2})} S_{n_+}^{\dagger(Q_{M_2})})(0)\,|0\rangle &= 1 + \tilde{\mu}^{2\epsilon} \int \frac{d^d k}{(2\pi)^d} \frac{-2i}{k^2 + i0} \frac{eQ_{M_2}}{n_- k + \delta_{\rm c}} \frac{eQ_{M_2}}{n_- k - \delta_{\bar{c}}} \qquad (4.46)\\ &= 1 - \frac{\alpha_{\rm em}}{4\pi} Q_M^2 \left[\frac{2}{\epsilon^2} + \frac{2}{\epsilon}\ln\frac{\mu}{-\delta_{\rm c}} + \frac{2}{\epsilon}\ln\frac{\mu}{-\delta_{\bar{c}}} - \frac{2i\pi}{\epsilon}\right.\\ &\quad \left. + \ln^2\frac{\mu}{-\delta_{\rm c}} + \ln^2\frac{\mu}{-\delta_{\bar{c}}} + 2\ln\frac{\mu}{-\delta_c}\ln\frac{\mu}{-\delta_{\bar{c}}} - \frac{\pi^2}{2} - 2i\pi\left(\ln\frac{\mu}{-\delta_{\rm c}} + \ln\frac{\mu}{-\delta_{\bar{c}}}\right)\right]\,.\end{aligned}$$

In the calculation, we assumed $\mathrm{Re}(\delta_{c,\bar{c}}) < 0$, which can be done since the UV renormalization of the entire effective operator does not depend on the IR regulators. The imaginary parts in the last line arise from logarithmic terms of the form $\ln(\mu/\delta_{\bar{c}}) = \ln(\mu/(-\delta_{\bar{c}})) - i\pi$ due to the $i0$-prescription of the regulators. To avoid the introduction of spurious rescattering phases in the (anti-)collinear sector, we take the absolute value of (4.46) and obtain

$$R_c^{(Q_{M_1})} = 1 - \frac{\alpha_{\rm em}}{4\pi} Q_{M_1}^2 \left[\frac{1}{\epsilon^2} + \frac{2}{\epsilon}\ln\frac{\mu}{-\delta_{\rm c}} + \ln^2\frac{\mu}{-\delta_{\rm c}} + \ln\frac{\mu}{-\delta_{\rm c}}\ln\frac{\mu}{-\delta_{\bar{c}}} - \frac{\pi^2}{4}\right], \tag{4.47}$$

$$R_{\bar{c}}^{(Q_{M_2})} = 1 - \frac{\alpha_{\rm em}}{4\pi} Q_{M_2}^2 \left[\frac{1}{\epsilon^2} + \frac{2}{\epsilon}\ln\frac{\mu}{-\delta_{\bar{c}}} + \ln^2\frac{\mu}{-\delta_{\bar{c}}} + \ln\frac{\mu}{-\delta_{\rm c}}\ln\frac{\mu}{-\delta_{\bar{c}}} - \frac{\pi^2}{4}\right]. \tag{4.48}$$

We emphasize that we *defined* the factor $R_{\rm c}$ such that the divergent part only contains the collinear off-shell regulator $\delta_{\rm c}$. In the same way, the divergent contribution of $R_{\bar{c}}$ only depends on $\delta_{\bar{c}}$. The finite terms are symmetric and hence $R_{\rm c}$ can be obtained from $R_{\bar{c}}$ by interchanging $n_+ \leftrightarrow n_-$ and $\delta_{\rm c} \leftrightarrow \delta_{\bar{c}}$.[5] To conveniently define the collinear

[4] In our convention n_-^μ, defines the direction of the positively charged M_1 meson in contrast to the direction chosen for ℓ^- in [60]. Moreover, the absolute value was not considered in this publication and the factors $R_{\rm c}$ and $R_{\bar{c}}$ were defined to include the *same* $\delta_{\rm c}$ and $\delta_{\bar{c}}$ dependence.

[5] The definition of $R_{\rm c}$ and $R_{\bar{c}}$ in [66] leaves an ambiguity for the finite terms. This is resolved by the choice in (4.47) and (4.48).

sector, we label the factor R_c with the charge $Q_{M_1} = -Q_{M_2}$.

For the generalized heavy-to-light current, a division by the factor $R_{\bar{\mathrm{c}}}$ in (4.48) yields

$$\begin{aligned} Z_J^{(1)} + R_{\bar{\mathrm{c}}}^{(Q_{M_2})(1)} = & -Q_d^2 \left\{ \frac{1}{\epsilon^2} + \frac{1}{\epsilon}\left[L + \frac{5}{2}\right]\right\} + 2Q_{M_2}Q_d \left\{ \frac{1}{\epsilon^2} + \frac{1}{\epsilon}\left[L + \frac{3}{2} + i\pi\right]\right\} \\ & - Q_{M_2}^2 \left\{ \frac{1}{\epsilon^2} + \frac{1}{\epsilon}\left[L + \frac{3}{2} + i\pi\right]\right\}. \end{aligned} \tag{4.49}$$

Indeed, we find that the total renormalization factor of the current does not contain the IR regulator $\delta_{\bar{\mathrm{c}}}$.

Light-meson LCDA

The soft rearrangement removes the IR regulator dependence in the renormalization factor of the anti-collinear kernel in (4.35). Hence, we multiply the operator $\mathcal{O}_{\bar{\mathrm{C}}}$ in (4.29) by the factor $R_{\bar{\mathrm{c}}}$ from (4.48) and define

$$\langle M_2(p)|R_{\bar{\mathrm{c}}}^{(Q_{M_2})}\,\bar{\chi}_{\bar{\mathrm{c}}}^{(q_1)}(tn_-)\frac{\not{n}_-}{2}(1-\gamma_5)\chi_{\bar{\mathrm{c}}}^{(u)}(0)|0\rangle = \frac{in_-p}{2}\int_0^1 du\, e^{iu(n-p)t} f_{M_2}\Phi_{M_2}(u;\mu)\,. \tag{4.50}$$

This is the operator definition of the leading-twist QED-generalized light-meson LCDA for the meson M_2. The function $\Phi_{M_2}(u;\mu)$ follows an RGE that describes its scale evolution. The anomalous dimension is defined by the equation

$$\frac{d}{d\ln\mu}\Phi_{M_2}(u;\mu) = -\int_0^1 dv\; \Gamma(u,v;\mu)\; \Phi_{M_2}(v;\mu)\,. \tag{4.51}$$

The evolution kernel is a combination of the counter term and the rearrangement factor

$$\Gamma(u,v;\mu) = -\int_0^1 dw\; \frac{dZ_{\bar{\mathrm{C}}}(u,w;\mu)}{d\ln\mu}\; Z_{\bar{\mathrm{C}}}^{-1}(w,v;\mu) - \frac{dR_{\bar{\mathrm{c}}}^{(Q_{M_2})(1)}}{d\ln\mu}\,. \tag{4.52}$$

The one-loop renormalization factor in (4.35), (2.82) and the factor $R_{\bar{\mathrm{c}}}$ from (4.48) yield the one-loop anomalous dimension in QED

$$\begin{aligned} \Gamma^{(1)}(u,v;\mu) = & -\frac{\alpha_\mathrm{em}Q_{M_2}}{\pi}\left(Q_{M_2}\left(\ln\frac{\mu}{2E}+\frac{3}{4}\right) - Q_{q_1}\ln u + Q_u \ln\bar{u}\right)\delta(u-v) \\ & - \frac{\alpha_\mathrm{em}Q_{q_1}Q_u}{\pi}\left[\left(1+\frac{1}{v-u}\right)\frac{u}{v}\theta(v-u) + \left(1+\frac{1}{u-v}\right)\frac{\bar{u}}{\bar{v}}\theta(u-v)\right]_+^{(u)}, \end{aligned} \tag{4.53}$$

which does not depend on $\delta_{\mathrm{c},\bar{\mathrm{c}}}$ anymore. Hence, the UV divergences of the operator in (4.50) have been renormalized consistently. As mentioned below (4.35), we recover the QCD result by sending $Q_{M_2} \to 0$ and $\alpha_\mathrm{em}Q_{q_1}Q_u \to \alpha_s C_F$. We emphasize that (4.53)

defines the scale evolution for both neutral and charged mesons $Q_{M_2} = 0, -1$. Note that we have $R_{\bar{c}}^{(0)} = 1$ by definition. We discuss the solution of (4.52) including the QCD kernel in Sec. 5.1.

The function $\Phi_{M_2}(u;\mu)$ in (4.50) is normalized with respect to the QCD decay constant f_{M_2}, that is defined by the local matrix element $t \to 0$ in the absence of QED. Since f_{M_2} does not evolve under the renormalization group, all QED effects are therefore absorbed into the evolution of Φ_{M_2}. This is a convenient choice since the local operator in QED would mix into higher logarithmic moments by scale evolution. In contrast to QCD-only, this implies that the normalization $\int_0^1 du\, \Phi(u;\mu) \neq 1$ will be violated when QED effects are considered.

We furthermore emphasize that the definition (4.50) is universal. Hence it also applies to the collinear meson M_1 after factorization in SCET_II. Note that the choice of the anti-collinear direction n_+ for the operator required a corresponding collinear vector n_- and vice versa. More generally, we can define for any light-like vector n_{i-} another back-to-back direction n_{i+} that fulfill $n_{i+}n_{i-} = 2$. Note that a specific (anti-)collinear direction does not necessarily need to correspond to a real particle in the process. The soft rearrangement (4.44) then defines a pair R_{c_i} and $R_{\bar{c}_i}$ computed from the corresponding soft Wilson lines for the i-th reference vectors. In this way, we can employ an arbitrary number of light-meson LCDAs after factorizing the soft-collinear interactions. For an n-jet SCET operator, we have

$$\mathcal{O}_\text{eff} = \mathcal{O}_s \times \mathcal{O}_{\text{c}_1}\mathcal{O}_{\text{c}_2}\dots\mathcal{O}_{\text{c}_n} = \frac{\mathcal{O}_s}{R_{\text{c}_1}R_{\text{c}_2}\dots R_{\text{c}_n}} \times (R_{\text{c}_1}\mathcal{O}_{\text{c}_1})(R_{\text{c}_2}\mathcal{O}_{\text{c}_2})\dots(R_{\text{c}_n}\mathcal{O}_{\text{c}_n})\,, \tag{4.54}$$

where each collinear sector is individually renormalized. Since the complete operator $\mathcal{O}_\text{eff}$ has to be renormalizable in a consistent effective theory, the same argument applies to the remaining soft operator. Based on this discussion, we conclude that the QED-generalized light-meson LCDA remains a relevant universal object for exclusive multi-body processes.

We finally remark that the boost invariance of the LCDA is broken due to the large energy dependence $E_{M_2} = m_B/2$ in (4.53). Hence, the definition (4.50) enforces the choice of a "soft reference frame" which is naturally given by the B-meson rest frame for this decay. Moreover, we note that the neutral π^0 meson needs to be described by two distinct quark LCDAs since QED breaks the isospin symmetry between the u- and d-quarks. We can choose between the pair $\Phi_{\pi^0}^{(u)}$ and $\Phi_{\pi^0}^{(d)}$ or the $SU(2)$ singlet and triplet representation. The LCDAs generally mix under renormalization which requires the definition of an additional two-gluon LCDA. In the following, we focus on the case of electrically charged mesons.

$\bar{B} \to M_1$ form factors

Since we multiplied the factor $R_{\bar{c}}$ in the anti-collinear sector, we subtract it in the soft-collinear building blocks. We therefore modify both SCET_I operators $\mathcal{O}^{\text{I/II}}$ according

to (4.54) and obtain

$$\langle M_1(p')|\frac{1}{R_{\bar{c}}^{(Q_{M_2})}}\bar{\chi}_C^{(q)}(0)\not{n}_+(1-\gamma_5)S_{n_+}^{\dagger(Q_{M_2})}h_v(0)|\bar{B}(v)\rangle = 4E_{M_1}\zeta_{Q_2}^{BM_1}(E_{M_1})\,, \tag{4.55}$$

$$\begin{aligned}\langle M_1(p')|&\frac{1}{R_{\bar{c}}^{(Q_{M_2})}}\,\frac{1}{m_b}\bar{\chi}_C^{(q)}(0)\frac{\not{n}_+}{2}\mathcal{A}_{C,\perp}(sn_+)(1+\gamma_5)S_{n_+}^{\dagger(Q_{M_2})}h_v(0)|\bar{B}(v)\rangle\\ &= -2E_{M_1}\int_0^1 d\tau e^{i\tau(n_+p')s}\,\Upsilon_{Q_2}^{BM_1}(E_{M_1},\tau)\,,\end{aligned} \tag{4.56}$$

which defines the generalized SCET$_\mathrm{I}$ $\bar{B}\to M_1$ form factors ζ^{BM_1} and Υ^{BM_1} in the presence of QED. The gluon form factor definition can be obtained from (4.56) upon replacing $\mathcal{A}\to\mathcal{G}$ and $\Upsilon_{Q_2}^{BM_1}(E_{M_1},\tau)\to\Sigma_{Q_2}^{BM_1}(E_{M_1},\tau)$. For vanishing mass $m_{M_1}=0$, the energy of the meson M_1 in the B-meson rest frame is given by $E_{M_1}=n_+p'/2=(m_B^2-q^2)/(2m_B)$. In the QCD-only limit, $\alpha_\mathrm{em}\to 0$ the form factors (ζ,Σ,Υ) turn into $(\xi,\Xi,0)$ in the convention of [49].

The discussion below (4.54) implies that the form factors (4.55) and (4.56) are well-defined. Due to the non-decoupling of the Wilson line $S_{n_+}^{\dagger(Q_{M_2})}$ and the soft rearrangement, these factors depend on the direction of flight n_+ and the charge Q_{M_2} of the outgoing anti-collinear meson through soft interactions. Finally, with the refinements in (4.55), (4.56) and (4.50), we find the SCET$_\mathrm{I}$ factorization formula

$$\begin{aligned}\big\langle M_1M_2\big|Q_i\big|\bar{B}\big\rangle = im_B^2\Big\{&\zeta_{Q_2}^{BM_1}\int_0^1 du\,H_{i,Q_2}^\mathrm{I}(u)f_{M_2}\Phi_{M_2}(u)\\ -\frac{1}{2}\int_0^1 du\,dz\Big[&H_{i,Q_2}^{\mathrm{II}\gamma}(u,z)\,\Upsilon_{Q_2}^{BM_1}(1-z)+H_{i,Q_2}^{\mathrm{II}g}(u,z)\,\Sigma_{Q_2}^{BM_1}(1-z)\Big]f_{M_2}\Phi_{M_2}(u)\Big\}\,.\end{aligned} \tag{4.57}$$

Note that we dropped the energy argument $E_{M_1}=m_B/2$ in the form factors. This completes the factorization proof in SCET$_\mathrm{I}$. For the results of the hard matching coefficients $H^{\mathrm{I/II}}$, we refer to Sec. 4.4.

4.2.4 Semi-leptonic QED factorization

The QED-generalized form factor $\zeta_{Q_2}^{BM_1}$ exclusively contains fields and states defined in the effective theory and is therefore a pure HQET×SCET$_\mathrm{I}$ quantity. In the following, we substitute this object by the full theory QCD×QED form factor

$$\zeta_{Q_2}^{BM_1}(E_{M_1}=m_B/2)\to\mathcal{F}_{Q_2}^{BM_1}(q^2=0),\qquad H_{i,Q_2}^\mathrm{I}(u)\to T_{i,Q_2}^\mathrm{I}(u)\,, \tag{4.58}$$

which can typically be determined with lattice or LCSR methods and hence represents a more suitable object in the factorization formula. The replacement uses a corresponding factorization for the full theory form factor and in general modifies the hard matching coefficient that we define to be T^I [83]. For neutral M_2, the form factor $\zeta_0^{BM_1}$ can

be expressed in terms of standard local heavy-to-light currents. For charged M_2, the additional soft Wilson lines however prevent the matching to local currents as it inherits the electrical charge and direction of flight of M_2. Nevertheless, we can relate the form factor to the semi-leptonic $\bar{B} \to M_1 \ell^- \bar{\nu}$ amplitude, in the kinematic limit where the neutrino becomes soft and the lepton carries almost everything of the momentum so that $q^2 = 0$ and $E_\ell = m_B/2$. In SCET_I, the non-radiative amplitude of $\bar{B} \to M_1 M_2$ contains the same IR behaviour after decoupling the anti-collinear sector, so that we can trade $\zeta_-^{BM_1}$ for $\mathcal{F}_-^{BM_1}$ as discussed below.

The semi-leptonic $b \to u$ transition is mediated by the Hamiltonian in (1.1). We emphasize that in QED the Wilson coefficient $C_\text{sl}(\nu) \neq 1$ is generally scale-dependent due to short-distance corrections from the electroweak scale. We refer to [131] for the one-loop result of C_sl in QED and use it to resum large logarithms $\alpha_\text{em}^n \ln^m(m_W/m_b)$ with $m \leq n$ between m_W and m_b by evolving the scale downwards to $\nu \sim \mathcal{O}(m_b)$. The semi-leptonic amplitude is

$$\begin{aligned}\mathcal{A}_\text{non-rad}^{\text{sl},M_1} &= \frac{G_F}{\sqrt{2}} V_{ub} C_\text{sl} \left\langle M_1 \ell^- \bar{\nu}_\ell \middle| Q_\text{sl} \middle| \bar{B} \right\rangle \\ &\equiv \frac{G_F}{\sqrt{2}} V_{ub}\, 4E_{M_1} [\bar{u}(p_\ell) \frac{\not{n}_-}{2} (1-\gamma_5) v_{\nu_\ell}(p_\nu)]\, \mathcal{A}_\text{red}^{\text{sl},M_1} \,. \end{aligned} \tag{4.59}$$

We define $\mathcal{A}_\text{red}^{\text{sl},M_1}$ in the second line as the "form factor" of this transition. Note that the factor does not depend on the renormalization scale ν since the product $C_\text{sl}\, Q_\text{sl}$ is ν-independent. We follow the same arguments for the factorization of the operators Q_i in the non-leptonic decay to obtain a factorization formula for Q_sl

$$\begin{aligned}\left\langle M_1 \ell^- \bar{\nu}_\ell \middle| Q_\text{sl} \middle| B \right\rangle =\, & 4E_{M_1} [\bar{u}(p_\ell) \frac{\not{n}_-}{2} (1-\gamma_5) v_{\nu_\ell}(p_\nu)]\, Z_\ell \left\{ H_\text{sl}^\text{I}(E_\ell)\, \zeta_-^{BM_1}(E_{M_1}) \right. \\ & \left. - \frac{1}{2} \int_0^1 dz \Big[H_\text{sl}^{\text{II}\gamma}(E_\ell, z)\, \Upsilon_-^{BM_1}(E_{M_1}, 1-z) + H_\text{sl}^{\text{II}g}(E_\ell, z) \Sigma_-^{BM_1}(E_{M_1}, 1-z) \Big] \right\} . \end{aligned} \tag{4.60}$$

In fact, we observe that the same SCET_I form factors appear in (4.57) for the charged meson $Q_{M_2} = -1$. Contrary to the meson M_2 in the non-leptonic decay, the lepton in the semi-leptonic decay is a point-like particle subject to QED-only interactions such that we can factor out the spinor structure in front. This simplifies the analysis of the anti-collinear sector compared to the convolution and renormalization of the light-meson LCDA defined by (4.50). The anti-collinear lepton can be parametrized by a $0 \to \ell$ matrix element of the lepton field $\chi_{\bar{C}}^{(\ell)} = [W_{\bar{C}}^{(\ell)}]^\dagger \xi_{\bar{C}}^{(\ell)}$ defining the renormalization factor Z_ℓ in (4.60) [60]. We regulate the IR divergences off-shell with momentum p_ℓ^2 for the lepton and calculate

$$\left\langle \ell^-(p_\ell) \middle| \bar{\chi}_{\bar{C}}^{(\ell)}(0) \middle| 0 \right\rangle = \bar{u}(p_\ell) \frac{\not{n}_- \not{n}_+}{4} \left\{ 1 + \frac{\alpha_\text{em}}{4\pi} Q_\ell^2 \left[\frac{2}{\epsilon^2} + \frac{3}{2\epsilon} + \frac{2}{\epsilon} \log \frac{\mu^2}{-p_\ell^2} + \mathcal{O}(\epsilon^0) \right] \right\} . \tag{4.61}$$

Once again, we observe that the UV structure depends on the IR regularization, which could be anticipated since the same form factors appear on the right-hand side of (4.57) and (4.60). We remove this dependence by multiplying with the soft rearrangement factor $R_{\bar{\mathrm{c}}}^{(Q_\ell)}$ that is obtained from (4.48) with $Q_{M_2} \to Q_\ell$ and $\delta_{\bar{\mathrm{c}}} \to p_\ell^2/n_-p_\ell$, where $n_-p_\ell = 2E_\ell$. Note that a corresponding factor is subtracted in the form factor definitions of (4.60). The UV renormalization factor for the on-shell matrix element $\langle \ell^-(p_\ell)\big|R_{\bar{\mathrm{c}}}^{(Q_\ell)}\bar{\chi}_{\bar{C}}^{(\ell)}(0)\big|0\rangle$ is then given by the sum of (4.61) and (4.48), that is

$$Z_\ell^{\text{bare}} = 1 + \frac{\alpha_{\text{em}}}{4\pi}Q_\ell^2\left[\frac{1}{\epsilon^2} + \frac{3}{2\epsilon} + \frac{2}{\epsilon}\ln\left(\frac{\mu}{n_-p_\ell}\right) + \mathcal{O}(\epsilon^0)\right]. \tag{4.62}$$

We emphasize that (4.62) is the point-like analogue to the QED-generalized ERBL kernel (4.36).

Finally, the above results can be used to eliminate the SCET$_\mathrm{I}$ form factor $\zeta_-^{BM_1}$ in favour of QCD×QED quantities. As mentioned beforehand, we use the traditional QCD treatment [106] for the neutral $Q_{M_2} = 0$ case. For $Q_{M_2} = -1$, we define

$$\mathcal{F}_-^{BM_1}(q^2=0) \equiv \frac{1}{C_{\text{sl}}Z_\ell}\,\mathcal{A}_{\text{red}}^{\text{sl},M_1}(q^2=0,\ E_\ell = m_B/2)\,. \tag{4.63}$$

Using (4.60), we exchange the SCET$_\mathrm{I}$ form factor in the non-leptonic decay and obtain

$$\begin{aligned}\langle M_1M_2|Q_i|\bar{B}\rangle = im_B^2\Bigg\{&\mathcal{F}_{Q_2}^{BM_1}(0)\int_0^1 du\,T_{i,Q_2}^{\mathrm{I}}(u)\,f_{M_2}\Phi_{M_2}(u) \\ &-\frac{1}{2}\int_0^1 du\,dz\,\Big[\hat{H}_{i,Q_2}^{\mathrm{II}\gamma}(u,z)\Upsilon_{Q_2}^{BM_1}(1-z) + \hat{H}_{i,Q_2}^{\mathrm{II}g}(u,z)\Sigma_{Q_2}^{BM_1}(1-z)\Big]\,f_{M_2}\Phi_{M_2}(u)\Bigg\},\end{aligned} \tag{4.64}$$

which parametrizes the first term in factorization formula (4.57) in terms of general QCD×QED form factors. The modifications for the hard-scattering kernels are given by

$$T_{i,0}^{\mathrm{I}}(u) \equiv \frac{H_{i,0}^{\mathrm{I}}(u)}{H_f^{\mathrm{I}}}\,, \qquad T_{i,-}^{\mathrm{I}}(u;E_\ell) \equiv \frac{H_{i,-}^{\mathrm{I}}(u)}{H_{\text{sl}}^{\mathrm{I}}(E_\ell)}\,. \tag{4.65}$$

In addition, the previously defined coefficients $H_{i,Q_2}^{\mathrm{I/II}}$ in (4.8) change according to

$$\begin{aligned}\hat{H}_{2,-}^{\mathrm{II}\gamma}(u,z;E_\ell) &= H_{2,-}^{\mathrm{II}\gamma}(u,z) - T_{2,-}^{\mathrm{I}}(u;E_\ell)H_{\text{sl}}^{\mathrm{II}\gamma}(z)\,, \\ \hat{H}_{1,0}^{\mathrm{II}\gamma}(u,z) &= C_F\hat{H}_{2,0}^{\mathrm{II}\gamma} = H_{1,0}^{\mathrm{II}\gamma}(u,z) - T_{1,0}^{\mathrm{I}}(u)H_f^{\mathrm{II}\gamma}(z)\,.\end{aligned} \tag{4.66}$$

Note that $\hat{H}_{1,-}^{\mathrm{II}\gamma}$ does not require a redefinition and therefore equals $H_{1,-}^{\mathrm{II}\gamma}$. The coefficients $H_f^{\mathrm{I}(1)}$ and $H_f^{\mathrm{II}\gamma}(z)$ appearing in (4.65) and (4.66) originate from the factorization of the full theory form factors. We can infer them from the semi-leptonic matching coefficients in (4.60) by setting $Q_\ell = 0$. Finally, we indicated an explicit dependence

on the lepton energy E_ℓ for the hard-scattering kernels when M_2 is charged. In fact, we can choose $E_\ell \sim \mathcal{O}(m_B/2)$ arbitrarily since the matching onto the semi-leptonic $\bar{B} \to M_1 \ell \bar{\nu}$ amplitude only requires $q^2 = 0$ to hold exactly. In the following, we drop this argument and calculate the kernels for $E_\ell = m_B/2$. The generalization follows directly from the results in Sec. 4.4.

4.3 $\mathsf{SCET}_{\mathrm{II}}$ factorization

In Sec. 4.2, we integrated out the hard modes and obtained formula (4.57) that describes the factorization of the anti-collinear sector from the $\bar{B} \to M_1$ transition, where the form factor $\mathcal{F}_{Q_2}^{BM_1}$ contains the soft spectator scattering interactions. The form factors Υ^{BM_1} and Σ^{BM_1} on the other hand can be further factorized into separate $\bar{B} \to 0$ and $0 \to M_1$ matrix elements in $\mathrm{SCET}_{\mathrm{II}}$. The corresponding matching coefficient encodes the hard-collinear spectator interactions and is represented by a jet function that convolutes the soft and collinear functions in the process. For QCD-only, one-loop computations have shown that the convolution integrals converge to all orders in the strong coupling [49,88,106]. For QED, we expect the same to hold true at $\mathcal{O}(\alpha_{\mathrm{em}})$ and thus perform the tree-level matching using generalized definitions for the LCDAs. The $\mathrm{SCET}_{\mathrm{I}} \to \mathrm{SCET}_{\mathrm{II}}$ matching equation reads

$$\Upsilon_{Q_2}^{BM_1}(1-z) = \frac{1}{4}\int_{-\infty}^{\infty} d\omega \int_0^1 dv\, J_\otimes(1-z;v,\omega) f_B \Phi_{B,\otimes}(\omega) f_{M_1} \Phi_{M_1}(v)\,, \tag{4.67}$$

where $\Phi_{B,\otimes}$, Φ_{M_1} and $J_\otimes$ are the soft, collinear and jet function respectively.[6]

Formally, we obtain (4.67) by first decoupling the collinear from the soft modes using the transformation (4.23) for the collinear fields with the soft $S_{n_-}^{(q)}$ Wilson line. Moreover, we integrate out the hard-collinear modes which can be trivially done on the Lagrangian level by sending $\xi_{\mathrm{C}} \to \xi_{\mathrm{c}}$. Since spectator-scattering requires a subleading $\mathcal{L}_{\xi q}^{(1/2)}$ interaction, the decoupling transformation leads to the appearance of $S_{n_-}^{(q)}(tn_-)S_{n_-}^{\dagger(q_2)}(0)$, where $t = vx$. The tn_--dependence enters from the multipole expansion of the position argument in the $\mathcal{L}_{\xi q}$ interaction. Alongside with an additional rearrangement factor $R_c^{(Q_M)}$ accounting for the light-meson LCDA, we absorb the soft contributions into the definition

$$\begin{aligned} & im_B \int_{-\infty}^{\infty} d\omega\, e^{-i\omega t} f_B \Phi_{B,\otimes}(\omega;\mu) \\ & \quad = \frac{1}{R_{\mathrm{c}}^{(Q_{M_1})} R_{\bar{\mathrm{c}}}^{(Q_{M_2})}} \big\langle 0 \big| \bar{q}_{\mathrm{s}}^{(q)}(tn_-)[tn_-,0]^{(q)} \not{n}_- \gamma_5 h_v(0) S_{n_-}^{\dagger(Q_{M_1})} S_{n_+}^{\dagger(Q_{M_2})} \big| \bar{B} \big\rangle\,. \end{aligned} \tag{4.68}$$

[6] Equivalently to (4.50), the LCDA for the meson M_1 is defined by

$$\langle M_1(p')| R_{\mathrm{c}}^{(Q_{M_1})}\, \bar{\chi}_{\mathrm{c}}^{(q_2)}(sn_+) \frac{\not{n}_+}{2}(1-\gamma_5)\chi_{\mathrm{c}}^{(q)}(0)|0\rangle = \frac{in_+p'}{2}\int_0^1 dv\, e^{iv(n_+p')s} f_{M_1}\Phi_{M_1}(v;\mu)\,,$$

obtained by the trivial replacements $n_- \to n_+$ and $R_{\bar{\mathrm{c}}}^{Q_{M_2}} \to R_{\mathrm{c}}^{(Q_{M_1})}$.

Note that we inserted unity $(S_{n_-}^{\dagger(q)} S_{n_-}^{(q)})(0)$ to obtain a QCD-like finite distance Wilson line $[tn_-, 0]^{(q)} = S_{n_-}^{(q)}(tn_-) S_{n_-}^{\dagger(q)}$ in analogy to (2.6) and the soft M_1 Wilson line $S_{n_-}^{\dagger(Q_{M_1})}$, similar to the anti-collinear case. Hence for electrically charged final states, the B-meson LCDA is fundamentally modified and we refer to it as soft function. Most generally, we distinguish in (4.68) between the four possible charge combinations $\otimes = \{(0,0), (-,0), (0,-), (+,-)\}$ that define four soft functions in total. The two distinct cases of electrically charged and neutral M_2 differ in particular. For $Q_{M_2} \neq 0$, the functions entail major phenomenological differences to the neutral case, namely that it contains soft-rescattering phases and the support has to be extended to $\omega < 0$ in contrast to QCD-only. We discuss the origin and the implications of these modifications in Chapter 5.

We refrain from giving an operator definition for the jet function $J_\otimes$ that contains the hard-collinear modes. In this regard, one might follow the discussion in Sec. 2.4.1 for a derivation. Instead, we compute the coefficient directly at tree level using a Fierz transformation for the four-quark operator

$$J_\otimes(\bar{z}; v, \omega) = -\frac{4\pi\alpha_{\text{em}} Q_{\text{sp}}}{N_c} \frac{1}{m_B \omega \bar{v}}\, \delta(\bar{z} - \bar{v}) \,. \tag{4.69}$$

The spectator quark charge is given by $Q_{\text{sp}} = Q_d - Q_{M_1} - Q_{M_2}$. The interplay between different photon polarizations to the operators $\mathcal{O}^{\text{I}}$ and $\mathcal{O}^{\text{II}}$ ensures that the jet function is purely determined from hard-collinear transverse photon exchange. Appendix C.2 shows the cancellation of the longitudinal polarization for the particular case of $\otimes = (+,-)$.

After inserting (4.67) into the SCET_I factorization formula (4.57), we obtain the final QCD×QED factorization

$$\begin{aligned}\left\langle M_1 M_2 | Q_i | \bar{B} \right\rangle = i m_B^2 \Bigg\{ & \mathcal{F}_{Q_2}^{BM_1}(0) \int_0^1 du\, T_{i,Q_2}^{\text{I}}(u) f_{M_2} \Phi_{M_2}(u) \\ & + \int_{-\infty}^{\infty} d\omega \int_0^1 du\, dv\, T_{i,\otimes}^{\text{II}}(u, v, \omega) f_{M_1} \Phi_{M_1}(v) f_{M_2} \Phi_{M_2}(u) f_B \Phi_{B,\otimes}(\omega) \Bigg\} ,\end{aligned} \tag{4.70}$$

which completes the separation of hard, hard-collinear, (anti-)collinear and soft modes in non-leptonic $\bar{B} \to M_1 M_2$ decays. We expressed the convolution of the hard coefficient with the jet function in terms of one the spectator-scattering term T^{II} in the second line

$$T_{i,Q_2}^{\text{II}}(\omega, u, v) = -\frac{1}{8} \int_0^1 dz\, \hat{H}_{i,Q_2}^{\text{II}}(u, z) J_\otimes(1 - z; v, \omega) \,. \tag{4.71}$$

4.4 Matching coefficients

We completed the formal derivation of the QCD×QED factorization and the results for the matching coefficients have yet to be listed. The computation for the form factor

term follows the arguments of the previous sections. We present the results at tree-level and one-loop separately. Moreover, we present the results for the kernels $H^{\mathrm{I/II}}$ as well as for the refinements $T^{\mathrm{I/II}}$.

4.4.1 Hard-scattering kernels H^{I}_{i,Q_2} and $H^{\mathrm{II}\gamma}_{i,Q_2}$

,At tree-level, the matching of the operators Q_i onto $\mathcal{O}^{\mathrm{I}}$ yields the coefficients $H^{\mathrm{I}(0)}_{i,Q_2}$ whose expressions are

$$H^{\mathrm{I}(0)}_{1,-}(u) = 0\,, \qquad H^{\mathrm{I}(0)}_{1,0}(u) = \frac{C_F}{N_c}\,, \tag{4.72}$$

$$H^{\mathrm{I}(0)}_{2,-}(u) = 1\,, \qquad H^{\mathrm{I}(0)}_{2,0}(u) = \frac{1}{N_c}\,. \tag{4.73}$$

The factors with $Q_{M_2} = 0, -1$ arise from the right and wrong insertion, respectively. As expected, these results agree with QCD-only. We emphasize that the contribution from the color-octet operator Q_1 vanishes for the charged M_2 case at LO in QCD and to all orders in QED. The same holds true for the relative factor C_F in the neutral case so that the identities are exact

$$H^{\mathrm{I}}_{1,-}(u) = 0, \qquad H^{\mathrm{I}}_{1,0}(u) = C_F H^{\mathrm{I}}_{2,0}(u)\,. \tag{4.74}$$

At the one-loop order, we evaluate the hard region of the diagrams in Fig. 4.2 which corresponds to the on-shell matrix elements $A_i^{(1)}$ defined in (4.17). We consider the general operator for the right insertion

$$[\bar{q}_2\gamma^\mu(1-\gamma_5)b][\bar{q}_1\gamma_\mu(1-\gamma_5)u]\,. \tag{4.75}$$

Including the corresponding renormalization factors, we find from (4.22)

$$\begin{aligned}
H^{\mathrm{I}(1)}_{2,-}(u) &= Q_{q_1}Q_{q_2}\left(L^2 - 4L_\nu + L\,(4 + 2i\pi - 2\ln u) + \ln^2 u - 2i\pi\ln u - \frac{7\pi^2}{6} + 1\right) \\
&\quad - Q_u Q_{q_2}\left(L^2 - L_\nu + L\,(4 + 2i\pi - 2\ln\bar{u}) - \ln\bar{u}\,(3 + 2i\pi - \ln\bar{u}) - \frac{7\pi^2}{6} + 3i\pi + 6\right) \\
&\quad + Q_u Q_d\left(\frac{1}{2}L^2 - 4L_\nu - 2L\,(-1 + \ln\bar{u}) + 2\ln^2\bar{u} - \frac{2}{u}\ln\bar{u} + 2\mathrm{Li}_2\,(u) + \frac{\pi^2}{12} - 3\right) \\
&\quad - Q_d Q_{q_1}\left(\frac{1}{2}L^2 - L_\nu + L(2 - 2\ln u) + 2\ln^2 u - 3\ln u + \frac{\ln u}{\bar{u}} + 2\mathrm{Li}_2(\bar{u}) + \frac{\pi^2}{12} + 2\right) \\
&\quad - 3\,(Q_{q_1} + Q_u)\,(Q_{q_2} + Q_d) \\
&\quad - Q_{q_2}Q_d\left(\frac{1}{2}L^2 - L_\nu + 2L + \frac{\pi^2}{12} + 4\right) - Q_d^2\left(\frac{1}{2}L_\nu + L + 2\right) - \frac{1}{2}Q_{q_2}^2\,(L_\nu - L)
\end{aligned}$$

$$-\frac{1}{2}\left(Q_{q_1}^2+Q_u^2-2Q_uQ_{q_1}\right)(L_\nu-L)\,. \tag{4.76}$$

We abbreviate the logarithm of the UV scale ν as

$$L_\nu \equiv \ln\left(\frac{\nu^2}{m_B^2}\right)\,, \tag{4.77}$$

which is distinguished from the factorization scale μ in L and matches to the scale evolution of the Wilson coefficients $C_i(\nu)$. Hence, the ν-dependence cancels with the QED corrections from the electroweak scale. On the other hand, the scale μ correlates to the scale dependence of the form factors in the $\mathrm{SCET_I}$ factorization formula (4.57). In (4.76), the first four lines correspond to the first four diagrams in Fig. (4.2), which can be identified from the quark charges. The fifth line originates from the finite terms of the evanescent operators as discussed in Sec. 4.1. The sixth line is a combination of the last diagram in Fig. 4.2 and the external quark field renormalization. The last line corresponds to the virtual corrections in between the anti-collinear q_1- and u-quark that are scaleless when UV and IR are not distinguished. We recover the QCD-only result by setting all charge factors to unity. In particular, the sixth line reproduces the renormalization factor C_{FF}/C_F in the notation of [53]. For the wrong insertion, we use the colour Fierz relation to obtain

$$H_{2,0}^{\mathrm{I}(1)}(u)=\frac{1}{N_c}H_{2,-}^{\mathrm{I}(1)}(u)-\frac{1}{N_c}\left(Q_d-Q_u\right)\left(Q_{q_2}-Q_{q_1}\right). \tag{4.78}$$

Finally, the all-order statement in (4.74) determines the coefficients $H_{1,-}^{\mathrm{I}(1)}$ and $H_{1,0}^{\mathrm{I}(1)}$.

At this point, we emphasize that the results (4.76) and (4.78) arising from the operator (4.75) are gauge-dependent due to the generalized quark charges. Our results have been computed in Feynman gauge. Once we insert the physical values for a specific process, the gauge dependence cancels. For an electrically charged meson M_2 with $q_1=d$ and $q_2=u$, we set the up- and down-type charges in (4.76) to $Q_{q_1}=Q_d=-1/3$ and $Q_{q_2}=Q_u=2/3$ and find

$$\begin{aligned}H_{2,-}^{\mathrm{I}(1)}(u)=&-\frac{13L^2}{18}+\frac{4}{3}L_\nu-L\left(\frac{41}{18}+\frac{4i\pi}{3}-\frac{4}{3}\ln(1-u)-\frac{2}{3}\ln u\right)\\&-\frac{2f(u)+4f(1-u)}{9}-\frac{(2-u)\ln(u)}{3(1-u)}+\frac{83\pi^2}{108}-\frac{4i\pi}{3}-\frac{19}{9}\,.\end{aligned} \tag{4.79}$$

For the neutral case with $q_1=u$ and $q_2=d$, we set $Q_{q_1}=Q_u=2/3$ and $Q_{q_2}=Q_d=-1/3$. Using (4.78), we have

$$H_{2,0}^{\mathrm{I}(1)}(u)=-\frac{1}{54}L^2+\frac{4}{9}L_\nu-\frac{5}{54}L-\frac{2}{27}g(u)-\frac{\pi^2}{324}+\frac{29}{27}\,. \tag{4.80}$$

To compactify our notation, we introduced the function

$$f(u)=\mathrm{Li}_2(1-u)+2\ln^2 u-(3+2i\pi)\ln u-\frac{\ln u}{1-u} \tag{4.81}$$

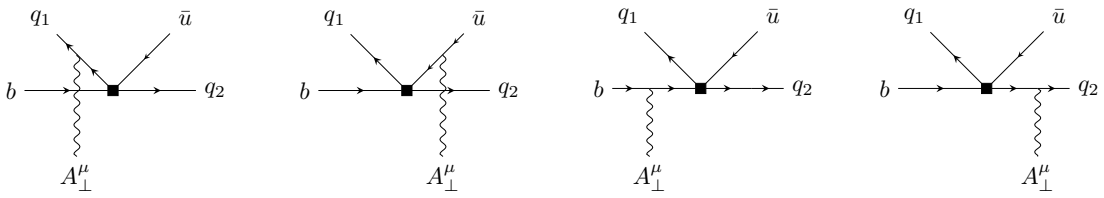

Figure 4.5: Five-point diagrams S_1-S_4 in the full theory that are matched onto the operator $\mathcal{O}^{\mathrm{II}\gamma}$ in spectator scattering. The index numbers are assigned to the order in which the diagrams are shown. The transverse photon carries outgoing momentum k.

as well as

$$g(u) = 3\left(\frac{1-2u}{1-u}\ln u - i\pi\right) + \Bigg[2\,\mathrm{Li}_2(u) - \ln^2 u + \frac{2\ln u}{1-u} - (3+2i\pi)\ln u \\ - (u \to 1-u)\Bigg]. \tag{4.82}$$

To calculate the hard matching coefficients of the tree-level spectator-scattering, we follow the arguments in [50]. Using the momentum prescription in (4.12), we compute the on-shell five-point amplitude

$$\langle q_1(k_{q_1})\bar{u}(k_{\bar{u}})q_2(k_{q_2})\gamma(k)|Q_i|b(p_b)\rangle \tag{4.83}$$

that describes the $b \to q_1\bar{u}\,q_2\gamma$ transition, where the outgoing photon gets connected to the spectator quark line. The matrix element (4.83) has to be equivalently considered for the $\mathrm{SCET_I}$ operators which results in a matching equation similar to (4.8)

$$\langle Q_2\rangle = \sum_{i=1}^{4} S_i = H_{2,Q_2}^{\mathrm{I}\gamma(0)} \otimes \langle\mathcal{O}^{\mathrm{I}}\rangle^{(0)} + H_{2,Q_2}^{\mathrm{II}\gamma(0)} \otimes \langle\mathcal{O}^{\mathrm{II}\gamma}\rangle^{(0)}\,, \tag{4.84}$$

where $\otimes$ denotes the convolution in the momentum variables u and v and the angle brackets correspond to the partonic matrix element in (4.83). At LO in α_{em}, there are four diagrams S_i shown in Fig. 4.5 that have to be considered. Based on the discussion in Appendix C.2, we recall that the longitudinal polarizations enter the hard coefficient H^{I} so that we assume the photon to be transversely polarized with one subtlety for diagram S_4. In this case, we need to distinguish between long- and short-distance effects arising from the q_2-propagator. When the momentum of the photon becomes soft, the q_2-propagator runs through its pole corresponding to a non-local long-distance contribution. On the SCET side, this contribution appears as a time-ordered product of the operator $\mathcal{O}^{\mathrm{I}}$ with subleading Lagrangian insertions [102]. Hence, these long-distance effects cancel on both sides of the matching equation. Therefore, only the

local short-distance contribution $S_4|_{\rm SD}$ enters the matching coefficient, which can be extracted by the replacement [50]

$$\frac{i(\not{k}_{q_2}+\not{k})}{(k_{q_2}+k)^2} \to \frac{i}{n_+(k_{q_2}+k)}\,\frac{\not{n}_+}{2}\,. \tag{4.85}$$

For the right insertion of Q_2, we find

$$\begin{aligned}
S_1 &= 0\,,\\
S_2 &= \frac{2eQ_u}{\bar{u}m_b}\left\langle\frac{\not{n}_-}{2}\right\rangle_{\bar{C}}\,[\bar{u}(k_{q_2})\gamma_\perp^\mu(1+\gamma_5)\,u(p_b)]\;\epsilon_{\perp\mu}^*\,,\\
S_3 &= \frac{2eQ_d}{m_b}\left\langle\frac{\not{n}_-}{2}\right\rangle_{\bar{C}}\,[\bar{u}(k_{q_2})\gamma_\perp^\mu(1+\gamma_5)\,u(p_b)]\;\epsilon_{\perp\mu}^*\,,\\
S_4|_{\rm SD} &= 0\,,
\end{aligned} \tag{4.86}$$

where we defined

$$\left\langle\frac{\not{n}_-}{2}\right\rangle_{\bar{C}} \equiv [\bar{u}(k_{q_1})\frac{\not{n}_-}{2}(1-\gamma_5)v(k_{\bar{u}})]\,. \tag{4.87}$$

The momenta in (4.86) refer to their LP expressions in (4.12). Note that QCD×QED and SCET spinors from contractions of $\xi_{\rm C,\bar{C}}$ and h_v fields are then equivalent. For transverse photons, we have $n_\pm\cdot\epsilon = 0$ and the matrix element $\langle\mathcal{O}^{\rm I}\rangle^{(0)}$ just corresponds to the long-distance contribution of S_4 since the coupling of the photon to (anti-)collinear Wilson lines vanishes. We already extracted the short-distance part $S_4|_{\rm SD}$, so that we can neglect the former term on the right-hand side of (4.84). The spinor structure of S_2 and S_3 matches the tree-level matrix element of the operator $\mathcal{O}^{\rm II\gamma}$. We can therefore read off the coefficients

$$H_{2,-}^{\rm II\gamma}(u,v) = N_c\,H_{2,0}^{\rm II\gamma}(u,v) = \frac{2}{\bar{u}}Q_u + 2Q_d\;. \tag{4.88}$$

The factor N_c accounts for the wrong insertion of Q_2. For the operator Q_1, we find similar to (4.74)

$$H_{1,0}^{\rm II\gamma}(u,v) = C_F H_{2,0}^{\rm II\gamma}\,, \qquad H_{1,-}^{\rm II\gamma}(u,v) = 0\;. \tag{4.89}$$

We remark that QED effects to the gluonic coefficient $H^{\rm IIg}$ are $\mathcal{O}(\alpha_s\alpha_{\rm em})$ and hence not considered to our accuracy.

Finally, we emphasize that in pure QCD only the diagrams S_1 and S_2 enter the hard-scattering coefficient $H^{\rm IIg}$. Since longitudinal gluon polarizations cancel among the diagrams, there is no need to assume a transverse polarization for the gluon in the

matching equation. In QED however, an equivalent computation would turn out to be too naive since the projection of S_2 onto the anti-collinear LCDA yields an integral of the form $\int_0^1 du\,\phi_{M_2}(u)/\bar{u}$ that is endpoint-divergent. As we discussed earlier and demonstrate in Appendix C.2, this contribution originates from longitudinal photons which are part of the generalized SCET_I form factor ζ^{BM_1} defined in (4.55).

4.4.2 Hard(-collinear)-scattering kernels T^I_{i,Q_2} and $T^{\text{II}\gamma}_{i,Q_2}$

In this section, we derive the physical hard-scattering kernels $T^{\text{I/II}}$ of the QCD×QED factorization formula (4.1). In order to trade the SCET_I for the full theory form factor, we require the semi-leptonic coefficients in (4.60). We obtain the both coefficients from the general result H^I in (4.76) and H^II in (4.88) upon sending $Q_{q_1} \to Q_\ell, Q_u \to 0$ and $u \to 2E_\ell/m_B$. For $E_\ell = m_B/2$, we drop the lepton-energy argument in the coefficients and find

$$\begin{aligned}
H_\text{sl}^{\text{I}(0)} &= 1\,, \\
H_\text{sl}^{\text{I}(1)} &= Q_\ell Q_u \left(L^2 - 3L_\nu + (3+2i\pi)\,L - \frac{7\pi^2}{6} - 2 \right) \\
&\quad - Q_d^2 \left(\frac{1}{2}L^2 + \frac{5}{2}L + \frac{\pi^2}{12} + 6 \right), \\
H_\text{sl}^{\text{II}\gamma}(z) &= 2Q_d\,.
\end{aligned} \tag{4.90}$$

The matching coefficients for the full theory QCD×QED form factor can be obtained by setting $Q_\ell = 0$ in the above[7]

$$\begin{aligned}
H_f^{\text{I}(1)} &= -Q_d^2 \left[\frac{1}{2}L^2 + \frac{5}{2}L + \frac{\pi^2}{12} + 6 \right], \\
H_f^{\text{II}\gamma(0)}(z) &= 2Q_d\,.
\end{aligned} \tag{4.91}$$

The hard-scattering kernels for the form factor term follow from (4.65) and the results in (4.79), (4.80), (4.90) and (4.91). We find

$$\begin{aligned}
T_{1,-}^{\text{I}(1)}(u) &= 0\,, \\
T_{2,-}^{\text{I}(1)}(u) &= -\frac{2}{3}L_\nu + \frac{2}{3}L\,(2\ln(1-u) + \ln u) \\
&\quad - \frac{2f(u) + 4f(1-u)}{9} - \frac{(2-u)\ln(u)}{3(1-u)} - \frac{4i\pi}{3} - \frac{25}{9}\,, \\
T_{1,0}^{\text{I}(1)}(u) &= C_F T_{2,0}^{\text{I}(1)}(u) = \frac{16}{27}L_\nu - \frac{8}{81}g(u) + \frac{140}{81}\,,
\end{aligned} \tag{4.92}$$

[7] Compared to [106], our convention differs by a factor $-1/2$ in the spectator-scattering terms. Hence, we identify $H_f^{\text{II}\gamma} \to -2C_{f_+}^{(B1)}$ in the QCD-only limit $Q_d \to 1$.

where $f(u)$ and $g(u)$ were defined in (4.81) and (4.82). Since the form factor renormalization enters at one-loop, the tree-level terms remain the same $T^{\mathrm{I}(0)}_{i,Q_2}(u) = H^{\mathrm{I}(0)}_{i,Q_2}(u)$.

For the spectator-scattering terms, the shift in (4.66) implies

$$\hat{H}^{\mathrm{II}\gamma}_{2,-}(u,z;E_\ell) = \frac{2}{\bar{u}}Q_u\,, \qquad \hat{H}^{\mathrm{II}\gamma}_{1,0}(u,z) = C_F\hat{H}^{\mathrm{II}\gamma}_{2,0}(u,z) = \frac{2C_F}{N_c\bar{u}}Q_u\,. \tag{4.93}$$

The right insertion of the octet operator Q_1 still vanishes, so that $\hat{H}^{\mathrm{II}\gamma}_{1,-}(u,z) = 0$. To obtain the entire kernel including the contribution from the jet function, we perform the integral (4.71) together with the expressions from (4.93) and (4.69). The results at $\mathcal{O}(\alpha_{\mathrm{em}})$ are given by

$$T^{\mathrm{II}}_{2,(Q_1,-)}(\omega,u,v) = N_c T^{\mathrm{II}}_{2,(Q_1,0)} = \frac{N_c}{C_F}T^{\mathrm{II}}_{1,(Q_1,0)} = \frac{\pi\alpha_{\mathrm{em}}Q_{\mathrm{sp}}Q_u}{N_c}\frac{1}{m_B\omega\bar{u}\bar{v}}\,, \tag{4.94}$$

while $T^{\mathrm{II}}_{1,(Q_1,-)}(\omega,u,v) = 0$ for an arbitrary charge of the meson M_1.

We conclude the analysis of the hard-scattering kernels with some important remarks. First, we emphasize that the double-logarithmic terms L^2 appearing in $H^{\mathrm{I}(1)}$ are absent in the result for $T^{\mathrm{I}(1)}_{2,-}(u)$ in (4.92). This is a consequence of the matching onto the semi-leptonic amplitude and the full theory form factors. The remaining single logarithm L corresponds to the scale dependence of the light-meson LCDA normalization appearing as a new feature in QED. The latter can be related to specific terms in the anomalous dimension as we discuss in Sec. 5.1. More precisely, the IR μ-dependence in $T^{\mathrm{I}(1)}_{2,-}(u)$ matches to the UV dependence of $f_{M_2}\Phi_{M_2}(u)/Z_\ell$ in the convolution (4.64). For $Q_{M_2} = -1$, this follows explicitly from (4.35), (4.48) and (4.62) due to the form factor replacement in (4.63). We have

$$R^{(Q_{M_2})(1)}_{\bar{\mathrm{c}}} + \frac{2}{\epsilon}\int_0^1 dv\, V(u,v)|_{Q_{q_1}=Q_d} - Z^{(1)}_\ell = -\frac{2}{\epsilon}Q_{M_2}\left[Q_d\ln u - Q_u\ln(1-u)\right]\,, \tag{4.95}$$

which exactly agrees to the coefficient of L in (4.92). The ν-dependence on the other hand is related to the renormalization of Q_i and Q_{sl} which cancels against the dependence of the Wilson coefficients $C_i(\nu)$ and $C_{\mathrm{sl}}(\nu)$ respectively.

As a second remark, we emphasize that the non-radiative $\bar{B} \to M_1M_2$ amplitude contains IR poles within the SCET form factors and LCDAs after matching on the EFT. These objects are defined as non-radiative hadronic matrix elements in presence of QCD and QED and correspond to non-perturbative but IR divergent quantities. At first sight, we might conclude that this renders the non-perturbative input ill-defined since the finite scale Λ_{QCD} may not serve as an IR regulator for soft QED divergences. However, one should regard these matrix elements as short-distance coefficients of a low-energy theory below a few times Λ_{QCD} obtained from $\mathrm{SCET}_{\mathrm{II}}$, where photons couple to point-like mesons. At this energy scale, we are free to choose a matching scale μ_{IR} at which the IR divergences cancel in the matching procedure. The scale μ_{IR} differs from the renormalization scale μ that corresponds to the UV renormalization of the

non-perturbative matrix elements which we calculated explicitly in perturbation theory by introducing off-shell IR regulators. Formally, the matching of SCET_{II} onto the effective theory of point-like mesons must be performed *non-perturbatively* at μ_{IR}. This leaves a hole in our ability to compute QED effects between scales above and below a few times Λ_{QCD}. Nevertheless, we can view the non-perturbative quantities in presence of QED as properly IR subtracted matching coefficients leaving a certain scheme dependence. Hence, the discussion justifies considering the form factors, LCDAs and the soft function in the conventional framework, in which experimental or lattice input, as well as general distribution models, can be used.

To demonstrate the central points listed above, we consider the anti-collinear leptonic matrix element

$$\left\langle \ell^-(p_\ell)\middle| R_{\bar{c}}^{(Q_\ell)} \bar{\chi}_{\bar{C}}^{(\ell)}(0)\middle|0\right\rangle = Z_\ell \bar{u}(p_\ell)\frac{\not{n}_-\not{n}_+}{4} \tag{4.96}$$

as a concrete example which we already used to define the UV renormalization factor Z_ℓ in Sec. 4.2.4. The matrix element (4.96) represents the point-particle equivalent to a hadronic LCDA that can be calculated perturbatively due to the absence of QCD at LO in $\mathcal{O}(\alpha_{\text{em}})$. The result for the bare UV coefficient Z_ℓ^{bare} was given in (4.62). To extract the IR dependence, we calculate the on-shell matrix element including the leptonic on-shell renormalization factor obtained from (4.18) by replacing $Q_d \to Q_\ell$ and $m_b \to m_\ell$. From the result, we subtract the UV pole given by the divergent part of Z_ℓ^{bare} and find

$$\begin{aligned} Z_\ell^{(1)} &= -\frac{1}{\epsilon_{\text{IR}}}\left(1+\ln\frac{m_\ell^2}{m_B^2}\right) + \frac{1}{2}\ln\frac{\mu^2}{m_\ell^2} + \frac{1}{2}\ln^2\frac{\mu^2}{m_\ell^2} + 2 + \frac{\pi^2}{12} \\ &= -\left(\frac{1}{\epsilon_{\text{IR}}} + \ln\frac{\mu_{\text{IR}}^2}{m_\ell^2}\right)\left(1+\ln\frac{m_\ell^2}{m_B^2}\right) + \frac{3}{2}\ln\frac{\mu_{\text{UV}}^2}{m_\ell^2} + \frac{1}{2}\ln^2\frac{\mu_{\text{UV}}^2}{m_B^2} - \frac{1}{2}\ln^2\frac{m_\ell^2}{m_B^2} + 2 + \frac{\pi^2}{12}\,, \end{aligned} \tag{4.97}$$

which corresponds to the UV-renormalized but IR-divergent matrix element. In the second line of (4.98), we separated the UV and IR scales $\mu_{\text{UV}} = \mu_{\text{IR}} = \mu$. The lepton mass m_ℓ acts as a regulator for the collinear divergences and hence the $1/\epsilon_{\text{IR}}$ pole originates from a soft singularity. Moreover, the large logarithm $\ln m_\ell/m_B$ reflects the relative boost between the external particle rest frames. While μ_{UV} gets canceled against the scale dependence of the hard-scattering kernel and the light-meson LCDA, see (4.95), the IR scale μ_{IR} is removed after matching onto the theory of point-like objects. In particular, we can relate μ_{IR} to the scale dependence of the ultrasoft function introduced in the next section that is associated with real soft photon emission much below Λ_{QCD}.

4.5 Ultrasoft photons

Throughout the analyses of the previous sections, we highlighted several times that the non-radiative amplitude of the exclusive $\bar{B} \to M_1 M_2$ decay contains IR singularities

arising from virtual QED corrections. To construct an IR finite observable, we must account for the emission of an arbitrary number of soft photons once the external states are electrically charged. In fact, experiments can not measure the difference between a charged final state and one that is accompanied by soft photons or electron-positron pairs below a certain energy threshold. Therefore, the relevant physical observable is the inclusive decay width

$$\Gamma[\bar{B} \to M_1 M_2](\Delta E) \equiv \Gamma[\bar{B} \to M_1 M_2 + X_\mathrm{s}]\big|_{E_{X_\mathrm{s}} \leq \Delta E}\,, \tag{4.98}$$

where X_s denotes all possible soft particle combinations with energy E_{X_s}. The total energy has to be smaller or equal to some energy cut $\Delta E \ll \Lambda_\mathrm{QCD}$ in the experiment. We refer to ΔE as the "ultrasoft" scale in the process and use $\Delta E \approx 60$ MeV for the soft emission. At leading power in $\Delta E/\Lambda_\mathrm{QCD}$, the inclusive $\bar{B} \to M_1 M_2 + X_\mathrm{s}$ amplitude factorizes into the non-radiative part and an ultrasoft matrix element

$$\mathcal{A}(\bar{B} \to M_1 M_2 + X_s) = \mathcal{A}(\bar{B} \to M_1 M_2)\, \langle X_s | (\bar{S}_v^{(Q_B)} S_{v_1}^{\dagger(Q_{M_1})} S_{v_2}^{\dagger(Q_{M_2})})(0)|0\rangle\,. \tag{4.99}$$

The outgoing time-like Wilson lines $S_{v_i}^{(Q_{M_i})}$ are given by (4.24) with the replacement $n_\pm \to v_i$, where v_i is the velocity label of the meson M_i obeying $v_i^2 = 1$. On the other hand, the incoming B meson gives rise to the Wilson line [60]

$$\bar{S}_v^{(Q_B)}(x) = \exp\left\{ +ieQ_B \int_{-\infty}^{0} ds\, v \cdot A_\mathrm{us}(x + sv) \right\}\,, \tag{4.100}$$

where the electric B-meson charge is fixed by conservation $Q_B = Q_{M_1} + Q_{M_2}$, ensuring gauge invariance of the ultrasoft function. We emphasize that the meson masses of order $m_{M_i} \sim \mathcal{O}(\Lambda_\mathrm{QCD})$ cannot be set to zero in the ultrasoft regime like we did in the hard(-collinear) matching. Hence, the ultrasoft function does not contain collinear divergences but large logarithms of the scale ratios $\Delta E/\Lambda_\mathrm{QCD}$ and $m_{M_i}/\Lambda_\mathrm{QCD}$. Formally, the factorization formula (4.99) can be derived from a non-perturbative matching at Λ_QCD on the EFT of mesons with point-like QED interactions [137]. We skip a precise derivation but note that each meson is treated in a (boosted) HQET framework. For a review of the theoretical concepts, we refer to [138–140]. In this approach, the Wilson lines in (4.99) ultimately arise from the decoupling of ultrasoft photons.

By squaring (4.99), we obtain the decay width

$$\Gamma[\bar{B} \to M_1 M_2](\Delta E) = |\mathcal{A}(\bar{B} \to M_1 M_2)|^2\, \mathcal{S}_\otimes(\{v_i\}, \Delta E)\,, \tag{4.101}$$

where the ultrasoft function is given by

$$\mathcal{S}_\otimes(\{v_i\}, \Delta E) = \sum_{X_s} |\langle X_s | (\bar{S}_v^{(Q_B)} S_{v_1}^{\dagger(Q_{M_1})} S_{v_2}^{\dagger(Q_{M_2})})(0)|0\rangle|^2\, \theta(\Delta E - E_{X_s})\,. \tag{4.102}$$

This function appears generally in the ultrasoft regime of cross sections and can be calculated perturbatively [141]. We expand the $\mathcal{O}(\alpha_\mathrm{em})$ corrections to leading power in $m_{M_i}/m_B \ll 1$ and obtain

$$\mathcal{S}_{(+,-)}^{(1)} = 8\left(\frac{1}{2} + \frac{1}{2}\ln\frac{m_{M_1}^2}{m_B^2}\right)\ln\frac{\mu}{2\Delta E} - \left(2 + \ln\frac{m_{M_1}^2}{m_B^2}\right)\ln\frac{m_{M_1}^2}{m_B^2} - \frac{2}{3}\pi^2$$

$$+ \quad (m_{M_1} \to m_{M_2}) \,, \tag{4.103}$$

$$\mathcal{S}^{(1)}_{(-,0)} = 8\left(1+\frac{1}{2}\ln\frac{m_{M_1}^2}{m_B^2}\right)\ln\frac{\mu}{2\Delta E} - \left(2+\ln\frac{m_{M_1}^2}{m_B^2}\right)\ln\frac{m_{M_1}^2}{m_B^2} + 4 - \frac{2}{3}\pi^2 \,. \tag{4.104}$$

We find $\mathcal{S}^{(1)}_{(0,0)} = 0$ trivially and the result for $\mathcal{S}^{(1)}_{(0,-)}$ can be inferred from the last line by sending $m_{M_1} \to m_{M_2}$. Our result for $\mathcal{S}^{(1)}_{(+,-)}$ agrees with [141].

The IR scale dependence of the non-radiative amplitude $\mathcal{A}(\bar{B} \to M_1 M_2)$ matches the μ-dependence of the ultrasoft function for the different charge cases. We choose $\mu \sim \mu_c$ of order of the hadronic scale $\Lambda_{\rm QCD}$ and derive the resummation of large logarithms in $\Delta E/\mu$ in Sec. 5.3. Finally, we emphasize once again that we are not able to determine QED corrections between the ultrasoft theory and SCET_{II} perturbatively in a small window around $\Lambda_{\rm QCD}$.[8] We further note that the exclusive matrix element defining the light-meson LCDA in (4.50) uses a frame in which the meson M_2 is ultrarelativistic with respect to the emitted radiation. Hence, the consistency of the factorization approach requires $\Delta E \ll \Lambda_{\rm QCD}$ for the applicability of the LCDA.

[8] The non-perturbative matching onto an EFT between the ultrasoft region and SCET_{II} which contains light-like operators, is generally challenging for lattice QCD/QED simulations. In recent years, different studies regarding this issue advanced in the context of (semi-)leptonic decays, see [142–145].

Chapter 5

Resummation of QED effects

The QCD×QED factorization formula obtained in Chapter 4 connects physics of different scales. In Sec. 2.5, we showed in a simplified environment how this affects the evaluation of matching coefficients and the non-perturbative input. For the non-leptonic $\bar{B} \to M_1 M_2$ decay, we encounter multi-layered scales that are more precisely associated to the hard, hard-collinear, (anti-)collinear, soft and ultrasoft region. Each object entering the factorization formula is naturally evaluated at its respective scale using a certain model, experimental/lattice input or theoretical calculation. For the calculation of observables, we use the factorization scale independence to choose a common reference scale, which typically has hard-collinear virtuality. A priori, the scale hierarchy introduces large logarithms involving the different scale ratios, which are then resummed by solving the RG. In what follows, we consider the scale evolution of the QED-generalized light and heavy meson LCDAs as well as the ultrasoft function. Since the jet function enters at tree-level, we do not require any RG improvement beyond the running of α_{em}. For the hard-matching coefficients that encode the structure-dependent logarithms between m_B and Λ_{QCD}, we disregard the resummation, leaving it for future work. The fixed-order expressions already yield a good approximation since QED logarithms $(\alpha_{\text{em}} \ln^2 m_b/\Lambda_{\text{QCD}})^n$ are expected to be small.

We recall that the QED-generalized LCDAs for charged light and heavy mesons acquire phenomenological modifications due to the non-decoupling of soft photons in the factorization approach. In the first place, this is related to an overlap of the soft and collinear region, which was discussed and removed in Sec. 4.2. For the light meson LCDA, the anomalous dimension (4.53) in QED contains additional local logarithmic terms that change the endpoint behaviour and renders the well-known scale evolution in terms of Gegenbauer coefficients non-diagonal. As a consequence, the LCDA loses its interpretation as probability distribution since its normalization becomes scale-dependent in contrast to QCD-only. For the heavy meson LCDA, the generalizations in QED are even more drastic. Due to the soft Wilson lines in the definition (4.68), the position space function develops singularities in the entire complex plane and hence acquires support for $\omega < 0$. Moreover, the Wilson line product introduces imaginary

soft rescattering phases. We therefore strictly refer to the QED-generalized heavy meson LCDA as soft function since the name "LCDA" is no longer justified. We remark that both hadronic matrix elements for light and heavy pseudoscalar mesons are chosen to be normalized with respect to the μ-independent QCD decay constant f_P in absence of QED, which implies that all QED effects are part of the wave functions.

To explain the fundamental new features, we proceed as follows: In Sec. 5.1, we focus on the endpoint behaviour and the solution in terms of Gegenbauer moments for the light meson LCDA. The latter can be only solved analytically to first order in $\alpha_{\rm em}$ on top of an all-order resummation for α_s. For the soft function discussed in Sec. 5.2, we first derive the renormalization factors and the corresponding anomalous dimension. Along these lines, we introduce the first inverse (logarithmic) moments of these functions that acquire a much simpler RGE. We further discuss the solution to the RGE and the phenomenological implications. Lastly, we derive the ultrasoft exponentiation factors in Sec. 5.3.

5.1 Light-meson LCDA

We defined the prototype for the light-meson LCDA in the case of the outgoing anti-collinear meson M_2 in Sec. 4.2. Including the soft rearrangement, we observed that the matrix element (4.50) has a well-defined UV anomalous dimension in QED. This generalizes the pure QCD twist-2 distribution amplitude as an essential and universal object in various exclusive processes accounting for an arbitrary number of virtual gluon and photon exchanges. To point out the differences between the pure QCD and the generalized QED behaviour, we first recall some of the basic properties of the light-meson LCDA in presence of QCD-only. In this case, the LCDA is defined by the non-local matrix element

$$\langle M(p)|\bar{q}_1(tn_+)[tn_+,0]\frac{\not{n}_+}{2}(1-\gamma_5)q_2(0)|0\rangle = \frac{in_+p}{2}\int_0^1 du\, e^{iu(n_+p)t} f_M \phi_M(u;\mu)\ , \quad (5.1)$$

where $[tn_+,0] = W(tn_+)W^\dagger(0)$ is a finite distance collinear Wilson line[1] and q_i are arbitrary quark flavours. Generally, the momentum $p^\mu = En_-^\mu + m_M^2/(4E)\, n_+^\mu$, expressed in terms of light-like reference vectors, indicates the direction of large momentum transfer $E \gg m_M$ in the process. We note that the function ϕ_M itself is boost-invariant and the scale-independent decay constant f_M defined in the local limit $t \to 0$, which yields the normalization $\int_0^1 du\, \phi_M(u;\mu) = 1$ at every scale.

In the neutral meson case, the QED generalization of ϕ_M corresponds to the trivial replacement $W \to W^{(q)}$ for each quark $q_1 = q_2 = q$. For a charged meson with $q_1 = D = d, s$ and $q_2 = u$, we observed that the gauge-invariant operator

$$\bar{D}(tn_+)W^{(d)}(tn_+)\frac{\not{n}_+}{2}(1-\gamma_5)W^{\dagger(u)}(0)u(0) \quad (5.2)$$

[1] $W(x)$ corresponds to $W_{\rm C}(x)$ in (2.48) without the collinear label for the gauge field, so that W represents the full QCD Wilson line. The same relation holds for $W^{(q)}$ obtained from $W_{\rm C}^{(q)}$ in (4.6).

corresponding to (4.29) in SCET retains soft IR divergences in collinear QED loops. The soft rearrangement cures this ill-definedness by multiplication with a factor of $R_{\mathrm{c}}^{(Q_M)}$. In fact, there must always exist such a factor and a corresponding soft function so that the complete process is IR finite, which justifies the possibility to rearrange the overlap as discussed in Sec. 4.2.3. Hence, we conclude that the LCDA remains universal to any exclusive decay when electromagnetic effects are included. In terms of QCD×QED fields, we define the charged light-meson LCDA generally as

$$\begin{aligned}\frac{in_+p}{2}\int_0^1 du\, e^{iu(n_+p)t} f_M \Phi_M(u;\mu) \\ = \langle M^-(p)|R_c^{(Q_M)}\,(\bar{D}W^{(d)})(tn_+)\frac{\not{n}_+}{2}(1-\gamma_5)(W^{\dagger(u)}u)(0)|0\rangle\,.\end{aligned} \tag{5.3}$$

Note that we can express the collinear Wilson line product in terms of a QED generalized finite distance and a semi-infinite line $W^{(d)}(tn_+)W^{\dagger(u)}(0) = [tn_+,0]^{(d)}W^{(Q_M)}(0)$. The latter Wilson line depends on the total electric charge $Q_M = Q_d - Q_u = -1$ of the meson and shows that the operator is not localized on a finite interval once the meson is charged. We remark that the QCD term in $W^{(Q_M)}(x)$ cancels exactly as the meson is colour-neutral. Hence, this effect is intrinsically related to QED.

In general, the LCDA follows equivalently to (4.51) the RGE

$$\frac{d}{d\ln\mu}\Phi_M(u;\mu) = -\int_0^1 dv\;\Gamma(u,v;\mu)\Phi_M(v;\mu)\,. \tag{5.4}$$

We explicitly derived the QED anomalous dimension in (4.53) from the one-loop counter term (4.35) and the rearrangement factor $R_{\bar{\mathrm{c}}}^{(Q_{M_2})}$ in (4.48). We do not recapitulate these arguments here and simply replace $Q_u \to Q_{q_2}$ upon adding the QCD limit [134–136], so that the complete QCD×QED anomalous dimension at one-loop reads

$$\begin{aligned}\Gamma(u,v;\mu) = -\frac{\alpha_{\mathrm{em}}}{\pi}\delta(u-v)Q_M\left(Q_M\left(\ln\frac{\mu}{2E}+\frac{3}{4}\right)-Q_{q_1}\ln u+Q_{q_2}\ln\bar{u}\right) \\ -\frac{\alpha_s C_F+\alpha_{\mathrm{em}}Q_{q_1}Q_{q_2}}{\pi}\left[\left(1+\frac{1}{v-u}\right)\frac{u}{v}\theta(v-u)+\left(1+\frac{1}{u-v}\right)\frac{\bar{u}}{\bar{v}}\theta(u-v)\right]_+^{(u)}\,.\end{aligned} \tag{5.5}$$

The definition of the evolution kernel applies to the charged as well as the neutral case. For a charged meson, the local logarithmic terms in the first line of (5.5) lead to a violation of the normalization $\int_0^1 du\,\Phi_M(u;\mu) \neq 1$.[2] Moreover, the LCDA becomes asymmetric under the exchange of $u \leftrightarrow \bar{u}$ due to the different quark charges which reflects the explicit isospin-symmetry breaking in QED. Thee logarithmic terms in

[2]The logarithmic corrections are entirely related to one-loop QED effects. Since the LCDA is normalized with respect to the μ-independent decay constant f_M, these are part of the dimensionless function Φ_M itself.

particular contain a dependence on the energy E of the meson that is of order of the hard scale, such that boost-invariance is explicitly broken. The latter is a remnant of the soft rearrangement and represents an example of the factorization (collinear) anomaly [146, 147] since the energy E implicitly defines the soft modes in the ultrarelativistic frame of the meson. We observe that the energy dependence is a global feature as it enters with the meson charge Q_M^2. The corresponding logarithmic term similarly arises in the point-like limit for the leptonic matrix element in (4.96) that is renormalized by $Z_\ell(\mu)$ in (4.62) with $Q_\ell, E_\ell \leftrightarrow Q_M, E$. The scale evolution is given by

$$\frac{d}{d\ln\mu} Z_\ell(\mu) = \frac{\alpha_{\text{em}}}{\pi} Q_\ell^2 \left(\ln\frac{\mu}{2E} + \frac{3}{4} \right) Z_\ell(\mu) \,, \tag{5.6}$$

which has a multiplicative solution $Z_\ell(\mu) = U_\ell(\mu,\mu_0) Z_\ell(\mu_0)$ determined by the "local" evolution factor[3]

$$U_\ell(\mu,\mu_0) = \exp\left\{ \int_{\mu_0}^{\mu} \frac{d\mu'}{\mu'} \frac{\alpha_{\text{em}}(\mu')}{\pi} Q_\ell^2 \left(\ln\frac{\mu'}{2E} + \frac{3}{4} \right) \right\} . \tag{5.7}$$

Since $U_\ell \neq 1$ for any two distinct scales, we directly observe that the normalization is no longer conserved. Motivated by the factorization theorem (4.70) which includes the semi-leptonic amplitude alongside with $1/Z_\ell$, we redefine the LCDA to $\hat{\Phi}_M = \Phi_M / Z_\ell$. Note that the logarithmic terms still change the overall normalization of $\hat{\Phi}_M$.

In QCD-only, the kernel (5.5) can be diagonalized in terms of Gegenbauer polynomials. The local logarithmic terms in QED produce non-diagonal coefficients that prevent us from finding a simple solution. Nevertheless, we can study the analytic structure of the evolution kernel to identify the endpoint behaviour of the all-order solution Φ_M compared to the asymptotic form of $\phi_M = 6u\bar{u}$ for $\mu \to \infty$ in QCD. In Sec. 5.1.2, we derive a fixed-order $\mathcal{O}(\alpha_{\text{em}})$ solution to the RGE (5.4) that resums QCD logarithms together with an α_{em} expansion. We recall that the light-meson LCDA in presence of QED naturally has to be understood as a matching coefficient of a low-energy effective theory and thus contains IR divergences that are minimally subtracted in dimensional regularization. The analytical and numerical results therefore apply to this particular scheme.

5.1.1 Endpoint behaviour

In QCD-only, the light-meson LCDA vanishes linearly at both endpoints $u, \bar{u} \to 0$, which is a consequence of conformal symmetry in QCD [148]. In Appendix B, we provided an explicit example of how the twist counting naturally constructs higher-twist operators of the B LCDA and determines their asymptotic behaviour. The general arguments apply to both heavy and light mesons and restrict the functional shape of the anomalous dimension. They are based on an OPE in terms of conformal operators

[3] We recall that the double-logarithmic expression in U_ℓ is a universal feature of the radiative amplitude including ultrasoft photons introduced in Sec. 4.5.

in QCD at the RG fixed point[4] in $d = 4 - 2\epsilon$ spacetime dimensions [149]. The running in QCD×QED depends however on both couplings $\beta(\alpha_s, \alpha_{\text{em}})$ such that there is no related fixed point to the RG. Hence, we do not expect conformal symmetry arguments to apply. We further note that QED becomes strongly coupled at scales of order 10^{12} GeV, which are physically irrelevant to the application range of the light meson LCDA. Nevertheless, this implies that the arguments below strictly apply to the one-loop RGE only and may be corrected by higher-loop orders.

The kernel (5.5) acts as a distribution in the variable u since it is convoluted with a hard function in exclusive processes. However, to analyze the behaviour of the function Φ_M under the RG, we rewrite the kernel to act in the variable v[5]

$$\Big[\dots\Big]_+^{(u)} = \Big[\dots\Big]_+^{(v)} + \left(u \ln \bar{u} + \bar{u} \ln u + \frac{3}{2}\right) \delta(u - v)\,. \tag{5.8}$$

In this way, the RGE (5.4) becomes self-consistent, meaning that for any initial function $\Phi_M(u;\mu_0)$ the infinitesimal evolution $d\Phi_M/d\ln\mu$ can be computed from the distribution in integral over v. In what follows, we construct an asymptotic expansion for $\Phi_M(u;\mu)$ in the endpoint regions $u \to 0$ and $u \to 1$. We restrict ourselves to the analysis of the $u \to 0$ case since $u \to 1$ can be inferred from $Q_{q_1} \leftrightarrow Q_{q_2}$ and consequently $Q_M \to -Q_M$. Near the endpoint $u \to 0$, the evolution equation is generally dominated by two momentum regions in which $v \sim u \ll 1$ (soft region) and $v \sim 1, u \ll 1$ ("true" collinear region). We approximate the distributions according to the power counting in a method of regions approach [84], see Sec. 2.2,

$$\text{Collinear region:} \qquad \int_0^1 dv \Big[\dots\Big]_+^{(v)} \to u \int_0^1 \frac{dv}{v} \left(1 + \frac{1}{v}\right)\,, \tag{5.9}$$

$$\text{Soft region:} \qquad \int_0^1 dv \Big[\dots\Big]_+^{(v)} \to u \int_0^\infty dv \left[\frac{\theta(v-u)}{v(v-u)} + \frac{\theta(u-v)}{u(u-v)}\right]_+^{(v)}\,. \tag{5.10}$$

In the first line, we neglected the plus-distribution as the additional term is power-suppressed. The soft region in the second line now acts as a distribution on functions with extended support $[0, \infty)$. Depending on the convoluted function $\Phi_M(v;\mu)$, both regions may diverge at $v \to 0$ and $v \to \infty$ respectively so that the integrals need to be regularized.[6]

In the following, we assume that the light meson LCDA near the endpoint $u \to 0$ exhibits the form $\Phi_M(u;\mu_0) \sim u^b$ for some initial scale μ_0. There are four distinct cases for the exponent b for which either one or both regions (5.9) and (5.10) dominate.

[4] The RG fixed point in QCD is sometimes referred to as the "Wilson-Fisher critical point". To any loop order, it is defined by the dimensional regulator ϵ^* at which the QCD beta function vanishes, i.e. $\beta^{\text{QCD}}(\alpha_s, \epsilon^*) = 0$.

[5] To show the equality in terms of distributions, we integrate both sides with respect to two test functions $\int_0^1 du \int_0^1 dv f(u)g(v)$.

[6] The method of regions approach yields an accurate power expansion in which power-suppressed terms can be disregarded even when they are divergent.

i) For $b > 1$, the collinear region dominates and the integral (5.4) counts in total as u^1. We neglect the local terms and the soft region that scales as $u^b \ll u^1$. As a consequence, the collinear RGE instantaneously reproduces linear endpoint behaviour for any $b > 1$ since after an infinitesimal evolution step $\mu_0 \to \mu_0 + d\mu$ the leading term $\Phi_M(u;\mu_0 + d\mu) \sim u^1$ supersedes the u^b initial condition.

ii) For $b = 1$, both regions and the local terms have the same power counting so that the full kernel contributes to the RGE. The asymptotic behaviour can be inferred as a limiting case from the soft approximation as discussed below.

iii) For $b < 1$, the soft region and the local terms both scale as u^b and dominate. In this case, the simplification allows us to analytically solve the RGE in Mellin space. Note that the result strictly depends on the initial condition $\Phi_M(u;\mu_0)$.

iv) For $b \leq -1$, the evolution equation becomes ill-defined since the distribution integral in (5.4) always diverges. The local terms in QED drive the LCDA unavoidably towards this regime when we evolve the function to exceptionally large scales.

Without further assumptions, only case iii) can be analytically solved to a satisfactory extent. We therefore focus on this case and assume $b < 1$ at the initial scale μ_0. To provide the basic ideas of the derivation for the asymptotic behaviour, we first recall some of the fundamental steps in QCD-only. In this case, the RGE in the soft region becomes

$$\Gamma(u,v;\mu)\big|^{\text{soft}}_{\alpha_{\text{em}}=0} = -\frac{\alpha_s C_F}{\pi}\left\{\left[\frac{u\theta(v-u)}{v(v-u)} + \frac{\theta(u-v)}{(u-v)}\right]_+^{(v)} + \delta(u-v)\left(\ln u + \frac{3}{2}\right)\right\}, \tag{5.11}$$

which exactly coincides with the kernel governing the evolution of the B LCDA ϕ_+ up to a constant in the local term. Physically, this configuration is in fact equivalent to a heavy-light system since for $u \to 0$, the q_1-quark in the light meson is restricted to soft momenta while the q_2-quark has a comparably large and relatively fixed momentum component $n_+ k_{q_2}$. The solution to (5.11) therefore involves the standard hypergeometric ${}_2F_1$ convolution given in [150]. We rederive this result in a slightly different form following the analyses in [35, 151]. The endpoint behaviour can be analyzed using a Mellin transformation for the LCDA

$$\tilde{\Phi}_M(\eta;\mu) \equiv \int_0^\infty du\, u^{-1-\eta}\,\Phi_M(u;\mu)\,, \qquad \Phi_M(u;\mu) = \int_{c-i\infty}^{c+i\infty}\frac{d\eta}{2\pi i}\,u^\eta\,\tilde{\Phi}_M(\eta;\mu)\,, \tag{5.12}$$

where c is a real parameter.[7] A posteriori, the function itself takes the form $\Phi_M(u;\mu) \sim u^{b_\mu}$ for $u \to 0$ with some scale-dependent exponent b_μ. Hence, we must choose $c < b_\mu$ in

[7] Note that we use the transformation prescription also for the LCDA $\phi_M(u;\mu)$ in QCD-only.

order for the Mellin transform to converge (the latter requires $\mathrm{Re}(\eta) < b_\mu$). Restricting to QCD-only, the RGE (5.11) in Mellin-space reads

$$\left[\frac{d}{d\ln\mu} + \frac{\alpha_s C_F}{\pi}\partial_\eta\right]\tilde{\phi}_M(\eta;\mu) = -\frac{\alpha_s C_F}{\pi}\left(H_\eta + H_{-\eta} - \frac{3}{2}\right)\tilde{\phi}_M(\eta;\mu)\,, \tag{5.13}$$

in which $H_n = \gamma_E + \psi(n+1)$ and $\psi(n) = \Gamma'(n)/\Gamma(n)$ are the harmonic number and the digamma function respectively. The solution to this equation is given by [150]

$$\tilde{\phi}_M(\eta;\mu) = e^{(2\gamma_E - 3/2)a}\,\frac{\Gamma(1-\eta)\Gamma(1+\eta+a)}{\Gamma(1+\eta)\Gamma(1-\eta-a)}\,\tilde{\phi}_M(\eta+a;\mu_0)\,. \tag{5.14}$$

The differential operator on the left-hand side of (5.13) leads to a shift in the η-variable of the Gamma functions and the initial condition. We define

$$a \equiv a(\mu,\mu_0) = -C_F\int_{\mu_0}^{\mu}\frac{d\tilde{\mu}}{\tilde{\mu}}\frac{\alpha_s(\tilde{\mu})}{\pi} = \frac{2C_F}{\beta_0^{\mathrm{QCD}}}\ln\frac{\alpha_s(\mu)}{\alpha_s(\mu_0)} + \mathcal{O}(\alpha_s)\,, \tag{5.15}$$

where β^{QCD} is the QCD β function given in (2.88). At one-loop, the relevant coefficient for n_f active quark flavours is

$$\beta_0^{\mathrm{QCD}} = \frac{11}{3}N_c - \frac{2}{3}n_f\,, \tag{5.16}$$

with $N_c = 3$. Since $\beta^{\mathrm{QCD}} < 0$ for $n_f \leq 6$, the evolution variable (5.15) is strictly negative when evolving to higher scales $\mu > \mu_0$. In fact, it turns out that the evolution factor is restricted to $-1 < a < 0$ in pure QCD.

The solution (5.14) holds to all orders in the strong coupling. In principle, we can obtain an analytic form in u-space by performing the inverse Mellin transformation. This is however not the goal of our analysis, since the soft approximation has no concrete application in the present context.[8] Instead, we determine the asymptotic behaviour from the analytic properties of the solution in Mellin space. To this end, we observe that (5.12) and (5.14) restrict the contour parameter c to the strip $-1-a < c < b_\mu \equiv b - a(\mu,\mu_0)$ so that the inverse transformation exists. We then deform the integration contour to enclose all singularities in the right half-plane of η. Note that the initial condition $\phi(u;\mu_0) \sim u^b$ leads to a pole at $\eta = b_\mu$ for the shifted function (5.14) in Mellin space. The left-most pole on the real axis for $\mathrm{Re}(\eta) > c$ in (5.14) dictates the asymptotic form of $\phi_M(u;\mu)$ for $u \to 0$. In our analysis, we strictly assume power-like behaviour for the initial condition without logarithmic $\ln u$ corrections that are only produced once QED is included. For $b_\mu < 1$, the contour picks up the pole of $\tilde{\phi}_M(\eta+a;\mu_0)$ and the asymptotic behaviour of the solution is given by $\phi_M(u;\mu) \sim u^{b_\mu}$. We present the precise analytic derivation in Appendix E.1. When μ is large enough, we generate linear behaviour $b_\mu = 1$ at which the $\Gamma(1-\eta)$ term becomes relevant. We neglect the $b_\mu > 1$ case since the collinear kernel automatically reproduces the

[8] The solution to these kinds of equations is discussed in more detail in Sec. 5.2.

linear endpoint behaviour. For $b_\mu = 1$, one might be tempted to directly extrapolate $\phi_M(u;\mu) \sim u^1$. However, we emphasize that the collinear kernel (5.9) enters at this power. Nevertheless, the soft approximation determines the asymptotic behaviour of the LCDA since the collinear region does not provide $\ln u$ enhanced terms that generate a different form. This is different to the soft region (5.10) in which the integral $\int_u^\infty \frac{dv}{v^2}\phi_M(v;\mu)$ for $\phi_M(v;\mu) \sim v^1$ does produce these terms.

For QCD, the above analysis is pictured in the left plot of Fig. 5.1, which shows the RG flow of the exponent $b_\mu = b - a(\mu,\mu_0)$ for given b to the scale $\mu > \mu_0$. While $b_\mu < 1$, the evolved function turns into $\phi_M(u;\mu) \sim u^{b_\mu}$ irrespective of the initial behaviour $\phi_M(u;\mu_0) \sim u^b$. As soon as we reach $b_\mu = 1$, the scale evolution does not change the asymptotic behaviour anymore which is consistent with the asymptotic form $\phi_M(u;\mu\to\infty) \to 6u\bar{u}$. Lastly, we note that $b > 1$ immediately becomes linear again. In the case of neutral mesons in QED, the same arguments apply since the evolution kernel just enters with the prefactor $\alpha_s C_F \to \alpha_s C_F + \alpha_{\rm em} Q_q^2$. A more sophisticated discussion in terms of Gegenbauer moments can be found below (5.31). In contrast to QCD-only, the one-loop results are not viable at extremely high scales when $\alpha_{\rm em}$ eventually tends to infinity and perturbation theory breaks down.

For charged mesons in QCD×QED, the analysis of the asymptotic behaviour becomes slightly more complicated due to the logarithmic terms in (5.5) but follows the same lines above. The small u behaviour is independent of the overall normalization and thus we redefine the LCDA

$$\Phi_M(u;\mu) = Z_\ell(\mu)\hat{\Phi}_M(u;\mu)\,. \tag{5.17}$$

which subtracts the point-like limit (5.6). The Mellin-space RGE for $\hat{\Phi}_M(u;\mu)$ in the soft approximation reads

$$\begin{aligned}\left[\frac{d}{d\ln\mu} + \frac{\alpha_s C_F + \alpha_{\rm em} Q_{q_1}(Q_{q_2}-Q_M)}{\pi}\partial_\eta\right]\tilde{\hat{\Phi}}_M(\eta;\mu)\\ = -\frac{\alpha_s C_F + \alpha_{\rm em} Q_{q_1}Q_{q_2}}{\pi}\left(H_\eta + H_{-\eta} - \frac{3}{2}\right)\tilde{\hat{\Phi}}_M(\eta;\mu)\,,\end{aligned} \tag{5.18}$$

where we adapted the Mellin transform (5.12) to the normalized LCDA $\tilde{\hat{\Phi}}_M(\eta;\mu)$. Following [151], we write down the ansatz

$$\begin{aligned}\tilde{\hat{\Phi}}_M(\eta;\mu) = e^{2\gamma_E a - 3\check{a}/2}\,\frac{\Gamma(1-\eta)\Gamma(1+\eta+a)}{\Gamma(1+\eta)\Gamma(1-\eta-a)}\tilde{\hat{\Phi}}_M(\eta+a;\mu_0)\\ \times\exp\left\{-\int_{\mu_0}^{\mu}\frac{d\mu'}{\mu'}\frac{\alpha_{\rm em}(\mu')Q_{q_1}Q_M}{\pi}\left(H_{\eta+a(\mu,\mu')} + H_{-\eta-a(\mu,\mu')}\right)\right\}\,,\end{aligned} \tag{5.19}$$

which provides a solution to (5.18) with the generalized evolution variable

$$a \equiv a(\mu,\mu_0) = -\int_{\mu_0}^{\mu}\frac{d\tilde{\mu}}{\tilde{\mu}}\frac{\alpha_s(\tilde{\mu})C_F + \alpha_{\rm em}(\tilde{\mu})Q_{q_1}(Q_{q_2}-Q_M)}{\pi}\,. \tag{5.20}$$

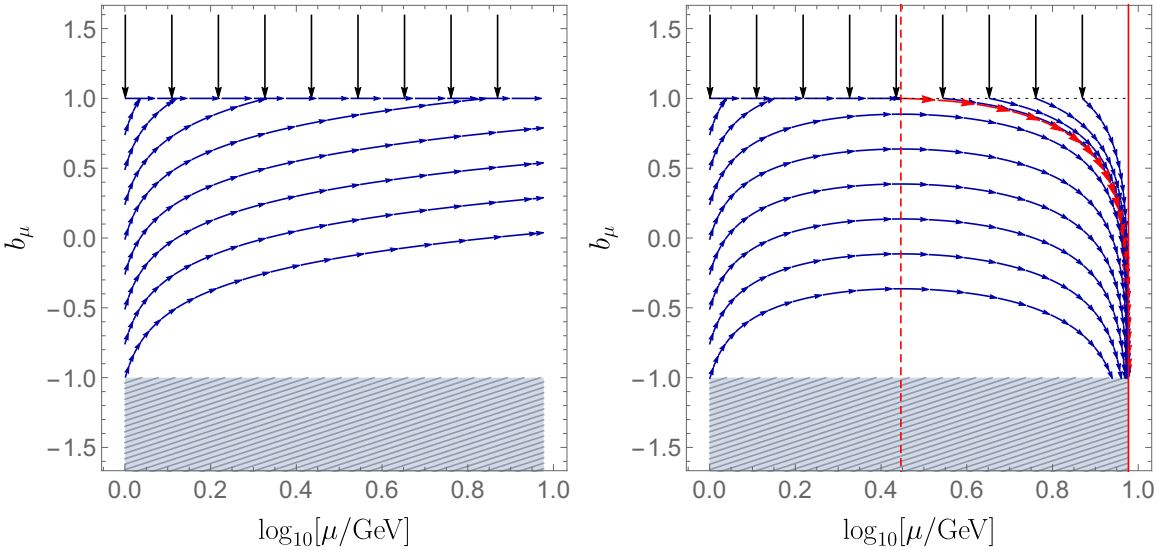

Figure 5.1: Instructive example of the RG flow for the exponent b_μ in the limit $u \to 0$: The left plot shows QCD-only, while the right plot pictures full QCD×QED. In a simplified model with one quark and lepton generation, we choose unphysical couplings $\alpha_s(\mu_0) = 4\pi$, $\alpha_{\mathrm{em}}(\mu_0) = \pi/4$ at the initial scale $\mu_0 = 1$ GeV. The running is determined by $\beta_0^{\mathrm{QCD}} = 29/3$ and $\beta_0^{\mathrm{QED}} = -32/9$. In the right plot, the solid vertical red line displays the QED Landau pole at $\mu_L \approx 9.5$ GeV while the dashed vertical red line marks the critical scale defined by (5.27) at $\mu_c \approx 2.8$ GeV. The red curve shows the evolution of $b_\mu = 1$ at μ_c towards the ill-defined, gray-shaded region with $b_\mu = -1$.

We additionally defined another global variable in the prefactor of the solution

$$\check{a} \equiv \check{a}(\mu, \mu_0) = -\int_{\mu_0}^{\mu} \frac{d\tilde{\mu}}{\tilde{\mu}} \frac{\alpha_s(\tilde{\mu}) C_F + \alpha_{\mathrm{em}}(\tilde{\mu}) Q_{q_1} Q_{q_2}}{\pi} \,. \tag{5.21}$$

The second line in (5.19) originates from the additional derivative term on the left-hand side of (5.18) which is related to the local logarithmic terms in the RGE. Its non-trivial analytic structure modifies the asymptotic behaviour of the evolved function. We discuss these properties including the full scale dependence in Appendix E.2. In the present context, we focus on two particular scenarios in which the analytic structure of the harmonic number exponential becomes "simple". We first consider i) the QED-only case with scale-dependent $\alpha_{\mathrm{em}}(\mu)$ and second ii) the case of scale-independent couplings α_s and α_{em} in QCD×QED. In both scenarios, we can perform the integral in the second line of (5.19) exactly and obtain

$$\tilde{\hat{\Phi}}_M(\eta;\mu) = e^{2\gamma_E a - 3\check{a}/2} \left[\frac{\Gamma(1-\eta)\Gamma(1+\eta+a)}{\Gamma(1+\eta)\Gamma(1-\eta-a)}\right]^{1+p} \tilde{\hat{\Phi}}_M(\eta+a;\mu_0)\,, \tag{5.22}$$

where, compared to the QCD solution (5.14), the Gamma functions are exponentiated by the non-integer $p = \alpha_{\rm em} Q_{q_1} Q_M / (\alpha_s C_F + \alpha_{\rm em} Q_{q_1}(Q_{q_2} - Q_M))$. The asymptotic behaviour then depends on the initial condition and the value of the exponent.

In case i), the exponent simplifies for QED-only to $p = Q_M/(Q_{q_2} - Q_M) = -3/5$ with $Q_M = -1$. Furthermore, the evolution variable

$$a = Q_{q_1}(Q_{q_2} - Q_M) \frac{2}{\beta_0^{\rm QED}} \ln \frac{\alpha_{\rm em}(\mu)}{\alpha_{\rm em}(\mu_0)} + \mathcal{O}(\alpha_{\rm em}) \tag{5.23}$$

turns out to be positive for $\mu > \mu_0$ due to the sign of the quark charges and the QED β function at one-loop

$$\frac{d\alpha_{\rm em}}{d\ln\mu} = -\frac{\alpha_{\rm em}^2}{2\pi}\beta_0^{\rm QED}\,, \qquad \beta_0^{\rm QED} = -\frac{4}{3}\left[N_c(n_u Q_u^2 + n_d Q_d^2) + n_\ell Q_\ell^2\right] < 0\,. \tag{5.24}$$

Above, $n_u(n_d)$ and n_ℓ are the number of active up (down) quark and lepton flavours respectively. In this case, we find the power-like behaviour for small u to be $\Phi_M(u;\mu) \sim u^{b_\mu}$ for $b < 1$, and $\Phi_M(u;\mu) \sim u^{1-a(\mu,\mu_0)}$ for $b \geq 1$. Since $a > 0$, the endpoint behaviour is generally pulled towards smaller values of the exponent and eventually to $b_\mu = -1$ when μ becomes large enough. As a consequence, the LCDA becomes divergent when going below $b_\mu = 0$. Furthermore, the evolution equation becomes ill-defined as (5.4) breaks down for $b_\mu < -1$. In the real world, this effect appears only at unphysically high scales and is prohibited by the strong interaction at low energies.

For ii) scale-independent couplings in QCD×QED, the evolution variable reads

$$a = -\frac{\alpha_s C_F + \alpha_{\rm em} Q_{q_1}(Q_{q_2} - Q_M)}{\pi} \ln \frac{\mu}{\mu_0} \tag{5.25}$$

and hence, QCD and QED effects in general compete due to the different relative signs induced by the electric charges of the meson and its constituents. The global sign of (5.25) then determines the asymptotic behaviour of the solution (5.22). For $\alpha_s C_F + \alpha_{\rm em} Q_{q_1}(Q_{q_2} - Q_M) < 0$, we have $a > 0$ so that b_μ decreases with increasing μ and the endpoint behaviour equals to the QED-only case i). For $\alpha_s C_F + \alpha_{\rm em} Q_{q_1}(Q_{q_2} - Q_M) > 0$, we have $a < 0$ and b_μ increases with μ, which is the phenomelogically relevant case comparable with QCD-only. The endpoint behaviour of the LCDA is $\Phi_M(u;\mu) \sim u^{b_\mu}$ for $b_\mu < 1$ and hence driven towards linear dependence so that we definitely reach $b_\mu = 1$ for a finite $\mu < \infty$. At $b_\mu = 1$, the analytic properties of the solution are more complicated, since the Gamma function $\Gamma^p(1-\eta)$ in (5.22) not only has a pole at $\eta = 1$, but also an attached branch cut extending to $\mathrm{Re}(\eta) \to \infty$. The integration along this cut yields

$$\Phi_M(u;\mu) \sim u(-\ln u)^p\,. \tag{5.26}$$

We conclude that at $b_\mu = 1$, the linear asymptotics of the light meson LCDA are enhanced by the logarithmic term $(-\ln u)^p$. For $\alpha_{\rm em} \to 0$, we restore the QCD-only

solution as the exponent p becomes zero. These relations can also be observed in an $\alpha_{\rm em}$ expansion since the first-order term enters with $\alpha_{\rm em} u \ln(-\ln u)$.

The two special cases above provide the discussion ground for the full QCD×QED theory, including running of the gauge couplings at one-loop. The exponent p introduced below (5.22) implicitly defines a critical scale through (5.20) given by

$$\alpha_s(\mu_c) C_F + \alpha_{\rm em}(\mu_c) Q_{q_1}(Q_{q_2} - Q_M) = 0\,. \tag{5.27}$$

For the critical scale, the power p has a singularity $p(\mu_c \mp 0) = \pm\infty$ with an opposite sign on both sides that marks the change from a QCD-like to a QED-like endpoint behaviour. The RG flow in terms of the asymptotic exponent b_μ is displayed in the right plot of Fig. 5.1. On a mathematical level, we conveniently distinguish between the cases $\mu_0 > \mu_c$ and $\mu < \mu_c$. In the former, we find $\alpha_s C_F + \alpha_{\rm em} Q_{q_1}(Q_{q_2} - Q_M) < 0$ so that the solution behaves like $\Phi_M(u;\mu) \sim u^{b_\mu}$, where $b_\mu < 1$ decreases as in QED-only, and we reach the ill-defined region of the RGE at a finite $\mu_L > \mu_0$. This only happens some orders of magnitude before entering the strong coupling regime in QED and hence, it is irrelevant for practical applications.[9] For $\mu < \mu_c$, we find again $\Phi_M(u;\mu) \sim u^{b_\mu}$ but for increasing $b_\mu < 1$. Interestingly, we observe for $b_\mu = 1$ that our result (5.26) also applies in this case even though it was derived for fixed couplings only. This fact emerges from the full scale-dependent discussion in Appendix E.2. The special case $\mu_0 < \mu_c < \mu$ is not listed since we can always split the evolution into smaller pieces.

In general, we conclude that the linear endpoint behaviour in physical scenarios is modified by an additional $(-\ln u)^p$ term. Hence, inverse moments like $\int_0^1 du \Phi_M(u;\mu)/u$ appearing in the factorization theorem (4.70) exist at realistic scales. In Fig. 5.2, we present the new qualitative features of the light meson LCDA involving the scale-dependent normalization, asymmetry as well as divergent endpoint behaviour for large artificial $\alpha_{\rm em}$. The plot is generated by discretization of the RGE (5.4), for which we refer to Chapter 6, providing more insights on the method.

5.1.2 Gegenbauer moments and analytic $\mathcal{O}(\alpha_{\rm em})$ solution

For realistic applications, we assume low scales at which $\alpha_{\rm em}$ is small. In this case, the first-order $\mathcal{O}(\alpha_{\rm em})$ solution to the RGE already provides an excellent approximation of the resummed result. This corresponds more precisely to a resummation of logarithms $\alpha_{\rm em}^k \alpha_s^n \ln^{n+k} \mu/\mu_0$ with $k = 0, 1$. Hence, QCD logarithms are summed on top of a fixed-order expansion in the electromagnetic coupling. We recall that in QCD-only, the kernel (5.5) can be diagonalized in terms of Gegenbauer polynomials. For this reason, we express the LCDA in (5.4) as

$$\hat{\Phi}_M(u;\mu) = 6u\bar{u} \sum_{n=0}^{\infty} a_n^M(\mu) C_n^{(3/2)}(2u-1)\,, \tag{5.28}$$

[9] In a theory with other quark and lepton flavours, the coefficient $\beta_0^{\rm QED}$ could be large enough to render the RGE for $\Phi_M(u;\mu)$ inconsistent much below the scale where QED becomes strongly coupled.

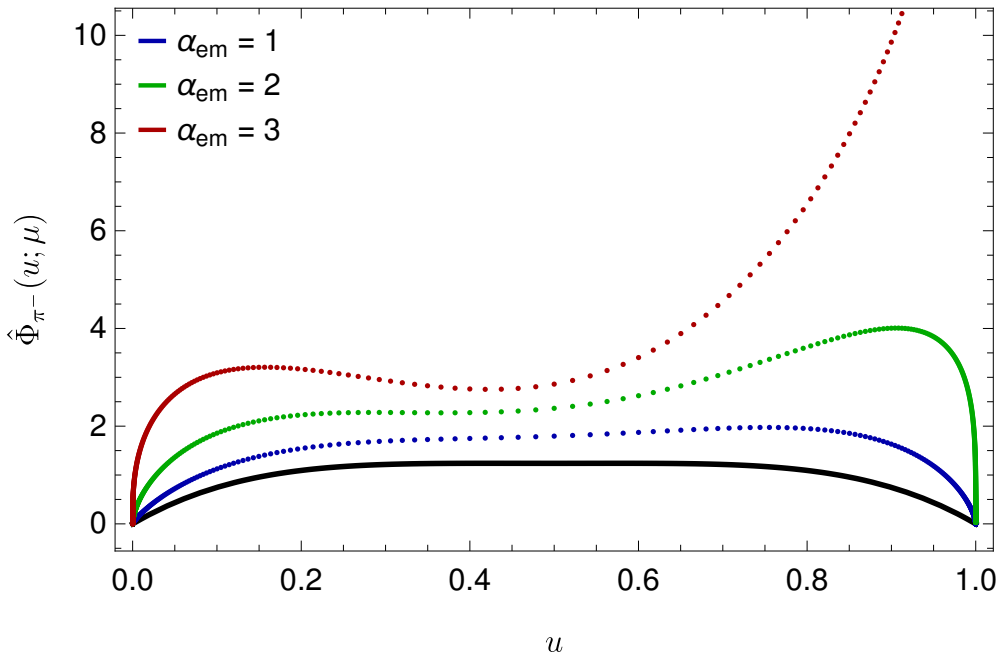

Figure 5.2: The plot shows a numerical solution to (5.4) for the LCDA of a negatively charged π^-. We discretize the u-interval $[0,1]$ to $N = 1001$ points that are logarithmically distributed and use lattice QCD results for the initial condition $\hat{\Phi}_{\pi^-}(u;\mu_{\rm lat}) = 6u\bar{u}(1+a_2^\pi(\mu_{\rm lat})C_2^{(3/2)}(2u-1))$ (black solid curve) at $\mu_{\rm lat} = 2$ GeV with $a_2^\pi(\mu_{\rm lat})$ from Table 6.3. The strong coupling $\alpha_s(\mu)$ runs at one-loop while the $\alpha_{\rm em}$ is fixed to three different, artificially large values. We evolve the LCDA to $\mu = 10$ GeV (dotted curves) and observe that i) the normalization is not conserved, the LCDA ii) gets asymmetric in $u \leftrightarrow \bar{u}$ and iii) begins to diverge at $u = 1$ for large $\alpha_{\rm em}$. The latter is a consequence of the larger charge Q_u leading to momentum configuration in which the u-quark is preferred to carry a higher momentum fraction in the meson.

which results in an infinite dimensional system of coupled ordinary differential equations for $a_n^M(\mu)$, where $C_n^{(3/2)}(2u-1)$ and $a_n^M(\mu)$ are the n-th Gegenbauer polynomial/moment respectively. Note that we subtracted the universal factor Z_ℓ according to (5.17). For the n-th coefficient in the expansion (5.28), the RGE is given by

$$\frac{d}{d\ln\mu}a_n^M(\mu) = -\frac{\alpha_s(\mu)C_F + \alpha_{\rm em}(\mu)Q_{q_1}Q_{q_2}}{2\pi}\gamma_n a_n^M(\mu) - \frac{\alpha_{\rm em}(\mu)}{\pi}Q_M\sum_{m=0}^{\infty} f_{nm}a_m^M(\mu)\,, \tag{5.29}$$

where the coefficients in the last term are given by

$$f_{nm} = \frac{4(2n+3)}{(n+2)(n+1)}\int_0^1 du\ (Q_{q_1}\ln u - Q_{q_2}\ln\bar{u})\ u\bar{u}\ C_n^{(3/2)}(2u-1)C_m^{(3/2)}(2u-1)$$

$$= \left(Q_{q_2} - (-1)^{n+m} Q_{q_1}\right) \times \begin{cases} \dfrac{(2n+3)}{(n-m)(n+m+3)} \times \dfrac{(m+1)(m+2)}{(n+1)(n+2)} & n > m \\ \dfrac{(2n+3)}{(m-n)(n+m+3)} & n < m \\ \dfrac{1}{2n+3} + H_{n+1/2} - H_{n+2} + \ln 4 & n = m\,. \end{cases} \tag{5.30}$$

The non-diagonal terms f_{nm} originate from the local logarithmic terms in the RGE so that Gegenbauer moments with different coefficients in general mix under scale evolution.

In the neutral case $Q_M = 0$ with $Q_{q_1} = Q_{q_2} = Q_q$, we find that (5.29) becomes diagonal and the solution is similar to the LL solution in QCD-only

$$a_n(\mu) = \left(\frac{\alpha_s(\mu)}{\alpha_s(\mu_0)}\right)^{C_F \gamma_n / \beta_0^{\mathrm{QCD}}} \left(\frac{\alpha_{\mathrm{em}}(\mu)}{\alpha_{\mathrm{em}}(\mu_0)}\right)^{Q_q^2 \gamma_n / \beta_0^{\mathrm{QED}}} a_n(\mu_0)\,, \tag{5.31}$$

with

$$\gamma_n = 1 - \frac{2}{(n+1)(n+2)} + 4 \sum_{m=2}^{n+1} \frac{1}{m} = 4H_{n+1} - 3 - \frac{2}{(n+1)(n+2)} \tag{5.32}$$

is the anomalous dimension [134] that asymptotically behaves like $\gamma_n \approx 4\ln(n)$ at large n. For the neutral case as well as in QCD-only the factors in (5.31) suppress the Gegenbauer moments for an upward scale evolution since $\alpha_s(\mu) < \alpha_s(\mu_0)$, $C_F \gamma_n / \beta_0^{\mathrm{QCD}} > 0$ and $\alpha_{\mathrm{em}}(\mu) > \alpha_{\mathrm{em}}(\mu_0)$, $Q_q^2 \gamma_n / \beta_0^{\mathrm{QED}} < 0$. Therefore, we can truncate the Gegenbauer expansion at some $n = n_0$ which is oftentimes chosen to be $n_0 = 2$ due to constraints from lattice QCD. Note that we argued before that QED in general prevents a truncation of the series, but only for charged mesons. Since $\gamma_0 = 0$, the zeroth moment is scale-independent so that the normalization $\int_0^1 du\, \Phi_M(u;\mu) = a_0 = 1$ is maintained for $Q_M = 0$.

In the case of $Q_M \neq 0$, the first term in (5.29) proportional to $Q_{q_1} Q_{q_2} < 0$ comes with the opposite sign compared to the QCD contribution and enhances the Gegenbauer moments with increasing μ. Nevertheless, we truncate the series at $n_0 = 2$ since we restrict ourselves to low scales at which $\alpha_{\mathrm{em}}(\mu)$ stays small in contrast to $\alpha_s(\mu)$.[10] Furthermore, the coefficients f_{nm} lead to a mixing of lower into higher Gegenbauer moments and vice versa. We especially emphasize that a_0 receives corrections from higher moments as $f_{0m} \neq 0$ such that the normalization of the LCDA is no longer conserved. For large n, the diagonal contribution $f_{nn} \approx Q_M \ln 4$ becomes constant and thus irrelevant with respect to the former logarithmically enhanced γ_n term in (5.29). The non-diagonal terms on the other hand fall off like $f_{nm} \sim 1/n^3$ for $n \gg m$ and

[10] Only at extremely large scales QED would turn the overall sign of the first term so that higher Gegenbauer moments get increasingly relevant.

$f_{nm} \sim 1/m^2$ for $m \gg n$. When $n \sim m$ are of the same order, the off-diagonal terms drop as $1/n$. We conclude that, independent of the QED coupling, the mixing between distant Gegenbauer moments gets strongly suppressed by the mixing matrix. Together with the truncation argument, this motivates to solve the resulting finite-dimensional coupled system (5.29) iteratively to first-order in $\alpha_{\rm em}$.

In the approximation where QED is small, we now solve the RGE analytically to $\mathcal{O}(\alpha_{\rm em})$ which sums the leading logarithms $\alpha_{\rm em}^k \alpha_s^n L^{n+k}$ with $k = 0, 1$ with $L = \ln \mu/\mu_0$. The resummation of QCD logarithms is in fact necessary since $\alpha_s \times L \sim \mathcal{O}(1)$ while $\alpha_{\rm em} \times L \ll 1$ justifies the first-order expansion in the electromagnetic coupling.[11] We expand the Gegenbauer moments to first order according to

$$a_n(\mu) = a_n^{\rm QCD}(\mu) + \frac{\alpha_{\rm em}(\mu)}{\pi} a_n^{(1)}(\mu) + \mathcal{O}(\alpha_{\rm em}^2) \,, \tag{5.33}$$

where we count the QCD moments as $a_n^{\rm QCD}(\mu) \sim \mathcal{O}(1)$ and the QED moments as $a_n^{(1)}(\mu) \sim \mathcal{O}(\ln(\mu/\mu_0), \alpha_s(\mu_0)/\alpha_s(\mu))$. Technically, one could expand also the initial condition $a_n(\mu_0)$ in the form of (5.33). This would however correspond to a resummation beyond the LL accuracy in QED. After inserting (5.33) into (5.29), we obtain the two differential equations

$$\frac{d}{d\ln\mu} a_n^{\rm QCD}(\mu) = -\frac{\alpha_s(\mu) C_F}{2\pi} \gamma_n a_n^{\rm QCD}(\mu) \tag{5.34}$$

and

$$\frac{d}{d\ln\mu} a_n^{(1)}(\mu) = -\frac{\alpha_s(\mu) C_F}{2\pi} \gamma_n a_n^{(1)}(\mu) - I_n(\mu) \tag{5.35}$$

where the inhomogeneous part is given by

$$I_n(\mu) = \frac{1}{2} Q_{q_1} Q_{q_2} \gamma_n a_n^{\rm QCD}(\mu) + Q_M \sum_{m=0}^{\infty} f_{nm} a_m^{\rm QCD}(\mu) \,. \tag{5.36}$$

For convenience, we neglected the index M of the Gegenbauer moments. The RGEs (5.34) and (5.35) correspond to the zeroth and first-order equations in $\alpha_{\rm em}$. We emphasize that the inhomogeneity (5.36) involves *all* QCD Gegenbauer moments. As expected, we recover from (5.34) the LL QCD solution

$$a_n^{\rm QCD}(\mu) = \left(\frac{\alpha_s(\mu)}{\alpha_s(\mu_0)}\right)^{C_F \gamma_n/\beta_0^{\rm QCD}} a_n^{\rm QCD}(\mu_0) \,. \tag{5.37}$$

For the QED corrections at $\mathcal{O}(\alpha_{\rm em})$, we obtain

$$a_n^{(1)}(\mu) = \left(\frac{\alpha_s(\mu)}{\alpha_s(\mu_0)}\right)^{C_F \gamma_n/\beta_0^{\rm QCD}} a_n^{(1)}(\mu_0) - \frac{1}{2} Q_{q_1} Q_{q_2} \gamma_n a_n^{\rm QCD}(\mu) \ln \frac{\mu}{\mu_0} \tag{5.38}$$

[11] For the universal factor Z_ℓ, we keep the double-logarithmic accuracy to all orders in $\alpha_{\rm em}$.

$$- Q_M \sum_{m=0}^{\infty} \frac{2\pi f_{nm}}{\beta_0^{\rm QCD} + (\gamma_n - \gamma_m) C_F} \left\{ \frac{a_m^{\rm QCD}(\mu)}{\alpha_s(\mu)} - \frac{a_m^{\rm QCD}(\mu_0)}{\alpha_s(\mu_0)} \left(\frac{\alpha_s(\mu)}{\alpha_s(\mu_0)} \right)^{C_F \gamma_n / \beta_0^{\rm QCD}} \right\} .$$

We recall that $a_n^{(1)}(\mu_0)$ represents the QED initial condition whose inclusion is beyond LL. In principle, this correction could be accessed by a future lattice simulation in the full QCD×QED theory. Nevertheless, the expansion of the initial condition according to (5.33) seems to be unnatural and we therefore send $a_n^{(1)}(\mu_0) \to 0$ in the numerical analysis of (5.38).

5.2 Soft functions

We defined the soft functions (4.68) in the framework of SCET_{II} factorization for the heavy B-meson decay into two light particles flying back-to-back. The precise definition depends on the soft rearrangement done in Sec. 4.2.3 and in particular the product of two soft Wilson lines from the decoupling of the two collinear sectors. As we will see in the following, the latter introduces imaginary parts, i.e. soft rescattering phases. We emphasize that the definition (4.68) still contained the B-meson decay constant in QCD to match the well-known factorization formula (4.70). It is however convenient to treat the soft functions entirely in HQET so that their natural definition becomes

$$\begin{aligned} & iF_B(\mu) \int_{-\infty}^{\infty} d\omega \; e^{-i\omega t} \Phi_{B,\otimes}(\omega;\mu) \\ & \quad = \frac{1}{R_{\rm c}^{(Q_{M_1})} R_{\bar{\rm c}}^{(Q_{M_2})}} \big\langle 0 \big| \bar{q}^{(q)}(tn_-)[tn_-,0]^{(q)} \not{n}_- \gamma_5 h_v(0) S_{n-}^{\dagger(Q_{M_1})} S_{n+}^{\dagger(Q_{M_2})} \big| \bar{B}(v) \big\rangle , \end{aligned} \tag{5.39}$$

where the HQET decay constant is given in (2.71). Since $F_B(\mu)$ is defined in the absence of QED, the entire electromagnetic corrections are contained in $\Phi_{B,\otimes}$.

Generally, the soft functions produce large logarithms when evaluated much above the soft scale $\Lambda_{\rm QCD}$ that require resummation. To this end, we analyze the behaviour under renormalization of these functions. We define the UV renormalization factor by

$$\mathcal{O}_{\otimes}^{\rm ren}(\omega;\mu) = \int_{-\infty}^{\infty} d\omega' \; Z_{\otimes}(\omega,\omega';\mu) \; \mathcal{O}_{\otimes}^{\rm bare}(\omega') , \tag{5.40}$$

where $\mathcal{O}_{\otimes}$ represents the Fourier-transformed operator with respect to the variable t on the right-hand side of (5.39). In (5.40), we include the $\overline{\rm MS}$ factors of the external quark fields as well as the soft rearrangement factors $R_{\rm c,\bar{c}}$. The one-loop diagrams contributing to the renormalization are depicted in Fig. 5.3. As for the light meson case, the ω'-convolution in (5.40) indicates a mixing of operators with different momentum variables. However, in the present context, one additional modification arises: Contrary to QCD-only, where the function is supported for $\omega > 0$ [152], the integration range for ω' extends to negative infinity for $Q_{M_2} \neq 0$. Hence, we most generally need to consider support for $-\infty < \omega < \infty$. The anomalous dimension for $\Phi_{B,\otimes}(\omega;\mu)$ is then defined

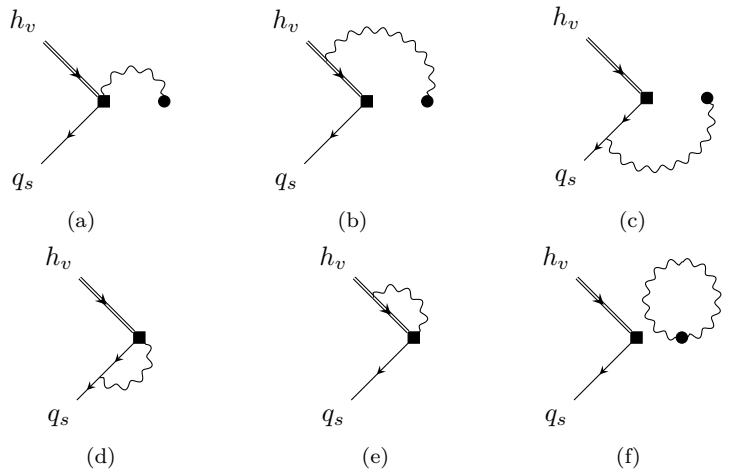

Figure 5.3: One-loop diagrams at $\mathcal{O}(\alpha_{\text{em}})$ for the soft function. The finite-distance Wilson line $[tn_-, 0]^{(q)}$ corresponds to the black square. An insertion of the product $S_{n_-}^{\dagger(Q_{M_1})} S_{n_+}^{\dagger(Q_{M_2})}$ is indicated by a black dot. We do not display the vertex correction since it is UV finite as we see from QCD in (A.14).

by

$$\frac{d}{d\ln\mu}\Phi_{B,\otimes}(\omega;\mu) = -\int_{-\infty}^{\infty} d\omega'\ \Gamma_{\otimes}(\omega,\omega';\mu)\Phi_{B,\otimes}(\omega';\mu)\,, \tag{5.41}$$

where the kernel can be computed from the $Z_{\otimes}$-factor and the scale-dependent decay constant $F_B(\mu)$ in (2.71)

$$\Gamma_{\otimes}(\omega,\omega';\mu) = -\int_{-\infty}^{\infty} d\hat{\omega}\ \frac{dZ_{\otimes}(\omega,\hat{\omega};\mu)}{d\ln\mu} Z_{\otimes}^{-1}(\hat{\omega},\omega';\mu) + \delta(\omega-\omega')\frac{dF_B(\mu)}{d\ln\mu}\,. \tag{5.42}$$

In the following, we calculate the renormalization factor and the anomalous dimension for $\Phi_{B,\otimes}$ in Sec. 5.2.1 and 5.2.2 respectively. Moreover, we introduce their first inverse (logarithmic) moments in 5.2.3 that play an essential role in factorization theorems like (1.7) or (4.70). The solution to the RGE of the soft functions alongside with the asymptotic behaviour and in terms of inverse moments is discussed in Sec. 5.2.5–5.2.6. We highlight that we obtain an all-order solution in both cases, even though the Laplace space solution for $\Phi_{B,\otimes}$ is only formal without concrete application. In the last Sec. 5.2.7, we therefore approximate the solution for the soft function again to first order in α_{em} for which we find an analytic form in ω-space.

5.2.1 Renormalization of $\Phi_{B,\otimes}$

We find the renormalization factor (5.40) by calculating the partonic matrix elements of the operator $\langle 0|\mathcal{O}_{\otimes}(\omega)|\bar{q}_s(\omega')h_v\rangle$ in momentum space. The variable $\omega' \equiv n_-l$ always

denotes the momentum variable of the incoming soft momentum l from the light spectator quark. We strictly assign ω to be the Fourier conjugate to the position space variable t on the right-hand side of (5.39). For convenience, we split the QCD from QED corrections and denote the counter term as

$$Z_\otimes(\omega,\omega',\mu) = \delta(\omega-\omega') + \frac{\alpha_s}{4\pi} Z^{\mathrm{QCD}}(\omega,\omega',\mu) + \frac{\alpha_{\mathrm{em}}}{4\pi} Z_\otimes^{\mathrm{QED}}(\omega,\omega',\mu)\,. \tag{5.43}$$

Without further notation, we identify $Z_\otimes$ and $\Gamma_\otimes$ with the one-loop expressions given below.

The computation of $Z_\otimes^{\mathrm{QED}}$ from the diagrams in Fig. 5.3 varies in multiple steps compared to the QCD calculation [152]. First and foremost, the extended support on the entire real axis for ω and ω' requires the introduction of two modified plus-distributions that mix the momentum variables $\omega' > 0$ into $\omega < 0$ and vice versa. To give a precise example, we derive the contribution for diagram (a). We use off-shell regularization for the spectator quark momentum $l^2 \neq 0$. As before, the soft Wilson lines in the operator definition carry the off-shell regulators $\delta_{\mathrm{c},\bar{\mathrm{c}}}$ in (4.39) and (4.45) after the decoupling from the collinear propagators. In addition to previous computations, we derive the Feynman rule for the finite-distance Wilson line $[tn_-,0]^{(q)}$ which is defined below (4.68). For outgoing photon momentum k, we have

$$\frac{Q_{\mathrm{sp}} e n_-^\mu}{n_-k+\delta_{\mathrm{c}}} \left(\delta(\omega+n_-k-\omega') - \delta(\omega-\omega')\right), \tag{5.44}$$

where the ω' denotes the incoming anti-quark momentum variable and δ_{c} arises from the Wilson line in the collinear decoupling. For (a), the finite-distance Wilson line only contributes together with the Wilson line of Q_{M_2} to the UV divergent terms. Dropping the charge factors $Q_{\mathrm{sp}}Q_{M_2}$, we find for diagram (a)

$$\begin{aligned}
&\tilde{\mu}^{2\epsilon}\int\frac{d^dk}{(2\pi)^d}\frac{-2i}{k^2+i0}\frac{e}{n_-k+\delta_{\mathrm{c}}}\frac{e}{n_+k-\delta_{\bar{\mathrm{c}}}}\left(\delta(\omega+n_-k-\omega')-\delta(\omega-\omega')\right) \qquad (5.45)\\
&= \frac{-2\alpha_{\mathrm{em}}}{(2\pi)^{d-2}}\tilde{\mu}^{2\epsilon}\int_0^\infty\frac{d(n_-k)}{n_-k+\delta_c}\int\frac{d^{d-2}k_\perp}{-k_\perp^2-\delta_{\bar{\mathrm{c}}}n_-k}\left(\delta(\omega+n_-k-\omega')-\delta(\omega-\omega')\right)\\
&= \frac{-2\alpha_{\mathrm{em}}}{(4\pi)^{1-\epsilon}}\left(\frac{\tilde{\mu}}{-\delta_{\bar{\mathrm{c}}}}\right)^\epsilon\Gamma(\epsilon)\int_0^\infty\frac{d(n_-k)}{n_-k+\delta_{\mathrm{c}}}\left(\frac{\tilde{\mu}}{n_-k}\right)^\epsilon\left(\delta(\omega+n_-k-\omega')-\delta(\omega-\omega')\right)\\
&= \frac{-2\alpha_{\mathrm{em}}}{(4\pi)^{1-\epsilon}}\left(\frac{\tilde{\mu}}{-\delta_{\bar{\mathrm{c}}}}\right)^\epsilon\Gamma(\epsilon)\left\{\frac{\theta(\omega'-\omega)}{\omega'-\omega+\delta_{\mathrm{c}}}\left(\frac{\tilde{\mu}}{\omega'-\omega}\right)^\epsilon-\Gamma(\epsilon)\Gamma(1-\epsilon)\left(\frac{\tilde{\mu}}{\delta_{\mathrm{c}}}\right)^\epsilon\delta(\omega-\omega')\right\}.
\end{aligned}$$

We recall our choice $\mathrm{Re}(\delta_{\mathrm{c},\bar{\mathrm{c}}}) < 0$ and note that we decomposed the loop momentum $k^2 = (n_-k)(n_+k)+k_\perp^2$ into light-cone components. We first integrated n_+k with the residue theorem enforcing $n_-k > 0$. We ultimately find two contributions that are proportional to $\delta(\omega-\omega')$ (local) and $\theta(\omega'-\omega)$ (non-local). The Heaviside function originates from the former $\delta(\omega+n_-k-\omega')$ term since n_-k must be positive. It contributes for $\omega < \omega'$ where, most importantly, ω is not necessarily positive in contrast

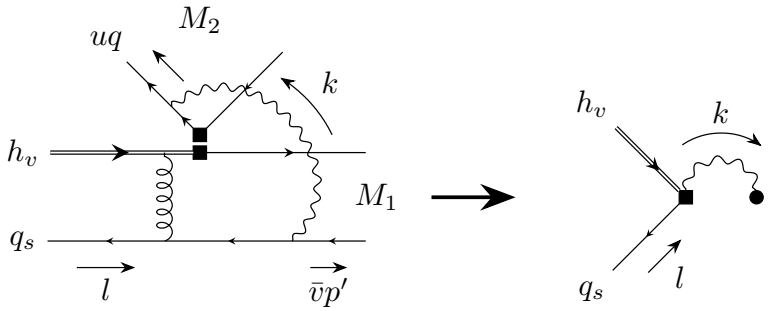

Figure 5.4: The two diagrams provide an example of how diagram (a) of Fig. 5.3 in the EFT arises from a full theory diagram in QCD×QED. The soft photon (wavy) line connects external (anti-)collinear fermions and internal hard(anti-)collinear propagators, where the latter gets contracted to the finite distance Wilson line in HQET×SCET$_{\rm II}$. In terms of momentum components, the difference $\ell - k - \bar{v}p'$ flows through the hard-collinear (curly) gluon line. At LP, the corresponding propagator turns into $1/\omega$ with $\omega = n_-(\ell - k) = \omega' - n_-k$. Even though the soft photon momentum counts formally as $\Lambda_{\rm QCD}$, it can become of order of the large component $n_-k \sim \mathcal{O}(u\ n_-q) \sim \mathcal{O}(m_b \to \infty)$. Hence, we always generate $\omega > 0$ from $\omega' > 0$ since n_-k has no upper bound in the heavy-quark limit.

to QCD-only. In fact, we require the $\omega < 0$ part of the diagram in order to obtain a consistent local limit $t \to 0$ of the operator (5.39). The local limit corresponds to an ω-integration of (5.45) over the entire real axis, which has to be performed before renormalizing the UV divergences.[12] Since the finite-distance line vanishes in this limit, diagram (a) should collapse to zero which is only the case by integrating $-\infty < \omega < \infty$. As a consequence, any initial $\omega' > 0$ will eventually result in $\omega < 0$ by scale evolution. This is an effect of diagram (a) only, so that we conclude $-\infty < \omega < \infty$ is generated only for $Q_{M_2} \neq 0$.

Similar to the light meson case in (5.8), we can understand the renormalization factor as a distribution in both variables ω and ω'. In ω, the soft functions act as an operator-valued distribution on the jet function (4.69). For ω' on the other hand, the RGE for the soft operators becomes self-consistent and $Z_\otimes$ as well as $\Gamma_\otimes$ has to be viewed as a kernel integrated against a test function $\phi(\omega')$.[13] To reveal the true UV structure of (5.45), we recast the non-local term into a generalized plus-distribution. We distinguish between *i)* $\omega > 0$ and *ii)* $\omega < 0$ and expand the result in both cases in terms of the regulators $\delta_{\rm c,\bar{c}}$ that will drop out after all diagrams have been summed.

i) For $\omega > 0$, we have $\omega' > 0$ imposed by $\theta(\omega' - \omega)$ and thus we can use the standard

[12] We discussed in Chapter 2 that the local limit does not commute with the operator renormalization according to [38].

[13] We provide the results for distributions in ω in Appendix D.2.

plus-distribution

$$\int_{-\infty}^{\infty} d\omega' \big[\dots\big]_+ \phi(\omega') = \int_{-\infty}^{\infty} d\omega' \big[\dots\big](\phi(\omega') - \phi(\omega)) \,. \tag{5.46}$$

The non-local term becomes

$$\begin{aligned}
&\theta(\omega) \int_{-\infty}^{\infty} d\omega' \frac{\theta(\omega'-\omega)}{\omega'-\omega+\delta_c} \left(\frac{\tilde{\mu}}{\omega'-\omega}\right)^{\epsilon} \phi(\omega') \\
&= \theta(\omega) \int_{-\infty}^{\infty} d\omega'\omega' \left[\frac{\theta(\omega'-\omega)}{\omega'(\omega'-\omega+\delta_c)}\right]_+ \phi(\omega') + \theta(\omega)\phi(\omega) \int_{\omega}^{\infty} d\omega' \frac{\omega}{\omega'(\omega'-\omega+\delta_c)} + \mathcal{O}(\epsilon) \\
&= \theta(\omega) \int_{-\infty}^{\infty} d\omega'\omega' \left[\frac{\theta(\omega'-\omega)}{\omega'(\omega'-\omega)}\right]_+ \phi(\omega') - \theta(\omega)\phi(\omega) \ln\frac{\delta_c}{\omega} + \mathcal{O}(\epsilon, \delta_c) \,.
\end{aligned} \tag{5.47}$$

We assume that the test function behaves like $\phi(\omega') \sim 1/\omega'$ and hence we do not obtain UV divergences from the ω' integration. Up to logarithmic corrections induced by higher loop orders, this behaviour can be inferred from the jet function in (4.69). Consequently, we can expand (5.47) up to $\mathcal{O}(\epsilon)$ that gives rise to an irrelevant constant for $\epsilon \to 0$. Since the plus-distribution including $1/(\omega' - \omega + \delta_c)$ produces IR finite results for $\delta_c \to 0$, we can set the regulator in this term to zero up to vanishing linear corrections $\mathcal{O}(\delta_c)$.

ii) For $\omega < 0$, the variable ω' can either be positive or negative. In this case, the region for $\omega' > 0$ requires no regularization while for $\omega' < 0$ we introduce the modified plus-distributions (comparable with the $+a$ distribution in [153])

$$\int_{-\infty}^{\infty} d\omega' \big[\dots\big]_{\oplus/\ominus} \phi(\omega') = \int_{-\infty}^{\infty} d\omega' \big[\dots\big](\phi(\omega') - \theta(\pm\omega')\phi(\omega)) \,. \tag{5.48}$$

For the case at hand, the $\ominus$-distribution regulates the $1/(\omega' - \omega)$ pole in (5.45) when $\omega < 0$ and $\omega' < 0$. We thus find for the $\omega < 0$ contribution of diagram (a)

$$\begin{aligned}
&\theta(-\omega) \int_{-\infty}^{\infty} d\omega' \frac{\theta(\omega'-\omega)}{\omega'-\omega+\delta_c} \left(\frac{\tilde{\mu}}{\omega'-\omega}\right)^{\epsilon} \phi(\omega') \\
&= \theta(-\omega) \int_{-\infty}^{\infty} d\omega' \left[\frac{\theta(\omega'-\omega)}{\omega'-\omega+\delta_c}\right]_\ominus \phi(\omega') + \theta(-\omega)\phi(\omega) \int_{\omega}^{0} d\omega' \frac{1}{\omega'-\omega+\delta_c} + \mathcal{O}(\epsilon) \\
&= \theta(-\omega) \int_{-\infty}^{\infty} d\omega' \left[\frac{\theta(\omega'-\omega)}{\omega'-\omega}\right]_\ominus \phi(\omega') - \theta(-\omega)\phi(\omega) \ln\frac{\delta_c}{-\omega} + \mathcal{O}(\epsilon, \delta_c) \,.
\end{aligned} \tag{5.49}$$

We require the second $\oplus$-distribution in (5.48) for the regularization of diagram (e) in case of $\omega > 0$ and $\omega' > 0$. All other diagrams involve the standard plus-distribution (5.46) and are not explicitly calculated. For diagram (e), we follow the same procedure above. Without giving specific details, this diagram evaluates to

$$\frac{2\alpha_{\text{em}}}{(4\pi)^{1-\epsilon}}\Gamma(\epsilon)\left\{\frac{\theta(\omega-\omega')}{\omega-\omega'-\delta_c}\left(\frac{\tilde{\mu}}{\omega-\omega'-\delta_c}\right)^{2\epsilon} - \Gamma(2\epsilon)\Gamma(1-2\epsilon)\left(\frac{\tilde{\mu}}{-\delta_c}\right)^{2\epsilon}\delta(\omega-\omega')\right\} , \tag{5.50}$$

where we stripped off the charge prefactor $Q_d Q_{\rm sp}$. Again, we consider the two distinct cases *i*) and *ii*) and rewrite the non-local term accordingly. For $\omega > 0$, we require the $\oplus$-distribution since ω' can be either positive or negative. We obtain

$$\begin{aligned}
&\theta(\omega)\int_{-\infty}^{\infty} d\omega' \frac{\theta(\omega-\omega')}{\omega-\omega'-\delta_{\rm c}}\left(\frac{\tilde{\mu}}{\omega-\omega-\delta_{\rm c}}\right)^{2\epsilon}\phi(\omega') \\
&= \theta(\omega)\int_{-\infty}^{\infty} d\omega' \left[\frac{\theta(\omega-\omega')}{\omega-\omega'}\right]_{\oplus}\phi(\omega') + \theta(\omega)\phi(\omega)\ln\frac{\omega}{-\delta_{\rm c}} + \mathcal{O}(\epsilon,\delta_{\rm c})\,. \qquad (5.51)
\end{aligned}$$

For $\omega < 0$, the standard distribution suffices in order to find

$$\begin{aligned}
&\theta(-\omega)\int_{-\infty}^{\infty} d\omega' \frac{\theta(\omega-\omega')}{\omega-\omega'-\delta_{\rm c}}\left(\frac{\tilde{\mu}}{\omega-\omega-\delta_{\rm c}}\right)^{2\epsilon}\phi(\omega') \\
&= \theta(-\omega)\int_{-\infty}^{\infty} d\omega'\,\omega' \left[\frac{\theta(\omega-\omega')}{\omega'(\omega-\omega')}\right]_{+}\phi(\omega') + \theta(-\omega)\phi(\omega)\ln\frac{-\omega}{-\delta_{\rm c}} + \mathcal{O}(\epsilon,\delta_{\rm c})\,, \qquad (5.52)
\end{aligned}$$

where we introduced a factor of $1/\omega'$ in the distribution to ensure convergence of the integration. We conclude by (5.51) that any $\omega' < 0$ can be pushed by diagram (e) to a positive ω up to infinity. Therefore, on the level of the anomalous dimension, diagrams (a) and (e) of Fig. 5.3 can mix positive into negative support and vice versa while the remaining contributions retain the sign of the initial momentum variable ω'.

Our findings are in fact consistent with the physical picture: In QCD-only, the static HQET field h_v provides an infinite source of momentum in the light-like directions n_+ and n_-. Hence, the spectator quark momentum $\omega' = n_-\ell$ can absorb an arbitrary amount of this momentum and extends to infinity in the heavy quark limit $m_b \to \infty$, which is reflected by diagram (e) that principally takes any ω' to infinity. In QED, the effect gets reversed since the spectator quark still couples to the outgoing charged mesons through soft photons. The spectator in particular couples to the outgoing anti-collinear meson M_2 whose constituents carry away large momentum $n_-q \sim \mathcal{O}(m_b)$ in the n_+-direction. For $m_b \to \infty$, this implies that the light quark loses momentum and ω' eventually extends to negative infinity. We present the latter scenario resulting from diagram (a) in Fig. 5.4. Altogether, we summarize that the soft functions have particularly distinguished to the B LCDA in QCD once M_2 is charged.

To obtain the final result for the renormalization factor of diagram (a), we insert the results from (5.47) and (5.49) corresponding to $\omega > 0$ and $\omega < 0$ into (5.45). We obtain the UV counter term

$$\begin{aligned}
Z_{\otimes}^{\rm QED,(a)} = Q_{\rm sp}Q_{M_2}\Bigg\{&\frac{2}{\epsilon}\theta(\omega)\omega'\left[\frac{\theta(\omega'-\omega)}{\omega'(\omega'-\omega)}\right]_{+} + \frac{2}{\epsilon}\theta(-\omega)\left[\frac{\theta(\omega'-\omega)}{\omega'-\omega}\right]_{\ominus} \\
&- \left(\frac{2}{\epsilon^2} + \frac{2}{\epsilon}\ln\frac{\mu}{-\delta_{\bar{c}}} + \frac{2}{\epsilon}\theta(\omega)\ln\frac{\mu}{\omega} + \frac{2}{\epsilon}\theta(-\omega)\ln\frac{\mu}{-\omega}\right)\delta(\omega-\omega')\Bigg\}, \qquad (5.53)
\end{aligned}$$

where the regulator δ_c drops out in the local terms. We give the results for diagrams (b)-(d) without further details. Diagram (b) only contains local terms that are given by

$$Z_{\otimes}^{\mathrm{QED,(b)}} = Q_d Q_{M_1} \left(\frac{1}{\epsilon^2} + \frac{2}{\epsilon} \ln \frac{\mu}{-\delta_c} \right) \delta(\omega - \omega') + Q_d Q_{M_2} \left(\frac{1}{\epsilon^2} + \frac{2}{\epsilon} \ln \frac{\mu}{-\delta_{\bar{c}}} \right) \delta(\omega - \omega') \,. \tag{5.54}$$

For both diagrams (c) and (d) we find non-local terms with support for $\omega > 0$ and $\omega < 0$ that originate from the integral

$$\int_0^{\omega'} d(n_{-}k) f(n_{-}k) \delta(\omega + n_{-}k - \omega') = f(\omega' - \omega) \left[\theta(\omega)\theta(\omega' - \omega) - \theta(-\omega)\theta(\omega - \omega') \right] \,. \tag{5.55}$$

We emphasize that the contributions from this integral do not mix positive into negative momentum variables and vice versa. In pure QCD, the last term in (5.55) vanishes as the heavy meson LCDA supports $\omega > 0$ exclusively. In QCD×QED however, this term needs to be included since diagram a) generates $\omega < 0$ after an infinitesimal evolution step. In total, we find the one-loop expressions

$$\begin{aligned} Z_{\otimes}^{\mathrm{QED,(c)}} = \frac{2}{\epsilon} Q_{\mathrm{sp}} Q_{M_1} \Bigg\{ & - \theta(\omega)\omega \left[\frac{\theta(\omega' - \omega)}{\omega'(\omega' - \omega)} \right]_+ - \theta(-\omega)\omega \left[\frac{\theta(\omega - \omega')}{\omega'(\omega - \omega')} \right]_+ \\ & + \ln \left(\frac{\mu}{\omega - i0} \right) \delta(\omega - \omega') - \ln \left(\frac{\mu}{-\delta_c} \right) \delta(\omega - \omega') \Bigg\} \,, \end{aligned} \tag{5.56}$$

$$Z_{\otimes}^{\mathrm{QED,(d)}} = \frac{2}{\epsilon} Q_{\mathrm{sp}}^2 \Bigg\{ - \theta(\omega)\omega \left[\frac{\theta(\omega' - \omega)}{\omega'(\omega' - \omega)} \right]_+ - \theta(-\omega)\omega \left[\frac{\theta(\omega - \omega')}{\omega'(\omega - \omega')} \right]_+ - \delta(\omega - \omega') \Bigg\} \,. \tag{5.57}$$

The UV divergent terms of diagram (c) do not mix positive into negative support. However, this contribution enters similar to diagram (a) in Fig. 5.4 with a coupling of the soft spectator quark to the collinear line next to the interaction vertex. Therefore, the meson M_1 may carry an infinite amount of momentum away so that $\omega < 0$ is generated through finite terms of the diagram. Diagram (e) is obtained by adding together (5.48)

$$\begin{aligned} Z_{\otimes}^{\mathrm{QED,(e)}} = Q_d Q_{\mathrm{sp}} \Bigg\{ & - \frac{2}{\epsilon} \theta(\omega) \left[\frac{\theta(\omega - \omega')}{\omega - \omega'} \right]_{\oplus} - \frac{2}{\epsilon} \theta(-\omega)\omega' \left[\frac{\theta(\omega - \omega')}{\omega'(\omega - \omega')} \right]_+ \\ & + \left(\frac{1}{\epsilon^2} + \frac{2}{\epsilon} \theta(\omega) \ln \frac{\mu}{\omega} + \frac{2}{\epsilon} \theta(-\omega) \ln \frac{\mu}{-\omega} \right) \delta(\omega - \omega') \Bigg\} \,. \end{aligned} \tag{5.58}$$

The remaining diagram (f) contracts the soft Wilson lines of M_1 and M_2 and contributes when both mesons are charged. We find

$$Z_{\otimes}^{\mathrm{QED,(f)}} = Q_{M_1} Q_{M_2} \left(-\frac{2}{\epsilon^2} - \frac{2}{\epsilon} \ln \frac{\mu}{-\delta_{\bar{c}}} - \frac{2}{\epsilon} \ln \frac{\mu}{-\delta_c} + \frac{2i\pi}{\epsilon} \right) \delta(\omega - \omega') \,. \tag{5.59}$$

Lastly, we include the external renormalization factors

$$Z_v^{\mathrm{QED}} = -\frac{Q_d^2}{\epsilon}\delta(\omega-\omega')\,, \qquad Z_q^{\mathrm{QED}} = \frac{Q_{\mathrm{sp}}^2}{2\epsilon}\delta(\omega-\omega')\,. \tag{5.60}$$

Most of the above results contain the IR regulators $\delta_{\mathrm{c},\bar{\mathrm{c}}}$. After including the rearrangement factors from (4.47) and (4.48) in (5.39), this dependence cancels and we obtain a well-defined UV renormalized matrix element. We recall that these factors were introduced through (4.44) together with the absolute value to avoid spurious imaginary parts in the collinear sector. Irrespective of the particular choice, the soft functions generally are complex-valued due to soft rescattering of the external states. We discuss the QCD limit of these expressions in the next step.

5.2.2 Anomalous dimension for $\Phi_{B,\otimes}$

Depending on the electric charge, the standard and generalized plus-distributions appear in certain linear combinations after adding the renormalization factors of each diagram together. To this end, we define Z^{QED}:

$$\begin{aligned}
F^{>}(\omega,\omega') &= \omega\left[\frac{\theta(\omega'-\omega)}{\omega'(\omega'-\omega)}\right]_+ + \left[\frac{\theta(\omega-\omega')}{\omega-\omega'}\right]_\oplus\,,\\
F^{<}(\omega,\omega') &= \omega\left[\frac{\theta(\omega-\omega')}{\omega'(\omega-\omega')}\right]_+ + \left[\frac{\theta(\omega'-\omega)}{\omega'-\omega}\right]_\ominus\,,\\
G^{>}(\omega,\omega') &= (\omega+\omega')\left[\frac{\theta(\omega'-\omega)}{\omega'(\omega'-\omega)}\right]_+ - i\pi\delta(\omega-\omega')\,,\\
G^{<}(\omega,\omega') &= (\omega+\omega')\left[\frac{\theta(\omega-\omega')}{\omega'(\omega-\omega')}\right]_+ + i\pi\delta(\omega-\omega')\,.
\end{aligned} \tag{5.61}$$

We indicate the $\omega>0$ ($\omega<0$) support by the superscript $>$ ($<$). For convenience in later computations, the G-distributions are defined with an additional imaginary part. Note that these distributions do not mix positive and negative momentum variables. Instead, only the distributions $F^{>}$ and $F^{<}$ contain the $\oplus$ and $\ominus$ distributions that cause a transition from $\omega'<0$ to $\omega>0$ and from $\omega'>0$ to $\omega<0$ respectively. We further combine the distributions (5.61) into

$$H_\pm(\omega,\omega') \equiv \theta(\pm\omega)F^{>(<)}(\omega,\omega') + \theta(\mp\omega)G^{<(>)}(\omega,\omega')\,. \tag{5.62}$$

with the upper (lower) sign corresponding to $>$ ($<$). Adding the contributions from (5.53)–(5.60) and (4.47) as well as (4.48), we receive

$$\begin{aligned}
Z_\otimes^{\mathrm{QED}}(\omega,\omega') = \Bigg[&(Q_{\mathrm{sp}}^2+2Q_{\mathrm{sp}}Q_{M_1})\left(\frac{1}{\epsilon^2}+\frac{2}{\epsilon}\ln\frac{\mu}{\omega-i0}\right)\\
&+\frac{2}{\epsilon}\left(i\pi(Q_{\mathrm{sp}}+Q_{M_1})Q_{M_2}-\frac{3}{4}Q_{\mathrm{sp}}^2-\frac{1}{2}Q_d^2\right)\Bigg]\delta(\omega-\omega')
\end{aligned}$$

$$-\frac{2}{\epsilon}Q_{\text{sp}}\Big[Q_d H_+(\omega,\omega') - Q_{M_2}H_-(\omega,\omega')\Big]\,, \tag{5.63}$$

where we used charge conservation $Q_d - Q_{\text{sp}} = Q_{M_1} + Q_{M_2}$ and recombined $\ln(\mu/[\omega - i0]) = \ln(\mu/[-\omega]) + i\pi$ for $\omega < 0$. As mentioned before, the IR regulators cancel in the sum of all diagrams. We find QCD limit of (5.63) by setting the meson charges to zero and $Q_{\text{sp}}^2, Q_d^2 \to C_F$:

$$Z^{\text{QCD}}(\omega,\omega') = C_F\left\{\left(\frac{1}{\epsilon^2} + \frac{2}{\epsilon}\ln\frac{\mu}{\omega - i0} - \frac{5}{2\epsilon}\right)\delta(\omega-\omega') - \frac{2}{\epsilon}H_+(\omega,\omega')\right\}. \tag{5.64}$$

We remark that this renormalization factor also contains terms for $\omega < 0$. In pure QCD, this contribution vanishes since we assume positive support due to the analytic structure of the position space operator defining the LCDA. Once QED effects are included, we generate negative support that then obtains a response from the QCD terms in (5.64). The traditional QCD expression in absence of QED can be obtained when restricting to test functions and integration for $\omega, \omega' > 0$ so that the distribution reduces to the well-known QCD result [152] $H_+ \to F$ with

$$F(\omega,\omega') = \omega\left[\frac{\theta(\omega'-\omega)}{\omega'(\omega'-\omega)}\right]_+ + \left[\frac{\theta(\omega-\omega')}{\omega-\omega'}\right]_+ . \tag{5.65}$$

Finally, we obtain the anomalous dimension for $\Phi_{B,\otimes}$ by plugging (5.63) and (5.64) into (5.42) together with (2.71)

$$\begin{aligned}\Gamma_{\otimes}(\omega,\omega') = {}& \frac{\alpha_s C_F}{\pi}\left[\left(\ln\frac{\mu}{\omega-i0} - \frac{1}{2}\right)\delta(\omega-\omega') - H_+(\omega,\omega')\right] \\ & + \frac{\alpha_{\text{em}}}{\pi}\Bigg[\Bigg((Q_{\text{sp}}^2 + 2Q_{\text{sp}}Q_{M_1})\ln\frac{\mu}{\omega-i0} - \frac{3}{4}Q_{\text{sp}}^2 - \frac{1}{2}Q_d^2 \\ & + i\pi(Q_{\text{sp}}+Q_{M_1})Q_{M_2}\Bigg)\delta(\omega-\omega') - Q_{\text{sp}}Q_d H_+(\omega,\omega') + Q_{\text{sp}}Q_{M_2}H_-(\omega,\omega')\Bigg]\,,\,.\end{aligned} \tag{5.66}$$

We recall that every distribution acts in the variable ω' and refer to the result in (D.9) as the distributions in ω. In what follows, we present the anomalous dimension for each charge combination explicitly.

$\bar{B}^0 \to M_1^0 M_2^0$ ($\otimes = (0,0)$)

For the neutral case $Q_{M_1} = Q_{M_2} = 0$, we have $Q_{\text{sp}} = Q_d$ and only diagrams (d) and (e) from Fig. 5.3 enter the anomalous dimension. Moreover, we can drop the $\omega < 0$ part of the $\oplus$-distribution and thus $F^{>}$ collapses to F in (5.65). The anomalous dimension becomes

$$\Gamma_{00}(\omega,\omega') = \frac{\alpha_s(\mu)C_F}{\pi}\left[\left(\ln\frac{\mu}{\omega} - \frac{1}{2}\right)\delta(\omega-\omega') - F(\omega,\omega')\right]$$

$$+\frac{\alpha_{\rm em}(\mu)Q_d^2}{\pi}\left[\left(\ln\frac{\mu}{\omega}-\frac{5}{4}\right)\delta(\omega-\omega')-F(\omega,\omega')\right], \tag{5.67}$$

which provides a trivial extension to the QCD result. Note that the QCD differs from the QED kernel by constant in the local term arising from $F_B(\mu)$ in the definition (5.42).

$\bar{B}^- \to M_1^- M_2^0$ $(\otimes = (-,0))$

For charged $Q_{M_1} = -1$ but still neutral $Q_{M_2} = 0$ implying $Q_{\rm sp} = Q_u$, the diagrams from Fig. 5.3(b)–(e) contribute. In this case, the soft function contains the rearrangement factor $1/R_c$ that cancels the IR regulator $\delta_{\rm c}$. We again neglect the $\omega < 0$ terms since M_2 is neutral and obtain

$$\begin{aligned}\Gamma_{-0}(\omega,\omega') = {}& \frac{\alpha_s(\mu)C_F}{\pi}\left[\left(\ln\frac{\mu}{\omega}-\frac{1}{2}\right)\delta(\omega-\omega')-F(\omega,\omega')\right]\\ &+\frac{\alpha_{\rm em}(\mu)}{\pi}\left[\left((Q_u^2+2Q_uQ_{M_1})\ln\frac{\mu}{\omega}-\frac{3}{4}Q_u^2-\frac{1}{2}Q_d^2\right)\delta(\omega-\omega')\right.\\ &\left.-(Q_u^2+Q_uQ_{M_1})F(\omega,\omega')\right].\end{aligned} \tag{5.68}$$

In fact, we restore the expression for Γ_{00} in (5.67) upon sending $Q_{M_1} \to 0$ and $Q_u \to Q_d$, where the latter refers to the spectator quark charge. We remark that the charge coefficients of the $\ln(\mu/\omega)$ term and the $-F$ distribution differ by $Q_uQ_{M_1}$ in contrast to QCD which turns out to be important for the solution of the corresponding RGE.

$\bar{B}^- \to M_1^0 M_2^-(\otimes = (0,-))$

Once $Q_{M_2} = -1$, we have to include the terms for $\omega < 0$ since the support will be generated for any initial condition. For $Q_{M_1} = 0$ the spectator charge is $Q_{\rm sp} = Q_u$. We divide the anomalous dimension in the two regions $\omega > 0$ and $\omega < 0$ by

$$\Gamma_\otimes(\omega,\omega') = \theta(\omega)\Gamma_\otimes^>(\omega,\omega') + \theta(-\omega)\Gamma_\otimes^<(\omega,\omega')\,. \tag{5.69}$$

For $\omega < 0$, we use $\ln\mu/(\omega - i0) = \ln\mu/(-\omega) + i\pi$ to make the imaginary contributions explicit. In total, we find

$$\begin{aligned}\Gamma_{0-}^>(\omega,\omega') = {}& \frac{\alpha_s(\mu)C_F}{\pi}\left[\left(\ln\frac{\mu}{\omega}-\frac{1}{2}\right)\delta(\omega-\omega')-F^>(\omega,\omega')\right]\\ &+\frac{\alpha_{\rm em}(\mu)}{\pi}\left[\left(Q_u^2\ln\frac{\mu}{\omega}-\frac{3}{4}Q_u^2-\frac{1}{2}Q_d^2\right)\delta(\omega-\omega')\right.\\ &\left.-(Q_u^2+Q_uQ_{M_2})F^>(\omega,\omega')+Q_uQ_{M_2}\left(G^>(\omega,\omega')+i\pi\delta(\omega-\omega')\right)\right],\end{aligned} \tag{5.70}$$

$$\Gamma^{<}_{0-}(\omega,\omega') = \frac{\alpha_s(\mu)C_F}{\pi}\left[\left(\ln\frac{\mu}{-\omega}-\frac{1}{2}\right)\delta(\omega-\omega') - G^{<}(\omega,\omega') + i\pi\delta(\omega-\omega')\right]$$
$$+\frac{\alpha_{\rm em}(\mu)}{\pi}\left[\left(Q_u^2\ln\frac{\mu}{-\omega}-\frac{3}{4}Q_u^2-\frac{1}{2}Q_d^2\right)\delta(\omega-\omega')\right.$$
$$\left.-\left(Q_u^2+Q_uQ_{M_2}\right)\left(G^{<}(\omega,\omega')-i\pi\delta(\omega-\omega')\right)+Q_uQ_{M_2}F^{<}(\omega,\omega')\right]. \quad (5.71)$$

Note that we can relate $\Gamma^{<}$ to $\Gamma^{>}$ by exchanging $F^{>} \leftrightarrow G^{<} - i\pi$ and $G^{>} + i\pi \leftrightarrow F^{<}$ respectively. The imaginary parts in particular match the ones from the G-distributions in (5.61). We conclude that Γ_{0-} and therefore $\Phi_{0-}(\omega;\mu)$ remains real-valued.

$\bar{B}^0 \to M_1^+ M_2^-$ $(\otimes = (+,-))$

For $\otimes = (+,-)$, every aspect of the previous calculation applies. In addition, we have $Q_{\rm sp} = Q_d$, $Q_{M_1} = -Q_{M_2}$. We observe that the off-shell regulators Fig. 5.3(a)–(e) already cancel amongst themselves. The real part of the remaining diagram f) is removed by $1/R_c$ and $1/R_{\bar{c}}$, leaving an explicit imaginary phase proportional to $Q_{M_1}Q_{M_2}$. According to the decomposition (5.69), we obtain

$$\Gamma^{>}_{+-}(\omega,\omega') = \frac{\alpha_s(\mu)C_F}{\pi}\left[\left(\ln\frac{\mu}{\omega}-\frac{1}{2}\right)\delta(\omega-\omega') - F^{>}(\omega,\omega')\right]$$
$$+\frac{\alpha_{\rm em}(\mu)}{\pi}\left[\left((Q_d^2-2Q_dQ_{M_2})\ln\frac{\mu}{\omega}+i\pi Q_{M_1}Q_{M_2}-\frac{5}{4}Q_d^2\right)\delta(\omega-\omega')\right.$$
$$\left.-Q_d^2F^{>}(\omega,\omega')+Q_dQ_{M_2}\left(G^{>}(\omega,\omega')+i\pi\delta(\omega-\omega')\right)\right], \quad (5.72)$$

$$\Gamma^{<}_{+-}(\omega,\omega') = \frac{\alpha_s(\mu)C_F}{\pi}\left[\left(\ln\frac{\mu}{-\omega}-\frac{1}{2}\right)\delta(\omega-\omega') - G^{<}(\omega,\omega') + i\pi\delta(\omega-\omega')\right]$$
$$+\frac{\alpha_{\rm em}(\mu)}{\pi}\left[\left((Q_d^2-2Q_dQ_{M_2})\ln\frac{\mu}{-\omega}+i\pi(Q_{M_1}-Q_d)Q_{M_2}-\frac{5}{4}Q_d^2\right)\delta(\omega-\omega')\right.$$
$$\left.-Q_d^2\left(G^{<}(\omega,\omega')-i\pi\delta(\omega-\omega')\right)+Q_dQ_{M_2}F^{<}(\omega,\omega')\right]. \quad (5.73)$$

The soft function for $\otimes = (+,-)$ turns out to be complex-valued due to soft rescattering of the final state mesons, reflected by the imaginary phase. Based on our discussion for diagram a) in the previous section, we observe that $Q_{M_2} = 0$ would remove the distribution $F^{<}$ in (5.73). In this case, we restore (5.67) and (5.68) depending on the charge of M_1 when positive support is assumed. Finally, we remark that $Q_{M_2} \to Q_\ell$ leads to the corresponding anomalous dimension for the soft function in the leptonic decay $B_q \to \mu^+\mu^-$ [60].

5.2.3 RGE of the first inverse (logarithmic) moments

In (4.70), we found that the soft functions $\Phi_{B,\otimes}$ are part of the LP factorization theorem in QCD×QED. As such, they are part of a convolution with a hard-collinear jet function that behaves like $1/\omega - i0$ up to logarithmic corrections from higher loop orders. Rather than solving the RGE for the soft functions themselves, it is oftentimes convenient to study the scale evolution of the inverse moments instead. To this end, we define for $n > 0$

$$\begin{aligned}\frac{1}{\lambda_B(\mu)} &= \int_{-\infty}^{\infty} \frac{d\omega}{\omega - i0}\, \Phi_{B,\otimes}(\omega;\mu)\,, \\ \sigma_n(\mu) &= \lambda_B(\mu) \int_{-\infty}^{\infty} \frac{d\omega}{\omega - i0} \ln^n\left(\frac{\tilde{\mu}}{\omega - i0}\right) \Phi_{B,\otimes}(\omega;\mu)\,. \end{aligned} \tag{5.74}$$

We emphasize that this definition differs to QCD in the sense that we generally integrate over the entire real axis, and in particular the origin so that the $i0$-prescription has to be included. Note that the $i0$ prescription arises from the hard-collinear propagator and is therefore inherited in the logarithmic terms. We normalize the logarithmic moments to $\lambda_B^{-1}(\mu)$, where $\tilde{\mu}$ serves as an arbitrary but fixed reference scale. Hence, the scale evolution only enters through the functions $\Phi_{B,\otimes}(\omega;\mu)$.

The existence of (5.74) for $\omega > 0$ in QCD can be inferred from the asymptotic behaviour $\phi_+(\omega) \propto \omega$ that follows from the conformal symmetry arguments in Appendix B. In the case of $Q_{M_2} = 0$, the soft functions are still restricted to $\omega > 0$ and the inverse moments are well-defined in QCD×QED due to their behaviour similar to the light meson LCDA that is discussed in Appendix E.3. When M_2 becomes charged, the soft function develops a non-zero value and potentially diverges logarithmically for $\omega \to 0$ in which case the $i0$-prescription in (5.74) is required to perform the integral consistently. We argue below that the inverse-logarithmic moments remain finite, but the analytic structure near $\omega = 0$ implies that higher inverse moments like $1/(\omega - i0)^2$ cannot exist.[14] Note that the integration in (5.74) over the origin provides an additional source of imaginary rescattering phases compared to QCD-only, where these arise through hard or hard-collinear loops.

The RGE for the inverse-logarithmic moments (5.74) corresponds to a coupled system obtained by calculating the $\ln\mu$-derivative of

$$\frac{d}{d\ln\mu}\left(\frac{\sigma_n(\mu)}{\lambda_B(\mu)}\right) = -\int_{-\infty}^{\infty} \frac{d\omega}{\omega - i0} \ln^n\left(\frac{\tilde{\mu}}{\omega - i0}\right) \int_{-\infty}^{\infty} d\omega'\, \Gamma_{\otimes}(\omega,\omega';\mu)\Phi_{B,\otimes}(\omega';\mu)\,, \tag{5.75}$$

using the scale evolution of the soft functions (5.66). In the further derivation, we exchange the integral order and perform the ω integration in advance. To this end,

[14] Contrary to QCD, where $1/\omega^2$ moments do not exist due to the linear endpoint behaviour, the existence $1/(\omega - i0)^2$ moments are forbidden by a different reason in QED: The analytic properties of the soft function are designed such that these moments diverge.

we conveniently view the plus-distributions $H_\pm$ as distributions in the variable ω. We denote these distributions with a superscript ω. The corresponding expressions for $F^{(\omega)}$ and $G^{(\omega)}$ are provided in (D.11). Both distributions equivalently define $H_\pm^{(\omega)}$ according to (5.62). Interestingly, we find for the integration over ω for $n \geq 0$

$$\int_{-\infty}^{\infty} d\omega \frac{\ln^n \frac{\tilde{\mu}}{\omega - i0}}{\omega - i0} H_+^{(\omega)}(\omega, \omega') = \frac{2n!}{\omega' - i0} \sum_{k=1}^{\lfloor n/2 \rfloor} \frac{\zeta_{2k+1}}{(n-2k)!} \ln^{n-2k} \frac{\tilde{\mu}}{\omega' - i0} , \tag{5.76}$$

where ζ_{2k+1} denotes the Riemann zeta function of odd numbers. This result agrees with the QCD result when restricting to positive support. In fact, the same equation holds true for F_ω with only $\omega > 0$. In (5.76), we find that the imaginary part defined in the distribution $G_\omega^>$ recombines to the final logarithmic term which was the original motivation to include the local $i\pi\delta(\omega - \omega')$ piece in (5.61). We further observe that (5.76) with $H_-^{(\omega)}$ evaluates to the same expression and thus conclude that

$$\int_{-\infty}^{\infty} d\omega \frac{\ln^n \frac{\tilde{\mu}}{\omega - i0}}{\omega - i0} \left(H_+^{(\omega)}(\omega, \omega') - H_-^{(\omega)}(\omega, \omega') \right) = 0 . \tag{5.77}$$

In other words, the distributions $H_\pm^{(w)}$ coincide on the function space of inverse moments including their logarithmic corrections.[15] From (5.77) follows directly that the ω-integral in (5.77) over $F_\omega^>(\omega, \omega') - G_\omega^>(\omega, \omega')$ and $G_\omega^<(\omega, \omega') - F_\omega^<(\omega, \omega')$ vanishes for $\omega' > 0$ and $\omega' < 0$, respectively. By using (5.77) we can therefore eliminate the distribution H_- which generates negative support in favour of H_+. As an important consequence, the RGE (5.66) greatly simplifies and allows us to construct an auxiliary function that produces the solution for the inverse moments in Sec. 5.2.5.

We obtain the RGE for the inverse moments by plugging (5.76) and (5.77) into (5.75). For $n = 0$, the plus-distributions do not contribute and the equation for the first inverse moment reads

$$\begin{aligned} \frac{d}{d\ln\mu} \lambda_B^{-1}(\mu) =& \frac{\alpha_s C_F}{\pi} \left[-\sigma_1(\mu) + \ln\frac{\tilde{\mu}}{\mu} + \frac{1}{2} \right] \lambda_B^{-1}(\mu) \\ &+ \frac{\alpha_{\rm em}}{\pi} \left[(Q_{\rm sp}^2 + 2Q_{\rm sp}Q_{M_1}) \left(-\sigma_1(\mu) + \ln\frac{\tilde{\mu}}{\mu} \right) + \frac{3}{4} Q_{\rm sp}^2 + \frac{1}{2} Q_d^2 \right. \\ &\left. - i\pi (Q_{\rm sp} + Q_{M_1}) Q_{M_2} \right] \lambda_B^{-1}(\mu) . \end{aligned} \tag{5.78}$$

For $n \geq 1$, we find the RGE of the logarithmic moments

$$\frac{d\sigma_n}{d\ln\mu} = \frac{\alpha_s C_F}{\pi} \left[-\sigma_{n+1} + \sigma_n \sigma_1 + 2n! \sum_{k=1}^{\lfloor n/2 \rfloor} \frac{\zeta_{2k+1}}{(n-2k)!} \sigma_{n-2k} \right]$$

[15] The relation does not apply to more general moments that are discussed in the conclusion of Section 5.2.5.

$$+\frac{\alpha_{\rm em}}{\pi}\Bigg[(Q_{\rm sp}^2+2Q_{\rm sp}Q_{M_1})(-\sigma_{n+1}+\sigma_n\sigma_1)$$

$$+(Q_{\rm sp}^2+Q_{\rm sp}Q_{M_1})\,2n!\sum_{k=1}^{\lfloor n/2\rfloor}\frac{\zeta_{2k+1}}{(n-2k)!}\sigma_{n-2k}\Bigg]\,. \tag{5.79}$$

Our results match in QCD limit $\alpha_{\rm em}\to 0$ the results in [154] up to an extra term of the form $n\sigma_{n-1}$ that appears due to the renormalization scale μ instead of $\tilde{\mu}$ in the definition of (5.74). The RGEs for the inverse moments differ in two aspects from the QCD result: First, the charge factor between the logarithmic terms and the summation in (5.79) do not agree, which only causes minor modifications. Second, the imaginary term in the last line (5.78) immediately produces a complex phase that can in principle be extracted by redefining

$$\lambda_B^{-1}(\mu)\to\exp\left\{-i\pi(Q_{\rm sp}+Q_{M_1})Q_{M_2}\int_{\mu_0}^{\mu}\frac{d\mu'}{\mu'}\frac{\alpha_{\rm em}(\mu')}{\pi}\right\}\lambda_B^{-1}(\mu)\,. \tag{5.80}$$

The imaginary contributions are absent in the evolution of the logarithmic moments $\sigma_n(\mu)$. Hence, these moments stay real when choosing entirely real $\sigma_n(\mu_0)$ at the initial scale since the first inverse moment does not mix into higher terms.

5.2.4 Evolution equation in Laplace space

In order to solve the RGE for the soft functions, we follow a similar yet more complex procedure as for the light meson LCDA in Sec. 5.1.1. In particular, we orientate ourselves at [150, 155] which uses a Mellin, or more generally Laplace transform to turn the evolution equation local in the conjugate η-space, allowing us to find a solution therein. We apply the method to the soft function by splitting it similar to the anomalous dimension in (5.69) into its respective support regions

$$\Phi_B(\omega;\mu)=\theta(\omega)\Phi_>(\omega;\mu)+\theta(-\omega)\Phi_<(\omega;\mu)\,. \tag{5.81}$$

In what follows, we neglect the charge index $\otimes$ for better readability. We consider the Laplace transform in the variable $\ln\mu/\omega$ separately for $\omega>0$ and $\omega<0$. In the first case similar to QCD-only, we have

$$\tilde{\Phi}_>(\eta;\mu)=\int_0^\infty\frac{d\omega}{\omega}\left(\frac{\mu}{\omega}\right)^\eta\Phi_>(\omega;\mu)\,,$$

$$\Phi_>(\omega;\mu)=\int_{c-i\infty}^{c+i\infty}\frac{d\eta}{2\pi i}\left(\frac{\mu}{\omega}\right)^{-\eta}\tilde{\Phi}_>(\eta;\mu)\,, \tag{5.82}$$

For the negatively supported part, we define

$$\tilde{\Phi}_<(\eta;\mu)=\int_0^\infty\frac{d\omega}{\omega}\left(\frac{\mu}{\omega}\right)^\eta\Phi_<(-\omega;\mu)$$

$$\Phi_<(-\omega;\mu) = \int_{c-i\infty}^{c+i\infty} \frac{d\eta}{2\pi i} \left(\frac{\mu}{\omega}\right)^{-\eta} \tilde{\Phi}_<(\eta;\mu) \,. \tag{5.83}$$

These transformations are connected to the inverse moment integration

$$\tilde{\Phi}_B(\eta;\mu) = \int_{-\infty}^{\infty} \frac{d\omega}{\omega - i0} \left(\frac{\mu}{\omega - i0}\right)^{\eta} \Phi_B(\omega;\mu) = \tilde{\Phi}_>(\eta;\mu) - e^{i\pi\eta}\tilde{\Phi}_<(\eta;\mu) \,. \tag{5.84}$$

Note that the integral over ω *defines* the function $\tilde{\Phi}_B$ on the left-hand side which cannot be viewed as an integral transformation. Besides, it is impossible to recover Φ_B from $\tilde{\Phi}_B$. Nevertheless, we can use (5.84) to derive the inverse-logarithmic moments in the limit $\eta \to 0$, for which we refer (5.94) and the follow-up arguments.

The evolution equation in Laplace space becomes a coupled differential equation for the two functions $\tilde{\Phi}_>$ and $\tilde{\Phi}_<$. In the derivation, we can either use the results as distributions in ω or ω'. We explicitly list the results for integration against pure powers ω^η in Appendix D.3. The RGEs are then commonly defined in the strip $-1 < \mathrm{Re}(\eta) < 0$ and we obtain

$$\begin{aligned}
\left(\frac{d}{d\ln\mu} - \eta\right)\tilde{\Phi}_>(\eta;\mu) &= \frac{\alpha_s C_F}{\pi}\bigg[- H_\eta - H_{-\eta} - \partial_\eta + \frac{1}{2}\bigg]\tilde{\Phi}_>(\eta;\mu) \\
&\quad + \frac{\alpha_s C_F}{\pi}\Gamma(-\eta)\Gamma(1+\eta)\tilde{\Phi}_<(\eta;\mu) \\
&\quad + \frac{\alpha_{\rm em}}{\pi}\bigg[- (Q_{\rm sp}^2 + 2Q_{\rm sp}Q_{M_1})\partial_\eta + \frac{3}{4}Q_{\rm sp}^2 + \frac{1}{2}Q_d^2 - i\pi Q_{M_1}Q_{M_2} \\
&\quad - Q_{\rm sp}Q_d(H_\eta + H_{-\eta}) + Q_{\rm sp}Q_{M_2}(H_{-\eta} + H_{-1-\eta})\bigg]\tilde{\Phi}_>(\eta;\mu) \\
&\quad + \frac{\alpha_{\rm em}}{\pi}Q_{\rm sp}Q_d\Gamma(-\eta)\Gamma(1+\eta)\tilde{\Phi}_<(\eta;\mu) \,.
\end{aligned} \tag{5.85}$$

$$\begin{aligned}
\left(\frac{d}{d\ln\mu} - \eta\right)\tilde{\Phi}_<(\eta;\mu) &= \frac{\alpha_s C_F}{\pi}\bigg[- H_{-\eta} - H_{-1-\eta} - \partial_\eta + \frac{1}{2}\bigg]\tilde{\Phi}_<(\eta;\mu) \\
&\quad + \frac{\alpha_{\rm em}}{\pi}\bigg[- (Q_{\rm sp}^2 + 2Q_{\rm sp}Q_{M_1})\partial_\eta + \frac{3}{4}Q_{\rm sp}^2 + \frac{1}{2}Q_d^2 - i\pi(Q_{\rm sp} + Q_{M_2})Q_{M_1} \\
&\quad - Q_{\rm sp}Q_d(H_{-\eta} + H_{-1-\eta}) + Q_{\rm sp}Q_{M_2}(H_\eta + H_{-\eta})\bigg]\tilde{\Phi}_<(\eta;\mu) \\
&\quad - \frac{\alpha_{\rm em}}{\pi}Q_{\rm sp}Q_{M_2}\Gamma(-\eta)\Gamma(1+\eta)\tilde{\Phi}_>(\eta;\mu) \,.
\end{aligned} \tag{5.86}$$

We combine the two equations to find the RGE for $\tilde{\Phi}_B$, that is

$$\left(\frac{d}{d\ln\mu} - \eta\right)\tilde{\Phi}_B(\eta;\mu) = \frac{\alpha_s C_F}{\pi}\bigg[- H_\eta - H_{-\eta} - \partial_\eta + \frac{1}{2}\bigg]\tilde{\Phi}_B(\eta;\mu)$$

$$+\frac{\alpha_{\rm em}}{\pi}\bigg[Q_{\rm sp}Q_{M_1}(H_\eta+H_{-\eta})-(Q_{\rm sp}^2+2Q_{\rm sp}Q_{M_1})\,(H_\eta+H_{-\eta}+\partial_\eta)$$
$$+\frac{3}{4}Q_{\rm sp}^2+\frac{1}{2}Q_d^2-i\pi(Q_{\rm sp}+Q_{M_1})Q_{M_2}\bigg]\tilde{\Phi}_B(\eta;\mu)\;. \tag{5.87}$$

Note that we implemented the relation $\Gamma(-\eta)\Gamma(1+\eta)=e^{i\pi\eta}(i\pi+H_\eta-H_{-1-\eta})$ which implies $H_{-1+\eta}+H_{-1-\eta}=H_\eta+H_{-\eta}$. We could have obtained (5.87) also differently by recalling that the distributions $H_\pm$ coincide (5.77) for inverse (logarithmic) moments. In fact, we can enlarge this statement to include pure powers as we show in Appendix D.3. In conclusion, we do not require the partition in (5.81) to arrive at the RGE (5.87), which is valid for $-1<\mathrm{Re}(\eta)<1$ since only H_η and $H_{-\eta}$ appear.

Before deriving the all-order solution of the soft functions and their inverse moments, we review the calculation of the QCD solution ϕ_+. The RGE for QCD is defined by

$$\frac{d}{d\ln\mu}\phi_+(\omega;\mu)=-\int_0^\infty d\omega'\;\Gamma^{\rm QCD}(\omega,\omega';\mu)\;\phi_+(\omega';\mu)\;, \tag{5.88}$$

where we set $\Gamma^{\rm QCD}=\Gamma_\otimes|_{\alpha_{\rm em}=0}$ in (5.66). In QCD-only, we consider only positive support for $\phi_+(\omega;\mu)$ so that the Laplace transform (5.82) applies and the QCD kernel $\Gamma^{\rm QCD}$ collapses to its conventional form [152] with the distribution F in (5.65). We find the RGE in Laplace space

$$\left(\frac{d}{d\ln\mu}-\eta\right)\tilde{\phi}_+(\eta;\mu)=\frac{\alpha_s C_F}{\pi}\left[-H_\eta-H_{-\eta}-\partial_\eta+\frac{1}{2}\right]\tilde{\phi}_+(\eta;\mu)\;, \tag{5.89}$$

where $-1<\mathrm{Re}(\eta)<1$. The analytical solution of this equation can be expressed in terms of the evolution variables

$$V^{\rm QCD}(\mu,\mu_0)=-\int_{\mu_0}^{\mu}\frac{d\mu'}{\mu'}\frac{\alpha_s(\mu')C_F}{\pi}\left[\ln\frac{\mu'}{\mu_0}-\frac{1}{2}\right]\;,$$
$$a^{\rm QCD}(\mu,\mu_0)=-\int_{\mu_0}^{\mu}\frac{d\mu'}{\mu'}\frac{\alpha_s(\mu')C_F}{\pi}\;. \tag{5.90}$$

We generally neglect the dependence of μ and μ_0 in these expressions. Together with the inverse transformation, the general solution becomes [150]

$$\tilde{\phi}_+(\eta;\mu)=e^{V+2\gamma_E a}\left(\frac{\mu}{\mu_0}\right)^\eta\frac{\Gamma(1-\eta)\Gamma(1+\eta+a)}{\Gamma(1+\eta)\Gamma(1-\eta-a)}\,\tilde{\phi}_+(\eta+a;\mu_0)\;, \tag{5.91}$$

$$\phi_+(\omega;\mu)=e^{V+2\gamma_E a}\int_0^\infty\frac{d\omega'}{\omega'}\left(\frac{\mu_0}{\omega'}\right)^a G_a\Big(\frac{\omega}{\omega'}\Big)\,\phi_+(\omega',\mu_0)\;, \tag{5.92}$$

which holds for any initial function. Note that we omit the QCD superscript above and in (5.93) to focus on the structure of the solution. The analytic structure of (5.91)

restricts the real contour parameter to the interval $-1 < c < 1$. For convenience, we express the kernel of the convolution in (5.92) in terms of the Meijer-G function

$$G_a\Big(\frac{\omega}{\omega'}\Big) \equiv G^{1,1}_{2,2}\left(\begin{matrix}-a\,, 1-a\\ 1\,, 0\end{matrix}\,\middle|\,\frac{\omega}{\omega'}\right) \tag{5.93}$$
$$= \frac{\Gamma(2+a)}{\Gamma(-a)}\left(\frac{\omega'}{\max(\omega,\omega')}\right)^a \frac{\min(\omega,\omega')}{\max(\omega,\omega')}\,{}_2F_1\left(1+a, 2+a; 2; \frac{\min(\omega,\omega')}{\max(\omega,\omega')}\right) .$$

Albeit these functions are more complicated and untypical to use, they allow us to cast results into compact expressions. We present the exact definition and some of the fundamental properties of Meijer-G functions in Appendix F. For QCD, we note that $G_a(z)$ has an integrable singularity for $z \to 1$ so that the integral in (5.92) exists.

5.2.5 Solution for inverse moments

The coupled evolution equations for the inverse-logarithmic moments in (5.78) and (5.79) can be solved exactly. We infer the solution from (5.84) which fulfills the RGE (5.87) so that we can calculate the moments by

$$\lambda_B^{-1}(\mu) = \lim_{\eta\to 0}\tilde\Phi_B(\eta;\mu) = \lim_{\eta\to 0}\left\{\tilde\Phi_>(\eta;\mu) - e^{i\pi\eta}\tilde\Phi_<(\eta;\mu)\right\} , \tag{5.94}$$

$$\sigma_n(\mu) = \lim_{\eta\to 0}\lambda_B(\mu)\left(\partial_\eta - \ln\frac{\mu}{\tilde\mu}\right)^n\tilde\Phi_B(\eta;\mu) . \tag{5.95}$$

While the limit $\eta \to 0$ corresponds to the first inverse moment, the limit $\eta \to 1$ produces the second inverse moment with $1/(\omega - i0)^2$, etc.

To provide a solution to (5.87), we introduce the QCD×QED evolution variables

$$V = V^{\rm QCD} - \int_{\mu_0}^{\mu}\frac{d\mu'}{\mu'}\frac{\alpha_{\rm em}(\mu')}{\pi}\left[(Q_{\rm sp}^2 + 2Q_{\rm sp}Q_{M_1})\ln\frac{\mu'}{\mu_0} - \frac{3}{4}Q_{\rm sp}^2 - \frac{1}{2}Q_d^2\right.$$
$$\left. + i\pi(Q_{\rm sp}+Q_{M_1})Q_{M_2}\right] ,$$
$$a = a^{\rm QCD} - \int_{\mu_0}^{\mu}\frac{d\mu'}{\mu'}\frac{\alpha_{\rm em}(\mu')}{\pi}(Q_{\rm sp}^2 + 2Q_{\rm sp}Q_{M_1}) , \tag{5.96}$$

with the QCD expressions $V^{\rm QCD}$ and $a^{\rm QCD}$ from (5.90) and the μ-dependence neglected. Note that we still expect $-1 < a < 0$ in practical applications since QED effects are small. We further define two evolution functions

$$\mathcal{F}(\eta;\mu,\mu_0) = \exp\left\{\int_{\mu_0}^{\mu}\frac{d\mu'}{\mu'}\frac{\alpha_{\rm em}(\mu')Q_{\rm sp}Q_{M_1}}{\pi}(H_{\eta+a(\mu,\mu')} + H_{-\eta-a(\mu,\mu')})\right\} , \tag{5.97}$$

$$\mathcal{G}(\eta;\mu,\mu_0) = \exp\left\{\int_{\mu_0}^{\mu}\frac{d\mu'}{\mu'}\frac{\alpha_{\rm em}(\mu')Q_{\rm sp}Q_{M_1}}{\pi}(H_{-\eta-a(\mu,\mu')} + H_{-1-\eta-a(\mu,\mu')})\right\} . \tag{5.98}$$

In the same manner of (5.19), we find the solution of (5.87) to be

$$\tilde{\Phi}_B(\eta;\mu) = e^{V+2\gamma_E a}\left(\frac{\mu}{\mu_0}\right)^{\eta}\frac{\Gamma(1-\eta)}{\Gamma(1+\eta)}\frac{\Gamma(1+\eta+a)}{\Gamma(1-\eta-a)}\mathcal{F}(\eta;\mu,\mu_0)\tilde{\Phi}_B(\eta+a;\mu_0)\,. \tag{5.99}$$

Using (5.95), we compute the first inverse moment at $\eta = 0$

$$\lambda_B^{-1}(\mu) = e^{V+2\gamma_E a}\frac{\Gamma(1+a)}{\Gamma(1-a)}\mathcal{F}(0;\mu,\mu_0)\int_{-\infty}^{\infty}\frac{d\omega}{\omega-i0}\left(\frac{\mu_0}{\omega-i0}\right)^a\Phi_B(\omega;\mu_0)\,. \tag{5.100}$$

To obtain σ_1, we similarly calculate the first derivative for $\eta \to 0$ with (5.95) and (5.99) and find[16]

$$\begin{aligned}\sigma_1(\mu) = H_a + H_{-a} + \ln\frac{\tilde{\mu}}{\mu_0} + \frac{\displaystyle\int_{-\infty}^{\infty}\frac{d\omega}{\omega-i0}\left(\frac{\mu_0}{\omega-i0}\right)^a\ln\frac{\mu_0}{\omega-i0}\,\Phi_B(\omega;\mu_0)}{\displaystyle\int_{-\infty}^{\infty}\frac{d\omega}{\omega-i0}\left(\frac{\mu_0}{\omega-i0}\right)^a\Phi_B(\omega;\mu_0)} \\ + \int_{\mu_0}^{\mu}\frac{d\mu'}{\mu'}\frac{\alpha_{\rm em}(\mu')Q_{\rm sp}Q_{M_1}}{\pi}(H'_{a(\mu,\mu')} - H'_{-a(\mu,\mu')})\,.\end{aligned} \tag{5.101}$$

By proceeding with this method, we can construct the solution to any inverse logarithmic moment. In the QCD limit $\alpha_{\rm em} \to 0$, we recover the results of λ_B and σ_1 in [154] up to the earlier mentioned difference regarding the reference scale. We emphasize (5.100) and (5.101) are the all-order solutions in both QCD and QED couplings. Their existence is tied to the asymptotic behaviour of Φ_B for $\omega \to 0$ and $\omega \to \pm\infty$ that ensures the convergence of the ω integral. We derive the details of this behaviour from the all-order statements for the soft functions in Sec. 5.2.6.

We remark that the simple form of the RGE (5.87) and its solution (5.99) emerges from the fact that the distributions $H_+ = H_-$ agree on the function space of inverse moments. In a complementary approach, we may assume this equality directly on the level of the anomalous dimension to eliminate the $\omega < 0$ support and obtain the solutions (5.100) and (5.101) thereafter. The soft function then has to be viewed as some auxiliary function $\Phi_B^{\rm red}$ that obeys the RGE for $\omega > 0$ only

$$\frac{d}{d\ln\mu}\Phi_B^{\rm red}(\omega;\mu) = -\int_0^{\infty}d\omega'\;\Gamma_{\otimes}^{\rm red}(\omega,\omega';\mu)\;\Phi_B^{\rm red}(\omega';\mu)\,. \tag{5.102}$$

The anomalous dimension reduces to

$$\Gamma_{\otimes}^{\rm red}(\omega,\omega') = \frac{\alpha_s C_F}{\pi}\left[\left(\ln\frac{\mu}{\omega}-\frac{1}{2}\right)\delta(\omega-\omega') - F(\omega,\omega')\right]$$

[16] Alternatively, the RGE (5.78) fixes the expression of σ_1 once the solution to λ_B^{-1} is known. With the result for σ_1, we then obtain σ_2 by (5.79) for $n = 1$. This allows us to build the complete tower of solutions.

$$+\frac{\alpha_{\text{em}}}{\pi}\Bigg[\Bigg((Q_{\text{sp}}^2+2Q_{\text{sp}}Q_{M_1})\ln\frac{\mu}{\omega}-\frac{3}{4}Q_{\text{sp}}^2-\frac{1}{2}Q_d^2$$
$$+i\pi(Q_{\text{sp}}+Q_{M_1})Q_{M_2}\Bigg)\delta(\omega-\omega')-(Q_{\text{sp}}^2+Q_{\text{sp}}Q_{M_1})F(\omega,\omega')\Bigg]\,, \tag{5.103}$$

where we defined the QCD distribution F in (5.65).

The solutions to the inverse moments (5.100) and (5.101) can be calculated in the same way from (5.94) but using the solution for $\widetilde{\Phi}_{B,\otimes}^{\text{red}}(\eta)$. In addition, we trade the integral expressions involving the soft function at the scale μ_0 for the sum over all initial inverse moments by

$$\int_0^\infty\frac{d\omega}{\omega}\left(\frac{\mu_0}{\omega}\right)^a\ln^n\frac{\mu_0}{\omega}\,\Phi_B^{\text{red}}(\omega;\mu_0)=\lambda_B^{-1}(\mu_0)\left(\frac{\mu_0}{\tilde{\mu}}\right)^a\sum_{k=0}^n\binom{n}{k}\ln^{n-k}\frac{\mu_0}{\tilde{\mu}}\sum_{l=0}^\infty\frac{a^l\sigma_{k+l}(\mu_0)}{l!}\,, \tag{5.104}$$

which holds for $\omega>0$ and $n\geq 0$. We find the same equation when extending to $\omega<0$, so that both approaches coincide. Let us emphasize that there is no physical interpretation of the reduced function Φ_B^{red} itself and hence it becomes most natural to use $\lambda_B(\mu_0)$ and $\sigma_n(\mu_0)$ instead.

The above discussion holds only true for the particular moments defined in (5.74). In general factorization theorems like (2.78) and (3.49), the inverse moment $1/(\omega-n_-p-i0)$ obtains a shift from the virtual photon momentum component. For these translated moments, the equality of distributions (5.77) does not apply and thus the evolution equation does not simplify. In this case, we require a proper all-order solution for $\tilde{\Phi}_>$ and $\tilde{\Phi}_<$ to calculate the inverse moments.

5.2.6 All-order solution for $\Phi_{B,\otimes}$

The complete RGE (5.41) can be solved in Laplace space to all orders in the strong and electromagnetic coupling upon taking linear combinations of the previous results. To begin with, we express the Laplace transformed function for the negative support via (5.84) as

$$\tilde{\Phi}_<(\eta;\mu)=e^{-i\pi\eta}(\tilde{\Phi}_>(\eta;\mu)-\tilde{\Phi}_{B,\otimes}(\eta;\mu))\,, \tag{5.105}$$

where $\tilde{\Phi}_B$ is the solution (5.99) that determines the first inverse moments. Then, the RGE for $\tilde{\Phi}_>$ given by (5.85) decouples and can be solved on its own. We find

$$\left(\frac{d}{d\ln\mu}-\eta\right)\tilde{\Phi}_>(\eta;\mu)=\frac{\alpha_s C_F}{\pi}\Bigg[-H_{-\eta}-H_{-1-\eta}-\partial_\eta+i\pi+\frac{1}{2}\Bigg]\tilde{\Phi}_>(\eta;\mu)$$
$$+\frac{\alpha_{\text{em}}}{\pi}\Bigg[(Q_{\text{sp}}^2+2Q_{\text{sp}}Q_{M_1})(-H_{-\eta}-H_{-1-\eta}-\partial_\eta)$$
$$+Q_{\text{sp}}Q_{M_1}(H_{-\eta}+H_{-1-\eta})+\frac{3}{4}Q_{\text{sp}}^2+\frac{1}{2}Q_d^2-i\pi(Q_{\text{sp}}+Q_{M_1})Q_{M_2}$$

$$+ i\pi(Q_{\rm sp}Q_d + Q_{\rm sp}Q_{M_2})\Big]\tilde{\Phi}_>(\eta;\mu)$$
$$- \frac{\alpha_s C_F + \alpha_{\rm em}Q_{\rm sp}Q_d}{\pi} e^{-i\pi\eta}\Gamma(-\eta)\Gamma(1+\eta)\tilde{\Phi}_{B,\otimes}(\eta;\mu)\,. \qquad (5.106)$$

The system $(\tilde{\Phi}_>, \tilde{\Phi}_B)$ strictly corresponds to two differential equations with an upper triangular form. It remains to find the solution for $\tilde{\Phi}_>$ that solves (5.106) with the inhomogeneous function $\tilde{\Phi}_B$. We solve the RGE by using variation of constants. To this end, we introduce a modified evolution variable

$$\hat{a}(\mu,\mu_0) = -\int_{\mu_0}^{\mu}\frac{d\mu'}{\mu'}\frac{\alpha_s(\mu')C_F + \alpha_{\rm em}(\mu')(Q_{\rm sp}Q_d + Q_{\rm sp}Q_{M_2})}{\pi}\,. \qquad (5.107)$$

The solution becomes

$$\begin{aligned}\tilde{\Phi}_>(\eta;\mu) = e^{V+2\gamma_E a}\left(\frac{\mu}{\mu_0}\right)^{\eta}\Bigg[&\frac{\Gamma(-\eta)\Gamma(1-\eta)}{\Gamma(-\eta-a)\Gamma(1-\eta-a)}e^{-i\pi\hat{a}}\mathcal{G}(\eta;\mu,\mu_0)\tilde{\Phi}_>(\eta+a;\mu_0)\\ &- \frac{\Gamma(-\eta)\Gamma(1-\eta)\Gamma(1+\eta+a)}{\Gamma(1-\eta-a)}\mathcal{F}(\eta;\mu,\mu_0)e^{-i\pi\eta}\tilde{\Phi}_B(\eta+a;\mu_0) \qquad (5.108)\\ &\times\int_{\mu_0}^{\mu}\frac{d\tilde{\mu}}{\tilde{\mu}}\frac{\alpha_s(\tilde{\mu})C_F + \alpha_{\rm em}(\tilde{\mu})Q_{\rm sp}Q_d}{\pi}e^{-i\pi a(\mu,\tilde{\mu})-i\pi\hat{a}(\mu,\tilde{\mu})}(\mathcal{F}^{-1}\mathcal{G})(\eta;\mu,\tilde{\mu})\Bigg]\,,\end{aligned}$$

where the combination $\mathcal{F}^{-1}\mathcal{G}$ simplifies to

$$(\mathcal{F}^{-1}\mathcal{G})(\eta;\mu,\tilde{\mu}) = \exp\left\{\int_{\tilde{\mu}}^{\mu}\frac{d\mu'}{\mu'}\alpha_{\rm em}(\mu')Q_{\rm sp}Q_{M_1}\cot\pi(\eta+a(\mu,\mu'))\right\} \qquad (5.109)$$

due to the identity $H_{-1-\eta} - H_\eta = \pi\cot\pi\eta$. Again, we restore the QCD result (5.91) for $\alpha_{\rm em}\to 0$. The solution for $\tilde{\Phi}_<$ can be constructed from (5.99), (5.105) and (5.108) and is not given explicitly. Afterwards, the inverse Laplace transform from (5.82) and (5.83) allows us to calculate the entire function $\Phi_B(\omega;\mu)$ numerically. We circumvent the numerical calculation by deriving analytical results at $\mathcal{O}(\alpha_{\rm em})$ in Sec. 5.2.7 which already provide an accurate estimate for soft QED effects.

The analytic structure of the all-order solution (5.108) dictates the asymptotic behaviour of the soft function Φ_B in momentum (ω) space. In the following, we study the behaviour for the two relevant cases *i)* $\omega\to 0$ and *ii)* $\omega\to\pm\infty$. We require knowledge about both limits to determine the convergence of the inverse moment integral in (5.74). While for *i)* we observe that the soft function develops a distinct $\omega - i0$ prescription for the leading term, we find for *ii)* that the power law dependence already ensures the convergence of the integration. We restrict ourselves to realistic scenarios in which the evolution variable is $-1 < a < 0$ due to the choice of $\mu,\mu_0 \ll \mu_L$. Moreover, we assume the exponential model $\Phi_B(\omega;\mu_0) = \omega/\omega_0^2\, e^{-\omega/\omega_0}\,\theta(\omega)$ at the initial scale μ_0. In Laplace space, this corresponds to

$$\tilde{\Phi}_>(\eta+a;\mu_0) = \frac{1}{\omega_0}\left(\frac{\mu_0}{\omega_0}\right)^{\eta+a}\Gamma(1-\eta-a)\,, \qquad \tilde{\Phi}_<(\eta+a;\mu_0) = 0\,. \qquad (5.110)$$

Up to the pole at $\eta = 1 - a$, the functional form of $\Phi_B(\omega;\mu)$ is then completely determined by the poles of the Gamma functions and the Harmonic numbers from the F- and G-distributions defined in (5.61). To extract the asymptotic behaviour, we perform the inverse transformation (5.82) for both cases and apply the same arguments of the previous discussion for the soft region $u \to 0$ in the light meson case from Sec. 5.1.1 and Appendix E.

i) For $\omega \to 0$, we shift the straight integration line $c \pm i\infty$ of the inverse transformation to a curve enclosing all poles and branch cuts of the right half-plane with respect to $\mathrm{Re}(\eta) = c$. The contour parameter is chosen to lie in the strip $-1-a < c < 0$ for which the contour integration converges. The left-most singular term in the right half-plane dominates and arises from $\eta \to 0$ through $\Gamma(-\eta)$ and $\mathcal{G}(\eta)$ in (5.108). Expanding these contributions in the limit $\eta \to 0$, we obtain

$$\Phi_>(\omega \to 0;\mu) \sim \frac{1}{\omega_0}\int_C \frac{d\eta}{2\pi i}\left(\frac{\omega}{\omega_0}\right)^{\eta}\left(\frac{1}{-\eta}\right)^{1+p(\mu)} = \frac{1}{\omega_0}\frac{1}{\Gamma(1+p(\mu))}\left(-\ln\frac{\omega}{\omega_0}\right)^{p(\mu)} . \tag{5.111}$$

We choose the same contour C as in E.2 and defined

$$p(\mu) = \frac{-\alpha_{\mathrm{em}}(\mu)Q_{\mathrm{sp}}Q_{M_1}}{\alpha_s(\mu)C_F + \alpha_{\mathrm{em}}(\mu)(Q_{\mathrm{sp}}^2 + 2Q_{\mathrm{sp}}Q_{M_1})} . \tag{5.112}$$

Note that $p(\mu)$ can easily be related to the result for the light meson LCDA by replacing $Q_{q_1} \to Q_{\mathrm{sp}}$ and $Q_{q_2} \to Q_{q_1}$ in the definition below (5.22) identifying $Q_{M_1} = Q_{q_1} - Q_{\mathrm{sp}}$ which was $Q_M = Q_{q_1} - Q_{q_2}$ before. The solution $\tilde{\Phi}_<$ uses the same contour parameter c and acquires an equivalent behaviour due to (5.105). The exponential prefactor in the latter equation recombines for $\omega < 0$ into $e^{-i\pi\eta}(-\omega)^\eta = (\omega - i0)^\eta$, so that the leading term becomes an analytic function of $\omega - i0$. In total, we obtain the asymptotic behaviour in the $\omega \to 0$ limit

$$\Phi_B(\omega \to 0;\mu) = \frac{1}{\omega_0}\frac{\kappa}{\Gamma(1+p(\mu))}\left(-\ln\frac{\omega - i0}{\omega_0}\right)^{p(\mu)} + \mathcal{O}\left(\frac{\omega}{\omega_0}\right) , \tag{5.113}$$

with the dimensionless constants κ. According to (5.105), the difference between the $\omega > 0$ and $\omega < 0$ functions in Laplace space is given by the solution for $\tilde{\Phi}_B$ in (5.99). The relevant branch cut for $\omega \to 0$ advances from the left-most pole $\mathrm{Re}(\eta) = 1$ to the right. Thus, it can only contribute to the $\mathcal{O}(\omega/\omega_0)$ terms in (5.113). Consequently, the linear corrections do not inherit the $i0$-prescription from the leading term in the asymptotic expansion. Overall, we observe that the soft function becomes finite at $\omega = 0$ for $p = 0$ ($\otimes = (0,-)$) while for $p > 0$ ($\otimes = (+,-)$) it logarithmically diverges. This conclusion is validated by the numerical results in Fig. X. We emphasize that the result in (5.113) only applies to the case of $Q_{M_2} \neq 0$ for which negative support is generated. For $Q_{M_2} = 0$, the support is restricted to $\omega > 0$ and the solution boils down to a product of Gamma functions multiplied with an exponential of Harmonic numbers

as shown in Appendix E.3. For $\omega \to 0$, the soft function then vanishes linearly up to logarithmic corrections.

ii) For $\omega \to \pm\infty$, the integration contour after deformation encircles all poles and cuts in the left half-plane with respect to $\mathrm{Re}(\eta) = c$. In this case, the right-most singular term located at $\eta \to -1 - a$ determines the asymptotic behaviour. We find the leading contribution

$$\Phi_B(\omega \to \pm\infty;\mu) \sim \frac{1}{\omega_0}\left(\frac{\pm\omega}{\omega_0}\right)^{-1-a} \ln^{p(\mu_0)}\left(\frac{\pm\omega}{\omega_0}\right) . \tag{5.114}$$

The power law behaviour ω^{-1-a} remains analogous to the QCD result [152] with the difference that a includes the QED corrections according to (5.96). We remark that the form of (5.113) and (5.114) strictly originates from the exponential model. However, the asymptotic behaviour in particular arises from the model-independent analytic structure of the solution (5.108). Therefore, different initial conditions will result in similar conclusions, up to exotic choices that collide with the relevant singular terms in Laplace space.

Existence of inverse moments

From the results in (5.113) and (5.114), we can infer the existence of the first inverse-logarithmic moments defined in (5.74). For comparison, we summarize that in QCD-only scale evolution generates a behaviour of the form $\phi_+(\omega;\mu) \propto \omega$ for $\omega \to 0$ and $\phi_+(\omega;\mu) \propto \omega^{-1-a^{\mathrm{QCD}}}$ for $\omega \to \infty$. The former implies that the second and higher inverse moments proportional to $1/\omega^n$ with $n \geq 2$ do not exist. Since $-1 < a^{\mathrm{QCD}} < 0$, the latter renders all non-negative moments ω^m with $m \geq 0$ divergent. Hence, only the $1/\omega$-moment including logarithmic corrections is well-defined in pure QCD. Even though QED effects are more complicated, they should retain the convergence of the inverse moment integrals in QCD×QED. In fact, the behaviour $\omega \to \pm$ agrees to the QCD-only result up to the trivial replacement $a^{\mathrm{QCD}} \to a$ yielding the same consequence. For $\omega \to 0$, the arguments become more subtle: The leading term in the asymptotic expansion is an analytic function in the variable $\omega - i0$ and thus it can be shifted away from the origin such that the inverse moment integrals converge. Along these lines, the linear terms of order $\mathcal{O}(\omega/\omega_0)$ give rise to finite corrections. For the $1/(\omega - i0)^n$ moments, however, the linear and higher order terms spoil the convergence of the integration at $\omega = 0$ since they are non-analytic in $\omega - i0$. As we discussed previously, this consequence emerges from the analytic structure in Laplace space, more specifically from the branch cuts beginning at $\eta = 1, 2, 3, \ldots$ in the solution of $\tilde{\Phi}_B$ in (5.99) that makes up the difference between the two support regimes $\omega > 0$ and $\omega < 0$.

Finally, we note that the second inverse moment can be rewritten in terms of the derivative with respect to the first argument of the soft function using integration by parts

$$\int_{-\infty}^{\infty} \frac{d\omega}{(\omega - i0)^2}\Phi_B(\omega;\mu) = \int_{-\infty}^{\infty} \frac{d\omega}{\omega - i0}\partial_\omega \Phi_B(\omega;\mu) , \tag{5.115}$$

where the boundary terms vanish due to the $\omega \to \pm\infty$ behaviour in (5.114). For $\otimes = (0,-)$, we found that the soft function is continuous so that we can directly conclude from (5.115) that it cannot be differentiable since the left-hand side diverges. For the general charge case $\otimes = (+,-)$ this has no further implications as the soft function becomes logarithmically divergent with $p(\mu) > 0$ in (5.113).

5.2.7 Analytic solution for $\Phi_{B,\otimes}$ to $\mathcal{O}(\alpha_{\text{em}})$

Once again, we recall that QED effects are assumed to be small. In Sec. 5.1.2, we introduced the first-order solution to $\mathcal{O}(\alpha_{\text{em}})$ in terms of Gegenbauer moments of the light meson LCDA that sums QCD logarithms $(\alpha_s L)^n$ to all orders on top of a fixed-order expansion in α_{em}. We apply the same arguments to the soft function and expand the evolution equation linearly in the electromagnetic coupling.[17] For the soft function, this implies

$$\Phi_B(\omega;\mu) = \phi_+(\omega;\mu) + \frac{\alpha_{\text{em}}}{\pi}\Phi^{(1)}(\omega;\mu) + \mathcal{O}(\alpha_{\text{em}}^2) \,, \tag{5.116}$$

where we expand around the QCD LCDA $\phi_+(\omega;\mu)$ with $\omega > 0$. As before, the QED corrections are entirely contained in $\Phi^{(1)}(\omega;\mu) \sim \mathcal{O}(\ln^2(\mu/\mu_0), \alpha_s(\mu_0)/\alpha_s(\mu))$. The expansion (5.116) motivates to divide the one-loop kernel into the corresponding QCD and QED terms

$$\Gamma_\otimes(\omega,\omega',\mu) = \Gamma^{\text{QCD}}(\omega,\omega',\mu) + \frac{\alpha_{\text{em}}}{\pi}\Gamma_\otimes^{\text{QED}}(\omega,\omega',\mu) \,. \tag{5.117}$$

Furthermore, we split the support of the first-order QED function according to (5.81)

$$\Phi^{(1)}(\omega;\mu) = \theta(\omega)\Phi_>^{(1)}(\omega;\mu) + \theta(-\omega)\Phi_<^{(1)}(\omega;\mu) \,. \tag{5.118}$$

The RGE at zeroth order in α_{em} is then given by (5.88). At first order, we obtain

$$\begin{aligned}\frac{d}{d\ln\mu}\Phi^{(1)}(\omega;\mu) = &-\int_{-\infty}^{\infty} d\omega'\, \Gamma^{\text{QCD}}(\omega,\omega';\mu)\, \Phi^{(1)}(\omega';\mu) \\ &-\int_0^{\infty} d\omega'\, \Gamma_\otimes^{\text{QED}}(\omega,\omega';\mu)\, \phi_+(\omega';\mu) \,.\end{aligned} \tag{5.119}$$

We emphasize that the QED anomalous dimension generates $\omega < 0$ support for the function $\Phi^{(1)}$ from $\omega' > 0$ in ϕ_+. Hence, we have to consider the full kernel Γ^{QCD} opposed to QCD-only and thus conclude that both convolutions on the right-hand side of (5.119) contribute to the negative support of the soft function. Using the decomposition (5.118) together with (5.61) and (5.65), we again find two coupled differential equations, but this time for the first order functions $\Phi_>^{(1)}$ and $\Phi_<^{(1)}$, reading

$$\frac{d}{d\ln\mu}\Phi_>^{(1)}(\omega;\mu) = \frac{\alpha_s C_F}{\pi}\int_0^{\infty} d\omega' \left[\left(-\ln\frac{\mu}{\omega} + \frac{1}{2}\right)\delta(\omega-\omega') + F(\omega,\omega')\right]\Phi_>^{(1)}(\omega';\mu)$$

[17] In principle, we can derive the first-order term from the formal all-order solution (5.108). Yet it seems convenient to restart from the evolution equations since this approach directly leads to a simpler result.

$$+\frac{\alpha_s C_F}{\pi}\int_{-\infty}^{0} d\omega' F^{>}(\omega,\omega')\Phi_{<}^{(1)}(\omega';\mu)+\int_{0}^{\infty} d\omega'\Bigg[(Q_{\rm sp}^2+Q_{\rm sp}Q_{M_1})F(\omega,\omega')$$

$$+Q_{\rm sp}Q_{M_2}(F(\omega,\omega')-G^{>}(\omega,\omega'))-\Bigg((Q_{\rm sp}^2+2Q_{\rm sp}Q_{M_1})\ln\frac{\mu}{\omega}$$

$$+i\pi(Q_{\rm sp}+Q_{M_1})Q_{M_2}-\frac{3}{4}Q_{\rm sp}^2-\frac{1}{2}Q_d^2\Bigg)\delta(\omega-\omega')\Bigg]\phi_+(\omega';\mu)\;, \tag{5.120}$$

$$\frac{d}{d\ln\mu}\Phi_{<}^{(1)}(\omega;\mu)=\frac{\alpha_s C_F}{\pi}\int_{-\infty}^{0} d\omega'\Bigg[\left(-\ln\frac{\mu}{-\omega}-i\pi+\frac{1}{2}\right)\delta(\omega-\omega')$$

$$+G^{<}(\omega,\omega')\Bigg]\Phi_{<}^{(1)}(\omega';\mu)-Q_{\rm sp}Q_{M_2}\int_{0}^{\infty} d\omega' F^{<}(\omega,\omega')\phi_+(\omega';\mu)\;. \tag{5.121}$$

Note that these equations are separately defined for $\omega>0$ and $\omega<0$ respectively. After applying the Laplace transformation (5.82) and (5.83) in both cases, we find

$$\left(\frac{d}{d\ln\mu}-\eta\right)\tilde{\Phi}_{>}^{(1)}(\eta;\mu)=\frac{\alpha_s C_F}{\pi}\left[-H_\eta-H_{-\eta}-\partial_\eta+\frac{1}{2}\right]\tilde{\Phi}_{>}^{(1)}(\eta;\mu)$$

$$-\frac{\alpha_s C_F}{\pi}\Gamma(\eta)\Gamma(1-\eta)\tilde{\Phi}_{<}^{(1)}(\eta;\mu)+\Bigg[Q_{\rm sp}Q_{M_1}(H_\eta+H_{-\eta})$$

$$+Q_{\rm sp}Q_{M_2}(H_{-1-\eta}-H_\eta)-(Q_{\rm sp}^2+2Q_{\rm sp}Q_{M_1})(H_\eta+H_{-\eta}+\partial_\eta)$$

$$-i\pi Q_{M_1}Q_{M_2}+\frac{3}{4}Q_{\rm sp}^2+\frac{1}{2}Q_d^2\Bigg]\tilde{\phi}_+(\eta;\mu)\;, \tag{5.122}$$

$$\left(\frac{d}{d\ln\mu}-\eta\right)\tilde{\Phi}_{<}^{(1)}(\eta;\mu)=\frac{\alpha_s C_F}{\pi}\left[-H_{-\eta}-H_{-1-\eta}-\partial_\eta+\frac{1}{2}\right]\tilde{\Phi}_{<}^{(1)}(\eta;\mu)$$

$$+Q_{\rm sp}Q_{M_2}\Gamma(\eta)\Gamma(1-\eta)\tilde{\phi}_+(\eta;\mu)\;, \tag{5.123}$$

with $-1<\mathrm{Re}(\eta)<0$.[18] Most importantly, we observe that the evolution equation for $\Phi_{<}^{(1)}$ does not depend on $\Phi_{>}^{(1)}$. As a consequence, we can obtain a self-consistent solution to (5.123) alone and insert the result into (5.122) to find a solution for thereafter.

Mathematically, we obtain the solution for (5.123) by a variation of constants which was already used to find (5.108). The general solution acquires a similar form to [151] and reads

$$\tilde{\Phi}_{<}^{(1)}(\eta;\mu)=e^{V+2\gamma_E a}\left(\frac{\mu}{\mu_0}\right)^{\eta}\frac{\Gamma(1-\eta)\Gamma(-\eta)}{\Gamma(1-\eta-a)\Gamma(-\eta-a)}\Bigg[\tilde{\Phi}_{<}^{(1)}(\eta+a;\mu_0)$$

$$-Q_{\rm sp}Q_{M_2}\Gamma(-\eta-a)\Gamma(1+\eta+a)\tilde{\phi}_+(\eta+a;\mu_0)\ln\frac{\mu}{\mu_0}\Bigg]\;. \tag{5.124}$$

[18] The convergence strip is based on the analytic structure induced by the distribution relations in Appendix D.3 and restricts the contour parameter to the interval $-1<c<0$ for both transformations.

Inserting (5.124) into (5.122), we find for $\tilde{\Phi}_>^{(1)}$ the solution

$$\begin{aligned}\tilde{\Phi}_>^{(1)}(\eta;\mu) = e^{V+2\gamma_E a}\left(\frac{\mu}{\mu_0}\right)^\eta \frac{\Gamma(1-\eta)\Gamma(1+\eta+a)}{\Gamma(1+\eta)\Gamma(1-\eta-a)}\Bigg[\tilde{\Phi}_>^{(1)}(\eta+a;\mu_0)\\ + \int_{\mu_0}^{\mu}\frac{d\mu'}{\mu'}\frac{\alpha_s(\mu')C_F}{\pi}\frac{\Gamma^2(-\eta-a(\mu,\mu'))\Gamma^2(1+\eta+a(\mu,\mu'))}{\Gamma(-\eta-a)\Gamma(1+\eta+a)}\Bigg\{\tilde{\Phi}_<^{(1)}(\eta+a;\mu_0)\\ - Q_{\rm sp}Q_{M_2}\Gamma(-\eta-a)\Gamma(1+\eta+a)\tilde{\phi}_+(\eta+a;\mu_0)\ln\frac{\mu'}{\mu_0}\Bigg\}\\ + \Bigg(\int_{\mu_0}^{\mu}\frac{d\mu'}{\mu'}\{Q_{\rm sp}Q_{M_1}(H_{\eta+a(\mu,\mu')}+H_{-\eta-a(\mu,\mu')})\\ + Q_{\rm sp}Q_{M_2}(H_{-1-\eta-a(\mu,\mu')}-H_{\eta+a(\mu,\mu')})\}\\ - (Q_{\rm sp}^2+2Q_{\rm sp}Q_{M_1})\left\{\frac{1}{2}\ln^2\frac{\mu}{\mu_0}+(H_{\eta+a}+H_{-\eta-a}+\partial_\eta)\ln\frac{\mu}{\mu_0}\right\}\\ + \left[\frac{3}{4}Q_{\rm sp}^2+\frac{1}{2}Q_d^2-i\pi Q_{M_1}Q_{M_2}\right]\ln\frac{\mu}{\mu_0}\Bigg)\tilde{\phi}_+(\eta+a;\mu_0)\Bigg]. \end{aligned} \tag{5.125}$$

For practical purposes, we did not perform the integral in the second line when it enters with $\tilde{\Phi}_<^{(1)}(\eta+a;\mu_0)$, even though it momentarily results in a simpler form. To recover $\Phi^{(1)}(\omega;\mu)$, we take the inverse transformation of (5.125) and (5.124). In doing so, we recast the harmonic numbers in terms of their plus-distribution expression

$$H_\eta = -\int_0^1 dx\left[\frac{1}{1-x}\right]_+ x^\eta = -\int_0^1\frac{dx}{1-x}\left(x^\eta-1\right). \tag{5.126}$$

In this way, we evaluate the μ'-integrals in (5.125) which then generally produce the function

$$h(x)\equiv\int_{\mu_0}^{\mu}\frac{d\mu'}{\mu'}x^{a(\mu,\mu')} = \frac{2\pi}{\beta_0^{\rm QCD}+2C_F\ln x}\left[\frac{1}{\alpha_s(\mu)}-\frac{1}{\alpha_s(\mu_0)}\left(\frac{\alpha_s(\mu)}{\alpha_s(\mu_0)}\right)^{\frac{2C_F}{\beta_0^{\rm QCD}}\ln x}\right], \tag{5.127}$$

and come along with several convolutions. Finally, we obtain

$$\begin{aligned}\Phi_>^{(1)}(\omega;\mu) = e^{V+2\gamma_E a}\int_0^\infty\frac{d\omega'}{\omega'}\left(\frac{\mu_0}{\omega'}\right)^a\Bigg[G_a\Big(\frac{\omega}{\omega'}\Big)\Phi_>^{(1)}(\omega';\mu_0)\\ + \int_0^1\frac{dx}{1-x}\Bigg\{(x^a-1)G_a^{1,0}\Big(\frac{x\omega}{\omega'}\Big)-(x^{-1-a}-x^{-1})G_a^{1,0}\Big(\frac{\omega}{x\omega'}\Big)\Bigg\}\Phi_<^{(1)}(-\omega';\mu_0)\\ - \int_{\mu_0}^{\mu}\frac{d\mu'}{\mu'}\frac{\alpha_s(\mu')C_F}{\pi}Q_{\rm sp}Q_{M_2}G_{a(\mu,\mu')}^{3,3}\Big(\frac{\omega}{\omega'}\Big)\ln\frac{\mu'}{\mu_0}\phi_+(\omega';\mu_0)\end{aligned}$$

$$
\begin{aligned}
&+\int_0^1 dx\left[\frac{1}{1-x}\right]_+\Bigg\{(Q_{\rm sp}^2+2Q_{\rm sp}Q_{M_1})\bigg(x^a G_a\Big(\frac{x\omega}{\omega'}\Big)+x^{-a}G_a\Big(\frac{\omega}{x\omega'}\Big)\bigg)\ln\frac{\mu}{\mu_0}\\
&-Q_{\rm sp}Q_{M_1}\bigg(h(x)G_a\Big(\frac{x\omega}{\omega'}\Big)+h(x^{-1})G_a\Big(\frac{\omega}{x\omega'}\Big)\bigg)\\
&-Q_{\rm sp}Q_{M_2}\bigg(-h(x)G_a\Big(\frac{x\omega}{\omega'}\Big)+x^{-1}h(x^{-1})G_a\Big(\frac{\omega}{x\omega'}\Big)\bigg)\Bigg\}\phi_+(\omega';\mu_0)\\
&+\Bigg\{-(Q_{\rm sp}^2+2Q_{\rm sp}Q_{M_1})\left(\frac{1}{2}\ln^2\frac{\mu}{\mu_0}+\ln\frac{\mu_0}{\omega'}\ln\frac{\mu}{\mu_0}\right)\\
&+\left(\frac{3}{4}Q_{\rm sp}^2+\frac{1}{2}Q_d^2-i\pi Q_{M_1}Q_{M_2}\right)\ln\frac{\mu}{\mu_0}\Bigg\}G_a\Big(\frac{\omega}{\omega'}\Big)\,\phi_+(\omega';\mu_0)\Bigg]\,, \qquad (5.128)
\end{aligned}
$$

$$
\begin{aligned}
\Phi_<^{(1)}(\omega;\mu)=e^{V+2\gamma_E a}\int_0^\infty\frac{d\omega'}{\omega'}\left(\frac{\mu_0}{\omega'}\right)^a\Bigg[&G_a^{2,0}\Big(\frac{-\omega}{\omega'}\Big)\,\Phi_<^{(1)}(-\omega';\mu_0)\\
&-Q_{\rm sp}Q_{M_2}G_a^{2,1}\Big(\frac{-\omega}{\omega'}\Big)\ln\frac{\mu}{\mu_0}\phi_+(\omega';\mu_0)\Bigg]\,. \qquad (5.129)
\end{aligned}
$$

For shorthand notation, we introduced

$$
\begin{aligned}
G_a^{m,n}\Big(\frac{\omega}{\omega'}\Big)&\equiv G_{2,2}^{m,n}\left(\begin{matrix}-a,\ 1-a\\ 1,\ 0\end{matrix}\middle|\frac{\omega}{\omega'}\right)\,,\\
G_{a(\mu,\mu')}^{m,n}\Big(\frac{\omega}{\omega'}\Big)&\equiv G_{4,4}^{m,n}\left(\begin{matrix}-a(\mu,\mu'),\ -a(\mu,\mu'),\ -a,\ 1-a\\ -a(\mu,\mu'),\ -a(\mu,\mu'),\ 1,\ 0\end{matrix}\middle|\frac{\omega}{\omega'}\right)\,, \qquad (5.130)
\end{aligned}
$$

based on the general Meijer-G functions $G_{p,q}^{m,n}$ defined in (F.1). The first-order solutions (5.128) and (5.129) provide the QED corrections to the QCD evolved function in (5.116). In practice, these $\mathcal{O}(\alpha_{\rm em})$ terms sufficiently describe the soft photon exchange in the exclusive $\bar{B}\to M_1M_2$ decays.

5.3 Ultrasoft QED effects

On top of the RGE evolution for the collinear and soft functions, we consider the resummation of QED logarithms in the ultrasoft regime. Opposed to the structure-dependent logarithms between $\Lambda_{\rm QCD}$ and m_B, these might result in percent level corrections to the decay rate (4.101). The ultrasoft logarithms can be universally obtained from an ultrasoft effective theory of point-like mesons or, equivalently, from scalar QED with point-like meson interaction vertices, see [137]. The RGE running from the hard scale $\mu_b\sim m_b$ to the collinear scale $\mu_c\sim\Lambda_{\rm QCD}$ in these objects produces universal Sudakov factors of the form

$$
e^{S_{M_i}(\mu_b,\mu_c)}=\exp\left\{-\frac{\alpha_{\rm em}}{2\pi}\,Q_{M_i}^2\ln^2\frac{\mu_c}{\mu_b}\right\}\,, \qquad (5.131)
$$

plus a term defining the difference between leading double and the structure-dependent QED logarithms according to [60]. We introduce (5.131) to factor out the contributions from the two final states in the exponentiated ultrasoft function. As discussed in Chapter 4, the ultrasoft logarithms are related to the IR dependence of the form factors and LCDAs appearing in the factorized amplitude. For $\mu = \mu_c$, the scale dependence therefore cancels in the combined expression

$$\begin{aligned}&\left|e^{S_{M_1}(\mu_b,\mu_c)+S_{M_2}(\mu_b,\mu_c)}\right|^2 e^{S_\otimes^{(1)}}\\ &\quad= \exp\left\{\frac{\alpha_{\rm em}}{\pi}\left(Q_B^2+Q_{M_1}^2\left[1+\ln\frac{m_{M_1}^2}{m_B^2}\right]+Q_{M_2}^2\left[1+\ln\frac{m_{M_2}^2}{m_B^2}\right]\right)\ln\frac{m_B}{2\Delta E}\right\}, \quad (5.132)\end{aligned}$$

where $S_\otimes^{(1)}$ is given in (4.103). Even though we consider the Sudakov factors $e^{S_{M_i}}$ in the double logarithmic approximation, we include the complete logarithmic dependence for ΔE in (4.103). We observe that the scale dependence in the ultrasoft logarithm of (5.132) has been promoted up to the hard scale m_B. At the level of the ultrasoft-inclusive decay rate (4.101), we obtain

$$\Gamma[\bar B\to M_1M_2](\Delta E) = \Gamma^{(0)}[\bar B\to M_1M_2]\; U(M_1M_2)\,, \quad (5.133)$$

with the all-order resummed ultrasoft function

$$U(M_1M_2) = \left(\frac{2\Delta E}{m_B}\right)^{-\frac{\alpha_{\rm em}}{\pi}\left(Q_B^2+Q_{M_1}^2\left[1+\ln\frac{m_{M_1}^2}{m_B^2}\right]+Q_{M_2}^2\left[1+\ln\frac{m_{M_2}^2}{m_B^2}\right]\right)}. \quad (5.134)$$

The factor $\Gamma^{(0)}$ in (5.133) contains the squared virtual amplitude $\left|\langle M_1M_2|Q_i|\bar B\rangle\right|^2$ modulo the Sudakov factors (5.131), which we reshuffled into the ultrasoft function. We emphasize that this choice is not unique. In the above approach however, the ultrasoft function (5.134) turns out to be universal and independent of the factorization scale in the logarithmic ΔE corrections. Hence, we most naturally refer to $\Gamma^{(0)}$ as the non-radiative decay width.

By comparison to [137], we find agreement when setting $\mu = m_B$ in (4.103) and (5.134) while neglecting virtual contributions as well as power corrections in m_{M_i}/m_B. From an EFT perspective, choosing the hard scale in the ultrasoft function is wrong a priori since the ultrasoft theory is only valid up to $\Lambda_{\rm QCD}$. However, the SCET analysis in Chapter 4 allows us to neglect the stucture-dependent terms in the reorganization of the Sudakov factors above, such that m_B appears in the final result. Below $\Lambda_{\rm QCD}$, our treatment of ultrasoft QED effects relies on the factorization in (4.99) including the static Wilson lines that contain ultrasoft flucations of $\mathcal{O}(\Delta E)$ in a similar manner to HQET. In the corresponding ultrasoft EFT, the logarithms of $m_{M_i}^2/m_B^2$ appear due to the large boost between the light and heavy meson rest frames. In contrast, the analysis in [137] keeps the point-like mesons as dynamical degrees of freedom, which eventually leads to unphysical multipole couplings in virtual corrections of $\mathcal{O}(\Lambda_{\rm QCD})$. These contributions do not enter the radiation factor (5.134) and may be understood as part of an unspecified non-radiative decay rate.

Chapter 6

Numerical results

In the previous chapters, we considered two cases for which we improved the QCD factorization analysis in the context of exclusive processes. The first one involved the computation of subleading power corrections to the Euclidean correlation functions (2.1) and (1.3) in an $1/E_\gamma$- and $1/m_b$-expansion. More precisely, we included hard-collinear as well as induced soft corrections to the LP factorization formula, where the latter have been obtained from a dispersive treatment. The second improvement regards the inclusion of QED effects in a combined QCD×QED factorization approach for non-leptonic B decays with light final states.

In a first numerical analysis, we present qualitative estimates for the respective cases. For the corrections to the B-meson correlators, we are mainly interested in the relative size of LP and NLP contributions, which are discussed in the first section. For the QED effects, we consider concrete applications to $\bar{B} \to \pi K$ observables. We separately discuss the various effects that enter the factorization formula, which involve electroweak QED effects, structure-dependent and ultrasoft contributions including their behaviour under scale evolution.

6.1 Subleading effects in QCD factorization

To estimate the magnitude of the subleading corrections, we consider the relative size of the LP and NLP contributions to the correlators (2.1) and (1.3) that enter the form factors in (3.2), (3.3) and (3.4). At LP, we use the factorization results from (2.78) and (3.49) as well as the one-loop resummation for the hard coefficients and the B LCDA. At NLP, we approximate the leading and subleading twist LCDAs by their tree-level matrix elements. Here and in what follows, we assume an exponential model for the B LCDAs, which is one of the simplest choices according to [36].[1] Within our analysis, we consider the combined model based on [124]. For the two-particle LCDAs, we use

$$\phi_+(\omega) = \frac{\omega}{\omega_0^2} e^{-\omega/\omega_0} \,, \tag{6.1}$$

[1] We postpone a more in-depth analysis involving different models to an upcoming publication [156].

Masses, decay constant and model parameters		
$m_b = 4.8\,\text{GeV}$	$m_B = 5.3\,\text{GeV}$	$\bar{\Lambda} = m_B - m_b$
$f_B = 0.19\,\text{GeV}$	$\lambda_E^2 = 0.03\,\text{GeV}^2$	$\lambda_H^2 = 0.06\,\text{GeV}^2$
Resonances, Borel parameter and condensate		
$m_\sigma = 0.500\,\text{GeV}$	$s_0 = 1.0\,\text{GeV}^2$	$M^2 = 1.25\,\text{GeV}^2$
$m_\rho = 0.775\,\text{GeV}$	$r_0 = 1.5\,\text{GeV}^2$	$\langle\bar{u}u\rangle(\mu_0) = -0.24\,\text{GeV}$

Table 6.1: Standard input values. We run the strong coupling at three-loop accuracy with $n_f = 4$ below m_b. For scale evolution from the initial scale $\mu_0 = 1\,\text{GeV}$ to $\mu = 1.5\,\text{GeV}$, we find $\alpha_s(\mu) = 0.348929$. The reference value at the electroweak scale is $\alpha_s(m_Z) = 0.118$. We estimate the continuum threshold for the scalar mesons based on [15]. The model parameters of the three-particle LCDAs have been taken from [157].

$$\phi_-^{\text{WW}}(\omega) = \frac{1}{\omega_0} e^{-\omega/\omega_0}\,, \qquad \phi_-^{\text{t3}}(\omega) = \frac{\lambda_E^2 - \lambda_H^2}{6\omega_0^5} e^{-\omega/\omega_0}(-\omega^2 + 4\omega\omega_0 - 2\omega_0^2)\,, \tag{6.2}$$

$$\begin{aligned} g_+(\omega) = &-\frac{\lambda_E^2}{6\omega_0^2}\left\{(\omega - 2\omega_0)\text{Ei}\left(-\frac{\omega}{\omega_0}\right) + (\omega + 2\omega_0)e^{-\omega/\omega_0}\left(\ln\frac{\omega}{\omega_0} + \gamma_E\right) - 2\omega e^{-\omega/\omega_0}\right\} \\ &+ \frac{e^{-\omega/\omega_0}}{2\omega_0}\omega^2\left\{1 - \frac{1}{36\omega_0^2}(\lambda_E^2 - \lambda_H^2)\right\}\,, \end{aligned} \tag{6.3}$$

where the exponential integral is defined by $\text{Ei}\,(-z) = \int_z^\infty e^{-x}dx/x$. For the three-particle LCDAs, we use

$$\begin{aligned} &\phi_3(\omega_1,\omega_2) = \frac{\lambda_E^2 - \lambda_H^2}{6\omega_0^5}\,\omega_1\omega_2^2\,e^{-(\omega_1+\omega_2)/\omega_0}\,, \quad \psi_4(\omega_1,\omega_2) = \frac{\lambda_E^2}{3\omega_0^4}\,\omega_1\omega_2\,e^{-(\omega_1+\omega_2)/\omega_0}\,, \\ &\phi_4(\omega_1,\omega_2) = \frac{\lambda_E^2 + \lambda_H^2}{6\omega_0^4}\,\omega_2^2\,e^{-(\omega_1+\omega_2)/\omega_0}\,, \qquad \widetilde{\psi}_4(\omega_1,\omega_2) = \frac{\lambda_H^2}{3\omega_0^4}\,\omega_1\omega_2\,e^{-(\omega_1+\omega_2)/\omega_0}\,. \end{aligned} \tag{6.4}$$

In the following, we consider scale evolution from $\mu_0 = 1\,\text{GeV}$ to $\mu = 1.5\,\text{GeV}$ and use three-loop running of α_s. When not specified otherwise, we employ the numerical values of Table 6.1.

6.1.1 LO+LP analysis

We first analyze the impact of different choices for p^2 to LO at LP. To this end, we recall that all form factors agree at this accuracy in the factorization approach, but differ in the soft correction due to different scalar and vector meson masses and effective continuum thresholds. We have

$$F_S^{(\text{LO})} = F_V^{(\text{LO})} = F_A^{(\text{LO})} = eQ_u f_B m_B \int_0^\infty \frac{d\omega}{2E_\gamma\omega - p^2}\,\phi_+(\omega)\,, \tag{6.5}$$

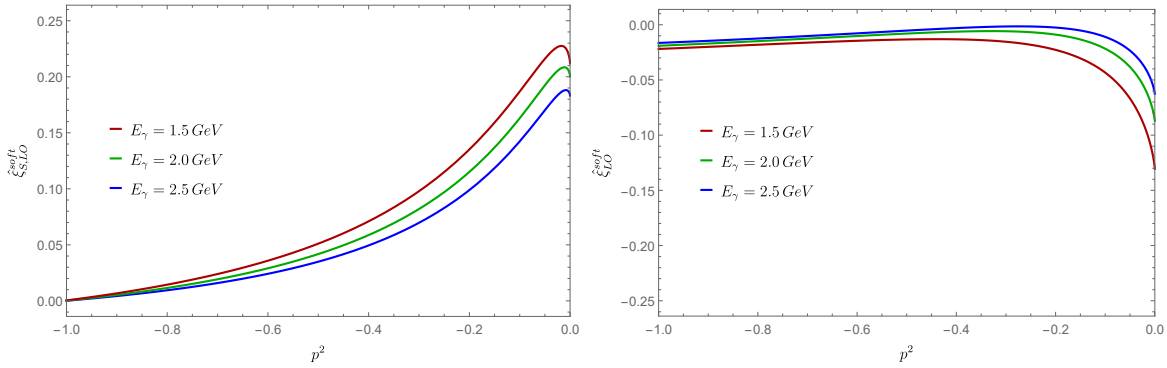

Figure 6.1: LO results for the soft correction $\hat{\xi} = \xi/F$ for different values of p^2. We use the reference value $\omega_0 = 0.35\,\text{GeV}$.

$$\xi^{\text{soft}}_{S,\text{LO}} = eQ_u f_B m_B \int_0^{\frac{s_0}{2E_\gamma}} \frac{d\omega'}{2E_\gamma\omega' - p^2} \left[\frac{2E_\gamma\omega' - p^2}{m_\sigma^2 - p^2} e^{-(2E_\gamma\omega' - m_\sigma^2)/M^2} - 1 \right] \phi_+(\omega) \,, \quad (6.6)$$

$$\xi^{\text{soft}}_{\text{LO}} = eQ_u f_B m_B \int_0^{\frac{r_0}{2E_\gamma}} \frac{d\omega'}{2E_\gamma\omega' - p^2} \left[\frac{2E_\gamma\omega' - p^2}{m_\rho^2 - p^2} e^{-(2E_\gamma\omega' - m_\rho^2)/M^2} - 1 \right] \phi_+(\omega) \,, \quad (6.7)$$

and $\Delta\xi^{\text{soft}}_{\text{LO}} = 0$. We present the relative size of the LO result with respect to the soft correction in Fig. 6.1 for different values of E_γ. The results for the scalar and vector case differ qualitatively, but show the largest variation in the low-p^2 region. In the following, we adopt the choice of $p^2 = -0.1\,\text{GeV}^2 \sim \Lambda^2_{\text{QCD}}$ which is a realistic value for lattice QCD simulations. For this particular value, we find at LO that the soft correction can be of order $\mathcal{O}(5\%)$ for the vector case, while the scalar corrections amount to an $\mathcal{O}(20\%)$ effect. Hence, we also expect the NLO contributions to be comparably large for the scalar case.

As mentioned beforehand, the expressions in (6.6) and (6.7) depend on the resonance masses, the continuum threshold and the Borel parameter. Due to the smaller parameter values in the scalar sector, we expect the dispersion relation to be less robust against variations of the Borel parameter M. Indeed, we observe from Fig. 6.2 that the choice of the parameter in the range of $M^2 = (1.25 \pm 0.25)\,\text{GeV}^2$ affects the scalar result at LO up to $\mathcal{O}(5\%)$. The vector form factors, on the other hand, vary with less than one percent.

Lastly, we remark that the limit $p^2 \to 0$ is not smooth in general. For $p^2 = 0$, some convolution integrals of the twist-5 and twist-6 contributions become divergent and require a special treatment according to [47]. In this case, Fig. 3.1(c) is promoted to an $\mathcal{O}(1/E_\gamma^2)$ correction.

6.1.2 NLO+NLP analysis

The aim of an advanced analysis [156] is to extract information about the leading-twist LCDA ϕ_+, in particular λ_B. In our model, this object can be naively related to the

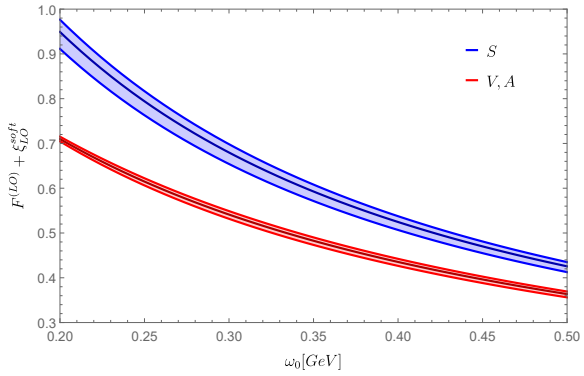

Figure 6.2: Dependence on the Borel parameter $M^2 = (1.25 \pm 0.25)\,\text{GeV}$ for the LO contributions plus the dispersive (soft) part for the scalar (S) and axial-vector (V,A) case. The central line in each region corresponds to the exact LO result.

input parameter ω_0. To obtain first numerical estimates, we consider three different values of this parameter, shown in Fig. 6.3. We include the complete results at NLP in our analysis and compare the NLO contributions from the LP factorization to the higher-twist effects. The resummation for the hard coefficients as well as the leading-twist LCDA is considered at LL accuracy. In this approximation, the evolved function $\phi_+(\omega;\mu)$ is given by

$$\phi_B^+(\omega;\mu) = \frac{1}{\omega_0} e^{V+2\gamma_E a} \left(\frac{\mu_0}{\omega_0}\right)^a F_a\left(\frac{\omega}{\omega_0}\right) , \tag{6.8}$$

which follows from (5.92) with $F_a(z) \equiv z\Gamma(2+a)\ {}_1F_1\,(2+a,2,-z)$.[2] We combine the higher-twist corrections from the OPE into

$$\xi_S^{\text{ht}} \equiv = \xi_S^{1/E_\gamma}\Big|_{(3.17)} + \xi_S^{1/m_b}\Big|_{(3.21)} + \xi_S^{(b)}\Big|_{(3.23)} + \xi_{S,\text{tw56}}\Big|_{(3.30)+(3.32)} , \tag{6.9}$$

$$\xi^{\text{ht}} \equiv = \xi^{1/E_\gamma}\Big|_{(3.27)} + \xi^{1/m_b}\Big|_{(3.21)} + \xi_{\text{tw56}}\Big|_{(3.30)+(3.33)} , \tag{6.10}$$

$$\Delta\xi^{\text{ht}} \equiv = \Delta\xi^{1/E_\gamma}\Big|_{(3.28)} + \Delta\xi^{(b)}\Big|_{(3.29)} + \Delta\xi_{\text{tw56}}\Big|_{(3.34)} . \tag{6.11}$$

In total, the subleading terms can be represented by the sum of these higher-twist parts and the soft corrections from the dispersive improvement

$$\xi_S = \xi_S^{\text{ht}}\Big|_{(6.9)} + \xi_{S,\text{NLO}}^{\text{soft}}\Big|_{(3.52)} + \xi_{S,\text{tw34}}^{\text{soft}}\Big|_{(3.57)} + \xi_{S,\text{tw56}}^{\text{soft}}\Big|_{(3.63)} , \tag{6.12}$$

[2]The evolution factors refer to the QCD definition in (5.90).

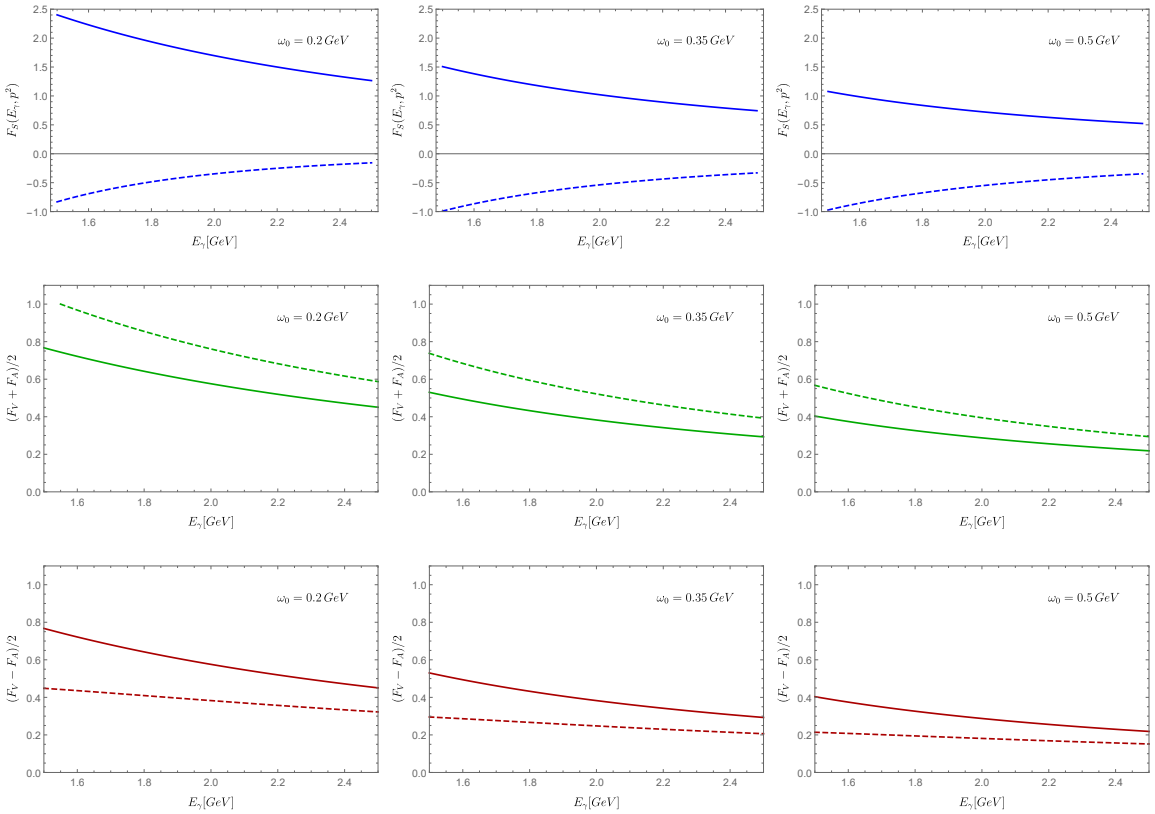

Figure 6.3: Form factors F_S and $(F_V \pm F_A)/2$ as a function of E_γ for different values of the parameter ω_0. We choose $p^2 = -0.1\,\text{GeV}^2$. The solid line refers to the NLO and its soft contribution, while the dashed curve includes all terms up to and including twist-5 and twist-6.

$$\xi = \xi^{\text{ht}}\Big|_{(6.10)} + \xi^{\text{soft}}_{\text{NLO}}\Big|_{(3.53)} + \xi^{\text{soft}}_{\text{tw34}}\Big|_{(3.58)} + \xi^{\text{soft}}_{\text{tw56}}\Big|_{(3.64)}\,, \tag{6.13}$$

$$\Delta\xi = \Delta\xi^{\text{ht}}\Big|_{(6.11)} + \Delta\xi^{\text{soft}}_{\text{tw34}}\Big|_{(3.62)} + \Delta\xi^{\text{soft}}_{\text{tw56}}\Big|_{(3.65)}\,. \tag{6.14}$$

We list three form factor combinations in Fig. 6.3, in which the NLO-only terms and the complete higher-twist results are displayed separately. The vector combinations $(F_V \pm F_A)/2$ eliminate the dependence on $\Delta\xi$ and ξ respectively and thus entirely reflect each correction at once. For both cases, the higher-twist contributions modify the NLO results by at least 20%. In the scalar sector, we expect a larger deviation to the NLO result due to the enhancement of the soft correction. We observe that the form factors depend only weakly on the value of E_γ. Furthermore, we find that the higher-twist contributions in $\Delta\xi$ decrease the value of the LP result while ξ overall increases the contribution.

In Fig. 6.3, we did not include uncertainties from the theoretical/experimental input. In this regard, the results only display a first estimate on the relative size of the LP

compared to NLP contributions. To obtain a proper estimate for λ_B, one has to incorporate these uncertainties and improve the resummation up to NLL, at which the dependence on the first logarithmic moment σ_1 becomes relevant, see [47]. For this analysis, we again refer to [156].

6.2 QED corrections in $\bar{B} \to \pi K$ observables

The analysis of QED corrections involves three major regimes, discussed in Chapter 4 and 5. To display their numerical relevance, we specifically consider the QED effects in context of $\bar{B} \to \pi K$ observables entering from i) the electroweak (above m_B), ii) the structure-dependent (between m_B and μ_c[3]) and the iii) ultrasoft region (below $\Lambda_{\rm QCD}$). The structure-dependent part in particular contains the contributions from the light-meson LCDA and the soft functions, which are treated separately.

As the structure-dependent terms ii) arise from weak operator insertions $Q_{1,2}$, we can view these corrections as modifications to the colour-allowed and colour-suppressed tree-amplitudes $\alpha_1(M_1M_2)$ and $\alpha_2(M_1M_2)$ in the notation of [158]. In QCD-only, the amplitudes are defined with respect to an overall factor

$$A_{M_1M_2} \equiv i\frac{G_F}{\sqrt{2}} m_B^2 F_0^{BM_1}(0) f_{M_2} \ , \tag{6.15}$$

subtracting the non-perturbative dependence on the QCD form factor $F_0^{BM_1}$ and decay constant f_{M_2}. In QCD×QED, we generally define

$$\mathcal{A}(M_1M_2) \equiv i\frac{G_F}{\sqrt{2}} m_B^2 \mathcal{F}_{Q_2}^{BM_1}(0) f_{M_2} \ , \tag{6.16}$$

which now depends on the electric charges Q_{M_1} and Q_{M_2} through the QED-generalized form factor $\mathcal{F}_{Q_2}^{BM_1}(0)$. We normalized the LCDAs with respect to the pure QCD decay constants, such that f_{M_2} appears in (6.16). The product of $\mathcal{A}\alpha_i$ generally does not factorize due to soft interactions. Therefore, we do not need to retain the QCD-like separation of $\mathcal{A}$ and α_i. Instead, we define

$$\mathcal{A}(M_1M_2)\alpha_i(M_1M_2) = A_{M_1M_2}\Big(\alpha_i^{\rm QCD}(M_1M_2) + \delta\alpha_i(M_1M_2)\Big) \,, \tag{6.17}$$

to directly compare QCD and QED contributions, where the latter are entirely contained within $\delta\alpha_i(M_1M_2)$. At $\mathcal{O}(\alpha_{\rm em})$, we decompose the various QED effects according to

$$\delta\alpha_i(M_1M_2) \equiv \delta\alpha_i^{\rm WC}(M_1M_2) + \delta\alpha_i^{\rm K}(M_1M_2) + \delta\alpha_i^{\rm F,V}(M_1M_2) + \delta\alpha_i^{\rm F,sp}(M_1M_2) \,. \tag{6.18}$$

The term (WC) refers to the electroweak Wilson coefficients, (K) to the hard and hard-collinear scattering kernels, (F,V) to the vertex and (F,sp) to the spectator terms

[3]The collinear scale μ_c of order of a few times $\Lambda_{\rm QCD}$ has been introduced in Sec. 5.3 to factor out the Sudakov factors for M_1 and M_2 into the ultrasoft function.

Coupling constants and masses [GeV]			
$\alpha_{\rm em}(m_Z) = 1/127.96$	$\alpha_s(m_Z) = 0.118$	$m_B = 5.297$	$m_Z = 91.19$
Decay constants [MeV] and form factors			
$f_\pi = 130$	$f_K = 160$	$f_B = 190$	$F_0^{B\pi} = 0.25$	$F_0^{BK} = 0.34$
CKM parameters and $R_{\pi K}$			
$\lvert\lambda_u/\lambda_c\rvert \equiv \lvert V_{us}V_{ub}^*/V_{cb}V_{cs}^*\rvert = 0.0206$		$R_{\pi K} = f_\pi F_0^{BK}/f_K F_0^{B\pi} = 1.11$	
Wilson coefficients and coupling constants at $\nu = 4.8$ GeV			
$C_1^{\rm QCD} = -0.26$	$C_2^{\rm QCD} = 1.01$	$\alpha_{\rm em} = 1/132.24$	$\alpha_s = 0.216$
Parameters of distributions amplitudes at $\mu = 1$ GeV			
$a_2^\pi = 0.138$	$a_1^{\bar{K}} = 0.061$	$a_2^{\bar{K}} = 0.124$	$\lambda_B = 250$ MeV
Coupling constants and $\hat{\alpha}_4^c$ at $\mu = 1$ GeV			
$\alpha_{\rm em} = 1/134.05$		$\hat{\alpha}_4^c = -0.104 - 0.015i$	

Table 6.2: Numerical values for the evaluation of QED effects. To obtain the Gegenbauer moments at 1 GeV, we consider downward scale evolution for the lattice results from [159] in the QCD LL approximation. We consider the Wilson coefficients in QCD-only at NNLL.

from the form factor and LCDAs. We neglect the spectator part since it is of order $\mathcal{O}(\alpha_{\rm em}\alpha_s)$. Moreover, we do not consider QED corrections to the form factor in this work. When M_2 is charged, we replace $\mathcal{F}_-^{BM_1}$ with the semi-leptonic factor (4.63). In this case, the Wilson coefficient $C_{\rm sl}$ will enter our analysis via $\delta\alpha^{\rm WC}$. Note that the point-like factor Z_ℓ is part of $\delta\alpha^{\rm F,V}$.

We consider the QED corrections to the light-meson LCDA and soft functions entering the factorization formula (4.70) separately. Both function types obey a first-order integro-differential equation that determines their scale evolution. On top of the evaluation of the analytical results in Chapter 5, we solve these equations numerically by discretizing the corresponding function domain. We discuss this procedure in more detail in Sec. 6.2.6 and Sec. 6.2.7.

6.2.1 Electroweak corrections

In the downward scale evolution of the QED-generalized Wilson coefficients from the electroweak scale, we sum the QCD but not the QED logarithms according to [160]. The results can be expressed in terms of two expansion parameters α_s and $\kappa \equiv \alpha_{\rm em}/\alpha_s$.[4]

[4]We expect the resummation of QED effects between m_B and the electroweak scale to be even less important than the resummation for the hard-scattering kernels, which we assumed to be negligible. Since we resum the large QCD logarithms $c_s = \alpha_s L$, the QED logarithms $\alpha_{\rm em} L = \kappa c_s$ will be pro-

We restrict ourselves to $\mathcal{O}(\kappa, \kappa\alpha_s)$ and to NLL accuracy. This implies the inclusion of QED corrections in $C_i(\mu_0)$ at the electroweak scale as well as $\mathcal{O}(\kappa, \kappa\alpha_s)$ terms in the anomalous dimension, see also [161] for comparison. We consider three-loop running for α_s and $\alpha_{\rm em}$ and include four-loop contributions from QCD as in Sec. 3.3 of [160]. We obtain the solution to the RGE for the Wilson coefficients from [160] with

$$\lambda \equiv \frac{\beta_0^{\rm QED}\alpha_{\rm em}(\mu_0)}{\beta_0^{\rm QCD}\alpha_s(\mu_0)}\,, \qquad \omega \equiv 2\beta_0^{\rm QCD}\,\frac{\alpha_s(\mu_0)}{4\pi}\,, \tag{6.19}$$

where $\beta_0^{\rm QCD} = 23/3$ and $\beta_0^{\rm QED} = 80/9$ for $n_f = 5$. Similar to (6.17), we split the QCD and QED contributions as

$$C_i(\nu) = C_i^{\rm QCD}(\nu) + \delta C_i(\nu)\ . \tag{6.20}$$

For the Wilson coefficients in QCD at NNLL as well as the value of the gauge couplings in the $\overline{\rm MS}$ scheme, we refer to Table 6.2. We choose the Z-boson mass m_Z as the initial scale for the downward scale evolution to $\nu = 4.8\,\text{GeV}$ with $n_f = 5$. For the QED corrections at the lower scale, we obtain

$$\delta C_1(\nu) = -1.66\frac{\alpha_{\rm em}(\nu)}{4\pi} = -1.00\cdot 10^{-3}\,, \tag{6.21}$$

$$\delta C_2(\nu) = 5.68\frac{\alpha_{\rm em}(\nu)}{4\pi} = 3.42\cdot 10^{-3}\ . \tag{6.22}$$

On the level of the tree amplitudes α_i, we find in consequence

$$\delta\alpha_1^{\rm WC}(M_1M_2) = \delta C_2 = 5.68\frac{\alpha_{\rm em}(\nu)}{4\pi} = 3.42\cdot 10^{-3}\ , \tag{6.23}$$

$$\delta\alpha_2^{\rm WC}(M_1M_2) = \frac{4}{9}\delta C_1 + \frac{1}{3}\delta C_2 = 1.16\frac{\alpha_{\rm em}(\nu)}{4\pi} = 0.695\cdot 10^{-3}\ . \tag{6.24}$$

For $Q_{M_2} = -1$, we need to include the semi-leptonic coefficient $C_{\rm sl}$ due to the normalization onto the semi-leptonic amplitude in the factorization formula. In this case, we use the fixed-order result at one-loop [131]

$$\delta C_{\rm sl}(\nu) = \frac{\alpha_{\rm em}(\nu)}{\pi}\ln\frac{m_Z}{\nu} = 11.78\frac{\alpha_{\rm em}(\nu)}{4\pi} = 7.09\cdot 10^{-3}\,. \tag{6.25}$$

In our specific analysis for $\bar{B}\to\pi K$, this modification only enters through the colour-allowed tree amplitude, for which we find

$$\delta\alpha_1^{\rm WC}(M_1M_2) = \delta C_2 - \delta C_{\rm sl}\,C_2^{\rm tree} = -3.88\cdot 10^{-3}\,. \tag{6.26}$$

Uniformly ignoring $\mathcal{O}(\alpha_s\alpha_{\rm em})$ contributions, we employ $C_2^{\rm tree}(\nu) = 1.03$. Compared to (6.23), we find that the QED contribution enters with an opposite sign but equivalent size after the $\text{SCET}_\text{I} \to \text{QCD}\times\text{QED}$ form factor replacement.

moted to $\kappa f(c_s)$, where $f(c_s)$ is the resummed QCD expression from the solution of the corresponding RGE in [160].

6.2.2 Hard-scattering kernels

In the second step, we consider the hard-scattering corrections to the amplitudes α_1 and α_2 which are given by

$$\delta\alpha_i^{\rm K}(M_1M_2) = \frac{\alpha_{\rm em}(\mu)}{4\pi}\sum_{j=1,2} C_j^{\rm QCD}(\nu)\left[\mathscr{V}_j^{(1)}(M_2) + H_{j,Q_2}^{\rm em}(M_1M_2)\right] . \tag{6.27}$$

The former contribution defines the convolution appearing in the form factor term

$$\mathscr{V}_i(M_2) = \int_0^1 du\, T_{i,Q_2}^{\rm I}(u)\,\phi_{M_2}(u)\,, \tag{6.28}$$

while the second involves the hard-collinear spectator scattering. In the present context, we use the naive lattice estimates from Table 6.2 for the Gegenbauer moments of ϕ_{M_2} in QCD and truncate the Gegenbauer expansion after the second moment. For $Q_{M_2} = 0$, this implies

$$\mathscr{V}_2^{(1)}(M_2^0) = -\frac{2}{27}\left[-6L_\nu - 18 - 3i\pi + \left(\frac{11}{2} - 3i\pi\right)a_1^{M_2} - \frac{21}{20}a_2^{M_2}\right] , \tag{6.29}$$

and $\mathscr{V}_1^{(1)}(M_2^0) = C_F\mathscr{V}_2^{(1)}(M_2^0)$. For $Q_{M_2} = 1$, we have

$$\begin{aligned}\mathscr{V}_2^{(1)}(M_2^-) = \Bigg[&-\frac{5}{3}L - \frac{2L_\nu}{3} - \frac{97}{18} - \frac{22i\pi}{9} - \frac{\pi^2}{9} \\ &- \left(\frac{1}{2}L + \frac{133}{72} + \frac{i\pi}{3}\right)a_1^{M_2} - \left(\frac{3}{5}L + \frac{184}{75} + \frac{2i\pi}{5}\right)a_2^{M_2}\Bigg] ,\end{aligned} \tag{6.30}$$

and $\mathscr{V}_1^{(1)}(M_2^-) = 0$. The normalization to the semi-leptonic amplitude removes some double logarithms of $H_{i,-}^{\rm I}(u)$ in (4.79), which shrinks the magnitude of the QED effect. The ν-dependent logarithms L_ν in the above results cancel against the corresponding electroweak coefficients, which corresponds to the cancellation of UV and IR divergences in the EFT picture. The μ dependence in L, on the other hand, matches the QED factorization scale in $f_{M_2}\Phi_{M_2}/Z_\ell$ which we treat separately such that $\mathscr{V}_2^{(1)}(M_2)$ stays μ-dependent. In the following, we choose $\mu = 1\,\text{GeV}$ for the collinear scale. We run the electromagnetic coupling at one-loop with flavour thresholds at $4.8\,\text{GeV}$ $(n_f = 4)$, $1.2\,\text{GeV}$ $(n_f = 3)$ for the b- and c-quark and at $\mu_\tau = 1.78\,\text{GeV}$ for the tau.

Finally, we note that the spectator-scattering term can be expressed as a sum of Gegenbauer moments

$$H_{2,-}^{\rm em}(M_1M_2) = \frac{4\pi^2 Q_{\rm sp}Q_u}{N_c}\frac{r_{\rm sp}(M_1)}{9}\int_0^1 du\,dv\,\frac{\phi_{M_2}(u)\phi_{M_1}(v)}{\bar{u}\bar{v}} , \tag{6.31}$$

$$= \frac{4\pi^2 Q_{sp}Q_u r_{\rm sp}(M_1)}{N_c}\sum_{i,j} a_i^{M_1}a_j^{M_2} , \tag{6.32}$$

multiplied with

$$r_{\rm sp}(M_1) \equiv \frac{9 f_B f_{M_1}}{m_B \lambda_B F_0^{BM_1}(0)} \ . \tag{6.33}$$

We use (4.94) applied to $H^{\rm em}_{2,-}(M_1M_2)$ in order to transition between different charge combinations. More precisely, we have

$$H^{\rm em}_{1,-}(M_1M_2) = 0\,, \quad H^{\rm em}_{1,0}(M_1M_2) = C_F H^{\rm em}_{2,0}(M_1M_2) = \frac{C_F}{N_c} H^{\rm em}_{2,-}(M_1M_2)\,. \tag{6.34}$$

6.2.3 Penguin-dominated $B \to \pi K$ decays

We parametrize the penguin-dominated $B \to \pi K$ decays by the four amplitudes [158]

$$\begin{aligned}
\mathcal{A}_{B^-\to\pi^-\bar K^0} &= A_{\pi K}\hat\alpha_4^p \ , \\
\sqrt{2}\mathcal{A}_{B^-\to\pi^0 K^-} &= A_{\pi K}\left[\delta_{pu}\alpha_1 + \hat\alpha_4^p\right] + A_{K\pi}\left[\delta_{pu}\alpha_2 + \delta_{pc}\frac{3}{2}\alpha^c_{3,\rm EW}\right] \ , \\
\mathcal{A}_{\bar B^0\to\pi^+ K^-} &= A_{\pi K}\left[\delta_{pu}\alpha_1 + \hat\alpha_4^p\right] \ , \\
\sqrt{2}\mathcal{A}_{\bar B^0\to\pi^0\bar K^0} &= A_{\pi K}\left[-\hat\alpha_4^p\right] + A_{K\pi}\left[\delta_{pu}\alpha_2 + \delta_{pc}\frac{3}{2}\alpha^c_{3,\rm EW}\right] \ .
\end{aligned} \tag{6.35}$$

The coefficients $\alpha_i(M_1M_2)$ denote the various topologies of the decay modes. In addition to the first two amplitudes we introduced earlier, $\hat\alpha_4$ and $\alpha^c_{3,\rm EW}$ refer to the QCD (electroweak) penguin amplitudes based on the notation in [158]. Every term in (6.35) further contains a multiplicative CKM factor $V_{pb}V_{ps}^*$ with a sum over $p = u, c$. The corrections from the hard-scattering kernels are

$$\delta\alpha_1^{\rm K}(\pi^+K^-) = \frac{\alpha_{\rm em}(\mu)}{4\pi} C_2^{\rm QCD}\left[\not{V}_2(K^-) + H^{\rm em}_{2,-}(\pi^+K^-)\right], \tag{6.36}$$

$$\delta\alpha_1^{\rm K}(\pi^0K^-) = \delta\alpha_1^{\rm K}(\pi^+K^-) + \frac{\alpha_{\rm em}(\mu)}{4\pi}\Delta_1^{\rm K}, \tag{6.37}$$

$$\delta\alpha_2^{\rm K}(\bar K^0\pi^0) = \frac{\alpha_{\rm em}(\mu)}{4\pi}(C_F C_1^{\rm QCD} + C_2^{\rm QCD})\left[\not{V}_2(\pi^0) + H^{\rm em}_{2,0}(\bar K^0\pi^0)\right], \tag{6.38}$$

$$\delta\alpha_2^{\rm K}(K^-\pi^0) = \delta\alpha_2^{\rm K}(\bar K^0\pi^0) + \frac{\alpha_{\rm em}(\mu)}{4\pi}\Delta_2^{\rm K} \ , \tag{6.39}$$

which can be read off from the right and wrong insertions of the operators $Q_{1,2}$. For two of these contributions, only the differences of the spectator scattering terms enter

$$\Delta_1^{\rm K} = C_2^{\rm QCD}(\nu)\left(H^{\rm em}_{2,-}(\pi^0K^-) - H^{\rm em}_{2,-}(\pi^+K^-)\right) = 8.03\,\frac{r_{\rm sp}(\pi)}{0.674} \ , \tag{6.40}$$

$$\Delta_2^{\rm K} = \left(C_F C_1^{\rm QCD}(\nu) + C_2^{\rm QCD}(\nu)\right)\left(H^{\rm em}_{2,0}(K^-\pi^0) - H^{\rm em}_{2,0}(\bar K^0\pi^0)\right) = 1.59\,\frac{r_{\rm sp}(K)}{0.610}\,, \tag{6.41}$$

which is related to the fact that the vertex terms $\mathscr{V}_i$ are independent of Q_{M_1}. The evaluation of these expressions yields

$$\begin{aligned}
\delta\alpha_1^{\mathrm{K}}(\pi^+K^-) &= \frac{\alpha_{\mathrm{em}}(\mu)}{4\pi}\left[-0.89 - 7.96i - 2.68\,\frac{r_{\mathrm{sp}}(\pi)}{0.674}\right] = (-2.12 - 4.73i)\cdot 10^{-3}\,,\\
\delta\alpha_1^{\mathrm{K}}(\pi^0K^-) &= \frac{\alpha_{\mathrm{em}}(\mu)}{4\pi}\left[-0.89 - 7.96i + 5.36\,\frac{r_{\mathrm{sp}}(\pi)}{0.674}\right] = (2.65 - 4.73i)\cdot 10^{-3}\,,\\
\delta\alpha_2^{\mathrm{K}}(\bar{K}^0\pi^0) &= \frac{\alpha_{\mathrm{em}}(\mu)}{4\pi}\left[0.83 + 0.46i - 0.53\,\frac{r_{\mathrm{sp}}(K)}{0.610}\right] = (0.18 + 0.27i)\cdot 10^{-3}\,,\\
\delta\alpha_2^{\mathrm{K}}(K^-\pi^0) &= \frac{\alpha_{\mathrm{em}}(\mu)}{4\pi}\left[0.83 + 0.46i + 1.06\,\frac{r_{\mathrm{sp}}(K)}{0.610}\right] = (1.12 + 0.27i)\cdot 10^{-3}\,. \qquad (6.42)
\end{aligned}$$

We observe that all QED corrections at this level are per mille effects. The choice of the factorization scale merely affects the numerical results above. To give an example, the first term in the square brackets change by $\mathcal{O}(1)$ when choosing the collinear scale to be $\mu = 1.5\,\mathrm{GeV}$ rather than $1\,\mathrm{GeV}$. Note that the factorization scale dependence cancels explicitly in the branching fractions and direct CP asymmetries considered below.

6.2.4 Ultrasoft factors

We defined the resummed ultrasoft exponentiation factor $U(M_1M_2)$ in (5.134) that multiplies the non-radiative decay rate to render the entire process IR finite. This requires a choice for ΔE, which refers in our case to the signal region of the πK invariant mass around m_B. The factorization approach relies on the hierarchy $\Delta E \ll \Lambda_{\mathrm{QCD}}$, so that we choose $\Delta E = 60\,\mathrm{MeV}$ in analogy to the treatment of $B_q \to \mu^+\mu^-$ in [60].[5] Compared to the previously investigated QED effects, the ultrasoft contributions turn out to be quite sizeable

$$\begin{aligned}
U(\pi^+K^-) &= 0.914\,,\\
U(\pi^0K^-) &= U(K^-\pi^0) = 0.976\,,\\
U(\pi^-\bar{K}^0) &= 0.954\,,\\
U(\bar{K}^0\pi^0) &= 1\,. \qquad (6.43)
\end{aligned}$$

For $Q_{M_2} = -1$, the form factor replacement including the normalization to the semi-leptonic amplitude modifies the branching ratio to

$$\mathrm{Br}(\pi^+K^-) \propto \left|\,\mathcal{A}^{\mathrm{sl,M_1}}_{\mathrm{non-rad}}\,\alpha_1(\pi^+K^-)\right|^2 U(\pi^+K^-)\,, \qquad (6.44)$$

[5] On the experimental side, the invariant mass spectrum including soft photon emission is currently generated by the PHOTOS algorithm which only uses an upper cutoff at $5\,\mathrm{GeV}$, see [162, 163]. Based on our framework, we suggest to focus on the signal window around m_B without additional extrapolations.

equivalently for $\mathrm{Br}(\pi^0 K^-)$, where we receive the non-radiative part from

$$\mathrm{Br}(M_1\ell^-) = U(M_1\ell^-)\,|\mathcal{A}^{\mathrm{sl},\mathrm{M}_1}_{\mathrm{non-rad}}|^2 \,. \tag{6.45}$$

The factor $U(M_1\ell^-)$ can be obtained from $U(M_1K^-)$ in (5.134) by replacing the mass dependence $m_K \to m_\ell$. We multiply the ultrasoft function in (6.45) to the semi-leptonic decay rate such that our determination of $\mathcal{A}^{\mathrm{sl},\mathrm{M}_1}_{\mathrm{non-rad}}$ is indeed given by the non-radiative part of the non-leptonic amplitude.

6.2.5 Branching ratios, isospin sum rule and direct CP asymmetries

The individual QED corrections studied so far only yield small corrections to the QCD results. This might be different for certain branching fractions in which QED effects are relatively enhanced compared to QCD. To this end, we introduce the ratio

$$R_L = \frac{2\,\mathrm{Br}(\pi^0\bar{K}^0) + 2\,\mathrm{Br}(\pi^0 K^-)}{\mathrm{Br}(\pi^-\bar{K}^0) + \mathrm{Br}(\pi^+ K^-)} = R_L^{\mathrm{QCD}} + \delta R_L \,, \tag{6.46}$$

where the pure QCD term is

$$R_L^{\mathrm{QCD}} = 1 + |r_{\mathrm{EW}}|^2 - \cos\gamma\ \mathrm{Re}\,(r_{\mathrm{T}} r_{\mathrm{EW}}^*) + \ldots \tag{6.47}$$

The factors r_{EW} and r_{T} denote the ratios of electroweak penguin $\alpha_{3,\mathrm{EW}}$ and tree coefficients α_1 divided by the QCD penguin $\hat{\alpha}_4^c$. These ratios are $\mathcal{O}(0.1)$, so that (6.46) may be understood as an expansion in terms of r_{EW} and r_{T}. While QCD corrections to unity enter quadratically in (6.47), we find that the QED effects provide linear terms

$$\delta R_L = \cos\gamma\ \mathrm{Re}\,(\delta_E) + \delta_{\mathrm{U}} \,, \tag{6.48}$$

where δ_E arises from the Wilson coefficients and hard-scattering kernels and δ_{U} from the ultrasoft function. In (6.48), only the differences of the spectator-scattering corrections Δ_i^{K} defined in (6.40) and (6.41) enter the coefficient δ_E at LO due to the dependence on the charge Q_{M_1}. As a consequence, the ratio R_L does not depend on the factorization scale μ in contrast to the individual corrections $\delta\alpha_i^{\mathrm{K}}$. Since the electroweak Wilson coefficients are also independent of Q_{M_1}, they do not appear in the coefficient δ_E. Numerically, we obtain

$$\begin{aligned}\delta_E &= \frac{\alpha_{\mathrm{em}}(\mu)}{4\pi}\left|\frac{\lambda_u}{\lambda_c}\right|\frac{\Delta_1^{\mathrm{K}} + \Delta_2^{\mathrm{K}} R_{\pi K}}{\hat{\alpha}_4^c(\pi K)} \\ &= (-1.89 + 0.27i)\,\frac{\alpha_{\mathrm{em}}(\mu)}{4\pi} = (-1.12 + 0.16i)\cdot 10^{-3} \,,\end{aligned} \tag{6.49}$$

using the CKM coefficient λ_u/λ_c, the QCD penguin amplitude $\hat{\alpha}_4^c$ and the form-factor ratio $R_{\pi K}$ in Table 6.3. Hence, QED again reduces to a per mille effect that is further suppressed by the CKM angle $\cos\gamma$. The ultrasoft coefficient is

$$\delta_U \equiv \frac{1 + U(\pi^0 K^-)}{U(\pi^-\bar{K}^0) + U(\pi^+ K^-)} - 1 = 5.8\% \,. \tag{6.50}$$

We recall that this number is obtained for $\Delta E = 60\,\text{MeV}$ and thus implicitly depends on the experimental analysis. Adding both results, we find with $\gamma = 70°$

$$\delta R_L = 5.7\% \,, \tag{6.51}$$

where the ultrasoft QED corrections make up almost the entire value. In this case, QED exceeds the corresponding QCD contribution $R_L^{\text{QCD}} - 1 = 0.01 \pm 0.02$ [158].

In addition to these kinds of ratios, direct CP asymmetries are frequently considered observables where QED might become relevant. Based on isospin relations, we find a sum rule

$$\begin{aligned}\Delta(\pi K) \equiv\, & A_{\text{CP}}(\pi^+K^-) + \frac{\Gamma(\pi^-\bar{K}^0)}{\Gamma(\pi^+K^-)} A_{\text{CP}}(\pi^-\bar{K}^0) - \frac{2\Gamma(\pi^0K^-)}{\Gamma(\pi^+K^-)} A_{\text{CP}}(\pi^0K^-) \\ & - \frac{2\Gamma(\pi^0\bar{K}^0)}{\Gamma(\pi^+K^-)} A_{\text{CP}}(\pi^0\bar{K}^0) \equiv \Delta(\pi K)^{\text{QCD}} + \delta\Delta(\pi K) \,,\end{aligned} \tag{6.52}$$

involving different asymmetries in $\bar{B} \to \pi K$ that sum up to zero apart from small corrections [164, 165]. In the expansion of small amplitude ratios, we find for QCD-only

$$\Delta(\pi K)^{\text{QCD}} = 2\sin\gamma \, [\text{Im}\,(r_T r_{\text{EW}}^*) + 2\,\text{Im}\,(r_C r_{\text{EW}}^*)] + \dots \,, \tag{6.53}$$

where r_C is the ratio of the colour-suppressed amplitude. Due to $\alpha_{3,\text{EW}}^c \sim \alpha_1$, we neglect the first term in (6.53) and thus the interference between r_C and r_{EW} determines the QCD part $\Delta(\pi K)^{\text{QCD}} = (0.5 \pm 1.1)\%$ [55]. The QED effects are given by

$$\delta\Delta(\pi K) = -2\sin\gamma\,\text{Im}\,(\delta_E) + \delta\Delta_U \,, \tag{6.54}$$

with the imaginary part of δ_E in (6.49) and a corresponding ultrasoft correction $\delta\Delta_U$. The former term is $\mathcal{O}(r^0)$ but dominated by the imaginary part of $\hat{\alpha}_4^c$ since the spectator-scattering terms Δ_i^{K} are real at $\mathcal{O}(\alpha_{\text{em}})$. Hence, this contribution is much smaller compared to the ultrasoft part

$$\begin{aligned}\delta\Delta_U =\, & 2\sin\gamma \Big[\text{Im}\,(r_P - r_T) + \text{Im}\,(r_P) \frac{U(\pi^-\bar{K}^0)}{U(\pi^+K^-)} \\ & + \text{Im}\,(r_T + r_C - r_P) \frac{U(\pi^0K^-)}{U(\pi^+K^-)} - \frac{\text{Im}\,(r_P + r_C)}{U(\pi^+K^-)} \Big] = -0.39\% \,,\end{aligned} \tag{6.55}$$

which first appears at $\mathcal{O}(r)$. The amplitude ratios given in [158] are $r_C = 0.06 - 0.016i$, $r_P = 0.018 + 0.0038i$ and $r_T = 0.18 - 0.030i$. The ultrasoft contribution (6.55) depends in particular on imaginary parts of the r-ratios in QCD and inherits large uncertainties as the determination of imaginary phases from experimental data turns out to be challenging. In total, we find

$$\delta\Delta(\pi K) = -0.42\% \,. \tag{6.56}$$

This result shows that QED only provides a small correction to the isospin sum rule in (6.52). According to [164], the same statement is true for QCD, such that larger deviations can not be explained in QCD×QED and may ultimately hint towards NP. To complete our analysis, we list each direct CP asymmetry for the amplitudes in (6.35). QED again enters linearly through a term $\delta A_{\rm CP}$, but the ultrasoft factors cancel in the ratio of CP-conjugated expressions. We obtain

$$\delta A_{\rm CP}(\pi^+K^-) = 2\sin\gamma \left|\frac{\lambda_u}{\lambda_c}\right| \operatorname{Im}\frac{\delta\alpha_1(\pi^+K^-)}{\hat\alpha_4^c(\pi K)} = 0.14\%\,, \tag{6.57}$$

$$\delta A_{\rm CP}(\pi^-\bar K^0) = 0\,,$$

$$\delta A_{\rm CP}(\pi^0\bar K^0) = -2\sin\gamma \left|\frac{\lambda_u}{\lambda_c}\right| R_{\pi K} \operatorname{Im}\frac{\delta\alpha_2(\bar K^0\pi^0)}{\hat\alpha_4^c(\pi K)} = 0.01\%\,,$$

$$\delta A_{\rm CP}(\pi^0K^-) = 2\sin\gamma \left(\left|\frac{\lambda_u}{\lambda_c}\right| \operatorname{Im}\left[\frac{\delta\alpha_1(\pi^+K^-) + R_{\pi K}\delta\alpha_2(\bar K^0\pi^0)}{\hat\alpha_4^c(\pi K)}\right] + \operatorname{Im}\delta_E \right) = 0.16\%\,.$$

Here, the corrections $\delta\alpha_{1,2}$ include both $\delta\alpha^{\rm K}$ and $\delta\alpha^{\rm WC}$. For $M_2 = K^-$, we consider the difference

$$\delta(\pi K) \equiv A_{\rm CP}(\pi^0K^-) - A_{\rm CP}(\pi^+K^-)\,, \tag{6.58}$$

for which we only find a tiny QED correction

$$2\sin\gamma \left(\left|\frac{\lambda_u}{\lambda_c}\right| R_{\pi K} \operatorname{Im}\frac{\delta\alpha_2(\bar K^0\pi^0)}{\hat\alpha_4^c(\pi K)} + \operatorname{Im}\delta_E \right) = 0.02\%\,. \tag{6.59}$$

All in all, the CP asymmetries do not contain sizeable QED corrections, in contrast to the ratio R_L. In fact, each term is strictly smaller than the QCD uncertainty from the experimental input.

6.2.6 Light-meson LCDA

For the light-meson LCDA, we discussed the phenomenological modifications of QED in Sec. 5.1 by solving the RGE in (5.4) to first order in $\alpha_{\rm em}$ (to all orders in the soft approximation near $u, \bar u \to 0$). Since we do not obtain analytical all-order results on the entire domain of the QED-generalized LCDAs, we focus on the first-order results of the Gegenbauer moments. In addition, we present the numerical solution of the RGE from which we calculated the graphs in Fig. 5.2. We remark that the results refer to the properly IR-subtracted matrix elements.

For the discretization of the RGE (5.4), we choose N points u_i that split the $u \in [0,1]$ interval into $N-1$ sub-intervals, where $i = 1, \ldots, N$. Taking N large, we replace the v-integral in the differential equation by a finite (Riemann) sum. In this way, we obtain N coupled differential equations that can be solved numerically. Regarding the precise summation, we implement the trapezoidal rule to decrease the error of the numerical

method.[6] At given u_i, we approximate the first distribution of (4.53) according to

$$\begin{aligned}\frac{d\Phi_M(u_i;\mu)}{d\ln\mu} &\propto \int_0^1 dv\ \theta(v-u_i)\left(1+\frac{1}{v-u_i}\right)\frac{u_i}{v}\Phi_M(u_i;\mu)\\ &\approx \frac{1}{2}\left(-\frac{1}{u_i}\Phi_M(u_i;\mu)+\Phi_M(u_{i+1};\mu)-\Phi_M(u_i;\mu)\right)\\ &\quad+\sum_{j=i+1}^{N-1}\frac{(u_{j+1}-u_j)}{2}\left(1+\frac{1}{u_j-u_i}\right)\left[\frac{u_i}{u_j}\Phi_M(u_j;\mu)-\Phi_M(u_i;\mu)\right]\ , \end{aligned} \tag{6.60}$$

where in the second line, for the limit $u_j \to u_i$, we replaced the function with its discretized derivative. The same treatment applies to the second distribution and the local terms. In our calculation, we formally exclude the endpoint $u = 0$ and $u = 1$ by reducing the entire interval $u \in [\epsilon, 1-\epsilon]$ for small $\epsilon \ll 1$ since the evolution kernel becomes divergent at these points. In practice, we choose $\epsilon = 10^{-10}$ and distribute the number of points u_i of the interval logarithmically increased towards both endpoints. For $N = 1001$ points, the numerical evaluation agrees with the LL result in QCD up to an error of less than 0.04%.[7] We calibrate this error in QCD-only, for which we know the analytical solution. Hence, it merely provides an estimate for the QED case, which is dominated by the endpoint contributions from the local terms at unrealistic high scales.

To parametrize the QED corrections for the light LCDA, we recall the decomposition in terms of Gegenbauer polynomials

$$\Phi_M(u;\mu) = Z_\ell(\mu)\, 6u\bar{u}\sum_{n=0}^{\infty} a_n^M(\mu) C_n^{(3/2)}(2u-1)\ , \tag{6.61}$$

where Z_ℓ is the point-like evolution factor defined in (5.6). In the following, we present the results for the evolved Gegenbauer moments based on the discussion in Sec. 5.1.2. At the initial scale μ_0, we use results obtained from lattice QCD $\mu_{\rm lat} = 2\,\text{GeV}$ evolved downwards in QCD-only at LL accuracy, given in Table 6.3. We emphasize that the initial function should be viewed as an IR-subtracted (scheme-dependent) model for the LCDA, for which we calculate the UV evolution numerically. In QCD×QED, we evolve the function to higher scales μ alongside with the gauge couplings, including the decoupling of the bottom and charm quark as well as the tau lepton at the flavour thresholds $\mu = m_{b,c,\tau}$.[8] In our analysis, we consider the scale evolution separately at LL, NLL and NNLL accuracy in QCD while keeping the LL evolution for QED by using the first-order results in (5.38).[9] To be consistent, we implement the NLO (NNLO) anomalous dimension and two-loop (three-loop) running for α_s at NLL (NNLL). We choose to

[6] The estimated error is proportional to $(\Delta u)^3$, where Δu refers to the difference of two neighboring points.

[7] The error refers to the initial function and scales chosen in Fig. 5.2.

[8] The decoupling of the tau is only required for the electromagnetic coupling $\alpha_{\rm em}(\mu)$.

[9] We neglect corrections at the threshold m_b induced by matching relations for the Gegenbauer moments at NNLL in QCD since they are expected to be small.

Quark and lepton masses		
$m_b = 4.78$ GeV	$m_c = 1.67$ GeV	$m_\tau = 1.78$ GeV
Gegenbauer moments at $\mu_{\text{lat}} = 2$ GeV		
$a_0^\pi = 1$	$a_1^\pi = 0$	$a_2^\pi = 0.116^{+19}_{-20}$
$a_0^K = 1$	$a_1^K = 0.0525^{+31}_{-33}$	$a_2^K = 0.106^{+15}_{-16}$
Gegenbauer moments at $\mu_0 = 1$ GeV		
$a_0^\pi = 1$	$a_1^\pi = 0$	$a_2^\pi = 0.140^{+23}_{-24}$
$a_0^K = 1$	$a_1^K = 0.0593^{+35}_{-37}$	$a_2^K = 0.128^{+18}_{-19}$

Table 6.3: Numerical values of the (two-loop pole) quark masses in the running of α_{em} and Gegenbauer coefficients at the initial scale $\mu_0 = 1\,\text{GeV}$ obtained from lattice QCD results at $\mu_{\text{lat}} = 2\,\text{GeV}$ in [159]. We neglect the four-loop QCD contribution in the strong coupling and increase one digit of precision, so that some values differ from Table 6.2. The value of m_c refers to the charm-quark pole mass.

evolve our results to $\mu = 5.3\,\text{GeV} \approx m_B$ and $\mu = 80.4\,\text{GeV} \approx M_W$ respectively. While the first value is chosen to obtain estimates in the environment of exclusive B decays, the evolution to the electroweak scale eventually becomes important in rare decays like $W^- \to \pi^-\gamma$ [166].

The lattice QCD calculations provide results for the first three Gegenbauer moments $a_{0,1,2}(\mu)$. Generally, the moments $a_n(\mu_0)$ with $n > 2$ mix into these first moments under QED evolution. In the initial model, we choose $a_n(\mu_0) = 0$ for $n > 0$, since we expect those contributions to be small. The QED evolution then again produces these higher coefficients in the upward scale evolution, which is also the case for pure QCD beyond LL. As we discussed earlier, we further neglect QED corrections at the initial scale which are currently not accessible.

At the scale $\mu = 5.3$ GeV, we find the moments of a negatively charged pion $\pi^-(d\bar{u})$ to be

$$\begin{aligned} a_0^{\pi^-} &= 1\big|_{\text{QCD}} + 0.0035\big|_{\text{QED}}\,, \\ a_1^{\pi^-} &= 0\big|_{\text{QCD}} + 0.0006\big|_{\text{QED}}\,, \\ a_2^{\pi^-} &= 0.0951\big|_{\text{LL}} - 0.0084\big|_{\text{NLL}} + 0.0001\big|_{\text{NNLL}} + 0.0010\big|_{\text{QED}}\,, \end{aligned} \tag{6.62}$$

For the kaon $K^-(s\bar{u})$, we have

$$\begin{aligned} a_0^{K^-} &= 1\big|_{\text{QCD}} + 0.0035\big|_{\text{QED}}\,, \\ a_1^{K^-} &= 0.0462\big|_{\text{LL}} - 0.0023\big|_{\text{NLL}} + 0.0001\big|_{\text{NNLL}} + 0.0009\big|_{\text{QED}}\,, \end{aligned}$$

$$a_2^{K^-} = 0.0869\big|_{\rm LL} - 0.0078\big|_{\rm NLL} - 0.0000\big|_{\rm NNLL} + 0.0010\big|_{\rm QED}\,. \tag{6.63}$$

At the scale $\mu = 80.4$ GeV, we find for the pion

$$\begin{aligned} a_0^{\pi^-} &= 1\big|_{\rm QCD} + 0.0094\big|_{\rm QED}\,, \\ a_1^{\pi^-} &= 0\big|_{\rm QCD} + 0.0015\big|_{\rm QED}\,, \\ a_2^{\pi^-} &= 0.0657\big|_{\rm LL} - 0.0098\big|_{\rm NLL} + 0.0002\big|_{\rm NNLL} + 0.0021\big|_{\rm QED}\,, \end{aligned} \tag{6.64}$$

and for the kaon

$$\begin{aligned} a_0^{K^-} &= 1\big|_{\rm QCD} + 0.0095\big|_{\rm QED}\,, \\ a_1^{K^-} &= 0.0365\big|_{\rm LL} - 0.0030\big|_{\rm NLL} + 0.0002\big|_{\rm NNLL} + 0.0020\big|_{\rm QED}\,, \\ a_2^{K^-} &= 0.0601\big|_{\rm LL} - 0.0091\big|_{\rm NLL} + 0.0002\big|_{\rm NNLL} + 0.0021\big|_{\rm QED}\,. \end{aligned} \tag{6.65}$$

In the above results, we do not provide uncertainties for our results since the QCD NLL contributions are typically larger than $\mathcal{O}(15\%)$, which is the order of the lattice error at the input scale $\mu_{\rm lat} = 2\,\text{GeV}$. Generally, we observe that the QED corrections are strictly below the NLL QCD evolution but one order of magnitude above the NNLL corrections. Depending on the high scale, the size of the relative QED correction in $a_2^{\pi^-}$ ranges between 1% and 4% compared to the LL and between 12% to 21% with respect to the NLL contributions. In the upward scale evolution, the QCD coupling decreases while the QED coupling increases so that naturally QED effects get more relevant. In contrast to QCD-only, the Gegenbauer moments do however not necessarily tend to zero which would asymptotically lead to $\phi_M(u;\mu\to\infty) = 6u\bar{u}$. Nevertheless, we expect the higher moments to be small at realistic scales where QCD still dominates. Since QED breaks the normalization condition and the isospin symmetry, the scale evolution changes QCD-fixed Gegenbauer moments such as $a_0^M|_{\rm QCD} = 0$ and $a_1^{\pi^-}|_{\rm QCD} = 0$.

The light-meson LCDA appears in the factorization theorem (4.1) through convolutions with a hard-collinear function. In earlier chapters of this thesis, we already stressed the importance of inverse moments for the soft function, appearing in these kinds of factorization theorems. The same discussion applies to the case of light mesons, for which the hard-collinear function typically behaves like u^{-1} or $\bar{u}^{-1}$. Hence, we define the inverse moments as

$$\left\langle \bar{u}^{-1} \right\rangle_{M^-}(\mu) = \int_0^1 \frac{du}{1-u} \Phi_{M^-}(u;\mu) = Z_\ell(\mu) \times 3 \sum_{n=0}^{\infty} a_n^{M^-}(\mu)\,, \tag{6.66}$$

$$\left\langle u^{-1} \right\rangle_{M^-}(\mu) = \int_0^1 \frac{du}{u} \Phi_{M^-}(u;\mu) = Z_\ell(\mu) \times 3 \sum_{n=0}^{\infty} (-1)^n a_n^{M^-}(\mu)\,, \tag{6.67}$$

which are given in terms of infinite sums over Gegenbauer moments. For the numerical values based on the previous analysis for the moments, we obtain for the π^- at the

scale $\mu = 5.3$ GeV

$$\begin{aligned}\left\langle \bar{u}^{-1}\right\rangle_{\pi^-} &= 0.9997\big|^{\text{QED}}_{\text{point charge}}(3.285^{+0.05}_{-0.05}\big|_{\text{LL}} - 0.020\big|_{\text{NLL}} + 0.017\big|^{\text{QED}}_{\text{partonic}}) \,, \\ \left\langle u^{-1}\right\rangle_{\pi^-} &= 0.9997\big|^{\text{QED}}_{\text{point charge}}(3.285^{+0.05}_{-0.05}\big|_{\text{LL}} - 0.020\big|_{\text{NLL}} + 0.012\big|^{\text{QED}}_{\text{partonic}}) \,, \end{aligned} \tag{6.68}$$

and at 80.4 GeV

$$\begin{aligned}\left\langle \bar{u}^{-1}\right\rangle_{\pi^-} &= 0.985\big|^{\text{QED}}_{\text{point charge}}(3.197^{+0.03}_{-0.03}\big|_{\text{LL}} - 0.022\big|_{\text{NLL}} + 0.042\big|^{\text{QED}}_{\text{partonic}}) \,, \\ \left\langle u^{-1}\right\rangle_{\pi^-} &= 0.985\big|^{\text{QED}}_{\text{point charge}}(3.197^{+0.03}_{-0.03}\big|_{\text{LL}} - 0.022\big|_{\text{NLL}} + 0.031\big|^{\text{QED}}_{\text{partonic}}) \,. \end{aligned} \tag{6.69}$$

For the kaon K^-, we obtain at $\mu = 5.3$ GeV

$$\begin{aligned}\left\langle \bar{u}^{-1}\right\rangle_{K^-} &= 0.9997\big|^{\text{QED}}_{\text{point charge}}(3.399^{+0.05}_{-0.05}\big|_{\text{LL}} - 0.026\big|_{\text{NLL}} + 0.018\big|^{\text{QED}}_{\text{partonic}}) \,, \\ \left\langle u^{-1}\right\rangle_{K^-} &= 0.9997\big|^{\text{QED}}_{\text{point charge}}(3.122^{+0.03}_{-0.03}\big|_{\text{LL}} - 0.011\big|_{\text{NLL}} + 0.011\big|^{\text{QED}}_{\text{partonic}}) \,, \end{aligned} \tag{6.70}$$

and at 80.4 GeV

$$\begin{aligned}\left\langle \bar{u}^{-1}\right\rangle_{K^-} &= 0.985\big|^{\text{QED}}_{\text{point charge}}(3.290^{+0.03}_{-0.03}\big|_{\text{LL}} - 0.029\big|_{\text{NLL}} + 0.044\big|^{\text{QED}}_{\text{partonic}}) \,, \\ \left\langle u^{-1}\right\rangle_{K^-} &= 0.985\big|^{\text{QED}}_{\text{point charge}}(3.071^{+0.02}_{-0.02}\big|_{\text{LL}} - 0.010\big|_{\text{NLL}} + 0.029\big|^{\text{QED}}_{\text{partonic}}) \,. \end{aligned} \tag{6.71}$$

In the above expressions, we explicitly factored out the point-like limit $Z_\ell(\mu)$, to which we refer as "point charge". The label "partonic" refers to the structure-dependent corrections, purely contained in the evolution of the Gegenbauer moments. In terms of precision, we use the evolution factor (5.7) for $Z_\ell(\mu)$ that resums the point-like logarithmic corrections to all orders while treating the Gegenbauer moments (5.38) to first order in α_{em}. At the initial scale, we impose $Z_\ell(\mu_0) = 1$. Moreover, we choose the hard scale $E = \mu/2$ of two-body decays for the energy dependence entering $Z_\ell(\mu)$. The results in (6.68)– (6.71) are obtained from the first $n_{\text{max}} = 100$ Gegenbauer moments, which are produced by QED as well as QCD NLL corrections. The convergence of the infinite sum in (6.66) and (6.67) differs for these two effects. For QCD NLL, we require a rather high truncation of the series to obtain reliable results while QED effects converge relatively fast so that we typically generate the given values already at $n_{\text{max}} = 10$. We do not consider the uncertainties from the lattice QCD input regarding the unknown coefficients $a_n(\mu_{\text{lat}})$ for $n > 2$. The results solely correspond to a comparison between different QCD and QED contributions for a particular model evolved to higher scales.

Compared to the analysis of the Gegenbauer moments in (6.62)–(6.65), the relative size of QCD and QED effects differs in the prediction for the inverse moments. Both QCD NLL and QED corrections are $\mathcal{O}(1\%)$, which is the same order of the lattice uncertainty of the input in Table 6.3. The uncertainties in (6.68)–(6.71) refer only to the QCD LL effects based on these input values. Beyond $\mathcal{O}(10$ GeV), the QED contributions exceed the QCD NLL results whereas at 80.4 GeV they also become

larger than the lattice uncertainty of the LL contribution. In contrast to QCD, QED in particular evolves the zeroth Gegenbauer moment a_0^M, which corresponds to the normalization in QCD of $\mathcal{O}(1)$ and explains the magnitude of this effect.[10] The isospin breaking effects caused by QED in $\langle \bar{u}^{-1} - u^{-1} \rangle_{\pi^-}$ turn out to be a few permille to 1% level.

Finally, we remark that the point-like and structure-dependent QED contributions have opposite effects on the Gegenbauer moments. The first one diminishes and the second one enhances the value of these objects. We still separate both effects since we shifted the point-like limit to the ultrasoft function in Sec. 5.3, which is by definition not contained in the non-radiative amplitude.

6.2.7 Soft functions

For the soft functions, we analyze the effects of the one-loop evolution in (5.66). The phenomenological modifications are generally more complicated compared to the light meson case. Nevertheless, some arguments of the discussion remain similar. At the low scale $\mu = \mu_0$, we separate the QED effects from the QCD initial condition in the spirit of (5.116)

$$\Phi_{B,\otimes}(\omega;\mu_0) = \phi_+(\omega;\mu_0) + \frac{\alpha_{\rm em}}{\pi}\Phi^{(1)}_{B,\otimes}(\omega;\mu_0) + \mathcal{O}(\alpha_{\rm em}^2) \,, \tag{6.72}$$

where we fix $\Phi^{(1)}(\omega;\mu_0) = 0$.[11] Here, we again choose the exponential model (6.1) with $\omega_0 = 0.3$ GeV for the initial function which carries an implicit $\theta(\omega)$ to indicate the domain. For the gauge couplings, we set $\alpha_{\rm em}(\mu) = 1/134$ and $\alpha_s(\mu_0) = 0.48$. In the present context, we evolve α_s at one-loop for $n_f = 4$ flavours and neglect threshold effects.

We solve the RGE (5.41) in a similar manner to the previous section by discretizing the domain and distributions according to (6.60). The main difference is that the soft function support extends to the entire real axis $\omega \in [-\infty, \infty]$. We introduce an upper and lower cutoff for ω and spare out a small window around the origin that regulates possible divergences from the distributions for $\omega \to 0$. The discretization procedure then applies to the two separate intervals $[-\epsilon, -\Omega]$ and $[\epsilon, \Omega]$ for which we choose $\epsilon = 10^{-7}$ and $\Omega = 10^4$ GeV. For each interval, we use $N+1$ points logarithmically concentrated towards the boundary at $|\omega_1| = \epsilon$. In total, we obtain $2(N+1)$ coupled first-order differential equations that we solve numerically. For the case of $Q_{M_2} = 0$, the support of the soft functions stays positive, so that we only encounter $N+1$ equations from the interval $[\epsilon, \Omega]$. As a benchmark, we recover the analytic QCD LL solution to a precision of 0.02% when evolving from $\mu_0 = 1$ GeV to $\mu = 2$ GeV. Since QED

[10] At $\mu = 80.4$ GeV, QED corrections change $a_0^{\pi^-} = 1$ by $\mathcal{O}(1\%)$. On the other hand, QCD NLL effects produce an $\mathcal{O}(15\%)$ variation on the LL result for $a_2^{\pi^-} = 0.0657$. Thus, the QED effects are relatively enhanced.

[11] We consider the QCD-only function for the initial condition since QED effects correspond to higher order corrections compared to our accuracy.

effects on this level are tiny, we choose the electromagnetic coupling fictitiously large to $\alpha_{\rm em} = 0.5$ and present the qualitative implications in Fig. 6.4 for both combinations $\otimes = (0,-)$ and $\otimes = (+,-)$. The red dots show the imaginary part produced in the latter scenario whereas the blue dots represent the real part in both cases. In addition, we depict the unevolved exponential model (grey) and the QCD LL result, given in (6.8).

In Sec. 5.2.7, we derived the analytic solution (5.128) and (5.129) to first order in the QED coupling. We compare this result to the numerical solution by inserting (6.1) together with $\Phi^{(1)}(\omega;\mu_0) = 0$ into these expressions. We then perform the corresponding ω'-integrals by applying the fundamental properties of Meijer-G functions, some of which are presented in Appendix F.[12] We find

$$\begin{aligned}
\Phi^{>(1)}_{B,\otimes}(\omega,\mu) = \frac{1}{\omega_0} e^{V+2\gamma_E a}\left(\frac{\mu_0}{\omega_0}\right)^a \Bigg[& - Q_{\rm sp}Q_{M_2}\int_{\mu_0}^{\mu}\frac{d\mu'}{\mu'}\frac{\alpha_s(\mu')C_F}{\pi} G^{33}_{34}\left(\frac{\omega}{\omega_0}\right)\ln\frac{\mu'}{\mu_0} \\
& + \int_0^1 dx \left[\frac{1}{1-x}\right]_+ \Bigg(- Q_{\rm sp}Q_{M_1}\left\{h(x)F_a\left(\frac{x\omega}{\omega_0}\right) + h(x^{-1})F_a\left(\frac{\omega}{x\omega_0}\right)\right\} \\
& + Q_{\rm sp}Q_{M_2}\left\{h(x)F_a\left(\frac{x\omega}{\omega_0}\right) - x^{-1}h(x^{-1})F_a\left(\frac{\omega}{x\omega_0}\right)\right\} \\
& + (Q^2_{\rm sp} + 2Q_{\rm sp}Q_{M_1})x^a F_a\left(\frac{x\omega}{\omega_0}\right)\ln\frac{\mu}{\mu_0}\Bigg) \\
& + \Bigg\{ - (Q^2_{\rm sp} + 2Q_{\rm sp}Q_{M_1})\left(\frac{1}{2}\ln^2\frac{\mu}{\mu_0} + \ln\frac{\mu_0 e^{\gamma_E}}{\omega_0}\ln\frac{\mu}{\mu_0}\right) \\
& + \left(\frac{3}{4}Q^2_{\rm sp} + \frac{1}{2}Q^2_d - i\pi Q_{M_1}Q_{M_2}\right)\ln\frac{\mu}{\mu_0}\Bigg\} F_a\left(\frac{\omega}{\omega_0}\right)\Bigg] ,
\end{aligned} \tag{6.73}$$

$$\Phi^{<(1)}_{B,\otimes}(\omega,\mu) = -\frac{Q_{\rm sp}Q_{M_2}}{\omega_0} e^{V+2\gamma_E a}\left(\frac{\mu_0}{\omega_0}\right)^a \Gamma(1+a)\Gamma(2+a)\, U\left(1+a,0,-\frac{\omega}{\omega_0}\right)\ln\frac{\mu}{\mu_0} . \tag{6.74}$$

We recall that V and a in the first-order solution are given by the QCD factors in (5.90). In the first line, we defined the short-hand notation

$$G^{33}_{34}(z) \equiv G^{33}_{34}\left(\begin{matrix} -a(\mu,\mu'),\ -a(\mu,\mu'),\ -a \\ -a(\mu,\mu'),\ -a(\mu,\mu'),\ 1,\ 0 \end{matrix}\middle| z\right) , \tag{6.75}$$

while in the last line we introduced the Tricomi confluent hypergeometric function

$$U(a,b,z) = \frac{\Gamma(b-1)}{\Gamma(a)} z^{1-b}\ {}_1F_1(a-b+1,2-b,z) + \frac{\Gamma(1-b)}{\Gamma(a-b+1)}\ {}_1F_1(a,b,z) . \tag{6.76}$$

[12] The result is most easily obtained by a calculation in Laplace space.

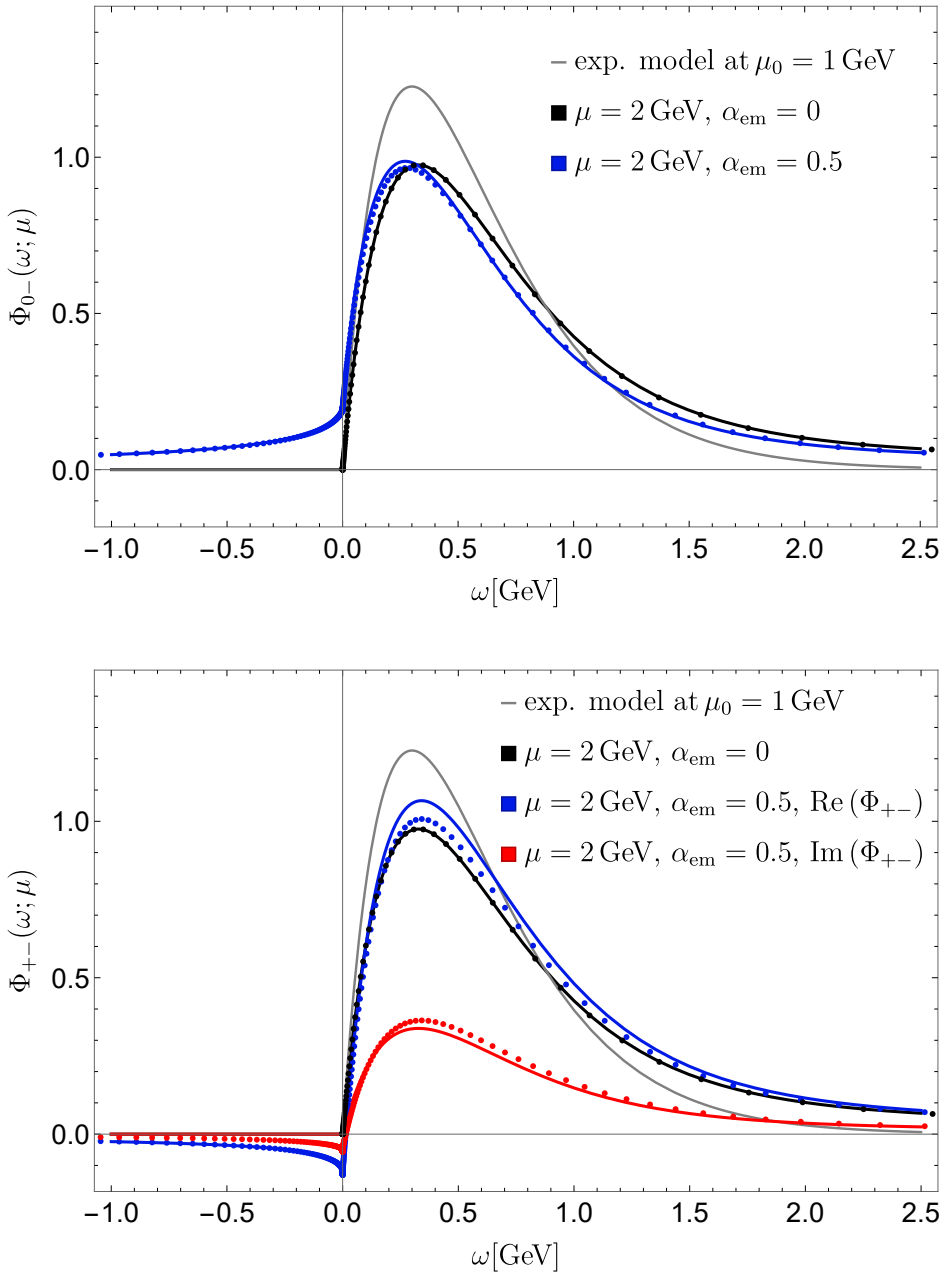

Figure 6.4: Upward scale evolution of the exponential model (6.1) (gray curve) for $\omega_0 = 0.3$ GeV from $\mu_0 = 1$ GeV to $\mu = 2$ GeV. The QCD-only LL solution (6.8) is represented by the black line. The upper and lower panel show the evolution of $\Phi_{0-}(\omega;\mu)$ and $\Phi_{+-}(\omega;\mu)$ respectively for $\alpha_{\text{em}} = 0.5$. In QCD×QED, the first-order $\mathcal{O}(\alpha_{\text{em}})$ corrections (6.73) and (6.74) generate real (blue curve) and imaginary (red curve) parts. The dotted curves are obtained from the discretization method applied to the full kernel (5.66). Note that $\Phi_{0-}(\omega;\mu)$ does not contain imaginary contributions due to the absence of soft rescattering.

	initial	QCD	$(0,0)$	$(-,0)$	$(0,-)$	$(+,-)$
λ_B^{-1}	3.3333	2.7922	2.7918	2.8018	$2.7900 + 0.0096i$	$2.7977 + 0.0096i$
σ_1	0	-0.2125	-0.2129	-0.2099	-0.2139	-0.2108

Table 6.4: Numerical results for λ_B^{-1} (in GeV^{-1}) and σ_1. We choose the reference scale to be $\tilde{\mu} = \omega_0 e^{-\gamma_E}$ and $\omega_0 = 0.3$ GeV for the exponential model. The initial value refers to the scale $\mu_0 = 1\,\text{GeV}$ while all other values represent the results at the high scale $\mu = 2\,\text{GeV}$.

In Fig. 6.4, the real and imaginary parts of the solution (6.73) and (6.74) correspond to the solid blue and red line respectively. We find excellent agreement to the numerical solution, even though we considered $\alpha_{\text{em}} = 0.5$ to be large. From our analysis about the asymptotic behaviour in (5.113), we recall that the soft function for $\otimes = (+,-)$ becomes log-divergent in the limit $\omega \to 0$. This divergence is absent in the first-order solution above since it enters at $\mathcal{O}(\alpha_{\text{em}}^2)$.

The realistic value of the electromagnetic coupling at $1 - 2$ GeV is $\alpha_{\text{em}} = 1/134$. In this case, we consider the evolution of the first inverse-logarithmic moments defined in (5.74). At $\mu_0 = 1$ GeV, the moments initially take the form

$$\lambda_B^{-1}(\mu_0) = \frac{1}{\omega_0}\,, \qquad \sigma_n(\mu_0) = \sum_{k=0}^{n} \binom{n}{k} (-1)^k\, \Gamma^{(k)}(1) \ln^{n-k} \frac{\tilde{\mu}}{\omega_0}\,, \tag{6.77}$$

with $\Gamma^{(k)}(1) = \partial_z^k \Gamma(z)\big|_{z=1}$. In what follows, we focus on the evolution of the first two moments λ_B and σ_1. To this end, we set $\tilde{\mu} = \omega_0 e^{-\gamma_E}$ according to [47] which implies $\sigma_1(\mu_0) = 0$. From the all-order solutions (5.100) and (5.101), we find for the exponential model

$$\lambda_B^{-1}(\mu) = e^{V+2\gamma_E a} \frac{\Gamma(1+a)}{\omega_0} \left(\frac{\mu_0}{\omega_0}\right)^a \mathcal{F}(0;\mu,\mu_0)\,, \tag{6.78}$$

$$\sigma_1(\mu) = H_a + \gamma_E + \ln\frac{\tilde{\mu}}{\omega_0} + \int_{\mu_0}^{\mu} \frac{d\mu'}{\mu'} \frac{\alpha_{\text{em}}(\mu') Q_{\text{sp}} Q_{M_1}}{\pi} \left\{ H'_{a(\mu,\mu')} - H'_{-a(\mu,\mu')} \right\}. \tag{6.79}$$

Here, a and V denote the QED-generalized variables in (5.96). The evolution function $\mathcal{F}$ is defined in (5.97). We list the numerical results for the scale evolution to $\mu = 2$ GeV in Table 6.4. Comparing these results to the discretization method, we achieve agreement at the permille level (equivalent to the numerical error). We find that the QED contributions maximally give rise to an 1.2% effect, which is less than the expected contribution from the two-loop QCD evolution [167].

Chapter 7

Conclusion

In this thesis, we investigated two different improvements to the QCD factorization framework in exclusive particle decays. Our main goal was to increase the accuracy of theoretical calculations in precision observables of charmless B decays. To this end, we considered generalized correlation functions related to the radiative $\bar{B} \to \gamma\ell\nu$ decay and derived a combined QCD×QED factorization approach for non-leptonic $\bar{B} \to M_1 M_2$ decays with light meson final states.

In the first part, we constructed the factorization theorem for a $\bar{B}$ to vacuum matrix element with space-like separated (pseudo-)scalar currents at LP in a $1/E_\gamma$- and $1/m_b$- expansion. We included NLP contributions by expanding the QCD fields in a soft background and derived sum rules to estimate the soft corrections. The results contain generalized inverse-logarithmic moments of the leading- and higher-twist B-meson LCDAs. We applied the same procedure to the transverse part of the $\bar{B} \to \gamma^*\ell\nu$ correlator with (axial-)vector currents. A first numerical analysis shows the qualitative dependence of the results on the off-shellness p^2 and the model parameter λ_B. In view of current perspectives for lattice QCD, we expect that these kinds of correlation functions can be calculated in the near future. From this, we can eventually extract more precise information about hadronic matrix elements of the B meson that enter various observables in exclusive decays.

The second and main part of this work focused on the development of a unified QCD×QED factorization framework in non-leptonic B decays. For the case of current-current operators Q_i in the weak effective Hamiltonian, we derived a consistent factorization theorem incorporating virtual QCD and QED corrections between scales of a few times Λ_{QCD} and m_B. Most notably, the formula retains the form of pure QCD regarding the appearance of form factors and hard(-collinear) matching coefficients convoluted with QED-generalized versions of the light and heavy meson LCDAs. To prove factorization, we calculated the hard-scattering kernels T_i at $\mathcal{O}(\alpha_s^0 \alpha_{\text{em}})$. The hadronic matrix elements entering the factorization formula generally become process-dependent as they retain information on the electric charge and direction of flight of the outgoing mesons through soft photon exchange. The light-meson LCDA, however,

remains universal in most of its aspects. Compared to pure QCD, we find that the normalization and the UV-fixed linear endpoint behaviour of the LCDA are modified by QED effects. Moreover, the definition of the LCDA is not boost-invariant and requires the choice of a soft reference frame. For charged π mesons in particular, QED generates an asymmetric distribution due to the breaking of isospin-symmetry. On the other hand, the heavy-meson LCDA involves soft rescattering physics and should rather be viewed as a soft function for a specific two-body back-to-back process with one of the four distinct charge combinations $\otimes = \{(0,0),(-,0),(0,-),(+,-)\}$. In the heavy-quark limit, soft photons coupling to M_2 can carry an infinite amount of energy away from the spectator quark. As a consequence, the soft function support in terms of the momentum variable ω extends over the entire real axis when M_2 is charged.

In presence of QED, the non-perturbative objects appearing in the factorization formula contain IR divergences. To construct IR-finite observables, we included ultrasoft photon emission with energy $\Delta E \ll \Lambda_{\rm QCD}$ and calculated the ultrasoft exponentiation factor that multiplies the non-radiative decay rate. In practice, we understand the IR divergences of the hadronic matrix elements in the factorization theorem as minimally IR-subtracted matching coefficients to an effective theory at scales below the validity of the factorization formula. Above the scale m_B, we employed QED effects from the electroweak scale within the Wilson coefficients of the weak effective theory. We solved the evolution equations of the Wilson coefficients, light-meson LCDA, the soft and ultrasoft function, which resums large logarithms of different scale ratios. The analytical results mostly refer to the resummation of QCD logarithms to all orders in the strong coupling, while QED effects are treated in a fixed-order expansion up to $\mathcal{O}(\alpha_{\rm em})$. An exception to this are the inverse-logarithmic moments of the soft functions, for which we obtain an all-order solution in both gauge couplings, as well as the ultrasoft function that is resummed to all orders in $\alpha_{\rm em}$.

In the numerical analysis, we considered QED corrections to branching fractions, CP asymmetries and hadronic functions appearing in $\bar{B} \to \pi K$ decays. We observe that the individual QED corrections in almost every case are smaller than the QCD uncertainties obtained from the experimental/lattice data. In two scenarios, we find sizable QED corrections: For the ratio R_L, the QED contributions sum up to an $\mathcal{O}(5\%)$ effect, which are dominated by ultrasoft effects. When evolving the light-meson LCDA to scales of order $\mathcal{O}(m_W)$, we also reach percent level corrections that may become relevant for electroweak precision observables.

The QCD×QED factorization approach has already been extended to the case of heavy-light final states in [67]. From a conceptional point of view, it might be interesting to include the remaining operators of the weak effective theory and the resummation of structure-dependent QED logarithms in future works. Finally, we note that our framework leaves a small window around $\Lambda_{\rm QCD}$, in which we are not able determine QED effects perturbatively. The corresponding matching corrections can potentially be determined from lattice calculations in the future.

Appendix A

Renormalization in HQET×SCET

In Sec. 2.4.2, we derived the one-loop expressions for the matching coefficients C_S and J_S in the factorization formula (2.78). Based on the structure of divergences in the one-loop results from Sec. 2.2, we argued that only the respectively renormalized hard and hard-collinear regions contribute to these coefficients. In the following, we prove this fact by calculating the hard-collinear and soft matrix elements on the HQET×SCET side. This finally shows how the hard-collinear and soft regions in the effective theory are reproduced and how they cancel on both sides of the matching equation.

A.1 Jet function in SCET

We defined the scalar jet function J_S by the two matrix elements (2.74) and (2.77). Now, we calculate the expressions J_1 and J_2 in SCET at one-loop using the Feynman rules in the effective theory, which can be derived from the leading power Lagrangian (2.43) and its subleading term (2.64). For an extensive review of SCET Feynman rules, we refer to Appendix A of [168]. Note that the collinear Wilson lines at any loop order can be replaced by inverse derivatives using

$$\int_{-\infty}^{0} ds n_+ G_{\mathrm{C}}(x + s n_+) = \frac{i}{i n_+ \partial + i0} n_+ G_{\mathrm{C}}(x) \,. \tag{A.1}$$

The computation of the function J_1 involves three diagrams, depicted in Fig. A.1a-c. We note that the two contributions from diagram (b) and (c) are identical. The one-loop results are

$$J_1^{(a)}(2E_\gamma\omega, p^2) = \frac{\alpha_s C_F}{4\pi}\left(-\frac{1}{\epsilon} - \ln\frac{\mu^2}{2E_\gamma\omega - p^2} - 1 \right) , \tag{A.2}$$

$$\begin{aligned} J_1^{(b)}(2E_\gamma\omega, p^2) = \frac{\alpha_s C_F}{4\pi}\Bigg(&\frac{2}{\epsilon^2} + \frac{2}{\epsilon} + \frac{2}{\epsilon}\ln\frac{\mu^2}{2E_\gamma\omega - p^2} - \frac{\pi^2}{6} + 4 \\ &+ 2\ln\frac{\mu^2}{2E_\gamma\omega - p^2} + \ln^2\frac{\mu^2}{2E_\gamma\omega - p^2} \Bigg) , \end{aligned} \tag{A.3}$$

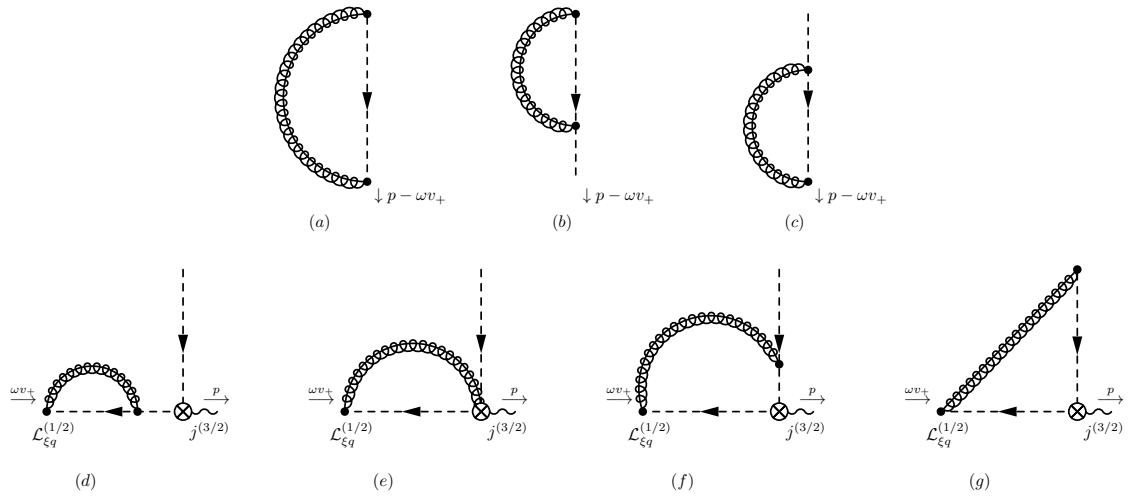

Figure A.1: One-loop contributions to the operators (2.74) and (2.77). (a)-(c) contribute to J_1 while (d)-(g) display corrections to J_2. Interactions at the edge of the fermion lines indicate the insertion of a hard-collinear Wilson line from the field $\chi_{\rm C}$ or the insertion of $\mathcal{L}_{\xi q}^{1/2}$. The electromagnetic current $j^{(3/2)}$ in SCET is defined in (2.60). Diagrams (d), (e) and (g) vanish in dimensional regularization.

$$J_1^{(c)}(2E_\gamma\omega,p^2)=J_1^{(b)}(2E_\gamma\omega,p^2)\;. \tag{A.4}$$

The $1/\epsilon$ divergences originate from both UV and IR and are renormalized in $\overline{\rm MS}$. In total, we obtain the renormalized function by the sum of (A.2)-(A.4)

$$J_1(2E_\gamma\omega,p^2;\mu)=1+\frac{\alpha_s C_F}{4\pi}\left(2\ln^2\frac{\mu^2}{2E_\gamma\omega-p^2}+3\ln\frac{\mu^2}{2E_\gamma\omega-p^2}-\frac{\pi^2}{3}+7\right). \tag{A.5}$$

The computation of the function J_2 is generically more complicated due to the structure of the current $j_{\xi\xi}^{(3/2)}$ defined in (2.60). In principle, we can emit an arbitrary number of collinear gluons from this current. At one-loop, there are four diagrams which could contribute to the function J_2, see Fig. A.1(d)-(g). As it turns out, only diagram (f) has a non-vanishing contribution. For simplicity, we concentrate on this diagram only. The Feynman rule for the subleading Lagrangian $\mathcal{L}_{\xi q}^{(1/2)}$ in (2.64) is known to be

$$ig_sT^A\left(\gamma_\perp^\mu-\frac{n_+^\mu}{n_+l}\right)\frac{\not n_+}{2}\;, \tag{A.6}$$

where l denotes the momentum of the incoming soft anti-quark. The Feynman rule for the $j_{\xi\xi}^{(3/2)}$ can be derived from two external quark fields with momentum k' and k

$$\int d^4x e^{ipx}\big\langle q(k')\big|T\left\{\bar\xi_{\rm C}\frac{1}{in_+D}i\not D_\perp\frac{\not n_+}{2}\xi_{\rm C}-\bar\xi_{\rm C}i\overleftarrow{\not D}_\perp\frac{1}{in_+\overleftarrow{D}}\frac{\not n_+}{2}\xi_{\rm C}\right\}\big|q(k)\big\rangle$$

$$= \int d^4x e^{ipx}\left[\bar{u}(k')e^{ik'x}\left(\frac{1}{in_+\partial}i\partial\!\!\!/_\perp - i\overleftarrow{\partial\!\!\!/}\frac{1}{in_+\overleftarrow{\partial}}\right)e^{-ikx}\frac{n\!\!\!/_+}{2}u(k)\right]$$

$$= \int d^4x e^{ipx+ik'x-ikx}\bar{u}(k')\left(\frac{k\!\!\!/_\perp}{n_+k} - \frac{k'\!\!\!/_\perp}{n_+k'}\right)k\!\!\!/_\perp\frac{n\!\!\!/_+}{2}u(k)$$

$$= (2\pi)^4\delta^{(4)}(k'-k+p)\bar{u}(k-p)\left[-\frac{n_+p}{n_+k(n_+k-n_+p)}k\!\!\!/_\perp\frac{n\!\!\!/_+}{2}\right]u(k)\,. \tag{A.7}$$

We conclude that the Feynman rule is given by

$$-\frac{n_+p}{n_+k(n_+k-n_+p)}k\!\!\!/_\perp\frac{n\!\!\!/_+}{2}\,. \tag{A.8}$$

The calculation of Fig. A.1(f) yields

$$J_2^{(f)}(2E_\gamma\omega,p^2;\mu) = \frac{\alpha_sC_F}{4\pi}\bigg(-\frac{2}{\epsilon^2}-\frac{2}{\epsilon}\ln\frac{\mu^2}{2E_\gamma\omega-p^2}-\frac{2}{\epsilon}\frac{p^2}{2E_\gamma\omega}\ln\frac{2E_\gamma\omega-p^2}{-p^2}-2+\frac{\pi^2}{6}$$
$$-\ln^2\frac{\mu^2}{2E_\gamma\omega-p^2}+\frac{p^2}{2E_\gamma\omega}\ln^2\frac{\mu^2}{2E_\gamma\omega-p^2}-\frac{p^2}{2E_\gamma\omega}\ln^2\frac{\mu^2}{-p^2}\bigg)\,. \tag{A.9}$$

Hence, the renormalized jet function is

$$J_2(2E_\gamma\omega,p^2;\mu) = \frac{\alpha_sC_F}{4\pi}\bigg(-2+\frac{\pi^2}{6}-\ln^2\frac{\mu^2}{2E_\gamma\omega-p^2}$$
$$+\frac{p^2}{2E_\gamma\omega}\ln^2\frac{\mu^2}{2E_\gamma\omega-p^2}-\frac{p^2}{2E_\gamma\omega}\ln^2\frac{\mu^2}{-p^2}\bigg)\,. \tag{A.10}$$

In sum, J_1 and J_2 reproduce the hard-collinear region of the full theory and in particular the hard-collinear matching coefficient J_S in (2.84).

A.2 Soft region in HQET

To complete the QCD → QET×SCET matching, it remains to show that the soft region is reproduced on both sides of the matching equation by calculating the matrix element 2.69 at NLO. There are three diagrams shown in Fig.A.2 in the effective theory. The Feynman rule for the soft operator is derived similarly to (A.7). For the two-particle case, it is only proportional to $n\!\!\!/_-\gamma_5\delta(\omega-\omega')$. For the three-particle case, we obtain

$$\Big(\delta(\omega-\omega')-\delta(\omega-\omega'+n_-k)\Big)n\!\!\!/_-\gamma_5\,, \tag{A.11}$$

where k denotes the momentum of the incoming/outgoing gluon from the finite distance Wilson line $[tn_-,0]$. Using the HQET Feynman rule for the heavy quark propagator, we obtain the contributions from the three diagrams

$$S^{(1a)} = -2ig_s^2C_F\bar{v}(l)n\!\!\!/_-\gamma_5u(v)\;\tilde{\mu}^{2\epsilon}\int\frac{d^dk}{(2\pi)^d}\frac{(\delta(\omega-n_-l)-\delta(\omega-n_-l+n_-k))}{[k^2+i0][2vk+i0][n_-k-i0]}$$

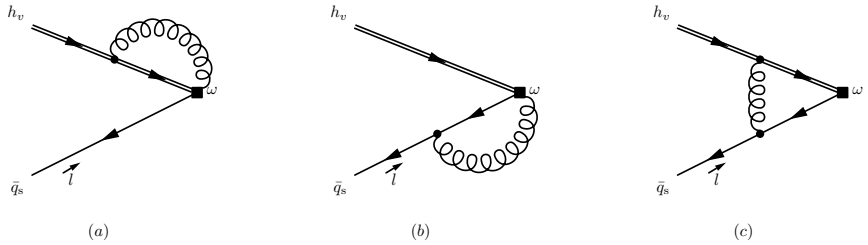

Figure A.2: NLO diagrams for the operator defined in (2.69). The double fermion line represents the heavy quark field. The finite distance Wilson line is denoted by the black square.

$$= \frac{\alpha_s C_F}{4\pi}\bar{v}(l)\not{n}_-\gamma_5 u(v) 2\Gamma(\epsilon)\frac{\theta(\omega - n_-l)}{\omega - n_-l}\left(\frac{4\pi\tilde{\mu}^2}{(n_-l-\omega)^2}\right)^{\epsilon} . \tag{A.12}$$

$$\begin{aligned} S^{(1b)} &= -2ig_s^2 C_F \bar{v}(l)\not{n}_-\gamma_5 u(v) \\ &\quad \times \tilde{\mu}^{2\epsilon}\int \frac{d^dk}{(2\pi)^d}\frac{(n_-k - n_-l)(\delta(\omega - n_-l) - \delta(\omega - n_-l + n_-k))}{[k^2+i0][(k-l)^2+i0][n_-k - i0]} \\ &= \frac{\alpha_s C_F}{4\pi}\bar{v}(l)\not{n}_-\gamma_5 u(v)\left(\frac{4\pi\tilde{\mu}^2}{-l^2}\right)^{\epsilon} 2\Gamma(\epsilon)\Bigg\{ - \frac{\Gamma(-\epsilon)\Gamma(2-\epsilon)}{\Gamma(2-2\epsilon)}\delta(\omega - n_-l) \\ &\quad + \frac{\omega\theta(n_-l-\omega)}{n_-l(n_-l-\omega)}\left(\frac{\omega}{n_-l} - \frac{\omega^2}{n_-l^2}\right)^{-\epsilon}\Bigg\} , \end{aligned} \tag{A.13}$$

$$S^{(1c)} = -2ig_s^2 C_F \int \frac{d^4k}{(2\pi)^4}\frac{\bar{v}(l)\not{v}\not{k}\not{n}_-\gamma_5 u(v)}{[k^2+i0][(k+l)^2+i0][2v\cdot k + 2v\cdot l + i0]} , \tag{A.14}$$

In order to compare the soft matrix element to the soft region from (2.25), (2.26) and (2.27), we integrate the results together with the tree-level jet function. We observe that each diagram (A.12)–(A.14) separately reproduces the soft region in (2.25)–(2.27). In total, we obtain

$$T_s^{(1)} = \int_0^\infty \frac{d\omega}{\omega - n_-p - i0} S^{(1)} . \tag{A.15}$$

We conclude that the soft region in the full theory exactly corresponds to the soft matrix element in the effective theory and hence cancels on both sides of the matching equation.

Appendix B

Twist expansion in QCD

Factorization theorems and NLP effects in exclusive B decays as discussed in Chapter 2 and 3 involve hadronic matrix elements of heavy-to-light operators on or near the light-cone $x^2 \to 0$. In pure QCD, the counting of the corresponding operators can be conveniently organised in terms of conformal (geometric) twist [148]. This allows in particular for a systematic parametrization of the bi- and trilocal operators

$$\bar{q}_{\rm s}(x)\Gamma h_v(0)\,, \qquad \bar{q}_{\rm s}(x_1)G_{\mu\nu}(x_2)\Gamma^{\mu\nu}h_v(0)\,. \tag{B.1}$$

To this end, one constructs the conformal spin and twist for each light field of the operator defined by

$$j = \frac{1}{2}(l+s)\,, \qquad t = l - s\,, \tag{B.2}$$

where l refers to the canonical mass-dimension of the field and s to its spin projection on the light-cone.[1] We present a list for some field projections in Table B.1. The total twist of an operator is defined by the sum of the light field twist plus one, following the convention in [124]. To give an example, the operator

$$\left\langle 0\middle|\bar{q}_{\rm s}(z_1 n_-)\not{n}_- G_{\perp+}(z_2 n_-)h_v(0)\middle|\bar{B}\right\rangle = 2F_B(\mu)\Phi_3(z_1,z_2)\,, \tag{B.3}$$

with $G_{\perp+} \equiv \gamma_\perp^\mu n_-^\nu G_{\mu\nu}$ contributes in total at twist-3. The conformal spin of the light fields dictates the behaviour of the LCDA for small arguments in momentum space according to $f(\omega_i) \sim \omega^{2j_i-1}$. Since the quark field has conformal spin $j = 1$ while the gluon field strength has $j = 3/2$, we find $\phi_3(\omega_1,\omega_2) \sim \omega_1\omega_2^2$. In the same way, the remaining operators are constructed up to a given twist counting. We refrain from giving the precise operator definitions but summarize the endpoint behaviour of each function in the main text. For the two-particle LCDAs, we find

$$\phi_+(\omega) \sim \omega\,, \qquad \phi_-(\omega) \sim \omega^0\,, \qquad g_+(\omega) \sim \omega^2\,, \qquad g_-(\omega) \sim \omega\,. \tag{B.4}$$

[1] More precisely, s is defined to be the eigenvalue of the operator $\Sigma_{+-} \equiv n_-^\mu n_+^\nu \Sigma_{\mu\nu}$, where the spin operator acts on the quark and gluon field as $\Sigma_{\mu\nu}q = i\sigma_{\mu\nu}/4$, with $\sigma^{\mu\nu} = i[\gamma^\mu,\gamma^\nu]/2$ and $\Sigma_{\mu\nu}G_\lambda = (g_{\nu\lambda}G_\mu - g_{\mu\lambda}G_\nu)/2$.

Fields	$\bar{q}_s \not{n}_-$	$\bar{q}_s \not{n}_+$	$G_{\perp +}$	$G_{+-}/G_{\perp\perp}$	$G_{\perp -}$
l	3/2		2		
s	1/2	−1/2	1	0	−1
t	1	2	1	2	3
$2j-1$	1	0	2	1	0

Table B.1: Values of the canonical dimension l, the light-cone spin projection s and twist t for the light fields of bi- and trilocal heavy-to-light operators. The conformal spin j dictates the small ω-behaviour of the LCDAs in the light quark field argument $f(\omega) \sim \omega^{2j-1}$.

For the three-particle LCDAs, we have

$$\phi_4(\omega_1,\omega_2) \sim \omega_1^0 \omega_2^2 \,, \qquad \psi_4(\omega_1,\omega_2) \sim \omega_1\omega_2 \,, \qquad \widetilde{\psi}_4(\omega_1,\omega_2) \sim \omega_1\omega_2 \,. \tag{B.5}$$

At LP in the heavy-quark expansion, we only expect the leading twist-2 amplitude ϕ_+ to contribute in physical processes. However, with increasing power of λ, the higher-twist LCDAs above generally appear in subleading terms. In fact, we observe that lower-twist amplitudes also enter in NLP corrections, which is a general feature of the twist expansion [169,170]. In the physical picture, the meson can be viewed as a multi-parton state, in which these different contributions are related by the equations of motions in QCD. For our purposes, we summarize some of the implications in Sec. B.2.

B.1 Fourier integrals

In Chapter 3, we perform several Fourier integrals from position to momentum space, for which we require some general identities. For $p^2 < 0$, we have most generally in d dimensions that

$$\int d^dx \frac{e^{ipx}}{(-x^2+i0)^n} = -i\pi^{\frac{d}{2}} \frac{\Gamma\left(\frac{d}{2}-n\right)}{\Gamma(n)} \left(\frac{4}{-p^2}\right)^{\frac{d}{2}-n} \,. \tag{B.6}$$

Taking suitable derivatives, we find explicitly

$$\begin{aligned} \int d^dx \frac{e^{ipx}}{(-x^2+i0)^{\frac{d}{2}-1}} x_\lambda x_\rho &= -\frac{8i\pi^{\frac{d}{2}}}{\Gamma\left(\frac{d}{2}-1\right)} \frac{(4p_\lambda p_\rho - p^2 g_{\lambda\rho})}{p^6} \,, \\ \int d^dx \frac{e^{ipx}}{(-x^2+i0)^{\frac{d}{2}-2}} x_\lambda &= \frac{64\pi^{\frac{d}{2}}}{\Gamma\left(\frac{d}{2}-2\right)} \frac{p_\lambda}{p^6} \,. \end{aligned} \tag{B.7}$$

For $d = 4$, we perform the Fourier transformation according to

$$\int d^4x \frac{e^{ipx}}{x^4} x^\lambda = 2\pi^2 \frac{p^\lambda}{p^2} \,, \qquad \int d^4x \frac{e^{ipx}}{x^4} x^\lambda x^\rho = \frac{2\pi^2 i}{p^2} \left(-g^{\lambda\rho} + 2\frac{p^\lambda p^\rho}{p^2}\right) \,,$$

$$\int d^4x \frac{e^{ipx}}{x^2} x^\lambda = 8\pi^2 \frac{p^\lambda}{p^4} \,, \qquad \int d^4x \frac{e^{ipx}}{x^2} = -\frac{4\pi^2 i}{p^2} \,. \tag{B.8}$$

We furthermore require

$$\int_0^\infty d\omega\, \phi(\omega) \int d^4x \frac{e^{i(p-\omega v)x}}{x^2(vx)} x^\lambda = 8\pi^2 i \int_0^\infty d\omega \frac{(p-\omega v)^\lambda}{(p-\omega v)^2} \int_0^\omega d\omega' \phi(\omega') \,, \tag{B.9}$$

which we obtain after integrating by parts. Note that the boundary term vanishes since the exponential factor $e^{-i\omega(vx-i0)}$ inherits the $i0$-prescription from the analytic structure of the LCDAs.

B.2 Wandzura-Wilczek relations

Under the assumption that we can neglect four-particle contributions like $\big|\bar{q}bgg\big\rangle$ or $\big|\bar{q}b\bar{q}q\big\rangle$, the equations of motion for the light fields impose connections between LCDAs of different twist, also known as Wandzura-Wilczek (WW) relations [171]. For the two-particle LCDA ϕ_-, this implies a decomposition of the form $\phi_- = \phi_-^{\mathrm{WW}} + \phi_-^{\mathrm{t3}}$, where the WW part can be written as

$$\phi_-^{\mathrm{WW}}(\omega) = \int_\omega^\infty \frac{d\omega'}{\omega'} \phi_+(\omega') \,, \tag{B.10}$$

which provides a solution to the equation of motion in the absence of the three-particle content while ϕ_-^{t3} represents the remaining twist-3 corrections [83]. The same separation applies to $g_+ = g_+^{\mathrm{WW}} + g_+^{\mathrm{t3+t4}}$, even though it is less relevant in our context. A simple application of (B.10) yields

$$\int_0^\omega d\omega' [\phi_+ - \phi_-](\omega') = -\int_0^\omega d\omega' \phi_-^{\mathrm{t3}}(\omega') - \omega \phi_-^{\mathrm{WW}}(\omega) \,. \tag{B.11}$$

This combination typically appears under the integral

$$\begin{aligned} &\int_0^\infty \frac{2E_\gamma d\omega}{2E_\gamma\omega - p^2} \int_0^\omega d\omega' [\phi_+ - \phi_-](\omega') = -\int_0^\infty d\omega \ln\left(\frac{2E_\gamma\omega - p^2}{4E_\gamma^2}\right) [\phi_+ - \phi_-](\omega) \\ &= \int_0^\infty d\omega \ln\left(\omega - \frac{p^2}{2E_\gamma}\right) \phi_-^{\mathrm{t3}}(\omega) - 1 - \frac{p^2}{2E_\gamma} \int_0^\infty \frac{d\omega}{\omega} \ln\left(\frac{2E_\gamma\omega - p^2}{-p^2}\right) \phi_+(\omega) \,, \end{aligned} \tag{B.12}$$

where we stripped of constant factors in the first term since $[\phi_+ - \phi_-]$ and therefore ϕ_-^{t3} are normalized to zero in the tree-level approximation according to (3.10).

The relations between two- and three-particle LCDAs in position space can be found in [47, 124]. For our purposes, we list some relevant equations in momentum space. The two-particle LCDA g_+ can be related to ψ_4 via

$$4E_\gamma^2 \int_0^\infty d\omega \frac{4g_+(\omega)}{(2E_\gamma\omega - p^2)^2} = \int_0^\infty \frac{2E_\gamma d\omega}{2E_\gamma\omega - p^2} 2(\bar{\Lambda} - \omega)\phi_+(\omega) \tag{B.13}$$

$$- \int_0^\infty \frac{2E_\gamma d\omega}{2E_\gamma\omega - p^2} \int_0^\omega d\omega' [\phi_+ - \phi_-](\omega')$$
$$- 4E_\gamma^2 \int_0^\infty d\omega_1 \int_0^\infty d\omega_2 \int_0^1 du \frac{2\bar{u}\psi_4(\omega_1,\omega_2)}{(2E_\gamma(\omega_1+u\omega_2)-p^2)^2} \,.$$

We note that the sum of the LCDAs $[\psi_4 + \widetilde{\psi}_4]$ is purely twist-4 whereas the difference $[\psi_4 - \widetilde{\psi}_4]^{\mathrm{t3+t4}}$ contains both twist-3 and twist-4 terms. The latter twist-3 contribution can be expressed in terms of ϕ_-^{t3} as

$$4E_\gamma^2 \int_0^\infty d\omega_1 \int_0^\infty d\omega_2 \int_0^1 du \frac{[\psi_4 - \widetilde{\psi}_4]^{\mathrm{t3}}(\omega_1,\omega_2)}{(2E_\gamma(\omega_1+u\omega_2)-p^2)^2} = \int_0^\infty d\omega \ln\left(\omega - \frac{p^2}{2E_\gamma}\right) \phi_-^{\mathrm{t3}}(\omega) \,. \tag{B.14}$$

For the twist-4 part, we find

$$4E_\gamma^2 \int_0^\infty d\omega_1 \int_0^\infty d\omega_2 \int_0^1 du \frac{[\psi_4 - \widetilde{\psi}_4]^{\mathrm{t4}}(\omega_1,\omega_2)}{(2E_\gamma(\omega_1+u\omega_2)-p^2)^2} \tag{B.15}$$
$$= \int_0^\infty \frac{2E_\gamma d\omega}{2E_\gamma\omega - p^2} \frac{d}{d\omega}\bigg(- \frac{\omega^2}{2}\phi_-^{\mathrm{WW}}(\omega) + \frac{1}{2}\int_0^\omega d\omega'\omega'\phi_+(\omega') + 2\int_0^\omega d\omega'(\bar{\Lambda}-\omega')\phi_+(\omega')\bigg)$$
$$- 4E_\gamma^2 \int_0^\infty d\omega_1 \int_0^\infty d\omega_2 \int_0^1 du \bigg(\frac{[\psi_4 + \widetilde{\psi}_4](\omega_1,\omega_2)}{(2E_\gamma(\omega_1+u\omega_2)-p^2)^2} + \frac{[\psi_4 + \widetilde{\psi}_4](\omega_1,\omega_2)}{(2E_\gamma(u\omega_1+\omega_2)-p^2)^2}\bigg) \,.$$

In the case of scalar currents, the subleading terms additionally contain a dependence on the LCDAs ϕ_3 and ϕ_4. These functions fulfill respectively

$$4E_\gamma^2 \int_0^\infty d\omega_1 \int_0^\infty d\omega_2 \int_0^1 du \frac{2u\phi_3(\omega_1,\omega_2)}{(2E_\gamma(\omega_1+u\omega_2)-p^2)^2}$$
$$= \int_0^\infty \frac{2E_\gamma d\omega}{2E_\gamma\omega - p^2}\bigg(\omega\phi_-(\omega) + \int_0^\omega d\omega'[\phi_+ - \phi_-](\omega')\bigg) \,, \tag{B.16}$$
$$4E_\gamma^2 \int_0^\infty d\omega_1 \int_0^\infty d\omega_2 \int_0^1 du \frac{2[u\phi_4 + \psi_4](\omega_1,\omega_2)}{(2E_\gamma(\omega_1+u\omega_2)-p^2)^2}$$
$$= \int_0^\infty \frac{2E_\gamma d\omega}{2E_\gamma\omega - p^2}\bigg((\bar{\Lambda}-\omega)\phi_+(\omega) - \int_0^\omega d\omega'[\phi_+ - \phi_-](\omega')\bigg) \,. \tag{B.17}$$

Appendix C

Diagrammatic results for $\bar{B} \to M_1 M_2$ decays

C.1 Vertex corrections

The hard matching coefficients of Sec. 4.4 are computed from the hard region of the diagrams depicted in Fig. 4.2. We presented the results of the right insertion for diagram 4.2(a) in (4.13). In the following, we complete the list for the wrong insertion and the remaining diagrams 4.2(b)-(e). We have

$$W_{\rm h}^{(1a)} = \frac{Q_{q_1}Q_u}{N_c}\bigg(\frac{1}{\epsilon_{\rm UV}} - \frac{1}{\epsilon^2} - \frac{1}{\epsilon}\left(2 + \log\frac{\mu^2}{u^2 m_B^2}\right) - 4 - \frac{\pi^2}{12} - \log^2 u \tag{C.1}$$
$$+ \frac{2-3u}{\bar{u}}\log u + 2\log u \log\frac{\mu^2}{m_B^2} - \log\frac{\mu^2}{m_B^2} - \frac{1}{2}\log^2\frac{\mu^2}{m_B^2} + 2{\rm Li}_2\left(-\frac{\bar{u}}{u}\right)\bigg)\langle\widetilde{\mathcal{O}}^{\rm I}\rangle\,.$$

For the second diagram, we find

$$R_{\rm h}^{(1b)} = Q_u Q_d\bigg\{\bigg(-\frac{4}{\epsilon_{\rm UV}} + \frac{1}{\epsilon^2} + \frac{1}{\epsilon}\left(2 + \ln\frac{\mu^2}{\bar{u}^2 m_B^2}\right) - 3 + \frac{\pi^2}{12} + \ln^2\bar{u} - \frac{2}{u}\ln\bar{u}$$
$$- 2\ln\bar{u}\ln\frac{\mu^2}{m_B^2} - 2\ln\frac{\mu^2}{m_B^2} + \frac{1}{2}\ln^2\frac{\mu^2}{m_B^2} - 2{\rm Li}_2\left(-\frac{u}{\bar{u}}\right)\bigg)\langle\mathcal{O}^{\rm I}\rangle + \frac{3}{4\epsilon_{\rm UV}}\langle\mathcal{E}^{\rm I}\rangle\bigg\}\,, \tag{C.2}$$

$$W_{\rm h}^{(1b)} = \frac{Q_u Q_d}{N_c}\bigg\{\bigg(-\frac{4}{\epsilon_{\rm UV}} + \frac{1}{\epsilon^2} + \frac{1}{\epsilon}\left(2 + \ln\frac{\mu^2}{\bar{u}^2 m_B^2}\right) - 5 + \frac{\pi^2}{12} + \ln^2\bar{u} - \frac{2}{u}\ln\bar{u} \tag{C.3}$$
$$- 2\ln\bar{u}\ln\frac{\mu^2}{m_B^2} - 2\ln\frac{\mu^2}{m_B^2} + \frac{1}{2}\ln^2\frac{\mu^2}{m_B^2} - 2{\rm Li}_2\left(-\frac{u}{\bar{u}}\right)\bigg)\langle\widetilde{\mathcal{O}}^{\rm I}\rangle + \frac{1}{4\epsilon_{\rm UV}}\langle\widetilde{\mathcal{E}}^{\rm I}\rangle\bigg\}\,.$$

For the third diagram, we have

$$R_{\rm h}^{(1c)} = Q_{q_1}Q_{q_2}\bigg\{\bigg(-\frac{4}{\epsilon_{\rm UV}} + \frac{2}{\epsilon^2} + \frac{2}{\epsilon}\left(2 + \ln\frac{\mu^2}{-u m_B^2}\right) + 1 - \frac{\pi^2}{6} + \ln^2\frac{\mu^2}{-u m_B^2}\bigg)\langle\mathcal{O}^{\rm I}\rangle$$
$$+ \frac{3}{4\epsilon_{\rm UV}}\langle\mathcal{E}^{\rm I}\rangle\bigg\}\,, \tag{C.4}$$

$$W_{\mathrm{h}}^{(1c)} = \frac{Q_{q_1} Q_{q_2}}{N_c} \bigg(-\frac{4}{\epsilon_{\mathrm{UV}}} + \frac{2}{\epsilon^2} + \frac{2}{\epsilon} \left(2 + \ln \frac{\mu^2}{-u m_B^2} \right) - 1 - \frac{\pi^2}{6} + \ln^2 \frac{\mu^2}{-u m_B^2} \bigg) \langle \widetilde{\mathcal{O}}^{\mathrm{I}} \rangle + \frac{1}{4\epsilon_{\mathrm{UV}}} \langle \widetilde{\mathcal{E}}^{\mathrm{I}} \rangle \bigg\} \,. \tag{C.5}$$

The fourth diagram yields

$$R_{\mathrm{h}}^{(1d)} = Q_u Q_{q_2} \bigg\{ \bigg(\frac{1}{\epsilon_{\mathrm{UV}}} - \frac{2}{\epsilon^2} - \frac{2}{\epsilon} \left(2 + \ln \frac{\mu^2}{-\bar{u} m_B^2} \right) - 6 + \frac{\pi^2}{6} - 3 \ln \frac{\mu^2}{-\bar{u} m_B^2} - \ln^2 \frac{\mu^2}{-\bar{u} m_B^2} \bigg) \langle \mathcal{O}^{\mathrm{I}} \rangle + \frac{\alpha Q_u^2}{4\pi} \frac{3}{4\epsilon_{\mathrm{UV}}} \langle \mathcal{E}^{\mathrm{I}} \rangle \bigg\} \,, \tag{C.6}$$

$$W_{\mathrm{h}}^{(1d)} = \frac{Q_u Q_{q_2}}{N_c} \bigg(\frac{1}{\epsilon_{\mathrm{UV}}} - \frac{2}{\epsilon^2} - \frac{2}{\epsilon} \left(2 - \ln \frac{\mu^2}{-\bar{u} m_B^2} \right) - 8 + \frac{\pi^2}{6} - 3 \ln \frac{\mu^2}{-\bar{u} m_B^2} - \ln^2 \frac{\mu^2}{-\bar{u} m_B^2} \bigg) \langle \widetilde{\mathcal{O}}^{\mathrm{I}} \rangle \,. \tag{C.7}$$

The fifth's diagram yields

$$R_{\mathrm{h}}^{(1e)} = Q_d Q_{q_2} \bigg(\frac{1}{\epsilon_{\mathrm{UV}}} - \frac{1}{\epsilon^2} - \frac{1}{\epsilon} \left(2 + \ln \frac{\mu^2}{m_B^2} \right) - 4 - \frac{\pi^2}{12} - \ln \frac{\mu^2}{m_B^2} - \frac{1}{2} \ln^2 \frac{\mu^2}{m_B^2} \bigg) \langle \mathcal{O}^{\mathrm{I}} \rangle \,, \tag{C.8}$$

$$W_{\mathrm{h}}^{(1e)} = \frac{Q_d Q_{q_2}}{N_c} \bigg\{ \bigg(\frac{1}{\epsilon_{\mathrm{UV}}} - \frac{1}{\epsilon^2} - \frac{1}{\epsilon} \left(2 + \ln \frac{\mu^2}{m_B^2} \right) - 4 - \frac{\pi^2}{12} - \ln \frac{\mu^2}{m_B^2} - \frac{1}{2} \ln^2 \frac{\mu^2}{m_B^2} \bigg) \langle \widetilde{\mathcal{O}}^{\mathrm{I}} \rangle + \frac{1}{4\epsilon_{\mathrm{UV}}} \langle \widetilde{\mathcal{E}}^{\mathrm{I}} \rangle \bigg\} \,. \tag{C.9}$$

For the wrong insertion, we additionally defined the matrix elements

$$\langle \widetilde{\mathcal{O}}^{\mathrm{I}} \rangle = [\bar{u}(k_{q_1}) \gamma_\perp^\mu (1 - \gamma_5) u(p_b)] [\bar{u}(k_{q_2}) \gamma_{\perp\mu} (1 - \gamma_5) v(k_{\bar{u}})] \,, \tag{C.10}$$

$$\langle \widetilde{\mathcal{E}}^{\mathrm{I}} \rangle = [\bar{u}(k_{q_1}) \gamma_\perp^\mu \gamma_\perp^\nu \gamma_\perp^\lambda (1 - \gamma_5) u(p_b)] [\bar{u}(k_{q_2}) \gamma_{\perp\mu} \gamma_{\perp\nu} \gamma_{\perp\lambda} (1 - \gamma_5) v(k_{\bar{u}})] \,. \tag{C.11}$$

Comparing right and wrong insertion, the result proportional to the Fierz equivalent operators $\mathcal{O}^{\mathrm{I}}$ and $\widetilde{\mathcal{O}}^{\mathrm{I}}$ only differs by a constant. We remark that the last contribution of diagram 4.2(e) is often referred to as "non-factorizable" since the results cancel with the corresponding renormalization of the full QCD×QED form factor.

C.2 Photon polarization and spectator scattering

According to the discussion in Sec. 4.4.2, the spectator scattering kernels $H_{i,-}^{\mathrm{II}\gamma}$ receive contributions from the first three diagrams S_1–S_3 that correspond to Fig. C.1(a)–(c)

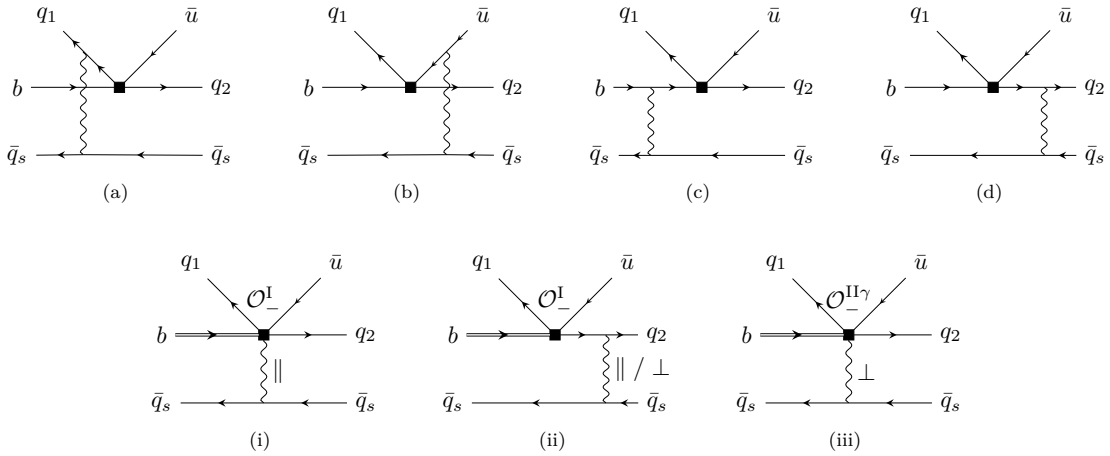

Figure C.1: Spectator scattering at tree-level in the QCD×QED (first line) compared to HQET×SCET$_{\rm I}$ (second line).

respectively. In the matching calculation, we assumed the photon to be transversely polarized. In a more precise treatment, the cancellation between different polarizations ensures the absence of endpoint divergences in the factorization formula (4.70). The longitudinal polarization states are in fact entirely contained in the time-ordered products of the operator $\mathcal{O}^{\rm I}$ in SCET$_{\rm I}$.

To prove these statements, we calculate the full theory and EFT diagrams in Fig. C.1 using the LCDA projector method [37, 48]. The method simplifies the computation in terms of hadronic matrix elements since it projects the on-shell spinors directly onto the light- and heavy-meson LCDAs. From the EFT viewpoint, this corresponds to a simultaneous elimination of hard and hard-collinear scales and thus a straightforward matching onto SCET$_{\rm II}$. In what follows, we neglect the three-particle LCDAs in the Wandzura-Wilcek approximation and only include two-particle contributions up to twist-3. The B-meson projector generalizes (2.11) and acts on the partonic amplitude with stripped off spinor (colour) indices $\beta\alpha$ (ba). We have [83]

$$M^B_{\alpha\beta} = -\frac{if_B m_B}{4}\,\frac{\delta_{ab}}{N_c}\left[\frac{1+\not v}{2}\left\{\phi^B_+(\omega)\,\not n_+ + \phi^B_-(\omega)\,\not n_- - \int_0^\omega d\eta\,\left(\phi^B_-(\eta)-\phi^B_+(\eta)\right)\,\gamma^\mu\frac{\partial}{\partial l^\mu_\perp}\right\}\gamma_5\right]_{\alpha\beta}. \tag{C.12}$$

For the case of light pseudoscalar mesons, we apply the projector [158]

$$M^P_{\alpha\beta} = \frac{if_P}{4}\,\frac{\delta_{ab}}{N_c}\left[\not p\,\gamma_5\,\phi_P(x)\right.$$

$$- \mu_M \gamma_5 \left(\phi_p(x) - i\sigma_{\mu\nu} \frac{p^\mu \bar{p}^\nu}{p\cdot\bar{p}} \frac{\phi_\sigma'(x)}{6} + i\sigma_{\mu\nu} p^\mu \frac{\phi_\sigma(x)}{6} \frac{\partial}{\partial k_{\perp\nu}} \right) \Bigg]_{\alpha\beta} , \tag{C.13}$$

where p denotes the total momentum of the meson and the spatial components of the light-like vector $\bar{p}$ are aligned in the opposite direction of p. For both kinds of projectors, the transverse derivatives are taken with respect to the quark momenta parametrized by (4.12), with the refinement $k_{q_1\perp} = -k_{\bar{u}\perp} = k_\perp$ for light mesons. Note that the definition of the LCDAs in (C.12) and (C.13) refers to their QCD-only expressions. For simplicity, we omit the QED generalization in this context, which would yield equivalent results. Moreover, we include the light and heavy LCDAs up to twist-3 to track the endpoint-divergent convolutions. These terms involve in particular ϕ_-, ϕ_p and ϕ_σ and appear at LP in the heavy-to-light form factors in [83]. The convolutions arise more precisely form time-ordered products with $\mathcal{O}^{\rm I}$ which is not matched further onto SCET$_{\rm I}$ as mentioned above.

We separate the polarization states of the hard-collinear photon in Fig. C.1 by decomposing the metric tensor according to $g^{\mu\nu} = (n_+^\mu n_-^\nu + n_-^\mu n_+^\nu)/2 + g_\perp^{\mu\nu}$ into longitudinal and transverse components. At LP, we obtain for diagrams (a) – (d) in Feynman gauge

$$\begin{aligned}
\langle Q_2\rangle_\parallel^{(a)} &= -Q_d Q_{\rm sp} \left\langle \bar{v}^{-2}\right\rangle_{M_1} \left\langle \omega^{-1}\right\rangle_- , \qquad \langle Q_2\rangle_\perp^{(a)} = 0 , \\
\langle Q_2\rangle_\parallel^{(b)} &= Q_u Q_{\rm sp} \left\langle \bar{v}^{-2}\right\rangle_{M_1} \left\langle \omega^{-1}\right\rangle_- , \qquad \langle Q_2\rangle_\perp^{(b)} = Q_u Q_{\rm sp} \left\langle \bar{v}^{-1}\right\rangle_{M_1} \left\langle \bar{u}^{-1}\right\rangle_{M_2} \left\langle \omega^{-1}\right\rangle_+ , \\
\langle Q_2\rangle_\parallel^{(c)} &= Q_d Q_{\rm sp} \left\langle \bar{v}^{-2}\right\rangle_{M_1} \left\langle \omega^{-1}\right\rangle_- , \qquad \langle Q_2\rangle_\perp^{(c)} = Q_d Q_{\rm sp} \left\langle \bar{v}^{-1}\right\rangle_{M_1} \left\langle \omega^{-1}\right\rangle_+ , \\
\langle Q_2\rangle_\parallel^{(d)} &= Q_u Q_{\rm sp} \frac{\mu_{M_1}}{3} \left\langle \bar{v}^{-2}\right\rangle_{\sigma 1} \left\langle \omega^{-2}\right\rangle_+ , \\
\langle Q_2\rangle_\perp^{(d)} &= Q_u Q_{\rm sp} \left\langle \bar{v}^{-1}\right\rangle_{M_1} \left\langle \omega^{-1}\right\rangle_- + Q_u Q_{\rm sp} \frac{\mu_{M_1}}{3} \left\langle v^{-1}\bar{v}^{-1}\right\rangle_{\sigma 1} \left\langle \omega^{-2}\right\rangle_+ .
\end{aligned} \tag{C.14}$$

We used $Q_{q_1} = Q_d$ and $Q_{q_2} = Q_u$ for the general case $\otimes = (+,-)$ in which the spectator quark charge is $Q_{\rm sp} = Q_d$ and normalized the results by subtracting the factor of $\mathcal{N} \equiv i\pi\alpha f_{M_1} f_{M_2} f_B m_B / N_c$. The angle brackets define the convolutions

$$\langle v^n\rangle_X \equiv \int_0^1 dv\, v^n \phi_X(v) , \qquad \langle \omega^n\rangle_\pm \equiv \int_0^\infty d\omega\, \omega^n \phi_\pm^B(\omega) . \tag{C.15}$$

In total, all contributions in (C.14) are summed to obtain the left-hand side of the matching equation (4.84).

From the RG evolution of the different LCDAs we conclude that the convolutions $\langle \bar{v}^{-2}\rangle_M , \langle \bar{v}^{-2}\rangle_\sigma$, $\langle \omega^{-2}\rangle_+$, $\langle \omega^{-1}\rangle_-$ are endpoint-divergent. We observe that diagrams (a) – (c) are individually ill-defined only when the photon is longitudinally polarized. For diagram d), both polarizations lead to divergent convolutions. In QCD-only, the spectator scattering diagrams (c) and (d) enter the $B \to M_1$ form factor while (a) and (b) cancel amongst each other. This differs to QED since longitudinal terms of (a) and

(b) sum up to a divergent contribution proportional to $Q_{M_2} = Q_u - Q_d$, which naively would spoil factorization. However, as we show in the following, this term originates from the hard-collinear Wilson line in $\mathcal{O}^{\rm I}$ that connects to the spectator quark and cancels in the matching equation.

We verify the cancellation by calculating the $\text{SCET}_{\rm I}$ matrix elements on the right-hand side of the matching equation (4.84). For $\mathcal{O}^{\rm I}$, this involves the computation of diagrams (i) and (ii) in Fig. C.1 and for $\mathcal{O}_-^{\rm II\gamma}$ the corresponding diagram (iii). Using the same methods as above, we find

$$\begin{aligned}\langle\widetilde{\mathcal{O}}^{\rm I}(u)\rangle &\equiv \int \frac{d\hat{t}}{2\pi}\, e^{-iu\hat{t}}\,\langle\mathcal{O}^{\rm I}(t)\rangle \qquad\qquad (C.16)\\ &= \mathcal{N} Q_u Q_{\rm sp}\,\phi_{M_2}(u)\Big[\big\langle\omega^{-1}\big\rangle_-\big\langle\bar v^{-2}+\bar v^{-1}\big\rangle_{M_1}+\frac{\mu_{M_1}}{3}\big\langle v^{-1}\bar v^{-2}\big\rangle_{\sigma 1}\big\langle\omega^{-2}\big\rangle_+\Big]\,,\\ \langle\widetilde{\mathcal{O}}_-^{\rm II\gamma}(u,v)\rangle &\equiv \int\frac{d\hat{s}}{2\pi}\frac{d\hat{t}}{2\pi}\,e^{-i(u\hat{t}+(1-v)\hat{s})}\,\langle\mathcal{O}_-^{\rm II\gamma}(t,s)\rangle = \mathcal{N}\,\frac{Q_{\rm sp}}{2}\,\frac{\phi_{M_1}(v)}{\bar v}\,\phi_{M_2}(u)\,\big\langle\omega^{-1}\big\rangle_+\,.\end{aligned}$$

We implicitly used $H^{\rm I}_{2,-}(u) = 1 + \mathcal{O}(\alpha_s, \alpha_{\rm em})$ that can be inferred from the matching of four-point matrix elements of $\mathcal{O}^{\rm I}$. The second line exactly reproduces the divergent contributions we obtained in (C.14). Hence, all endpoint-divergent convolutions are part of the form factor $\zeta_{Q_2}^{BM_1}$. From the last line of (C.16) we recover the matching coefficient (4.88)

$$H^{\rm II\gamma}_{2,-}(u,v) = \frac{2Q_u}{\bar u} + 2Q_d\,, \qquad (C.17)$$

which we already found from the matching in (4.84) assuming only transverse photon polarizations. The precise combinations between the full-theory and SCET diagrams are given by

$$\begin{aligned}\langle Q_2\rangle_\parallel^{(a)+(b)+(c)} &= \int_0^1 du\; H^{\rm I}_{2,-}(u)\langle\widetilde{\mathcal{O}}^{\rm I}(u)\rangle^{(i)}\,,\\ \langle Q_2\rangle_\parallel^{(d)} + \langle Q_2\rangle_\perp^{(d)} &= \int_0^1 du\; H^{\rm I}_{2,-}(u)\langle\widetilde{\mathcal{O}}^{\rm I}(u)\rangle^{(ii)}\,,\\ \langle Q_2\rangle_\perp^{(a)+(b)+(c)} &= \int_0^1 dvdu\; H^{\rm II\gamma}_{2,-}(u,v)\langle\widetilde{\mathcal{O}}_-^{\rm II\gamma}(u,v)\rangle^{(iii)}\,, \qquad (C.18)\end{aligned}$$

which finally justifies to consider only transversely polarized photons in the derivation of $H^{\rm II\gamma}_{2,-}(u,v)$.

Appendix D

Relations for distribution amplitudes

D.1 Dispersive integrals

The dispersive treatment for the soft form factor in (3.46) requires the calculation of imaginary parts from the QCD factorization results. In the simplest case, the imaginary part is picked up from the hard-collinear propagator

$$\text{Im}\frac{1}{\omega-\omega'-i0} = \pi\delta(\omega-\omega')\,, \tag{D.1}$$

which follows from the Sokhotksi-Plemelj theorem involving the principal value for the real part. For higher integer powers $1/(\omega-\omega'-i0)^n$ we generally integrate by parts to reduce the expression to (D.1). For non-integer powers or logarithmic corrections, we rewrite

$$\begin{aligned}\frac{1}{\omega-\omega'-i0}\ln^{n-1}\frac{\omega'-\omega}{\omega'} &= \frac{d}{d\omega}\frac{1}{n}\ln^n\frac{\omega'-\omega-i0}{\omega'} \\ &= \frac{d}{d\omega}\frac{1}{2}\left(\theta(\omega'-\omega)\ln\frac{\omega'-\omega}{\omega'}+\theta(\omega-\omega')\left(\ln\frac{\omega-\omega'}{\omega'}+i\pi\right)\right)^n\end{aligned} \tag{D.2}$$

and again integrate by parts. For the NLO corrections of the LP factorization formula in (2.78) and (3.49) to the soft form factor, we use the following identities

$$\begin{aligned}&\frac{\text{Im}}{\pi}\int_0^\infty\frac{d\omega}{\omega-\omega'-i0}\ln^2\frac{\mu^2}{2E_\gamma(\omega-\omega')}\phi_+(\omega;\mu) \\ &\quad= \ln^2\frac{\mu^2}{2E_\gamma\omega'}\phi_+(\omega';\mu)-2\ln\frac{\mu^2}{2E_\gamma\omega'}\int_0^{\omega'}d\omega\ln\frac{\omega'-\omega}{\omega'}\frac{d}{d\omega}\phi_+(\omega;\mu) \\ &\quad-\frac{\pi^2}{3}\phi_+(\omega';\mu)+\int_0^{\omega'}d\omega\ln^2\frac{\omega'-\omega}{\omega'}\frac{d}{d\omega}\phi_+(\omega;\mu)\,,\end{aligned} \tag{D.3}$$

$$\frac{\text{Im}}{\pi}\int_0^\infty\frac{d\omega}{\omega-\omega'-i0}\frac{\omega'}{\omega}\ln\frac{\omega'-\omega}{\omega'}\left(\ln\frac{\mu^2}{2E_\gamma\omega'}+i\pi\right)\phi_+(\omega;\mu)$$

$$= -\ln\frac{\mu^2}{2E_\gamma\omega'}\int_{\omega'}^{\infty}d\omega\ln\frac{\omega-\omega'}{\omega'}\frac{d}{d\omega}\frac{\omega'}{\omega}\phi_+(\omega;\mu)-\frac{\pi^2}{2}\phi_+(\omega';\mu)$$

$$-\frac{1}{2}\int_0^{\omega'}d\omega\ln^2\frac{\omega'-\omega}{\omega'}\frac{d}{d\omega}\frac{\omega'}{\omega}\phi_+(\omega;\mu)-\frac{1}{2}\int_{\omega'}^{\infty}d\omega\ln^2\frac{\omega-\omega'}{\omega'}\frac{d}{d\omega}\frac{\omega'}{\omega}\phi_+(\omega;\mu)\ , \quad \text{(D.4)}$$

$$\frac{\mathrm{Im}}{\pi}\int_0^{\infty}\frac{d\omega}{\omega-\omega'-i0}\frac{\omega'}{\omega}\ln\frac{\omega'-\omega}{\omega'}\left(\ln\frac{\mu^2}{2E_\gamma\omega'}-\ln\frac{\omega-\omega'}{\omega'}\right)\phi_+(\omega;\mu)$$

$$= -\ln\frac{\mu^2}{2E_\gamma\omega'}\int_{\omega'}^{\infty}d\omega\ln\frac{\omega-\omega'}{\omega'}\frac{d}{d\omega}\frac{\omega'}{\omega}\phi_+(\omega;\mu)-\frac{\pi^2}{6}$$

$$-\frac{1}{2}\int_0^{\omega'}d\omega\ln^2\frac{\omega'-\omega}{\omega'}\frac{d}{d\omega}\frac{\omega'}{\omega}\phi_+(\omega;\mu)+\frac{1}{2}\int_{\omega'}^{\infty}d\omega\ln^2\frac{\omega-\omega'}{\omega'}\frac{d}{d\omega}\frac{\omega'}{\omega}\phi_+(\omega;\mu)\ , \quad \text{(D.5)}$$

$$\frac{\mathrm{Im}}{\pi}\int_0^{\infty}\frac{d\omega}{\omega-\omega'-i0}\frac{\omega'}{\omega}\ln\frac{\omega'-\omega}{\omega'}\phi_+(\omega;\mu)=-\int_{\omega'}^{\infty}d\omega\ln\frac{\omega-\omega'}{\omega'}\frac{d}{d\omega}\frac{\omega'}{\omega}\phi_+(\omega;\mu)\ . \quad \text{(D.6)}$$

Note that the logarithm in the first line of the third equation corresponds to the term $\ln\mu^2/2E_\gamma(\omega-\omega')$ appearing in the jet functions (2.84) and (3.51).

D.2 Distributions in ω

For the self-consistent treatment of the soft function RGE, it appeared natural to introduce the plus-distributions (5.46) and (5.48) in the variable ω'. To obtain the evolution equations for the first inverse-logarithmic moments (5.78) and (5.79), we conveniently consider the distributions to act in the variable ω instead. Here, we present the corresponding alternative results from Sec. 5.2 for the distributions and the anomalous dimension.

The fundamental linear combinations of ω'-distributions are displayed in (5.61). To let these distributions act in ω, we define analogous plus-distributions

$$\int_{-\infty}^{\infty}d\omega\big[\dots\big]_+^{(\omega)}f(\omega)=\int_{-\infty}^{\infty}d\omega\big[\dots\big](f(\omega)-f(\omega'))\ ,$$

$$\int_{-\infty}^{\infty}d\omega\big[\dots\big]_{\oplus/\ominus}^{(\omega)}f(\omega)=\int_{-\infty}^{\infty}d\omega\big[\dots\big](f(\omega)-\theta(\pm\omega)f(\omega'))\ . \quad \text{(D.7)}$$

By integrating against test functions $\int d\omega d\omega'\phi(\omega)\psi(\omega')$, we find the relations:

$$\theta(\omega)\omega'\left[\frac{\theta(\omega'-\omega)}{\omega'(\omega'-\omega)}\right]_+=\theta(\omega')\left[\frac{\theta(\omega'-\omega)}{\omega'-\omega}\right]_\oplus^{(\omega)}-\frac{\theta(-\omega)\theta(\omega')}{\omega'-\omega}\ ,$$

$$\theta(-\omega)\left[\frac{\theta(\omega'-\omega)}{\omega'-\omega}\right]_\ominus=\theta(-\omega')\omega\left[\frac{\theta(\omega'-\omega)}{\omega(\omega'-\omega)}\right]_+^{(\omega)}+\frac{\theta(-\omega)\theta(\omega')}{\omega'-\omega}\ ,$$

$$\theta(\omega)\omega\left[\frac{\theta(\omega'-\omega)}{\omega'(\omega'-\omega)}\right]_+=\theta(\omega')\omega\left[\frac{\theta(\omega'-\omega)\theta(\omega)}{\omega'(\omega'-\omega)}\right]_+^{(\omega)}\ ,$$

$$\theta(-\omega)\omega\left[\frac{\theta(\omega-\omega')}{\omega'(\omega-\omega')}\right]_+ = \theta(-\omega')\omega\left[\frac{\theta(\omega-\omega')\theta(-\omega)}{\omega'(\omega-\omega')}\right]_+^{(\omega)},$$

$$\theta(\omega)\left[\frac{\theta(\omega-\omega')}{\omega-\omega'}\right]_\oplus = \theta(\omega')\omega\left[\frac{\theta(\omega-\omega')}{\omega(\omega-\omega')}\right]_+^{(\omega)} + \frac{\theta(\omega)\theta(-\omega')}{\omega-\omega'},$$

$$\theta(-\omega)\omega'\left[\frac{\theta(\omega-\omega')}{\omega'(\omega-\omega')}\right]_+ = \theta(-\omega')\left[\frac{\theta(\omega-\omega')}{\omega-\omega'}\right]_\ominus^{(\omega)} - \frac{\theta(\omega)\theta(-\omega')}{\omega-\omega'}. \tag{D.8}$$

The terms proportional to $\theta(-\omega)\theta(\omega')$ or $\theta(\omega)\theta(-\omega')$ disappear after taking the linear combinations according to (5.61) so that every diagram of Fig. 5.3 and consequently the anomalous dimension can entirely be written in terms of the ω-distributions in (D.7).

Using (D.8), we obtain the anomalous dimension equivalent to (5.66)

$$\begin{aligned}\Gamma_\otimes^{(\omega)}(\omega,\omega') = \frac{\alpha_s C_F}{\pi}\left[\left(\ln\frac{\mu}{\omega-i0}-\frac{1}{2}\right)\delta(\omega-\omega') - H_+^{(\omega)}(\omega,\omega')\right] \\ + \frac{\alpha_{\rm em}}{\pi}\left[\left((Q_{\rm sp}^2+2Q_{\rm sp}Q_{M_1})\ln\frac{\mu}{\omega-i0} - \frac{3}{4}Q_{\rm sp}^2 - \frac{1}{2}Q_d^2\right.\right. \\ \left.\left. + i\pi(Q_{\rm sp}+Q_{M_1})Q_{M_2}\right)\delta(\omega-\omega') - Q_{\rm sp}Q_d H_+^{(\omega)}(\omega,\omega') + Q_{\rm sp}Q_{M_2}H_-^{(\omega)}(\omega,\omega')\right],\end{aligned} \tag{D.9}$$

but with the distributions in ω as can be indicated by the replacement $H \to H^{(\omega)}$. Equivalently to (5.62), we define

$$H_\pm^{(\omega)}(\omega,\omega') \equiv \theta(\pm\omega')F_\omega^{>(<)}(\omega,\omega') + \theta(\mp\omega')G_\omega^{<(>)}(\omega,\omega'), \tag{D.10}$$

where the F and G distributions that mimic (5.61) in ω are given by

$$\begin{aligned}F_\omega^>(\omega,\omega') &= \omega\left[\frac{\theta(\omega'-\omega)\theta(\omega)}{\omega'(\omega'-\omega)}\right]_+^{(\omega)} + \omega\left[\frac{\theta(\omega-\omega')}{\omega(\omega-\omega')}\right]_+^{(\omega)}, \\ G_\omega^>(\omega,\omega') &= \omega\left[\frac{\theta(\omega'-\omega)\theta(\omega)}{\omega'(\omega'-\omega)}\right]_+^{(\omega)} + \left[\frac{\theta(\omega'-\omega)}{\omega'-\omega}\right]_\oplus^{(\omega)} - i\pi\delta(\omega-\omega'), \\ F_\omega^<(\omega,\omega') &= \omega\left[\frac{\theta(\omega-\omega')\theta(-\omega)}{\omega'(\omega-\omega')}\right]_+^{(\omega)} + \omega\left[\frac{\theta(\omega'-\omega)}{\omega(\omega'-\omega)}\right]_+^{(\omega)}, \\ G_\omega^<(\omega,\omega') &= \omega\left[\frac{\theta(\omega-\omega')\theta(-\omega)}{\omega'(\omega-\omega')}\right]_+^{(\omega)} + \left[\frac{\theta(\omega-\omega')}{\omega-\omega'}\right]_\ominus^{(\omega)} + i\pi\delta(\omega-\omega').\end{aligned} \tag{D.11}$$

Note that the superscript $>$ ($<$) indicates the support $\omega' > 0$ ($\omega' < 0$) respectively. In contrast to the $F^>$ and $F^<$ distributions in ω', the distributions $G_\omega^>$ and $G_\omega^<$ cause the mixing between different support regimes in this representation. We thus obtain

(D.10) by sending $\theta(\pm\omega)F^{>(<)} \to \theta(\pm\omega')F_\omega^{>(<)}$ and $\theta(\pm\omega)G^{>(<)} \to \theta(\pm\omega')G_\omega^{>(<)}$ in (5.62). This implies furthermore that the results in (5.67)–(5.73) for the explicit charge four charge cases can be inferred from the replacement $F \to F_\omega$ and $G \to G_\omega$. Then for $Q_{M_2} \neq 0$, the subscripts $>$ and $<$ on the anomalous dimension separate $\omega' > 0$ and $\omega' < 0$, contrary to (5.69).

D.3 Distributions acting on pure powers

In Sec. 5.2, we translate the evolution equation (5.41) to Laplace space in order to find analytic solutions thereafter. There are two ways to obtain the form of the RGEs in Laplace space using the transformation (5.82). In the first approach, we integrate the RGE by $\int \frac{d\omega}{\omega}(\frac{\mu}{\omega})^\eta$ and therefore use the representation in terms of ω-distributions. The second way uses distributions in ω' that affect factors $(\frac{\mu}{\omega'})^{-\eta}$ that enter by expressing the soft function directly in terms of its Laplace transform for $\omega' > 0$ and $\omega' < 0$ respectively. Both strategies lead to the same final results. However, the intermediate steps differ by the outcome of the distributions when they act on pure powers. For distributions in ω, we have

$$\begin{aligned}
\theta(\pm\omega')\int_{-\infty}^{\infty}\frac{d\omega}{\omega-i0}\left(\frac{\mu}{\omega-i0}\right)^\eta F_\omega^{>(<)}(\omega,\omega') &= \theta(\pm\omega')\,\frac{\left(\frac{\mu}{\omega'-i0}\right)^\eta}{\omega'-i0}\,(-H_\eta - H_{-\eta})\,,\\
\theta(\pm\omega')\int_{-\infty}^{\infty}\frac{d\omega}{\omega-i0}\left(\frac{\mu}{\omega-i0}\right)^\eta G_\omega^{>(<)}(\omega,\omega') &= \theta(\pm\omega')\,\frac{\left(\frac{\mu}{\omega'-i0}\right)^\eta}{\omega'-i0}\,(-H_\eta - H_{-\eta})\,, \qquad \text{(D.12)}
\end{aligned}$$

where $-1 < \mathrm{Re}(\eta) < 1$. Note that we implemented $H_\eta - H_{-1-\eta} + \pi\cot(\pi\eta) = 0$, which altogether yields

$$\int_{-\infty}^{\infty}\frac{d\omega}{\omega-i0}\left(\frac{\mu}{\omega-i0}\right)^\eta H_\pm^{(\omega)}(\omega,\omega') = \frac{\left(\frac{\mu}{\omega'-i0}\right)^\eta}{\omega'-i0}(-H_\eta - H_{-\eta})\,. \qquad \text{(D.13)}$$

Hence, the difference $H_+^{(\omega)} - H_-^{(\omega)}$ integrated against pure powers vanishes, which generalizes (5.76) and (5.77). In fact, we recover the latter two equations by taking the η-derivative in (D.13) and setting $\eta \to 0$. As an equivalent observation, we state that $F_\omega^> - G_\omega^>$ and $G_\omega^< - F_\omega^<$ vanish for the two respective support regimes $\omega' > 0$ and $\omega' < 0$.

For the separate transformations that enter with factors of $(\frac{\mu}{-\omega})^\eta$ for $\omega < 0$, we consider the combined expressions for the distributions G_ω which yield

$$\begin{aligned}
\int_{-\infty}^{\infty}\frac{d\omega}{\omega}\left[\theta(\omega)\left(\frac{\mu}{\omega}\right)^\eta + \theta(-\omega)\left(\frac{\mu}{-\omega}\right)^\eta\right]\theta(\pm\omega')G_\omega^{>(<)}(\omega,\omega')&\\
= \frac{\theta(\pm\omega')}{\omega'}\left(\frac{\mu}{\pm\omega'}\right)^\eta(-H_{-\eta} - H_{-1-\eta} - \Gamma(-\eta)\Gamma(1+\eta) \mp i\pi)\,,&
\end{aligned} \qquad \text{(D.14)}$$

that converges in the strip $-1 < \mathrm{Re}(\eta) < 0$. The term the F-distributions in (D.12) remains equivalent and is therefore not listed. To complete our summary, we present the analogous results for the distributions in ω', that are given by

$$\int_{-\infty}^{\infty} d\omega' \left[\theta(\omega') \left(\frac{\mu}{\omega'} \right)^{-\eta} + \theta(-\omega') \left(\frac{\mu}{-\omega'} \right)^{-\eta} \right] \theta(\pm\omega) F^{>(<)}(\omega, \omega') = \theta(\pm\omega) \left(\frac{\mu}{\pm\omega} \right)^{-\eta} \left(-H_\eta - H_{-\eta} + \Gamma(-\eta)\Gamma(1+\eta) \right) , \quad \text{(D.15)}$$

$$\int_{-\infty}^{\infty} d\omega' \left[\theta(\omega') \left(\frac{\mu}{\omega'} \right)^{-\eta} + \theta(-\omega') \left(\frac{\mu}{-\omega'} \right)^{-\eta} \right] \theta(\pm\omega) G^{>(<)}(\omega, \omega') = \theta(\pm\omega) \left(\frac{\mu}{\pm\omega} \right)^{-\eta} \left(-H_{-\eta} - H_{-1-\eta} \mp i\pi \right) . \quad \text{(D.16)}$$

Appendix E

Asymptotic behaviour of hadronic functions

In QCD-only, the asymptotic behaviour of LCDAs can be inferred from conformal symmetry at the critical point of the QCD β function. For the B-LCDA, we explicitly made use of the implications in Appendix B. However, once QED gets involved, we cannot rely on these arguments anymore as we already discussed in Sec. 5.1.1. In that case, we need to study the evolution equations of the hadronic objects analytically and develop different solution strategies. Throughout Chapter 5, we performed Mellin/Laplace transformations to extract the analytic structure of the RGEs and their solutions. Most notably, we found that the asymptotic behaviour for the light meson LCDA and the soft functions receive logarithmic modifications near the "endpoints" $u, \bar{u} = 0$ and $\omega = 0, \omega \to \pm\infty$ respectively.

We derived these modifications for the first time in (5.26) in the case of scale-independent strong and electromagnetic couplings. In the following sections, we provide more details on the derivation of these results and in particular show that the analysis even applies when the one-loop running for the gauge couplings $\alpha_s(\mu)$ and $\alpha_{\text{em}}(\mu)$ is included. For the light meson LCDA, we first consider the inverse Mellin transform in QCD-only to illustrate the strategy of the derivation. For the soft function, we present additional special cases in which we can solve the RGE analytically to all orders in both couplings.

E.1 Inverse Mellin transform in QCD

Before turning to the solution in QCD-only, we begin with some general remarks: The central result of Sec. 5.1.1 shows that the light meson LCDA for $u \to 0$ approaches its asymptotic form $\Phi_M(u;\mu) \sim u(-\ln u)^p$, where the logarithm gets exponentiated with the non-integer power $p = \alpha_{\text{em}} Q_{q_1} Q_M / (\alpha_s C_F + \alpha_{\text{em}} Q_{q_1}(Q_{q_2} - Q_M))$. We obtained this expression from the soft approximation of the evolution kernel in (5.10) and stated that the collinear region of the RGE does not alter this result even with an initial condition of the form $\Phi_M(u;\mu) \sim u^b$ and $b = 1$, for which the soft region diverges in the UV. To this end, we recall that the method of regions relies on the expansion of the integrand irrespective of the fact whether the individual separation converges or

not. In consequence, we introduce an upper cut-off $\Lambda \sim \mathcal{O}(1)$ for the initial function $\hat{\Phi}_M(u;\mu_0) = \theta(\Lambda - u)u^b$ that regulates the UV divergence in the soft region and cancels after the collinear approximation has been added to the result. Since the latter may only supply subleading logarithms $\ln u$, we conclude that the soft approximation already determines the complete asymptotic behaviour for small u. For this particular initial condition, the computation of the small-u behaviour becomes simple since the Mellin transform corresponds to a simple pole at $\eta = b$ given by

$$\tilde{\hat{\Phi}}_M(\eta;\mu_0) = \frac{\Lambda^{b-\eta}}{b-\eta}\,. \tag{E.1}$$

Note that the Mellin transform converges for $\mathrm{Re}(\eta) < b$ and hence we choose $c < b$ for the integration contour of the inverse transformation. We remark that the choice (E.1) captures all important implications for the asymptotic behaviour and can be used without loss of generality.

Now for QCD-only, the above discussion implies that the Mellin space solution for the soft approximation (5.14) including (E.1) becomes

$$\phi_M(u;\mu) = \Lambda^{b_\mu}\, e^{(2\gamma_E - 3/2)a} \int_{c-i\infty}^{c+i\infty} \frac{d\eta}{2\pi i} \left(\frac{u}{\Lambda}\right)^\eta \frac{\Gamma(1-\eta)\Gamma(1+\eta+a)}{\Gamma(1+\eta)\Gamma(1-\eta-a)} \frac{1}{b_\mu - \eta}\,. \tag{E.2}$$

We defined the QCD evolution variable a in (5.15) and $b_\mu \equiv b - a(\mu,\mu_0)$, where the renormalization-scale dependence has been neglected. The integrand of (E.2) is an analytic function in the complex η-plane, except for the points where the numerator Gamma functions and the initial condition is singular. More precisely, there are two strings of poles that are associated to the Gamma functions with $\eta = -1-a-n$ and $\eta = 1+n$ extending to the left and right respectively for non-negative integers $n = 0, 1, 2, \ldots$. The single pole of the initial condition is located at $\eta = b_\mu$. For $u \to 0$, we assume $u < \Lambda$ so that the factor $(u/\Lambda)^\eta$ provides an exponential suppression for the integrand in the limit $\mathrm{Re}(\eta) \to \infty$. We can then deform the integration contour $c \pm \infty$ to a curve enclosing the poles in the right-half plane with respect to c. Due to the asymptotic behaviour of the Gamma functions for $\mathrm{Re}(\eta) \to -\infty$, the contour parameter c must be chosen in the strip $-1-a < c < \min(1, b_\mu)$, which constrains $b > -1$ and $a > -2$ that avoids an overlap between the two sets of Gamma function poles.[1] From the analyticity, we thus conclude that the contour can be further divided into small circles enclosing the poles at $\eta = b_\mu, 1+n$ in mathematically negative direction. Hence, the integral in (E.2) evaluates to the sum of all residues corresponding to these poles. The leading contribution in the limit $u \to 0$ is given by the left-most pole with respect to $\mathrm{Re}(\eta) > c$. We find

$$\phi_M(u;\mu) = e^{(2\gamma_E - 3/2)a} \Lambda^{b_\mu} \sum_{\eta = b_\mu, 1+n} (-1) \cdot \mathrm{Res}\left[\left(\frac{u}{\Lambda}\right)^\eta \frac{\Gamma(1-\eta)\Gamma(1+\eta+a)}{\Gamma(1+\eta)\Gamma(1-\eta-a)} \frac{1}{b_\mu - \eta} \right]$$

[1] At unrealistically high scales, we eventually encounter $a > -2$. In this scenario, we divide the evolution into smaller steps and glue the solutions together in order to obtain an analytic continuation for the entire scale domain.

$$= e^{(2\gamma_E-3/2)a}\left(\frac{\Gamma(1+b)\Gamma(1-b_\mu)}{\Gamma(1-b)\Gamma(1+b_\mu)}\,u^{b_\mu}+\frac{\Lambda^{b_\mu-1}}{b_\mu-1}\frac{\Gamma(2+a)}{\Gamma(-a)}u+\mathcal{O}(u^2)\right). \quad \text{(E.3)}$$

Note that the former term does not depend on the UV regulator Λ, which can be anticipated since it yields the asymptotic behaviour for $b_\mu < 1$ for which the collinear region does not contribute. In this case, the small-u behaviour is entirely dictated by the pole of the initial condition at μ_0. For $b_\mu \to 1$, the regulator Λ cancels after adding the previously suppressed collinear region and the result (E.3) collapses to a finite constant multiplied with u, reflecting the linear endpoint behaviour.

Finally, we summarize that the endpoint behaviour for $u \to 0$ is determined by the exponent b_μ. When the exponent is smaller or larger than one, the solution becomes proportional to u^{b_μ} or linear, respectively. In QCD-only, the evolution variable $a < 0$ is negative such that b_μ always tends to the linear solution. The same arguments apply for the soft approximation in the limit $u \to 1$, which matches the asymptotic form $\phi_M(u;\mu\to\infty) \to 6u\bar{u}$ found by conformal symmetry.

E.2 Inverse Mellin transform in QCD×QED

For the general analysis in QCD×QED, we now prove how the inverse transformations generates the logarithmic modifications of $\ln u$ for the light meson LCDA in (5.26). The derivation directly carries over to the soft functions for which we omit the detailed derivation in the following sections. We separate our discussion into two different cases with respect to the evolution below and above the critical scale (5.27). The phenomenologically relevant case is $\mu < \mu_c$ whereas $\mu_0 > \mu_c$ entails only conceptually interesting corrections. We focus on the former, for which $\mu_0 < \mu < \mu_c$ and the evolution variable $a(\mu,\mu_0) < 0$ is strictly negative. For the QED-generalized solution of the soft region in Mellin space (5.19) together with the initial condition (E.1), we have

$$\begin{aligned}\tilde{\hat{\Phi}}_M(\eta;\mu) &= e^{2\gamma_E a-3\check{a}/2}\,\frac{\Gamma(1-\eta)\Gamma(1+\eta+a)}{\Gamma(1+\eta)\Gamma(1-\eta-a)}\,\frac{\Lambda^{b_\mu-\eta}}{b_\mu-\eta}\\ &\quad\times\exp\left\{-\int_{\mu_0}^{\mu}\frac{d\mu'}{\mu'}\frac{\alpha_{\rm em}(\mu')Q_{q_1}Q_M}{\pi}\left(H_{\eta+a(\mu,\mu')}+H_{-\eta-a(\mu,\mu')}\right)\right\}. \quad \text{(E.4)}\end{aligned}$$

Here, the definition of $b_\mu = b-a$ contains the QCD×QED evolution variable (5.20). The evaluation of the inverse transformation of (E.4) becomes more difficult in the present context due to the non-trivial analytical structure of the exponential containing an additional integration over harmonic numbers in the second line. For negative integers, the harmonic numbers acquire simple pole and thus the μ' integration generates branch cuts along the real η-axis. We recall that for QCD-only, the contour parameters must lie in the strip $-1-a < c < \min(1,b_\mu)$ that divides the non-analytic poles and cuts into strings extending to the left and right, where $H_{\eta+a(\mu,\mu')}$ and $H_{-\eta-a(\mu,\mu')}$ contribute to each region respectively. The asymptotic expansion $H_\eta \sim \ln\eta$ for $|\eta|\to\infty$ justifies that we can shift the contour to encircle the discontinuities on the right-hand side of

$\mathrm{Re}(\eta) = c$ in the small-u limit as in QCD. In complete analogy, the left-most pole or cut for $\mathrm{Re}(\eta) > c$ yields the dominant contribution to the asymptotic expansion of $\Phi_M(u;\mu)$. As long as $b_\mu < 1$, the residue for $\eta = b_\mu$ defines the leading term and thus the LCDA at μ is proportional to u^{b_μ}. For $b_\mu = 1$ or better $b = 1$[2], the structure of the harmonic numbers becomes relevant. More precisely, the exponential factor in (E.4) develops a branch point for $\eta \to 1$ through the simple pole of $H_{-\eta-a(\mu,\mu')} = -1/(1-\eta-a(\mu,\mu')) + \ldots$ The omitted terms correspond to regular terms and poles/cuts advancing further to the right. We thus expand the μ' integral according to

$$-\int_{\mu_0}^{\mu} \frac{d\mu'}{\mu'} \frac{\alpha_{\mathrm{em}}(\mu') Q_{q_1} Q_M}{\pi} H_{-\eta-a(\mu,\mu')} = \int_{\mu_0}^{\mu} \frac{d\mu'}{\mu'} \frac{\alpha_{\mathrm{em}}(\mu') Q_{q_1} Q_M}{\pi} \frac{1}{1-\eta-a(\mu,\mu')} + \text{regular terms and poles/cuts to the right}\,. \tag{E.5}$$

The domain of μ' corresponds to the interval $[a,0]$ for the evolution variable $a(\mu,\mu')$, where $a = a(\mu,\mu_0) < 0$, and hence the entire branch cut in the left-most term acquires a finite length from $\eta = 1$ to $\eta = 1-a$. In general, the exponential of (E.5) generates cuts along the intervals $[1+n, 1-a+n]$ for non-negative integers $n = 0, 1, 2, \ldots$. Since the left-most part for $\eta \to 1$ dominates the asymptotic behaviour, which corresponds to $\mu' \to \mu$, we further expand the integrand denominator in (E.5) to

$$a(\mu,\mu') = -\frac{\alpha_s(\mu) C_F + \alpha_{\mathrm{em}}(\mu) Q_{q_1}(Q_{q_2} - Q_M)}{\pi} \ln\frac{\mu}{\mu'} + \ldots \tag{E.6}$$

Note that we also expanded $\alpha_{\mathrm{em}}(\mu') \to \alpha_{\mathrm{em}}(\mu)$ up to logarithmic corrections from the QED running. Altogether, the integration inside the exponential boils down to

$$-\int_{\mu_0}^{\mu} \frac{d\mu'}{\mu'} \frac{\alpha_{\mathrm{em}}(\mu') Q_{q_1} Q_M}{\pi} H_{-\eta-a(\mu,\mu')} = p(\mu) \ln\frac{1}{1-\eta} + \text{regular terms and poles/cuts further to the right}, \tag{E.7}$$

which formally equals to the scale-independent result in the first term but with one-loop dependence $p(\mu) = \alpha_{\mathrm{em}}(\mu) Q_{q_1} Q_M / (\alpha_s(\mu) C_F + \alpha_{\mathrm{em}}(\mu) Q_{q_1}(Q_{q_2} - Q_M))$. Note that for $\mu < \mu_c$, the exponent $p(\mu) > 0$ is strictly positive. In addition to (E.7), the Laurent expansion $\Gamma(1-\eta)$ contributes with another singular term in (E.4). The remaining terms do not affect the endpoint behaviour for $u \to 1$. Hence, we absorb these terms into a dimensionless constant κ and find for the inverse Mellin transform

$$\hat{\Phi}_M(u;\mu) = \kappa \int_C \frac{d\eta}{2\pi i}\, u^\eta \left(\frac{1}{1-\eta}\right)^{1+p(\mu)} + \mathcal{O}(u^2)\,. \tag{E.8}$$

Based on [172], the choice of the contour C that encircles the discontinuity for $\mathrm{Re}(\eta) > 1$ requires a "careful" decomposition. We divide the contour into a small circle C_ϵ around $\eta = 1$ and two straight lines C_{cut} along the real axis, with a small positive and negative

[2]The initial condition for $b = 1$ below μ_c reflects a stable point of the evolution equation.

imaginary part. More precisely, we parametrize the circle of radius ϵ by $\eta = 1 + \varepsilon e^{i\varphi}$ with $\varphi \in (2\pi, 0)$ and the straight lines by a linear function from $1 + \varepsilon$ to ∞ and vice versa. For these separate contributions, we obtain

$$\hat{\Phi}_M^{C_{\text{cut}}}(u;\mu) = \kappa \int_{1+\varepsilon}^{\infty} \frac{d\eta}{2\pi i}\, u^{\eta}\, \text{disc}\left[\left(\frac{1}{1-\eta}\right)^{1+p}\right] = \kappa\, \frac{u(-\ln u)^p}{\Gamma(1+p)\Gamma(-p)}\Gamma(-p, -\varepsilon \ln u)\ ,$$

$$\hat{\Phi}_M^{C_{\varepsilon}}(u;\mu) = \kappa\, \frac{u(-\ln u)^p}{\Gamma(1+p)\Gamma(-p)} \sum_{n=0}^{\infty} \frac{(-1)^n(-\varepsilon \ln u)^{n-p}}{n!(n-p)}\ . \tag{E.9}$$

In the above, we defined the discontinuity of a function f as $\text{disc}(f(\eta)) = f(\eta + i0) - f(\eta - i0)$ and $\Gamma(-p, -\varepsilon \ln u)$ as the incomplete gamma function

$$\Gamma(-p, -\varepsilon \ln u) = \Gamma(-p) - \sum_{n=0}^{\infty} \frac{(-1)^n(-\varepsilon \ln u)^{n-p}}{n!(n-p)}\ . \tag{E.10}$$

Note that the first $n < p$ terms with $p(\mu) > 0$ diverge for $\epsilon \to 0$ due to ϵ^{n-p}. However, these terms cancel in the sum of both results in (E.9) so that we ultimately find

$$\hat{\Phi}_M(u;\mu) = \hat{\Phi}_M^{C_{\text{cut}}}(u;\mu) + \hat{\Phi}_M^{C_{\varepsilon}}(u;\mu) + \mathcal{O}(u^2) = \frac{\kappa}{\Gamma(1+p(\mu))}\, u(-\ln u)^{p(\mu)} + \mathcal{O}(u^2)\,. \tag{E.11}$$

Finally, this result proves our claim (5.26) for running couplings in QCD×QED.

Lastly, we remark that the above analysis differs for a scale evolution beyond the critical scale with $\mu > \mu_0 > \mu_c$. In this case, the evolution variable $a(\mu, \mu_0) < 0$ turns negative and thus the left-most branch cut of the harmonic number $H_{-\eta - a(\mu,\mu')}$ in (E.4) begins at $\eta = 1 - a$. Hence, depending on the initial condition, the endpoint behaviour for $u \to 0$ either becomes u^{b_μ} or u^{1-a}. For the latter, logarithmic enhancements from $\eta \to 1$ may be generated even though they will not play a physical role, since any evolution at these scale instantaneously produces a behaviour proportional to $u^{1-a(\mu_0+d\mu,\mu_0)}$ where $1 - a(\mu_0 + d\mu, \mu_0) < 1$. We conclude that only the power-like behaviour is relevant, and we can safely assume $b < 1$ for the initial function such that $b_\mu < 1 - a < 1$ and the endpoint behaviour is dictated by the single pole at $\eta = b_\mu$. Hence, above the critical scale in QED, the LCDA always behaves like u^{b_μ}, and eventually the RGE will reach u^{-1} at some finite $\mu \gg \mu_c$, where the evolution equation becomes ill-defined since the convolution with the anomalous dimension (5.5) diverges.

E.3 Soft function for $Q_{M_2} = 0$

In the case of $Q_{M_2} = 0$, the negative supported part of the anomalous dimension (5.66) decouples so that we consider only positive support for each soft function $\Phi_{B,(Q_1,0)}(\omega;\mu)$. This is in fact dictated by the analytic structure of the position space matrix element,

which again allows to consider $t - i0$ and $\omega > 0$ as in QCD-only.[3] The kernel (5.66) then collapses to QCD-like expressions, and we find for the RGE in Laplace space

$$\begin{aligned}\left(\frac{d}{d\ln\mu} - \eta\right)\tilde{\Phi}_{B,(Q_1,0)}(\eta;\mu) = \frac{\alpha_s C_F}{\pi}\bigg[- H_\eta - H_{-\eta} - \partial_\eta + \frac{1}{2}\bigg]\tilde{\Phi}_{B,(Q_1,0)}(\eta;\mu) \\ + \frac{\alpha_{\rm em}}{\pi}\bigg[- (Q_{\rm sp}^2 + 2Q_{\rm sp}Q_{M_1})\,(H_\eta + H_{-\eta} + \partial_\eta) \\ + Q_{\rm sp}Q_{M_1}(H_\eta + H_{-\eta}) + \frac{3}{4}Q_{\rm sp}^2 + \frac{1}{2}Q_d^2\bigg]\tilde{\Phi}_{B,(Q_1,0)}(\eta;\mu)\ ,\end{aligned} \tag{E.12}$$

which agrees to (5.87) for $Q_{M_2} = 0$. Therefore, we obtain an equivalent solution to (5.99), namely

$$\tilde{\Phi}_{B,(Q_1,0)}(\eta;\mu) = e^{V+2\gamma_E a}\left(\frac{\mu}{\mu_0}\right)^\eta \frac{\Gamma(1-\eta)}{\Gamma(1+\eta)}\frac{\Gamma(1+\eta+a)}{\Gamma(1-\eta-a)}\mathcal{F}(\eta;\mu,\mu_0)\tilde{\Phi}_{B,(Q_1,0)}(\eta+a;\mu_0)\ . \tag{E.13}$$

Alternatively, we obtain this result by sending $\tilde{\Phi}_< \to 0$ in (5.108). As a crosscheck, we recover the $\mathcal{O}(\alpha_{\rm em})$ solution (5.125) by expanding (E.13) and the initial condition with (5.116) to first order in $\alpha_{\rm em}$ upon replacing $Q_{M_2} \to 0$.

For the rather simple solution (E.13), we can derive the asymptotic behaviour similar to the light meson LCDA. However, in this context, we are interested in two different limites, that are *i*) $\omega \to 0$ and *ii*) $\omega \to \infty$. We restrict ourselves to the analysis of the exponential model $\Phi_{B,(Q_1,0)}(\omega;\mu_0) = \omega/\omega_0^2 e^{-\omega/\omega_0}\,\theta(\omega)$ at the initial scale, for which the inverse transformation of the solution reads

$$\Phi_{B,(Q_1,0)}(\omega;\mu) = \frac{e^{V+2\gamma_E a}}{\omega_0}\int_{c-i\infty}^{c+i\infty}\frac{d\eta}{2\pi i}\left(\frac{\mu_0}{\omega_0}\right)^a\left(\frac{\omega}{\omega_0}\right)^\eta\frac{\Gamma(1-\eta)\Gamma(1+\eta+a)}{\Gamma(1+\eta)}\mathcal{F}(\eta;\mu,\mu_0)\ , \tag{E.14}$$

where $-1 < a < 0$ and $-1 - a < c < 1 + a$. The function (E.14) acquires the same form as in (E.4) for the soft region of the light meson LCDA. We therefore apply the same procedure of the previous section to the two cases above sparing out particular details.

i) The contour for $\omega \to 0$ encloses the pole and branch cuts to the right of $\mathrm{Re}(\eta) = c$. For $\eta \to 1$, the leading contribution comes from $\Gamma(1-\eta)$ and $\mathcal{F}(\eta;\mu,\mu_0)$ given in (5.97). We find

$$\Phi_{B,(Q_1,0)}(\omega \to 0;\mu) \sim \frac{\omega}{\omega_0^2}\left(-\ln\frac{\omega}{\omega_0}\right)^{p(\mu)}\ , \tag{E.15}$$

[3]The soft Wilson line proportional to Q_{M_2} in the n_+-direction enters with a different relative sign of the $i0$-prescription in the denominator of diagram (a) in (5.45). Hence, the operator acquires singularities in the entire complex plane of the position space variable.

with $p(\mu)$ defined in (5.112). Similar to QCD-only, the soft function for $Q_{M_2} = 0$ becomes linear near the origin, but with a logarithmic modification as in the light LCDA case (5.26). Note that the pole at $\eta = 0$ from the all-order solution does not contribute in this case, so that the results differs to (5.113).

ii) The contour for $\omega \to \infty$ encloses the poles and cuts on the left-hand side of $\mathrm{Re}(\eta) = c$. In this limit, we obtain

$$\Phi_{B,(Q_1,0)}(\omega \to \infty;\mu) \sim \frac{1}{\omega_0}\left(\frac{\omega}{\omega_0}\right)^{-1-a} \ln^{p(\mu_0)}\left(\frac{\omega}{\omega_0}\right) , \tag{E.16}$$

that matches the asymptotic expansion of the all-order result in (5.114) since the evolution variable only contains the charge of Q_{M_1}.

E.4 Soft function for $Q_{M_i} \gg Q_{u,d}$

To understand the structure of the evolution equation for the soft functions, it is instructive to consider a specific unphysical limit, in which the electric quark charges are assumed to be small with respect to the meson charges. For $\otimes = (+,-)$, this implies that we can neglect the Q_{sp}^2 and $Q_{\mathrm{sp}}Q_d$ terms in the anomalous dimension so that the kernel becomes

$$\begin{aligned}\Gamma_{\otimes}^{(a)-(c)}(\omega,\omega';\mu) \approx \frac{\alpha_{\mathrm{em}}}{\pi}\Bigg[&\left(2Q_{\mathrm{sp}}Q_{M_1}\ln\frac{\mu}{\omega - i0} + i\pi(Q_{\mathrm{sp}}+Q_{M_1})Q_{M_2}\right)\delta(\omega-\omega') \\ &+ Q_{\mathrm{sp}}Q_{M_2}H_-(\omega,\omega')\Bigg] ,\end{aligned} \tag{E.17}$$

We further neglect the QCD terms proportional to α_s and thus the kernel (E.17) effectively corresponds to diagrams (a)–(c) of Fig. 5.3 in QED-only. Hence, the $\ominus$-distribution of diagram (a) generates negative support for the soft function, but there is no opposite effect since the $\oplus$-distribution of diagram (e) does not appear. As a consequence, the RGE for $\Phi^{>}$ decouples (in Laplace space), which is the opposite effect of the decoupling from $\Phi_{<}$ in the case of $Q_{M_2} = 0$. In detail, the evolution equations are

$$\begin{aligned}\left(\frac{d}{d\ln\mu} - \eta\right)\tilde{\Phi}_{>}(\eta;\mu) = \frac{\alpha_{\mathrm{em}}}{\pi}\Bigg[&2Q_{\mathrm{sp}}Q_{M_1}(-\partial_\eta - H_{-\eta} - H_{-1-\eta}) \\ &+ Q_{\mathrm{sp}}Q_{M_1}(H_{-\eta}+H_{-1-\eta}) - i\pi Q_{M_1}Q_{M_2}\Bigg]\tilde{\Phi}_{>}(\eta;\mu) ,\end{aligned} \tag{E.18}$$

$$\begin{aligned}\left(\frac{d}{d\ln\mu} - \eta\right)\tilde{\Phi}_{<}(\eta;\mu) = \frac{\alpha_{\mathrm{em}}}{\pi}\Bigg[&2Q_{\mathrm{sp}}Q_{M_1}(-\partial_\eta - H_{\eta} - H_{-\eta}) \\ &+ Q_{\mathrm{sp}}Q_{M_1}(H_{\eta}+H_{-\eta}) - i\pi(Q_{\mathrm{sp}}+Q_{M_2})Q_{M_1}\Bigg]\tilde{\Phi}_{<}(\eta;\mu)\end{aligned}$$

$$+\frac{\alpha_{\rm em}}{\pi}Q_{\rm sp}Q_{M_1}\Gamma(-\eta)\Gamma(1+\eta)\tilde{\Phi}_>(\eta;\mu)\;. \tag{E.19}$$

To solve these equations, we proceed with the methods developed in Sec. 5.2.7 by first solving the first equation on its own and infer the latter by variation of constants. For simplicity, we further consider the electromagnetic coupling to be scale independent. We define the two evolution variables

$$\begin{aligned} V^{\rm QED} &= -\frac{\alpha_{\rm em}}{\pi}\left[Q_{\rm sp}Q_{M_1}\ln^2\frac{\mu}{\mu_0}+i\pi Q_{M_1}Q_{M_2}\ln\frac{\mu}{\mu_0}\right]\,,\\ a^{\rm QED} &= -\frac{\alpha_{\rm em}}{\pi}2Q_{\rm sp}Q_{M_1}\ln\frac{\mu}{\mu_0}\,, \end{aligned} \tag{E.20}$$

for which we drop the QED label in the following. We find the particular solution as a limiting case of (5.108). More precisely, we have

$$\tilde{\Phi}_>(\eta;\mu) = e^V\left(\frac{\mu}{\mu_0}\right)^\eta\left[\frac{\Gamma(-\eta)\Gamma(1-\eta)}{\Gamma(-\eta-a)\Gamma(1-\eta-a)}\right]^{1/2}\tilde{\Phi}_>(\eta+a,\mu_0)\,, \tag{E.21}$$

$$\begin{aligned} \tilde{\Phi}_<(\eta;\mu) &= e^V\left(\frac{\mu}{\mu_0}\right)^\eta\left[\frac{\Gamma(1-\eta)\Gamma(1+\eta+a)}{\Gamma(1+\eta)\Gamma(1-\eta-a)}\right]^{1/2}\left\{\tilde{\Phi}_<(\eta+a,\mu_0)\right.\\ &\quad+\frac{\alpha_{\rm em}Q_{\rm sp}Q_{M_1}}{\pi}\frac{\tilde{\Phi}_>(\eta+a,\mu_0)}{\Gamma^{1/2}(-\eta-a)\Gamma^{1/2}(1+\eta+a)}\\ &\quad\left.\times\int_{\mu_0}^{\mu}\frac{d\mu'}{\mu'}\Gamma^{3/2}(-\eta-a(\mu,\mu'))\Gamma^{3/2}(1+\eta+a(\mu,\mu'))e^{i\alpha_{\rm em}Q_{\rm sp}Q_{M_1}\ln(\mu'/\mu)}\right\}\\ &= e^V\left(\frac{\mu}{\mu_0}\right)^\eta e^{-i\pi\eta}\left[\frac{\Gamma(-\eta)\Gamma(1-\eta)}{\Gamma(-\eta-a)\Gamma(1-\eta-a)}\right]^{1/2}\tilde{\Phi}_>(\eta+a,\mu_0)\\ &\quad\times\left\{1-e^{-i\pi a/2}\left[\frac{\Gamma(-\eta-a)\Gamma(1+\eta+a)}{\Gamma(-\eta)\Gamma(1+\eta)}\right]^{1/2}\right\}\,. \end{aligned} \tag{E.22}$$

The exponent of $1/2$ arises through the Harmonic number exponential that can be calculated exactly for the case of fixed gauge couplings:

$$\frac{\alpha_{\rm em}Q_{\rm sp}Q_{M_1}}{\pi}\int_{\mu_0}^{\mu}\frac{d\mu'}{\mu'}(H_{\eta+a(\mu,\mu')}+H_{-\eta-a(\mu,\mu')}) = -2\gamma_E a-\frac{1}{2}\ln\frac{\Gamma(1-\eta)\Gamma(1+\eta+a)}{\Gamma(1+\eta)\Gamma(1-\eta-a)}\,. \tag{E.23}$$

The scale independence of $\alpha_{\rm em}$ further allows to perform the μ'-integral in the third line of (E.22) explicitly. Rather than in the precise form of the general solution, we are interested in the asymptotic behaviour near the origin. For this purpose, we assume the exponential model (6.1) for which $\tilde{\Phi}_<(\eta,\mu_0)=0$ and

$$\tilde{\Phi}_>(\eta+a,\mu_0) = \frac{1}{\omega_0}\Gamma(1-\eta-a)\left(\frac{\mu_0}{\omega_0}\right)^{\eta+a}\,. \tag{E.24}$$

Applying the inverse transformation to (E.21) and (E.22) with (E.24), we have

$$\Phi_>(\omega;\mu) = \frac{e^V}{\omega_0}\left(\frac{\mu_0}{\omega_0}\right)^a \int_{c-i\infty}^{c+i\infty} \frac{d\eta}{2\pi i}\left(\frac{\omega}{\omega_0}\right)^\eta \left[\frac{\Gamma(-\eta)\Gamma(1-\eta)\Gamma(1-\eta-a)}{\Gamma(-\eta-a)}\right]^{1/2},$$

$$\Phi_<(\omega;\mu) = \frac{e^V}{\omega_0}\left(\frac{\mu_0}{\omega_0}\right)^a \int_{c-i\infty}^{c+i\infty} \frac{d\eta}{2\pi i}\left(\frac{-\omega}{\omega_0}\right)^\eta e^{-i\pi\eta}\left[\frac{\Gamma(-\eta)\Gamma(1-\eta)\Gamma(1-\eta-a)}{\Gamma(-\eta-a)}\right]^{1/2}$$
$$\times\left\{1 - e^{-i\pi a/2}\left[\frac{\Gamma(-\eta-a)\Gamma(1+\eta+a)}{\Gamma(-\eta)\Gamma(1+\eta)}\right]^{1/2}\right\}. \tag{E.25}$$

For QED-only, we have $a > 0$ such that the contour must be chosen in the interval $-1-a < \eta < -a$ based on the analytic structure of the Gamma functions. In the limit $\omega \to 0$, we deform the contour to enclose the cuts extending to the right of $\mathrm{Re}(\eta) = c$. The left-most contributions starts at the branch-point $\eta = -a$ and determines the asymptotic expansion near the origin

$$\Phi_B(\omega;\mu) = \frac{e^V}{\omega_0}\left(\frac{\mu_0}{\omega_0}\right)^a \frac{\Gamma^{1/2}(a)\Gamma^{1/2}(1+a)}{\Gamma(-1/2)} \times \begin{cases} \left(\dfrac{\omega}{\omega_0}\right)^{-a}\left[-\ln\dfrac{\omega}{\omega_0}\right]^{-3/2} & \omega > 0 \\ \left(\dfrac{-\omega}{\omega_0}\right)^{-a} e^{i\pi a}\left[-\ln\dfrac{-\omega}{\omega_0} + i\pi\right]^{-3/2} & \omega < 0 \end{cases}$$
$$= \frac{e^V}{\omega_0}\left(\frac{\mu_0}{\omega_0}\right)^a \frac{\Gamma^{1/2}(a)\Gamma^{1/2}(1+a)}{\Gamma(-1/2)}\left(\frac{\omega - i0}{\omega_0}\right)^{-a}\left[-\ln\frac{\omega-i0}{\omega_0}\right]^{-3/2}. \tag{E.26}$$

In another toy world, we could even change the sign of the quark charges such that $a < 0$. For this case, the pole at $\eta = 0$ dominates the asymptotic expansion and we find

$$\Phi_B(\omega;\mu) = \frac{e^V}{\omega_0}\left(\frac{\mu_0}{\omega_0}\right)^a \frac{\Gamma^{1/2}(1-a)}{\Gamma^{1/2}(-a)\Gamma(1/2)}\left[-\ln\frac{\omega-i0}{\omega_0}\right]^{-1/2}, \tag{E.27}$$

which implies a logarithmic vanishing of the soft function for $\omega \to 0$.

We remark that both results in (E.26) and (E.27) show that the leading term in an asymptotic expansion around the origin for the soft function with $Q_{M_2} \neq 0$ retains the $i0$-prescription of the first inverse-logarithmic moments. Moreover, we can directly observe from (E.25) that the linear term proportional to $\Gamma(1-\eta)$ differs for the negatively supported solution $\Phi_<$. Hence, the $i0$-prescription is broken explicitly at $\mathcal{O}(\omega/\omega_0)$ as expected such that the second inverse moment does not exist in QCD×QED.

Appendix F

Meijer-G functions

The results of Sec. 5.2 are represented most generally in terms of convolution integrals over the so-called Meijer-G functions. These functions arise through complex line integrals of the inverse Laplace transformation in (5.82). To supplement our analysis, we present some fundamental features of the Meijer-G functions based on [173]. For integers $0 \leq m \leq q$ and $0 \leq n \leq p$, we define a Meijer-G function via the complex contour integral

$$G_{p,q}^{m,n}\left(\left.\begin{matrix}\mathbf{a}\\ \mathbf{b}\end{matrix}\right| z\right) = \int_{\mathcal{C}} \frac{d\eta}{2\pi i} z^{\eta} \frac{\prod_{j=1}^{m}\Gamma(b_j-\eta)\prod_{j=1}^{n}\Gamma(1-a_j+\eta)}{\prod_{j=m+1}^{q}\Gamma(1-b_j+\eta)\prod_{j=n+1}^{p}\Gamma(a_j-\eta)}\,, \tag{F.1}$$

with arbitrary coefficients $\mathbf{a} = (a_1, \ldots, a_p)$ and $\mathbf{b} = (b_1, \ldots, b_q)$. In general, there are three possibilities for the choice of the contour $\mathcal{C}$ determined by the analytic properties of the Gamma functions that appear in the integrand. For our studies, we only regard one specific type, that is a straight line from $c - i\infty$ to $c + i\infty$ with the real contour parameter c. The latter is chosen such that the chains of Gamma function poles in the numerator get separated. Then, the contour integral (F.1) yields a finite result as long as $p + q < 2(n + m)$ and $|\arg(z)| < (n + m - (p + q)/2)\pi$. To discuss the asymptotic behaviour, we consider the two relevant limits $z \to 0$ and $z \to \infty$. In the former, we can deform the contour $\mathcal{C}$ to a line beginning and ending at $\mathrm{Re}(\eta) = \infty$ enclosing all poles of $\Gamma(b_j - \eta)$ in the mathematically negative direction. In the latter, we enclose the string of poles from $\Gamma(1 - a_j + \eta)$ in the positive direction with start and end at $\mathrm{Re}(\eta) = -\infty$. Note that for large integers n, m, p, q, the numerical evaluation of the complex contour integral in (F.1) generally becomes difficult.

In our calculations, we used two relevant identities

$$\begin{aligned}\int_0^{\infty} dz\; G_{p,q}^{m,n}\left(\left.\begin{matrix}\mathbf{a}\\ \mathbf{b}\end{matrix}\right|\lambda z\right) G_{\sigma,\tau}^{\mu,\nu}\left(\left.\begin{matrix}\mathbf{c}\\ \mathbf{d}\end{matrix}\right|\omega z\right)\\ = \frac{1}{\lambda} G_{q+\sigma,p+\tau}^{n+\mu,m+\nu}\left(\left.\begin{matrix}-b_1,\cdots-b_m,\mathbf{c},-b_{m+1},\ldots,-b_q\\ -a_1,\ldots,-a_n,\mathbf{d},-a_{n+1},\ldots,-a_p\end{matrix}\right|\frac{\omega}{\lambda}\right),\end{aligned}$$

$$G_{p,q}^{m,n}\left(\begin{matrix}\mathbf{a}\\ \mathbf{b}\end{matrix}\middle| z\right) = G_{q,p}^{n,m}\left(\begin{matrix}1-\mathbf{a}\\ 1-\mathbf{b}\end{matrix}\middle| \frac{1}{z}\right) . \tag{F.2}$$

We refer to the first one as the closure property under integration over positive valued arguments. The latter serves as an inversion formula. From the first identity, we can infer from the Laplace transformation that

$$\int_0^\infty dz\; z^\alpha e^{-\omega z} G_{p,q}^{m,n}\left(\begin{matrix}\mathbf{a}\\ \mathbf{b}\end{matrix}\middle| \lambda z\right) = \omega^{-\alpha-1} G_{p+1,q}^{m,n+1}\left(\begin{matrix}-\alpha,\; \mathbf{a}\\ \mathbf{b}\end{matrix}\middle| \frac{\lambda}{\omega}\right) . \tag{F.3}$$

The above relations were implicitly used for the numerical evaluation of the first-order solution (5.128) and (5.129) in Sec. 6.2.7, for which the exponential model was implemented as the initial condition. One peculiarity is that the Meijer-G functions depending on their coefficients may acquire a singular behaviour at the point $z = 1$. This is in fact already the case in the QCD-only scenario for the function $G_a(z)$ that is defined in (5.93). Since the singularity for $z \to 1$ appears in a convolution, we have to prove on a technical level that the integral exists for any regular initial condition so that the singular term remains integrable. According to [151], we can derive this from an asymptotic expansion of (5.93) around $z = 1$ for which we obtain

$$\lim_{z\to 1} G_{2,2}^{1,1}\left(\begin{matrix}-a,\; 1-a\\ 1,\; 0\end{matrix}\middle| z\right) = -\frac{\sin \pi a}{\pi}\frac{\Gamma(1+2a)}{|1-z|^{1+2a}} + \mathcal{O}(1) . \tag{F.4}$$

Note that for realistic cases, we consider $-1 < a < 0$ such that the singular term becomes integrable. We neglect the explicit analysis for the remaining Meijer-G functions in the main text since it is generally more complicated. However, from the coefficients that enter these functions, we conclude that the singular terms behave like $|1-z|^{-1-2a}$ such that we only encounter integrable singularities and hence $\Phi_{B,\otimes}^{(1)}$ in (5.128) and (5.129) remains finite at any point.

Bibliography

[1] ATLAS collaboration, *Observation of a new particle in the search for the Standard Model Higgs boson with the ATLAS detector at the LHC*, *Phys. Lett. B* **716** (2012) 1 [1207.7214].

[2] CMS collaboration, *Observation of a New Boson at a Mass of 125 GeV with the CMS Experiment at the LHC*, *Phys. Lett. B* **716** (2012) 30 [1207.7235].

[3] S. L. Glashow, *Partial Symmetries of Weak Interactions*, *Nucl. Phys.* **22** (1961) 579.

[4] N. Cabibbo, *Unitary Symmetry and Leptonic Decays*, *Phys. Rev. Lett.* **10** (1963) 531.

[5] A. Salam and J. C. Ward, *Electromagnetic and weak interactions*, *Phys. Lett.* **13** (1964) 168.

[6] F. Englert and R. Brout, *Broken Symmetry and the Mass of Gauge Vector Mesons*, *Phys. Rev. Lett.* **13** (1964) 321.

[7] P. W. Higgs, *Broken Symmetries and the Masses of Gauge Bosons*, *Phys. Rev. Lett.* **13** (1964) 508.

[8] S. Weinberg, *A Model of Leptons*, *Phys. Rev. Lett.* **19** (1967) 1264.

[9] M. Kobayashi and T. Maskawa, *CP Violation in the Renormalizable Theory of Weak Interaction*, *Prog. Theor. Phys.* **49** (1973) 652.

[10] H. Fritzsch, M. Gell-Mann and H. Leutwyler, *Advantages of the Color Octet Gluon Picture*, *Phys. Lett. B* **47** (1973) 365.

[11] SLAC-SP-017 collaboration, *Discovery of a Narrow Resonance in e^+e^- Annihilation*, *Phys. Rev. Lett.* **33** (1974) 1406.

[12] E598 collaboration, *Experimental Observation of a Heavy Particle J*, *Phys. Rev. Lett.* **33** (1974) 1404.

[13] E288 collaboration, *Observation of a Dimuon Resonance at 9.5-GeV in 400-GeV Proton-Nucleus Collisions*, *Phys. Rev. Lett.* **39** (1977) 252.

[14] CDF collaboration, *Observation of top quark production in $\bar{p}p$ collisions*, *Phys. Rev. Lett.* **74** (1995) 2626 [hep-ex/9503002].

[15] Particle Data Group collaboration, *Review of Particle Physics*, *PTEP* **2022** (2022) 083C01.

[16] LIGO Scientific, Virgo collaboration, *Observation of Gravitational Waves from a Binary Black Hole Merger*, *Phys. Rev. Lett.* **116** (2016) 061102 [1602.03837].

[17] D. Clowe, M. Bradac, A. H. Gonzalez, M. Markevitch, S. W. Randall, C. Jones et al., *A direct empirical proof of the existence of dark matter*, *Astrophys. J. Lett.* **648** (2006) L109 [astro-ph/0608407].

[18] B. T. Cleveland, T. Daily, R. Davis, Jr., J. R. Distel, K. Lande, C. K. Lee et al., *Measurement of the solar electron neutrino flux with the Homestake chlorine detector*, *Astrophys. J.* **496** (1998) 505.

[19] Super-Kamiokande collaboration, *Measurements of the solar neutrino flux from Super-Kamiokande's first 300 days*, *Phys. Rev. Lett.* **81** (1998) 1158 [hep-ex/9805021].

[20] T. Aoyama et al., *The anomalous magnetic moment of the muon in the Standard Model*, *Phys. Rept.* **887** (2020) 1 [2006.04822].

[21] FCC collaboration, *FCC Physics Opportunities: Future Circular Collider Conceptual Design Report Volume 1*, *Eur. Phys. J. C* **79** (2019) 474.

[22] FCC collaboration, *FCC-ee: The Lepton Collider: Future Circular Collider Conceptual Design Report Volume 2*, *Eur. Phys. J. ST* **228** (2019) 261.

[23] FCC collaboration, *FCC-hh: The Hadron Collider: Future Circular Collider Conceptual Design Report Volume 3*, *Eur. Phys. J. ST* **228** (2019) 755.

[24] BaBar, Belle collaboration, *The Physics of the B Factories*, *Eur. Phys. J. C* **74** (2014) 3026 [1406.6311].

[25] Belle-II collaboration, *The Belle II Physics Book*, *PTEP* **2019** (2019) 123C01 [1808.10567].

[26] HFLAV collaboration, *Averages of b-hadron, c-hadron, and τ-lepton properties as of 2021*, 2206.07501.

[27] LHCb collaboration, *Test of lepton universality in $b \to s\ell^+\ell^-$ decays*, 2212.09152.

[28] LHCb collaboration, *Measurement of lepton universality parameters in $B^+ \to K^+\ell^+\ell^-$ and $B^0 \to K^{*0}\ell^+\ell^-$ decays*, 2212.09153.

[29] K. G. Wilson, *Nonlagrangian models of current algebra*, *Phys. Rev.* **179** (1969) 1499.

[30] K. G. Wilson and W. Zimmermann, *Operator product expansions and composite field operators in the general framework of quantum field theory*, *Commun. Math. Phys.* **24** (1972) 87.

[31] D. Becirevic, B. Haas and E. Kou, *Soft Photon Problem in Leptonic B-decays*, *Phys. Lett. B* **681** (2009) 257 [0907.1845].

[32] A. J. Buras, *Weak Hamiltonian, CP violation and rare decays*, in *Les Houches Summer School in Theoretical Physics, Session 68: Probing the Standard Model of Particle Interactions*, pp. 281–539, 6, 1998, hep-ph/9806471.

[33] M. Beneke and J. Rohrwild, *B meson distribution amplitude from $B \to \gamma \ell \nu$*, *Eur. Phys. J. C* **71** (2011) 1818 [1110.3228].

[34] E. Lunghi, D. Pirjol and D. Wyler, *Factorization in leptonic radiative $B \to \gamma e \nu$ decays*, *Nucl. Phys. B* **649** (2003) 349 [hep-ph/0210091].

[35] S. W. Bosch, R. J. Hill, B. O. Lange and M. Neubert, *Factorization and Sudakov resummation in leptonic radiative B decay*, *Phys. Rev. D* **67** (2003) 094014 [hep-ph/0301123].

[36] A. G. Grozin and M. Neubert, *Asymptotics of heavy meson form-factors*, *Phys. Rev. D* **55** (1997) 272 [hep-ph/9607366].

[37] M. Beneke, G. Buchalla, M. Neubert and C. T. Sachrajda, *QCD factorization for $B \to \pi\pi$ decays: Strong phases and CP violation in the heavy quark limit*, *Phys. Rev. Lett.* **83** (1999) 1914 [hep-ph/9905312].

[38] V. M. Braun, D. Y. Ivanov and G. P. Korchemsky, *The B meson distribution amplitude in QCD*, *Phys. Rev. D* **69** (2004) 034014 [hep-ph/0309330].

[39] V. Pilipp, *Matching of lambda$_B$ onto HQET*, hep-ph/0703180.

[40] W. Wang, Y.-M. Wang, J. Xu and S. Zhao, *B-meson light-cone distribution amplitude from Euclidean quantities*, *Phys. Rev. D* **102** (2020) 011502 [1908.09933].

[41] S. Zhao and A. V. Radyushkin, *B-meson Ioffe-time distribution amplitude at short distances*, *Phys. Rev. D* **103** (2021) 054022 [2006.05663].

[42] C. Kane, D. Giusti, C. Lehner, S. Meinel and A. Soni, *Controlling unwanted exponentials in lattice calculations of radiative leptonic decays*, *PoS* **LATTICE2021** (2022) 162 [2110.13196].

[43] P. A. Boyle et al., *A lattice QCD perspective on weak decays of b and c quarks Snowmass 2022 White Paper*, in *2022 Snowmass Summer Study*, 5, 2022, 2205.15373.

[44] D. Giusti, C. F. Kane, C. Lehner, S. Meinel and A. Soni, *High-precision determination of radiative-leptonic-decay form factors using lattice QCD: a study of methods*, 2302.01298.

[45] M. Beneke, P. Böer, P. Rigatos and K. K. Vos, *QCD factorization of the four-lepton decay $B^- \to \ell\bar{\nu}_\ell\ell^{(\prime)}\bar{\ell}^{(\prime)}$*, *Eur. Phys. J. C* **81** (2021) 638 [2102.10060].

[46] C. Wang, Y.-M. Wang and Y.-B. Wei, *QCD factorization for the four-body leptonic B-meson decays*, *JHEP* **02** (2022) 141 [2111.11811].

[47] M. Beneke, V. M. Braun, Y. Ji and Y.-B. Wei, *Radiative leptonic decay $B \to \gamma\ell\nu_\ell$ with subleading power corrections*, *JHEP* **07** (2018) 154 [1804.04962].

[48] M. Beneke, G. Buchalla, M. Neubert and C. T. Sachrajda, *QCD factorization for exclusive, nonleptonic B meson decays: General arguments and the case of heavy light final states*, *Nucl. Phys. B* **591** (2000) 313 [hep-ph/0006124].

[49] M. Beneke and S. Jager, *Spectator scattering at NLO in non-leptonic b decays: Tree amplitudes*, *Nucl. Phys. B* **751** (2006) 160 [hep-ph/0512351].

[50] M. Beneke and S. Jager, *Spectator scattering at NLO in non-leptonic B decays: Leading penguin amplitudes*, *Nucl. Phys. B* **768** (2007) 51 [hep-ph/0610322].

[51] G. Bell, *NNLO vertex corrections in charmless hadronic B decays: Imaginary part*, *Nucl. Phys. B* **795** (2008) 1 [0705.3127].

[52] G. Bell, *NNLO vertex corrections in charmless hadronic B decays: Real part*, *Nucl. Phys. B* **822** (2009) 172 [0902.1915].

[53] M. Beneke, T. Huber and X.-Q. Li, *NNLO vertex corrections to non-leptonic B decays: Tree amplitudes*, *Nucl. Phys. B* **832** (2010) 109 [0911.3655].

[54] C. S. Kim and Y. W. Yoon, *Order α_s^2 magnetic penguin correction for B decay to light mesons*, *JHEP* **11** (2011) 003 [1107.1601].

[55] G. Bell, M. Beneke, T. Huber and X.-Q. Li, *Two-loop current–current operator contribution to the non-leptonic QCD penguin amplitude*, *Phys. Lett. B* **750** (2015) 348 [1507.03700].

[56] G. Bell, M. Beneke, T. Huber and X.-Q. Li, *Two-loop non-leptonic penguin amplitude in QCD factorization*, *JHEP* **04** (2020) 055 [2002.03262].

[57] A. J. Buras, R. Fleischer, S. Recksiegel and F. Schwab, *Anatomy of prominent B and K decays and signatures of CP violating new physics in the electroweak penguin sector*, *Nucl. Phys. B* **697** (2004) 133 [hep-ph/0402112].

[58] N. B. Beaudry, A. Datta, D. London, A. Rashed and J.-S. Roux, *The $B \to \pi K$ puzzle revisited*, *JHEP* **01** (2018) 074 [1709.07142].

[59] M. Beneke, C. Bobeth and R. Szafron, *Enhanced electromagnetic correction to the rare B-meson decay $B_{s,d} \to \mu^+\mu^-$*, *Phys. Rev. Lett.* **120** (2018) 011801 [1708.09152].

[60] M. Beneke, C. Bobeth and R. Szafron, *Power-enhanced leading-logarithmic QED corrections to $B_q \to \mu^+\mu^-$*, *JHEP* **10** (2019) 232 [1908.07011].

[61] M. Bordone, G. Isidori and A. Pattori, *On the Standard Model predictions for R_K and R_{K^*}*, *Eur. Phys. J. C* **76** (2016) 440 [1605.07633].

[62] G. Isidori, S. Nabeebaccus and R. Zwicky, *QED corrections in $\bar{B} \to \bar{K}\ell^+\ell^-$ at the double-differential level*, *JHEP* **12** (2020) 104 [2009.00929].

[63] D. Mishra and N. Mahajan, *Impact of soft photons on $B \to K\ell^+\ell^-$*, *Phys. Rev. D* **103** (2021) 056022 [2010.10853].

[64] G. Isidori, D. Lancierini, S. Nabeebaccus and R. Zwicky, *Qed in $\bar{B} \to \bar{K}\ell^+\ell^-$ lfu ratios: theory versus experiment, a monte carlo study*, *JHEP* **10** (2022) 146 [2205.08635].

[65] T. Feldmann, N. Gubernari, T. Huber and N. Seitz, *On the contribution of the electromagnetic dipole operator $\mathcal{O}_7$ to the $\bar{B}_s \to \mu^+\mu^-$ decay amplitude*, 2211.04209.

[66] M. Beneke, P. Böer, J.-N. Toelstede and K. K. Vos, *QED factorization of non-leptonic B decays*, *JHEP* **11** (2020) 081 [2008.10615].

[67] M. Beneke, P. Böer, G. Finauri and K. K. Vos, *QED factorization of two-body non-leptonic and semi-leptonic B to charm decays*, 2107.03819.

[68] M. Beneke, P. Böer, J.-N. Toelstede and K. K. Vos, *Light-cone distribution amplitudes of heavy mesons with QED effects*, *JHEP* **08** (2022) 020 [2204.09091].

[69] Flavour Lattice Averaging Group (FLAG) collaboration, *FLAG Review 2021*, *Eur. Phys. J. C* **82** (2022) 869 [2111.09849].

[70] P. Ball and R. Zwicky, *New results on $B \to \pi, K, \eta$ decay formfactors from light-cone sum rules*, *Phys. Rev. D* **71** (2005) 014015 [hep-ph/0406232].

[71] F. De Fazio, T. Feldmann and T. Hurth, *Light-cone sum rules in soft-collinear effective theory*, *Nucl. Phys. B* **733** (2006) 1 [hep-ph/0504088].

[72] A. Khodjamirian, T. Mannel and N. Offen, *B-meson distribution amplitude from the $B \to \pi$ form-factor*, *Phys. Lett. B* **620** (2005) 52 [hep-ph/0504091].

[73] T. Hurth, F. De Fazio and T. Feldmann, *The $B \to \pi$ form-factor from light-cone sum rules in soft-collinear effective theory*, *PoS* **HEP2005** (2006) 215 [hep-ph/0509167].

[74] Y.-M. Wang and Y.-L. Shen, *QCD corrections to $B \to \pi$ form factors from light-cone sum rules*, *Nucl. Phys. B* **898** (2015) 563 [1506.00667].

[75] N. Gubernari, A. Kokulu and D. van Dyk, *$B \to P$ and $B \to V$ Form Factors from B-Meson Light-Cone Sum Rules beyond Leading Twist*, *JHEP* **01** (2019) 150 [1811.00983].

[76] J. Gao, C.-D. Lü, Y.-L. Shen, Y.-M. Wang and Y.-B. Wei, *Precision calculations of $B \to V$ form factors from soft-collinear effective theory sum rules on the light-cone*, *Phys. Rev. D* **101** (2020) 074035 [1907.11092].

[77] A. Khodjamirian, T. Mannel and M. Melcher, *Kaon distribution amplitude from QCD sum rules*, *Phys. Rev. D* **70** (2004) 094002 [hep-ph/0407226].

[78] S. S. Agaev, V. M. Braun, N. Offen and F. A. Porkert, *Light Cone Sum Rules for the $\pi^0 \to \gamma^\gamma$ Form Factor Revisited*, *Phys. Rev. D* **83** (2011) 054020 [1012.4671].

[79] S. Cheng, A. Khodjamirian and A. V. Rusov, *Pion light-cone distribution amplitude from the pion electromagnetic form factor*, *Phys. Rev. D* **102** (2020) 074022 [2007.05550].

[80] BaBar collaboration, *Precise Measurement of the $e^+e^- \to \pi^+\pi^-(\gamma)$ Cross Section with the Initial-State Radiation Method at BABAR*, *Phys. Rev. D* **86** (2012) 032013 [1205.2228].

[81] S. S. Agaev, V. M. Braun, N. Offen and F. A. Porkert, *BELLE Data on the $\pi^0\gamma^*\gamma$ Form Factor: A Game Changer?*, *Phys. Rev. D* **86** (2012) 077504 [1206.3968].

[82] P. Böer, A. Kokulu, J.-N. Toelstede and D. van Dyk, *Angular Analysis of $\Lambda_b \to \Lambda_c(\to \Lambda\pi)\ell\bar{\nu}$*, *JHEP* **12** (2019) 082 [1907.12554].

[83] M. Beneke and T. Feldmann, *Symmetry breaking corrections to heavy to light B meson form-factors at large recoil*, *Nucl. Phys. B* **592** (2001) 3 [hep-ph/0008255].

[84] M. Beneke and V. A. Smirnov, *Asymptotic expansion of Feynman integrals near threshold*, *Nucl. Phys. B* **522** (1998) 321 [hep-ph/9711391].

[85] V. A. Smirnov, *Applied asymptotic expansions in momenta and masses*, *Springer Tracts Mod. Phys.* **177** (2002) 1.

[86] K. H. Phan and T. Riemann, *Scalar 1-loop Feynman integrals as meromorphic functions in space-time dimension d*, *Phys. Lett. B* **791** (2019) 257 [1812.10975].

[87] J. Blümlein, M. Saragnese and C. Schneider, *Hypergeometric Structures in Feynman Integrals*, 2111.15501.

[88] M. Beneke and T. Feldmann, *Factorization of heavy to light form-factors in soft collinear effective theory*, *Nucl. Phys. B* **685** (2004) 249 [hep-ph/0311335].

[89] M. Beneke and V. M. Braun, *Heavy quark effective theory beyond perturbation theory: Renormalons, the pole mass and the residual mass term*, *Nucl. Phys. B* **426** (1994) 301 [hep-ph/9402364].

[90] H. Georgi, *An Effective Field Theory for Heavy Quarks at Low-energies*, *Phys. Lett. B* **240** (1990) 447.

[91] M. Neubert, *Heavy quark symmetry*, *Phys. Rept.* **245** (1994) 259 [hep-ph/9306320].

[92] M. Neubert, *Reparametrization invariance and the expansion of currents in the heavy quark effective theory*, *Phys. Lett. B* **306** (1993) 357 [hep-ph/9302269].

[93] A. G. Grozin, *Heavy quark effective theory*, *Springer Tracts Mod. Phys.* **201** (2004) 1.

[94] C. W. Bauer, S. Fleming and M. E. Luke, *Summing Sudakov logarithms in $B \to X_s\gamma$ in effective field theory*, *Phys. Rev. D* **63** (2000) 014006 [hep-ph/0005275].

[95] C. W. Bauer, D. Pirjol and I. W. Stewart, *Soft collinear factorization in effective field theory*, *Phys. Rev. D* **65** (2002) 054022 [hep-ph/0109045].

[96] C. W. Bauer and I. W. Stewart, *Invariant operators in collinear effective theory*, *Phys. Lett. B* **516** (2001) 134 [hep-ph/0107001].

[97] M. Beneke, A. P. Chapovsky, M. Diehl and T. Feldmann, *Soft collinear effective theory and heavy to light currents beyond leading power*, *Nucl. Phys. B* **643** (2002) 431 [hep-ph/0206152].

[98] C. W. Bauer, D. Pirjol and I. W. Stewart, *Factorization and endpoint singularities in heavy to light decays*, *Phys. Rev. D* **67** (2003) 071502 [hep-ph/0211069].

[99] M. Beneke and T. Feldmann, *Multipole expanded soft collinear effective theory with non Abelian gauge symmetry*, *Phys. Lett. B* **553** (2003) 267 [hep-ph/0211358].

[100] C. W. Bauer, D. Pirjol and I. W. Stewart, *On Power suppressed operators and gauge invariance in SCET*, *Phys. Rev. D* **68** (2003) 034021 [hep-ph/0303156].

[101] T. Becher, A. Broggio and A. Ferroglia, *Introduction to Soft-Collinear Effective Theory*, vol. 896. Springer, 2015, 10.1007/978-3-319-14848-9, [1410.1892].

[102] M. Beneke, Y. Kiyo and D. s. Yang, *Loop corrections to subleading heavy quark currents in SCET*, *Nucl. Phys. B* **692** (2004) 232 [hep-ph/0402241].

[103] M. E. Luke and A. V. Manohar, *Reparametrization invariance constraints on heavy particle effective field theories*, *Phys. Lett. B* **286** (1992) 348 [hep-ph/9205228].

[104] A. V. Manohar, T. Mehen, D. Pirjol and I. W. Stewart, *Reparameterization invariance for collinear operators*, *Phys. Lett. B* **539** (2002) 59 [hep-ph/0204229].

[105] R. J. Hill, T. Becher, S. J. Lee and M. Neubert, *Sudakov resummation for subleading SCET currents and heavy-to-light form-factors*, *JHEP* **07** (2004) 081 [hep-ph/0404217].

[106] M. Beneke and D. Yang, *Heavy-to-light B meson form-factors at large recoil energy: Spectator-scattering corrections*, *Nucl. Phys. B* **736** (2006) 34 [hep-ph/0508250].

[107] G. Bell, M. Beneke, T. Huber and X.-Q. Li, *Heavy-to-light currents at NNLO in SCET and semi-inclusive $\bar{B} \to X_s l^+ l^-$ decay*, *Nucl. Phys. B* **843** (2011) 143 [1007.3758].

[108] C. W. Bauer, S. Fleming, D. Pirjol and I. W. Stewart, *An Effective field theory for collinear and soft gluons: Heavy to light decays*, *Phys. Rev. D* **63** (2001) 114020 [hep-ph/0011336].

[109] T. Becher, M. Neubert and B. D. Pecjak, *Factorization and Momentum-Space Resummation in Deep-Inelastic Scattering*, *JHEP* **01** (2007) 076 [hep-ph/0607228].

[110] A. M. Polyakov, *Gauge Fields as Rings of Glue*, *Nucl. Phys. B* **164** (1980) 171.

[111] G. P. Korchemsky and A. V. Radyushkin, *Loop Space Formalism and Renormalization Group for the Infrared Asymptotics of QCD*, *Phys. Lett. B* **171** (1986) 459.

[112] P. A. Baikov, K. G. Chetyrkin and J. H. Kühn, *Five-Loop Running of the QCD coupling constant*, *Phys. Rev. Lett.* **118** (2017) 082002 [1606.08659].

[113] Y. Schroder and M. Steinhauser, *Four-loop decoupling relations for the strong coupling*, *JHEP* **01** (2006) 051 [hep-ph/0512058].

[114] K. G. Chetyrkin, J. H. Kuhn and C. Sturm, *QCD decoupling at four loops*, *Nucl. Phys. B* **744** (2006) 121 [hep-ph/0512060].

[115] Y.-M. Wang, *Factorization and dispersion relations for radiative leptonic B decay*, *JHEP* **09** (2016) 159 [1606.03080].

[116] M. A. Ebert, I. Moult, I. W. Stewart, F. J. Tackmann, G. Vita and H. X. Zhu, *Subleading power rapidity divergences and power corrections for q_T*, *JHEP* **04** (2019) 123 [1812.08189].

[117] P. Böer, *QCD Factorisation in Exclusive Semileptonic B Decays New Applications and Resummation of Rapidity Logarithms*, Ph.D. thesis, Siegen U., 2018.

[118] M. Beneke, M. Garny, R. Szafron and J. Wang, *Violation of the Kluberg-Stern-Zuber theorem in SCET*, *JHEP* **09** (2019) 101 [1907.05463].

[119] Z. L. Liu, B. Mecaj, M. Neubert and X. Wang, *Factorization at subleading power and endpoint divergences in $h \to \gamma\gamma$ decay. Part II. Renormalization and scale evolution*, *JHEP* **01** (2021) 077 [2009.06779].

[120] Z. L. Liu, B. Mecaj, M. Neubert and X. Wang, *Factorization at subleading power, Sudakov resummation, and endpoint divergences in soft-collinear effective theory*, *Phys. Rev. D* **104** (2021) 014004 [2009.04456].

[121] G. Bell, P. Böer and T. Feldmann, *Muon-electron backward scattering: a prime example for endpoint singularities in SCET*, *JHEP* **09** (2022) 183 [2205.06021].

[122] M. Beneke, M. Garny, S. Jaskiewicz, J. Strohm, R. Szafron, L. Vernazza et al., *Next-to-leading power endpoint factorization and resummation for off-diagonal "gluon" thrust*, *JHEP* **07** (2022) 144 [2205.04479].

[123] I. I. Balitsky and V. M. Braun, *Evolution Equations for QCD String Operators*, *Nucl. Phys. B* **311** (1989) 541.

[124] V. M. Braun, Y. Ji and A. N. Manashov, *Higher-twist B-meson Distribution Amplitudes in HQET*, *JHEP* **05** (2017) 022 [1703.02446].

[125] H. Kawamura, J. Kodaira, C.-F. Qiao and K. Tanaka, *B-meson light cone distribution amplitudes in the heavy quark limit*, *Phys. Lett. B* **523** (2001) 111 [hep-ph/0109181].

[126] A. Khodjamirian, *Form-factors of $\gamma^*\rho \to \pi$ and $\gamma^*\gamma \to \pi^0$ transitions and light cone sum rules*, *Eur. Phys. J. C* **6** (1999) 477 [hep-ph/9712451].

[127] V. M. Braun and A. Khodjamirian, *Soft contribution to $B \to \gamma\ell\nu_\ell$ and the B-meson distribution amplitude*, *Phys. Lett. B* **718** (2013) 1014 [1210.4453].

[128] T. Muta, *Foundations of Quantum Chromodynamics: An Introduction to Perturbative Methods in Gauge Theories, (3rd ed.)*, vol. 78 of *World scientific Lecture Notes in Physics*. World Scientific, Hackensack, N.J., 3rd ed., 2010.

[129] P. Colangelo and A. Khodjamirian, *QCD sum rules, a modern perspective*, hep-ph/0010175.

[130] M. Beneke, P. Böer, J.-N. Toelstede and K. K. Vos, *Light-cone distribution amplitudes of light mesons with QED effects*, *JHEP* **11** (2021) 059 [2108.05589].

[131] A. Sirlin, *Large m_W, m_Z Behavior of the $\mathcal{O}alpha_s$ Corrections to Semileptonic Processes Mediated by W*, *Nucl. Phys. B* **196** (1982) 83.

[132] K. G. Chetyrkin, M. Misiak and M. Munz, *$|\Delta F| = 1$ nonleptonic effective Hamiltonian in a simpler scheme*, *Nucl. Phys.* **B520** (1998) 279 [hep-ph/9711280].

[133] B. O. Lange and M. Neubert, *Factorization and the soft overlap contribution to heavy to light form-factors*, *Nucl. Phys. B* **690** (2004) 249 [hep-ph/0311345].

[134] G. P. Lepage and S. J. Brodsky, *Exclusive Processes in Quantum Chromodynamics: Evolution Equations for Hadronic Wave Functions and the Form-Factors of Mesons*, *Phys. Lett.* **87B** (1979) 359.

[135] G. P. Lepage and S. J. Brodsky, *Exclusive Processes in Perturbative Quantum Chromodynamics*, *Phys. Rev.* **D22** (1980) 2157.

[136] A. V. Efremov and A. V. Radyushkin, *Factorization and Asymptotical Behavior of Pion Form-Factor in QCD*, *Phys. Lett.* **94B** (1980) 245.

[137] E. Baracchini and G. Isidori, *Electromagnetic corrections to non-leptonic two-body B and D decays*, *Phys. Lett. B* **633** (2006) 309 [hep-ph/0508071].

[138] S. Fleming, A. H. Hoang, S. Mantry and I. W. Stewart, *Jets from massive unstable particles: Top-mass determination*, *Phys. Rev. D* **77** (2008) 074010 [hep-ph/0703207].

[139] C. Lee, P. Shrivastava and V. Vaidya, *Predictions for energy correlators probing substructure of groomed heavy quark jets*, *JHEP* **09** (2019) 045 [1901.09095].

[140] L. Dai, C. Kim and A. K. Leibovich, *Heavy quark jet production near threshold*, *JHEP* **09** (2021) 148 [2104.14707].

[141] A. von Manteuffel, R. M. Schabinger and H. X. Zhu, *The two-loop soft function for heavy quark pair production at future linear colliders*, *Phys. Rev. D* **92** (2015) 045034 [1408.5134].

[142] D. Giusti, V. Lubicz, G. Martinelli, C. T. Sachrajda, F. Sanfilippo, S. Simula et al., *First lattice calculation of the QED corrections to leptonic decay rates*, *Phys. Rev. Lett.* **120** (2018) 072001 [1711.06537].

[143] C. T. Sachrajda, M. Di Carlo, G. Martinelli, D. Giusti, V. Lubicz, F. Sanfilippo et al., *Radiative corrections to semileptonic decay rates*, *PoS* **LATTICE2019** (2019) 162 [1910.07342].

[144] G. M. de Divitiis et al., *Real photon emissions in leptonic decays*, 1908.10160.

[145] C. Kane, C. Lehner, S. Meinel and A. Soni, *Radiative leptonic decays on the lattice*, *PoS* **LATTICE2019** (2019) 134 [1907.00279].

[146] M. Beneke, *Helmholtz International Summer School on "Heavy Quark Physics", Lectures on Soft-Collinear Effective Theory*, *Dubna* (2005) .

[147] T. Becher and M. Neubert, *Drell-Yan Production at Small q_T, Transverse Parton Distributions and the Collinear Anomaly*, *Eur. Phys. J. C* **71** (2011) 1665 [1007.4005].

[148] V. M. Braun, G. P. Korchemsky and D. Müller, *The Uses of Conformal Symmetry in QCD*, *Prog. Part. Nucl. Phys.* **51** (2003) 311 [hep-ph/0306057].

[149] V. M. Braun, A. N. Manashov, S. O. Moch and M. Strohmaier, *Conformal symmetry of QCD in d-dimensions*, *Phys. Lett. B* **793** (2019) 78 [1810.04993].

[150] G. Bell, T. Feldmann, Y.-M. Wang and M. W. Y. Yip, *Light-Cone Distribution Amplitudes for Heavy-Quark Hadrons*, *JHEP* **11** (2013) 191 [1308.6114].

[151] Z. L. Liu, B. Mecaj, M. Neubert, X. Wang and S. Fleming, *Renormalization and Scale Evolution of the Soft-Quark Soft Function*, *JHEP* **07** (2020) 104 [2005.03013].

[152] B. O. Lange and M. Neubert, *Renormalization-Group Evolution of the B-Meson Light-Cone Distribution Amplitude*, *Phys. Rev. Lett.* **91** (2003) 102001 [hep-ph/0303082].

[153] S. Actis, M. Beneke, P. Falgari and C. Schwinn, *Dominant NNLO corrections to four-fermion production near the W-pair production threshold*, *Nucl. Phys. B* **807** (2009) 1 [0807.0102].

[154] G. Bell and T. Feldmann, *Modelling light-cone distribution amplitudes from non-relativistic bound states*, *JHEP* **04** (2008) 061 [0802.2221].

[155] V. M. Braun and A. N. Manashov, *Conformal symmetry of the Lange-Neubert evolution equation*, *Phys. Lett. B* **731** (2014) 316 [1402.5822].

[156] M. Beneke, P. Boeer, Y. Ji and J.-N. Toelstede, *Euclidean QCD correlators with subleading power corrections*, *in preparation* (2023) .

[157] T. Nishikawa and K. Tanaka, *QCD Sum Rules for Quark-Gluon Three-Body Components in the B Meson*, *Nucl. Phys. B* **879** (2014) 110 [1109.6786].

[158] M. Beneke and M. Neubert, *QCD factorization for $B \to PP$ and $B \to PV$ decays*, *Nucl. Phys.* **B675** (2003) 333 [hep-ph/0308039].

[159] RQCD collaboration, *Light-cone distribution amplitudes of pseudoscalar mesons from lattice QCD*, *JHEP* **08** (2019) 065 [1903.08038].

[160] T. Huber, E. Lunghi, M. Misiak and D. Wyler, *Electromagnetic logarithms in $\bar{B} \to X_s l^+ l^-$*, *Nucl. Phys. B* **740** (2006) 105 [hep-ph/0512066].

[161] C. Bobeth, P. Gambino, M. Gorbahn and U. Haisch, *Complete NNLO QCD analysis of $\bar{B} \to X_s \ell^+ \ell^-$ and higher order electroweak effects*, *JHEP* **04** (2004) 071 [hep-ph/0312090].

[162] A. Carbone, D. Galli, U. Marconi, S. Perazzini, A. Sarti, V. Vagnoni et al., *Invariant mass line shape of $B \to PP$ decays at LHCb*, .

[163] LHCb collaboration, *Measurement of CP asymmetries in two-body $B^0_{(s)}$-meson decays to charged pions and kaons*, *Phys. Rev. D* **98** (2018) 032004 [1805.06759].

[164] M. Gronau and J. L. Rosner, *Rate and CP-asymmetry sum rules in $B \to K\pi$*, *Phys. Rev. D* **74** (2006) 057503 [hep-ph/0608040].

[165] M. Gronau, *A Precise sum rule among four $B \to K\pi$ CP asymmetries*, *Phys. Lett. B* **627** (2005) 82 [hep-ph/0508047].

[166] Y. Grossman, M. König and M. Neubert, *Exclusive Radiative Decays of W and Z Bosons in QCD Factorization*, *JHEP* **04** (2015) 101 [1501.06569].

[167] V. M. Braun, Y. Ji and A. N. Manashov, *Two-loop evolution equation for the B-meson distribution amplitude*, *Phys. Rev. D* **100** (2019) 014023 [1905.04498].

[168] M. Beneke, M. Garny, R. Szafron and J. Wang, *Anomalous dimension of subleading-power N-jet operators. Part II*, *JHEP* **11** (2018) 112 [1808.04742].

[169] R. L. Jaffe, *Spin, twist and hadron structure in deep inelastic processes*, in *Ettore Majorana International School of Nucleon Structure: 1st Course: The Spin Structure of the Nucleon*, pp. 42–129, 1, 1996, hep-ph/9602236.

[170] C. W. Bauer, D. Pirjol and I. W. Stewart, *Power counting in the soft collinear effective theory*, *Phys. Rev. D* **66** (2002) 054005 [hep-ph/0205289].

[171] S. Wandzura and F. Wilczek, *Sum Rules for Spin Dependent Electroproduction: Test of Relativistic Constituent Quarks*, *Phys. Lett. B* **72** (1977) 195.

[172] M. Beneke and P. Ruiz-Femenia, *Threshold singularities, dispersion relations and fixed-order perturbative calculations*, *JHEP* **08** (2016) 145 [1606.02434].

[173] Y. L. Luke, *The Special Functions and Their Approximations*, *New York: Academic Press* (1969) .

Acknowledgements

First of all, I would like to thank my advisor Prof. Dr. Martin Beneke, who instructed me over the past years. From our meetings and discussions, I substantially learned novel and valuable methods to tackle conceptually interesting problems. Along the way, this guided me to turn proper TMP math into actual phenomenological relevance, for which I am highly grateful. The second person I want to thank is Dr. Philipp Böer, for his day-to-day supervision up to the very end. This includes all the feedback on calculations, presentations, drafts, and in particular many text messages over the weekends. In a similar manner, I am grateful to Prof. Dr. Keri Vos, who sometimes motivated me to leave the calculation machine deck and take a view on the precision horizon. For her administrative support and efforts, especially during the application phase, I thank Elke Hutsteiner. At the beginning of my work, Prof. Dr. Danny van Dyk provided me the opportunity to participate in an additional project and different theory workshops, for which I owe him a special thanks.

For financial support, I thank Studienstiftung des deutschen Volkes for their Ph.D. scholarship and the possibility to extend my research within the Marianne Plehn program. The Max Planck Institute for Physics and the IMPRS program, supervised by Dr. Frank Steffen, supported me in particular during my first year. In this context, I would like to thank Prof. Dr. Gerhard Buchalla for mentoring my progress in the IMPRS program.

Special thanks also go to Dr. Matthias König, with whom I had many enlightening and joyful discussions about the fundamental concepts of HQET and SCET over the last months of my Ph.D. Furthermore, I would like to thank Dr. Kai Urban, who has been my long-term office mate, as well as Gael Finauri and Andrea Sanfilippo for relaxing coffee and lunch breaks. I am thankful to Dr. Yao Ji for his help and comments about LCDAs and their evolution, and to Dr. Lennart Laude and Mathias Geiger for feedback on language style. Finally, I would like to thank my mother and my father for their endless support.